

**COORDINATING VERSATILITY OF TRANSITION
METAL COMPLEXES DERIVED FROM NNO DONOR
AROYLHYDRAZONES: SPECTRAL AND BIOLOGICAL
STUDIES**

*Thesis submitted to
Cochin University of Science and Technology
In partial fulfillment of the requirements for the degree of*

***Doctor of Philosophy
in
Chemistry***

Under the Faculty of Science

By

FOUSIAMOL M. M.



**Department of Applied Chemistry
Cochin University of Science and Technology
Kochi 682 022**

May 2019

**COORDINATING VERSATILITY OF TRANSITION METAL
COMPLEXES DERIVED FROM NNO DONOR
AROYLHYDRAZONES: SPECTRAL AND BIOLOGICAL
STUDIES**

Ph. D. Thesis under the Faculty of Science

Author:

Fousiamol M. M.

Research Fellow, Department of Applied Chemistry
Cochin University of Science and Technology
Kochi 682 022
India
Email: fousia27@gmail.com

Research Advisor:

Dr. M.R. Prathapachandra Kurup

Professor (Rtd.)
Department of Applied Chemistry
Cochin University of Science and Technology
Kochi 682 022, India
Email: mrp@cusat.ac.in

Department of Applied Chemistry
Cochin University of Science and Technology
Kochi 682 022
India

May 2019

*“AND MY SUCCESS CAN ONLY COME
FROM ALLAH. IN HIM I TRUST, AND
UNTO HIM I RETURN.”*

Quran (11: 88)

*To my dearest
Ikka, daughter & my mother.....*

**DEPARTMENT OF APPLIED CHEMISTRY
COCHIN UNIVERSITY OF SCIENCE AND TECHNOLOGY
KOCHI - 682022, INDIA**



Dr. M. R. Prathapachandra Kurup
Professor (Rtd.)

Mob: 9895226115
Phone Res. 0484-2626904
Email: mrp@cusat.ac.in
mrp_k@yahoo.com
mrpcusat@gmail.com

30-04-2019

Certificate

This is to certify that the thesis entitled **“COORDINATING VERSATILITY OF TRANSITION METAL COMPLEXES DERIVED FROM NNO DONOR AROYLHYDRAZONES: SPECTRAL AND BIOLOGICAL STUDIES”** submitted by **Mrs. Fousiamol M. M.**, in partial fulfillment of the requirements for the degree of Doctor of Philosophy, to the Cochin University of Science and Technology, Kochi-22, is an authentic record of the original research work carried out by her under my guidance and supervision. The results embodied in this thesis, in full or in part, have not been submitted for the award of any other degree. All the relevant corrections and modifications suggested by the audience and recommended by the doctoral committee of the candidate during the presynopsis seminar have been incorporated in the thesis.

Dr. M.R. Prathapachandra Kurup
(Supervising Guide)

Declaration

I hereby declare that the work presented in this thesis entitled **“COORDINATING VERSATILITY OF TRANSITION METAL COMPLEXES DERIVED FROM NNO DONOR AROYLHYDRAZONES: SPECTRAL AND BIOLOGICAL STUDIES”** is entirely original and was carried out independently under the supervision of **Dr. M. R. Prathapachandra Kurup** (Rtd. Professor), Department of Applied Chemistry, Cochin University of Science and Technology and has not been included in any other thesis submitted previously for the award of any other degree.

30-04-2019
Kochi-22

Fousiamol M. M.

Acknowledgements.....

A piece of work to become perfect, one needs the blessings and help of many. For the completion of this research work, I'm indebted to many for their generous contributions, be it in the form of a piece of advice or suggestions for improvement.

First of all, let me bow my head in reverent gratitude to Allah for the immense blessings showered on me and for the undeserving grace shown to me for the successful completion of this work.

First and foremost, I wish to place on record my heartfelt gratefulness to my supervising guide Dr. M.R. Prathapachandra Kurup, Rtd. Professor of the Department of Applied Chemistry, Cochin University of Science and Technology for his intensive guidance and whole hearted support and inspiration throughout my research work. Especially I was very inspired in the interest and eagerness shown by him to study how to solve crystal structure for long time eventhough we get bored and tired. I am very much thankful to him for the valuable time spent by him for me during his busy schedule as Dean of Science, CUSAT & HOD, Department of Chemistry, Central University, Kasargod and for correcting my thesis with positive criticisms, valuable suggestions and corrections. I express my sincere thanks to Dr. P. A. Unnikrishnan as my doctoral committee member.

I express my sincere thanks to former H. O. D's Prof. K. Sreekumar & Dr. N. Manoj for their encouragement and support. I am very much thankful to Prof. K. Gireeshkumar, Head, Department of Applied Chemistry, CUSAT for the support and cooperation during my research period.

Let me place on record my gratitude to all my former teachers who made me what I am today especially to Smt. Rosaline Francis and my teachers of Newman College, Thodupuzha. I also thank all my friends of Newman College Thodupuzha.

I would like to acknowledge my deep gratitude to Prof. K.K. Mohammed Yusuff (Rtd.), for his group theoretical classes. Also I extent my heartfelt gratitude to Dr. S. Prathapan, who

taught me the principles of spectroscopy during my M.Phil course which proved to be of great use in my research field also. I sincerely thank all other faculty members and non-teaching staffs especially Smt. Bindhu (S. O., Department of Applied Chemistry) for the assistance to conduct this research.

I sincerely thank the Cochin University of Scientific and Technology & DST-PURSE, for financial support offered in the form of JRF and SRF. I am indebted to all the staff of SAIIF, Kochi, IIT Bombay for the services rendered for sample analyses. I place my special thanks to Dr. Shibu Eapen, SAIIF, Kochi, Prof. Jerry P. Jasinski, Department of Chemistry, Keene State College, 229 Main Street, Keene, USA, Dr. Matthias Zeller, Purdue University, West Lafayette, USA and Dr. Krishna K. Damodaran, Department of Chemistry, University of Iceland for Single crystal XRD studies.

I am grateful to my senior researchers Dr. Roji J. Kunnath, Dr. Jinsa Mary Jacob, Dr. Bibitha Joseph, Dr. Nisha K. and Dr. Sajitha N. R. for their support. It is a pleasure to thank Dr. Aiswarya N. for her valuable suggestions, inspiring words and support offered throughout my research period. I also thank Dr. Sreejith S. S. for installing various programmes, technical help and valuable advices. My senior labmates Dr. Ambily Aravindakshan and Ms. Ambily K.U. helped me a lot during my thesis writing. Positive energy is always obtained from Seena Chechi, my best friend of M. Phil course. Her support helped me a lot during crucial situations.

I am grateful to Dr. M. Sithambaresan for his patience and timely help for the EPR simulations and his countless support. I am especially thankful to my first friend in the lab Nithya for her all the moments of help and support offered by you in my CUSAT days. I also extend my thanks to Ms. Sameeha A. P. of Inorganic lab for her countless help. If I need any help, Lincy is always ready and also she gives valuable suggestions and criticisms whenever I needed. Thanks a lot Lincy... All my agonies, worries and day to day moments are shared with my junior labmate and my best friend Asha. Her advices helped me a lot in all situations. I wish to express special thanks to all my labmates - Daly, Manjari, Nimya and Vineetha chechi – you all are helped me in various situations. I also thank all junior students of Kala miss especially Aswathy.

My uncle, Mr. Nazar Saidumuhammed (S. O., School of Legal Studies, CUSAT) encouraged me a lot in various stages of my education and showered his love and affection enabling me to complete this work successfully.

Another person who deserves a special mention is Dr. Laly K, of our senior. She gave me a peaceful atmosphere for thesis writing and also full freedom in her house. It is a pleasure to pay tribute for the motherly care and prayers given by her mother Bhavani teacher. Also her husband Er. V. S. Thankappan helped me a lot. Thank you very much for the whole family....

Words are not enough to express the gratitude towards family - It's only God's grace to become a daughter of my parents Mr. Moosa & Mrs. Ramla Moosa. Also I am very much thankful to my mother-in-law and father-in-law for all the sacrifices that you have made on my behalf. I am very lucky and proud of you my partner Muhammad Sha. He is the driving force behind the research. My little daughter Amna, the most precious gift in my life, missed my care but she adjusted all the circumstances like an adult. I also thank my brother and family for the support during my work. I thank all my family members and appreciate the support and comfort that they gave me throughout my life.

Thank you all, who has directly and indirectly extended a helping hand in this endeavor of mine.

Fousiamol M. M.

Contents

Chapter 1

A PREAMBLE ON AROYLHYDRAZONES AND THEIR BIOLOGICAL

APPLICATIONS 01 - 20

1.1	Introduction.....	01
1.1.1	Aroylhydrazones.....	02
1.1.2	Diversity of coordination in the chelation of aroylhydrazones	03
1.2	Applications of aroylhydrazones and its complexes.....	08
1.2.1	Biological activity	08
1.2.1.1	Antimicrobial activity.....	08
1.2.1.2	Analgesic and anti-inflammatory activity.....	09
1.2.1.3	Anticancer activity.....	09
1.2.1.4	Central nervous system activity.....	10
1.2.1.5	Antiprotozoal activity.....	10
1.2.1.6	Cardioprotective activity	10
1.2.1.7	Antiplatelet activity	11
1.2.1.8	DNA binding	11
1.2.1	Catalytic applications	12
1.2.2	Analytical applications.....	12
1.2.2.1	Spectrophotometric applications	12
1.2.2.2	Spectrofluorimetric applications.....	12
1.3	Objectives of the present work	13
1.4	Physicochemical methods.....	14
1.2.1	Elemental analyses	14
1.2.3	Molar conductivity measurements	14
1.2.3	Infrared spectroscopy	14
1.2.4	Electronic spectroscopy.....	15
1.2.5	¹ HNMR spectroscopy.....	16
1.2.6	EPR Spectroscopy	16
1.2.7	Hirshfeld Surface Analysis.....	18
1.2.8	X-ray crystallography.....	19
1.2.9	Antibacterial Activity.....	20
1.2.10	<i>In vitro</i> Cytotoxicity Studies	20

Chapter 2

SYNTHESES AND CHARACTERIZATION OF AROYLHYDRAZONES...21 - 41

2.1	Introduction.....	21
2.2	Experimental.....	22
2.2.1	Materials.....	22
2.2.2	Syntheses of aroylhydrazones	22

2.2.2.1	Synthesis of 2-benzoylpyridine-3-methoxybenzhydrazone (H _{bpm}).....	22
2.2.2.2	Synthesis of di-2-pyridyl ketone-3-methoxybenzhydrazone (H _{dkm}).....	23
2.2.3	Refinement.....	23
2.3	Results and discussion	24
2.3.1	Infrared spectra.....	24
2.3.2	Electronic spectra.....	25
2.3.3	¹ HNMR spectral studies.....	26
2.3.4	Hirshfeld Surface and 2D Fingerprint Plot Analysis	28
2.3.5	X-ray crystallography.....	34
2.3.5.1	Crystal structure of 2-benzoylpyridine-3-methoxybenzhydrazone (H _{bpm}).....	34
2.3.5.2	Crystal structure of di-2-pyridyl ketone-3-methoxybenzhydrazone (H _{bpm}).....	37

Chapter 3

SYNTHESES AND CHARACTERIZATION OF HALIDE BRIDGED BOX

DIMER COPPER(II) COMPLEXES OF AROYLHYDRAZONES 43 - 75

3.1	Introduction.....	43
3.2	Experimental	44
3.2.1	Materials.....	44
3.2.2	Syntheses of copper(II) complexes	44
3.2.2.1	Synthesis of [Cu(bpm)Cl] ₂ (1).....	44
3.2.2.2	Synthesis of [Cu(bpm)Br] ₂ (2).....	45
3.2.2.3	Synthesis of [Cu(dkm)Br] ₂ (3).....	45
3.3	Results and discussion	46
3.3.1	Infrared spectra.....	46
3.3.2	Electronic spectra.....	48
3.3.3	EPR spectra	50
3.3.4	Hirshfeld Surface and 2D Fingerprint Plot Analysis.....	55
3.3.5	X-ray crystallography.....	59
3.3.5.1	Crystal structure description of [Cu(bpm)Cl] ₂ (1) and [Cu(bpm)Br] ₂ (2).....	59
3.3.5.2	Crystal structure of [Cu(dkm)Br] ₂ (3)	69

Chapter 4

SYNTHESES AND CHARACTERIZATION OF COPPER(II) AND NICKEL(II) COMPLEXES OF AROYLHYDRAZONES CONTAINING PSEUDOHALIDES AS COLIGANDS

77 - 116

4.1	Introduction.....	77
4.1.1	The pseudohalogens – azide and thiocyanate.....	78
4.1.1.1	Azide anion.....	78
4.1.1.2	Thiocyanate anion	80

4.2	Experimental.....	80
4.2.1	Materials.....	80
4.2.2	Syntheses of azide bridged complexes.....	81
4.2.2.1	Synthesis of [Cu(bpm)N ₃] ₂ (4).....	81
4.2.2.1	Synthesis of [Cu(dkm)N ₃] ₂ (5).....	82
4.2.2.1	Synthesis of [Ni(dkm)N ₃] ₂ (6).....	82
4.2.2.1	Synthesis of [Cu(bpm)NCS] _n (7).....	83
4.3	Results and discussion.....	84
4.3.1	Infrared spectra.....	84
4.3.2	Electronic spectra.....	86
4.3.3	EPR spectra.....	88
4.3.4	Hirshfeld Surface Analysis.....	92
4.3.5	X-ray crystallography.....	96
4.3.5.1	General features in the crystal structures of [Cu(bpm)N ₃] ₂ (4) and [Cu(dkm)N ₃] ₂ (5).....	97
4.3.5.2	Crystal structure of [Cu(bpm)N ₃] ₂ (4).....	98
4.3.5.3	Crystal structure of [Cu(dkm)N ₃] ₂ (5).....	99
4.3.5.4	Crystal structure of [Ni(dkm)N ₃] ₂ (6).....	108
4.3.5.5	Crystal structure of [Cu(dkm)NCS] _n (7).....	114

Chapter 5

SYNTHESES AND CHARACTERIZATION OF BISLIGATED

COMPLEXES OF AROYLHYDRAZONES..... 117 - 154

5.1	Introduction.....	117
5.2	Experimental.....	118
5.2.1	Materials.....	118
5.2.2	Syntheses of bisligated copper(II) complexes.....	118
5.2.2.1	Synthesis of [Cu(dkm)] ₂ (8).....	118
5.2.2.2	Synthesis of [Cu(dkm)(Hdkm)](ClO ₄)·0.8H ₂ O (9).....	119
5.2.2.3	Synthesis of [Ni(bpm)] ₂ (10).....	119
5.2.2.3	Synthesis of [Ni(dkm)] ₂ (11).....	120
5.2.2.3	Synthesis of [Co(bpm) ₂](ClO ₄) (12).....	121
5.2.2.3	Synthesis of [Zn(bpm)] ₂ (13).....	121
5.3	Results and discussion.....	122
5.3.1	Infrared spectra.....	122
5.3.2	Electronic spectra.....	124
5.3.3	EPR spectra.....	126
5.3.4	Hirshfeld Surface Analysis.....	129
5.3.5	X-ray crystallography.....	133
5.3.5.1	Crystal structure of [Cu(dkm)] ₂ (8).....	133
5.3.5.2	Crystal structure of [Cu(dkm)(Hdkm)](ClO ₄)·0.8H ₂ O (9).....	139
5.3.5.3	General features in the crystal structure of [Ni(bpm)] ₂ (10) and [Ni(dkm)] ₂ (11).....	142

5.3.5.4	Crystal structure of [Co(bpm) ₂](ClO ₄) (12).....	148
5.3.5.5	Crystal structure of [Zn(bpm) ₂] (13).....	151

Chapter 6

ANTIBACTERIAL AND CYTOTOXICITY STUDIES OF SELECTED

COMPLEXES	155 - 175
------------------------	------------------

6.1	General Introduction	155
-----	----------------------------	-----

Section A

ANTIBACTERIAL ACTIVITY

6.2	Introduction.....	156
-----	-------------------	-----

6.2.1	Mode of action	159
-------	----------------------	-----

6.3	Experimental	159
-----	--------------------	-----

6.3.1	Materials and methods	159
-------	-----------------------------	-----

6.3.1.1	Bacterial cultures used.....	159
---------	------------------------------	-----

6.3.1.1	Media used.....	159
---------	-----------------	-----

6.3.2	Well diffusion method	160
-------	-----------------------------	-----

6.4	Results and discussions.....	160
-----	------------------------------	-----

Section B

CYTOTOXICITY STUDY

6.5	Introduction.....	170
-----	-------------------	-----

6.6	Experimental	171
-----	--------------------	-----

6.6.1	<i>In vitro</i> cytotoxicity study – Trypan Blue Exclusion Method	171
-------	---	-----

6.7	Results and discussions.....	172
-----	------------------------------	-----

Chapter 7

SUMMARY AND CONCLUSION.....	177 – 183
------------------------------------	------------------

REFERENCES.....	185 - 201
------------------------	------------------

LIST OF PUBLICATIONS	203
-----------------------------------	------------

||| Preface |||

Aroylhydrazones are an important class of compounds exhibiting a wide spectrum of activities in the biological, medicinal, catalytic and photoluminescence fields. They are resourceful compounds which can act as potential multifunctional ligands with interesting coordination modes in either neutral, monoanionic, dianionic or tetraanionic forms bearing unusual coordination numbers. Among the various transition metals, dinuclear copper(II) complexes are gaining more importance because of their relevance in biological fields. Copper exhibits rich coordination chemistry with complexes and has its own footprint in both magnetic susceptibility and EPR. Copper(II) complexes of diverse drugs have been the subject of a large number of research studies due to its synergic activity with the drug. The design and synthesis of halide/pseudohalide bridged dinuclear copper(II) complexes of hydrazones have been an attractive area of research. The cobalt(III), nickel(II), copper(II) and Zinc(II) complexes of these aroylhydrazones are prepared. The in vitro cytotoxicity of the synthesized aroylhydrazones and the selected complexes were assayed against lymphoma ascites cell line. The antibacterial activity of the aroylhydrazones and its selected complexes have been screened against bacterial species *Staphylococcus aureus*, *Bacillus subtilis*, *Escherichia coli* and *Pseudomonas*.

The thesis is divided into seven chapters. Chapter 1 gives an idea about the general introduction of aroylhydrazones, coordinating properties, coordination diversity and objectives of the present work. Various physicochemical techniques are also discussed in this chapter. Chapter 2 describes the syntheses and characterization of two aroylhydrazones 2-benzoylpyridine-3-methoxybenzhydrazone and di-2-pyridyl ketone-3-methoxybenzhydrazone. Chapter 3 deals with the syntheses and characterization of three single crystals of halogen bridged box dimer copper(II) complexes of these two aroylhydrazones. Chapter 4 discusses the syntheses and characterization of copper(II) and nickel(II)

complexes of aroylhydrazones containing pseudohalides as coligand. Two pseudohalides, azide and thiocyanate are used as coligands. Chapter 5 portrays syntheses and characterization of six bisligated transition metal complexes of copper(II), nickel(II), cobalt(III) and zinc(II). In chapter 6, we are discussing about biological applications like antibacterial activity and cytotoxicity studies of selected complexes. The antibacterial activities of the complexes have been screened *in vitro* against both Gram(+) and Gram(-) bacterial stains. In vitro cytotoxicity of the selected complexes have been tested by Trypan blue exclusion method. Chapter 7 explains the conclusion and future aspects of our work.

||| List of Abbreviations |||

Hbpm	2-benzoylpyridine-3-methoxybenzhydrazone
Hdkm	di-2-pyridyl ketone-3-methoxybenzhydrazone
DMF	<i>N,N</i> -dimethylformamide
CH ₃ OH	methanol
N ₃	azide
KSCN	potassium thiocyanate
Complex 1	[Cu(bpm)Cl] ₂
Complex 2	[Cu(bpm)Br] ₂
Complex 3	[Cu(dkm)Br] ₂
Complex 4	Cu(bpm)N ₃ ₂
Complex 5	[Cu(dkm)N ₃] ₂
Complex 6	[Ni(dkm)N ₃] ₂
Complex 7	[Cu(bpm)NCS] _n
Complex 8	[Cu(dkm)] ₂
Complex 9	[Cu(dkm)(Hdkm)](ClO ₄)·0.8H ₂ O
Complex 10	[Ni(bpm)] ₂
Complex 11	[Ni(dkm)] ₂
Complex 12	[Co(bpm) ₂](ClO ₄)
Complex 13	[Zn(bpm)] ₂

.....

Chapter 1

A PREAMBLE ON AROYLHYDRAZONES AND THEIR BIOLOGICAL APPLICATIONS

Contents

- 1.1. Introduction*
- 1.2. Applications of aroylhydrazones and its complexes*
- 1.3. Objectives of the present work*
- 1.4. Physico-chemical methods*

1.1. Introduction

Coordination chemistry emerged from the work of Alfred Werner, a Swiss chemist and he was awarded the Nobel Prize in 1913 for his coordination theory. Coordination compounds are molecules that possess a metal center that is bound to ligands (atoms, ions, or molecules that donate electrons to the metal). These complexes can be neutral or charged. When the complex is charged, it is stabilized by neighboring counter-ions. Several thousands of coordination complexes have been synthesized and investigated during the past few decades. Coordination chemistry will continue to strengthen its role as a central expertise and authority for material science. Nowadays coordination chemistry comprises a major portion of current inorganic research.

Metal coordination complexes have a wide variety of technological and industrial application ranging from catalysis to anticancer drugs. In these compounds the metal atom itself may have a number of roles, based on its coordination geometry, oxidation state, magnetic, electronic and photochemical behaviours. Among the nitrogen-oxygen donor ligands, hydrazone compounds have revealed very versatile behaviour in metal coordination and it possesses a special place due to its ease of synthesis.

1.1.1. Aroylhydrazones

Aroylhydrazones, versatile ligand systems in coordination chemistry are a class of compounds having the group $-C=N-N-$ obtained by the action of aldehydes or ketones with aroylhydrazides (Fig. 1.1). The desirable characteristics of hydrazones are the ease of preparation, tendency towards crystallinity and increased hydrolytic stability relative to imines. The nitrogen atoms of the hydrazones are nucleophilic and the carbon atom has both electrophilic and nucleophilic nature [1]. The α -hydrogen atom of hydrazone is more nucleophilic as compared to ketones because α -hydrogen atom of hydrazone is 10 times more acidic than ketones [2,3]. The combination of hydrazones with other functional group leads to compounds with unique physical and chemical character [4]. They act as reactants in various important reactions such as hydrazone iodination, Shapiro reaction and Bamford- Stevans reaction to form vinyl compounds. They act as intermediate in Wolff-Kishner reaction.

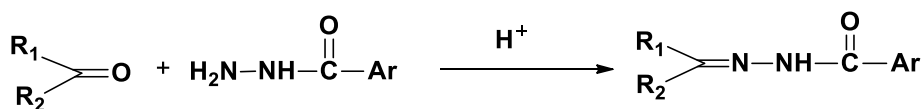


Fig.1.1. Formation of aroylhydrazone.

Amido - iminol tautomerism occurs readily in hydrazones and has an important role in determining the overall charge on the ligands. Hydrazones generally exist in the amido form in the solid state but in solution they tend to exist as an equilibrium mixture of amido and iminol forms (Fig. 1.2).

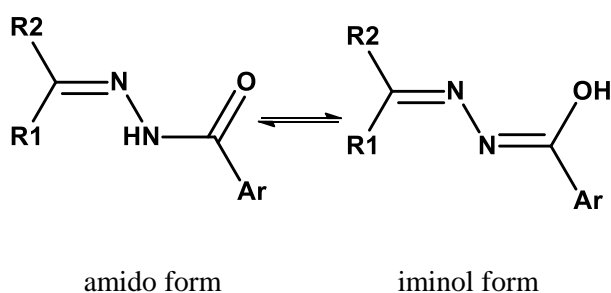
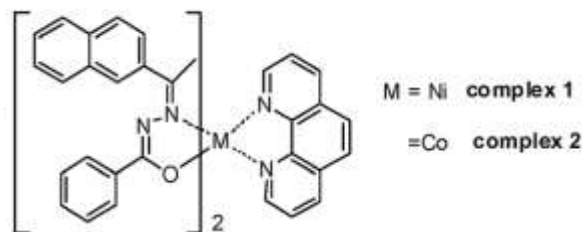


Fig.1.2. Tautomerism in aroylhydrazones.

1.1.2. Diversity of coordination in the chelation of aroylhydrazones

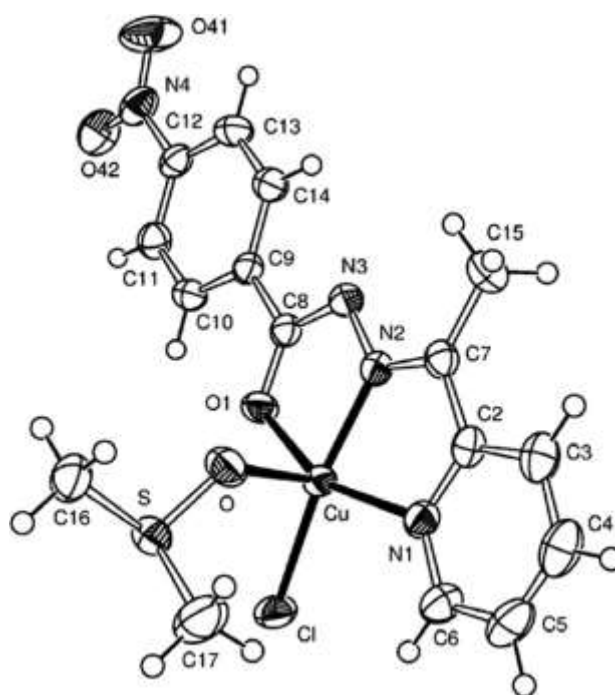
Aroylhydrazone are an important class of ligands in coordination chemistry and their complexing ability containing different donor atoms are widely reported. Various factors like reaction time, temperature, solvent, number and nature of substituents, stability of complex formed etc. are affected the coordination modes of hydrazones. The structural changes of the segment attached to the hydrazone will affect the metal binding of the ligand and exhibit interesting coordination modes with transition metal ions to form octahedral, square planar, square pyramidal and tetrahedral complexes.

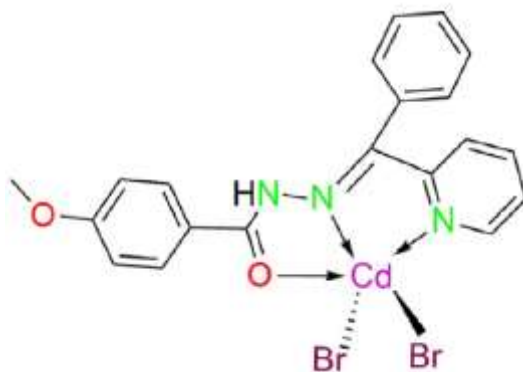
In the absence of side chains with donor atoms, aroylhydrazones are bidentate ligands with carbonyl oxygen and amine nitrogen as possible donors. X-ray crystallography of two new nickel(II) and cobalt(II) benzhydrazone complexes reveals a distorted octahedral coordination environment around the metal center, with the hydrazone ligand acting as a monoanionic bidentate N,O-donor (Structure 1) [5-7].



Structure 1

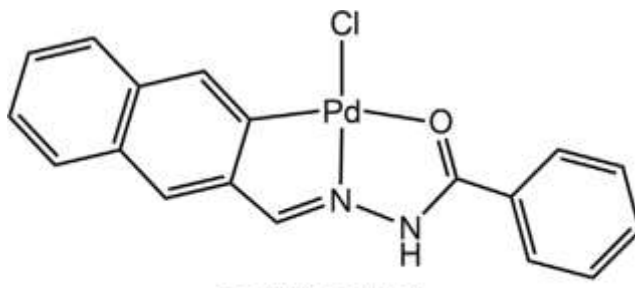
Introduction of suitable substituent containing donor atoms on the hydrazide part as well as on the carbonyl part should increase the coordination possibility. If the carbonyl part contains a pyridyl group, it can coordinate to the central metal by adopting an NNO coordination mode, either through deprotonated iminolic form (Structure 2) [8,9] or neutral amido form (Structure 3) [10,11].





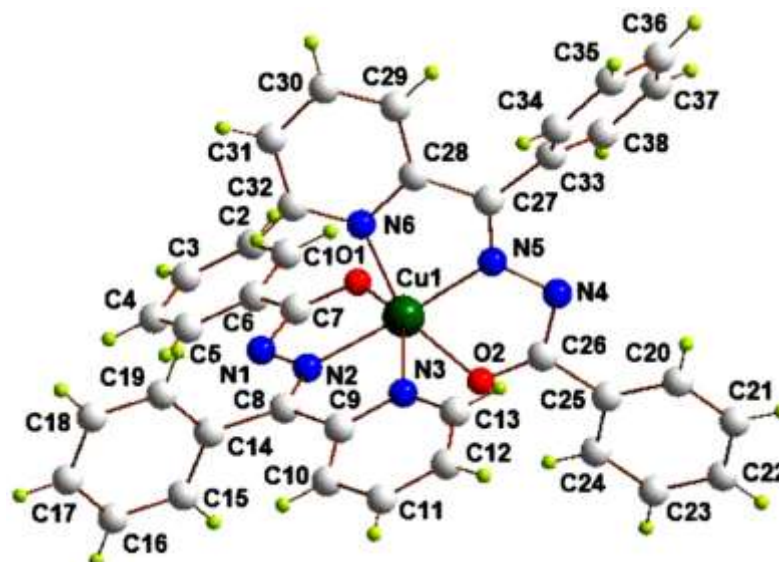
Structure 3

Babu *et al* synthesized a cyclometallated palladium(II) complex of N'-(2-naphthylidene)benzohydrazide in which the tridentate ligand acts as pincer-like CNO-donor (Structure 4) [12].



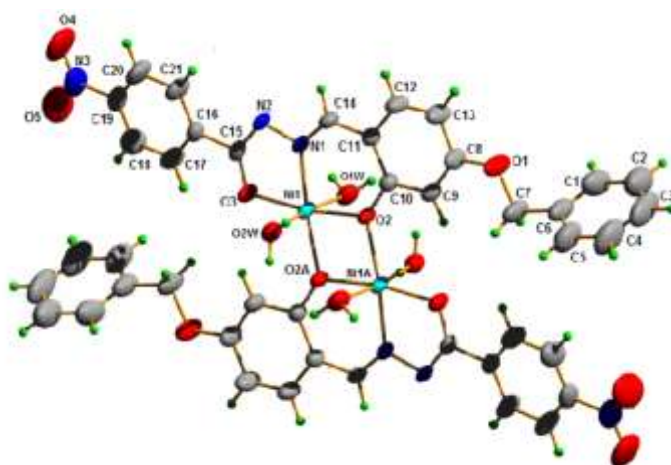
Structure 4

Another possibility is the formation of bisligated six coordinated complex with two NNO donor aroylhydrazones in monoanionic form (Structure 5) [13].



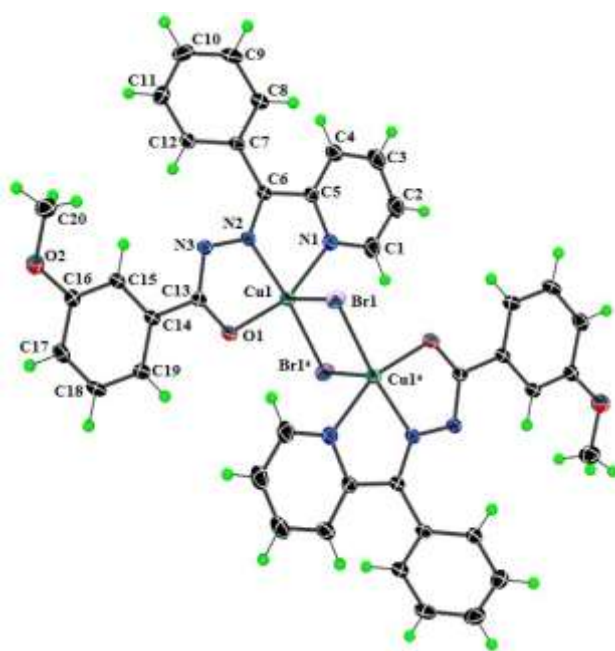
Structure 5

Sometimes hydrazones can form bridged complexes. If the tridentate ONO donor hydrazone possesses a phenolic group, the phenolate oxygen can form a bridge between the metal centers and thus forming dimeric complexes (Structure 6) [14].



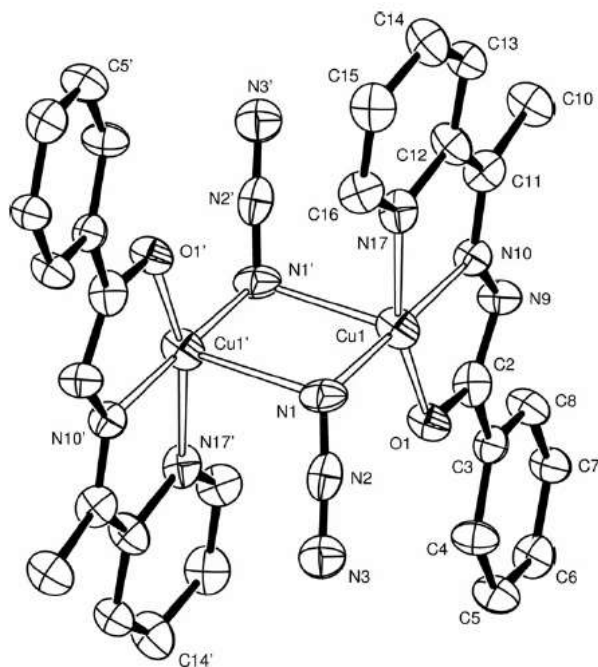
Structure 6

Attractive bridging ligands like halides, azide, thiocyanate, acetate etc. have been reported to bind divalent transition metal ions in a variety of coordination modes where, in addition to the formation of mononuclear species, it led to the construction of polynuclear metal complexes of different nuclearity and dimensionality (Structure 7) [15-21].



Structure 7

A synthetic strategy that is generally applied to build exchange interactions between the metal centers is to use pseudohalides as ligands, because they provide versatile coordination behavior and generates dimeric and multidimensional polymeric magnetic materials that facilitate ferro and antiferromagnetic interactions among the metal centers [22-29]. Depending upon the steric and electronic demand of coligands, azide can serve as *end-on* (1-1,1 or EO) or an *end-to-end* (1-1,3 or EE) bridging ligand. Such azido-bridged copper(II) complexes are of great interest in magnetism, material chemistry and biology (Structure 8) [30].



Structure 8

1.2. Applications of aroylhydrazones and its complexes

1.2.1. Biological activity

Hydrazone ligands and their metal complexes have attracted many authors due to their wide applications in biological, pharmaceutical, analytical, catalytic and industrial fields.

1.2.1.1. Antimicrobial activity

The emerging bacterial resistance causes a widespread problem for the treatment of various infections. Therefore, the search for antimicrobials is a never-ending task. Now-a-days a number of hydrazone derivatives have been developed and evaluated for their antibacterial activity [31]. Angel *et al* studied 2-

acetylpyridine and 2-benzoylpyridine derived hydrazones and showed their poor antimicrobial effect against Gram-positive *S. aureus* and *E. faecalis* and Gram-negative *P. aeruginosa* bacteria, but exhibited significant antifungal activity against *C. albicans*. Upon coordination to copper(II) the antimicrobial activity of 2-acetylpyridine and 2-benzoylpyridine derived hydrazones increases [8]. Cu(II) complexes of pyridoxal isonicotinoyl hydrazone can be considered an important potential alternative class of compounds for new antimicrobial agents development [32].

1.2.1.2. Analgesic and anti-inflammatory activity

Non-steroidal anti-inflammatory drugs (NSAIDs) have a wide clinical use for the treatment of inflammatory and painful conditions including rheumatoid arthritis, soft tissue and oral cavity lesions, respiratory tract infections and fever. A number of hydrazone derivatives have been developed to overcome gastrointestinal disturbance and toxicity. The most important antiinflammatory derivative 2-(2-formylfuryl)pyridylhydrazone presented a 79% inhibition of pleurisy at a dose of 80.1 $\mu\text{mol/kg}$ [33].

The salicylaldehyde-*N*-acylhydrazone derivatives and their zinc(II) complexes showed comparable or superior inhibition of cell-migration process to indomethacin, indicating an expressive anti-inflammatory profile [34].

1.2.1.3. Anticancer activity

A comparative analysis of the cytotoxic effect of three new 2-oxo-1,2-dihydrobenzo[h]quinoline-3-carbaldehyde terminal substituted aroylhydrazone ligands and their copper(II) complexes on a panel of human cancer cell lines showed that the copper complexes exhibited *in vitro* antitumor activity significantly higher than that of the free ligands and also of cisplatin [35].

Cytotoxicity evaluated by MTT assay, suggested that the aroylhydrazones 4-nitro-N'-(1-(pyridin-2-yl)ethylidene)benzohydrazide and 4-nitro-N'-(1-(thiophen-2-yl)ethylidene)benzohydrazide significantly reduce the cell viability of breast cancer cell lines (MCF7) and human prostate adenocarcinoma (DU145) in a dose dependent manner [36]. Copper(II) complex of mixed ligand aroylhydrazone and N-donor heterocyclic lewis base exhibits a high cytotoxic activity against ovarian and colorectal carcinoma cells (A2780, HCT116 respectively), with IC₅₀ much lower than those for normal primary fibroblasts [37].

1.2.1.4. Central nervous system (CNS) activity

CNS diseases can affect either brain or the spinal cord resulting in psychological and neurological disorder. Hydrazones are reported to have activity against various disorders of CNS [38]. Novel 2-methoxyacylhydrazone derivatives synthesized by Cutshall *et al.*, [39] were evaluated for inhibition of phosphodiesterase 10A (PDE10A), a PDE responsible for neurological and psychological disorders like schizophrenia.

1.2.1.5. Antiprotozoal activity

Protozoa are a diverse group of unicellular eukaryotic organisms affecting human beings, especially in tropical countries. Carvalho *et al.*, synthesized cinamic N-acylhydrazones with good anti-Trypanosomal activity [40,41].

1.2.1.6. Cardio protective activity

Cardiovascular disease is a class of diseases that involve the heart and blood vessels. Cardiovascular diseases (CVDs) are the number one killer and thrombosis in particular is accountable for the majority of CVD-related mortalities. Antihypertensive profile of 2-thienyl-3,4-methylenedioxybenzoylhydrazone have been reported by Leal *et al* [42].

1.2.1.7. Antiplatelet activity

Antiplatelet drugs are the agents which decrease platelet aggregation and inhibit thrombus formation. A series of indole-based aryl(aroyl)hydrazone analogs of antiplatelet indole-3- carboxaldehyde phenylhydrazone were synthesized by Tehrani *et al* [43]. Anti-platelet activity of novel arylsulfonate–acylhydrazone derivatives were evaluated by Lima *et al* [44].

1.2.1.8. DNA binding

The DNA-binding interaction of the Ni(II) and Co(II) complexes containing 2-acetonaphthone benzoylhydrazone (HL) and 1,10-phenanthroline revealed that both complexes can bind to DNA *via* intercalation in the order of HL < Co(II) complex < Ni(II) complex. The Ni(II) complex displays higher DNA and BSA-binding affinity than the corresponding Co(II) analogue, which is expected of its smaller size [45].

Competitive binding of Cu(II), Co(II) and Ni(II) complexes of (*E*)-*N'*-(2-oxo-1-phenylindolin-3-ylidene)isonicotinohydrazide for DNA indicated that complexes could interact as a groove binder. It should be noted that the observed intrinsic binding constant ($5.88\text{--}10.50 \times 10^4 \text{ M}^{-1}$) is comparable to other groove binders as well and complexes Cu and Ni have stronger binding affinity than Co. The complexes bind to super coiled plasmid pUC19 DNA and display efficient hydrolytic cleavage and are a specific groove binder [46].

The Cu(II), Ni(II) and Zn(II) complexes of 4-*N'*-[(*Z*)-furan-2-ylmethylidene]-4 hydroxybenzohydrazide and hydroxymethyl (4-[[(*Z*)-2- (furan-2ylmethylidene)hydrazinyl]carbonyl}phenoxy)acetate bind slightly to calf thymus DNA and effectively cleave pBR322 DNA whereas the nickel and zinc complexes have only slight interactions with DNA [47].

1.2.2. Catalytic applications

The nickel(II) complexes of benzoyl hydrazone derivatives catalyze the oligmerization of ethylene with methylaluminumoxane [48]. Manganese(II), cobalt(II), nickel(II) and copper(II) complexes of bis(salicylaldiminato) hydrazone catalyze the oxidation of cyclohexene with *tert*-butylhydroperoxide [49]. Another example is the catalytic activity of copper(II) complexes of picolylhydrazone derivatives toward ascorbic oxidation of vitamin C [50]. A Zn(II) complex with coumarin-hydrazone ligand is an active catalyst for green synthesis of tetrazole compounds and the electronic properties of substrate has considerable effect on the activity of this catalytic system [51].

1.2.3. Analytical applications

1.2.3.1. Spectrophotometric applications

Di-2-pyridyl ketone benzoylhydrazone is used for the spectrophotometric determination of Pd(II), Fe(II) and Ni(II) and di-2-pyridyl ketone benzoylhydrazone for Fe(II), Fe(III), Co(II) and Ni(II) [52-57].

1.2.3.2. Spectrofluorimetric applications

Di-2-pyridylketone-2-furoylhydrazone was used for the determination of gallium(III) by Salgado et al [58]. O-vanillin furfuralhydrazone and o-vanillin furoylhydrazone were used for the spectrofluorimetric determination of Os(VIII) and Cd(II) respectively [59,60].

1.3. Objectives of the present work

Extensive research has been devoted to the syntheses and studies of halide and pseudohalide bridged binuclear transition metal complexes with characteristic physical and/or chemical properties for biologists and bioinorganic chemists to investigate the structural and functional role of active sites in copper proteins, and also for physical inorganic chemists seeking to design new magnetic materials. The azide displays versatile bridging modes in polynuclear transition metal complexes. Among which the $\mu_{(1,1)}$ singly (EO), di- $\mu_{1,1}$ -N₃ (double EO) and $\mu_{1,3}$ -N₃ (single EE) are common. Depending on these bridging modes, the azido group can efficiently transmit different magnetic interactions in them. The type and the magnitude of the magnetic exchange interactions depend on the metal–metal separation, the metal bridging ligand bond lengths, the bridge identity, the dihedral angles between the planes containing the metal ions, the metal ion stereochemistries, the bond angles subtended to the bridging atoms [61]. As a part of our continuous effort to explore the coordination chemistry of metal-halide/pseudohalide bridged complexes, we report the syntheses and characterization of three halide bridged box dimers, three azide bridged box dimers and a thiocyanate bridged 1-D polymer. Rest of them are bisligated complexes. We formulated the following objectives for our present work.

- Syntheses of two NNO donor ligands and their metal complexes
- Characterization of compounds by IR, UV-Vis, SCXRD, ¹H NMR, EPR, elemental analysis and Hirshfeld Surface Analysis
- Study of various interactions present in the synthesized compounds by SCXRD and Hirshfeld Surface Analysis
- To study the antibacterial activity of selected complexes
- To study the cytotoxicity studies of selected complexes

1.4. Physicochemical Methods

The physicochemical methods used for the present study are given below.

1.4.1. Elemental analyses

Elemental analysis is a process where a sample of a chemical compound is analyzed for its elemental and sometimes isotopic composition. Elemental analysis can be qualitative and it can be quantitative. This information is important to help to determine the purity of a synthesised compound. Carbon, hydrogen, nitrogen and sulfur present in all the compounds were estimated by a Vario EL III CHNS elemental analyzer at the Sophisticated Analytical Instrument Facility, Cochin University of Science and Technology, Kochi-22, Kerala, India.

1.4.2. Molar conductivity measurements

The conductivity (specific conductance) of an electrolytic solution is a measure of its ability to conduct electricity. The molar conductivities of the complexes in DMF solutions (10^{-3} M) at room temperature were measured using a Systronic model 303 direct reading conductivity meter at the Department of Applied Chemistry, CUSAT, Kochi, India.

1.4.3. Infrared spectroscopy

Infra-red spectroscopy is an important spectroscopy which gives almost complete information about the functional groups present in a compound. The absorption of infrared radiations is possible only by those bonds of molecule which can show a change in dipole moment by the absorption of radiations. Such types of vibrational transitions which involve the change in dipole moment are known as infra-red transitions. However those vibrational transitions which are not accompanied by the change in dipole moment are not directly observed and called

as infra-red inactive transition. One of the great advantage of IR spectroscopy is that virtually any sample in any state may be studied. Infrared spectra of the ligand and the complexes were recorded on a JASCO FT-IR-5300 Spectrometer in the range 4000-400 cm^{-1} using KBr pellets at the Department of Applied Chemistry, CUSAT, Kochi, India.

1.4.4. Electronic spectroscopy

Electronic spectroscopy is an analytical technique to study the electronic structure and its dynamics in atoms and molecules. It is a technique in which intensity of light passing through a sample (I) is measured and is compared to the intensity of light before it passes through the sample (I_0). The ratio (I/I_0) is called the transmittance and is usually expressed as a percentage (%T). Electronic spectroscopy consists of monitoring the absorption of light by the sample or monitoring the emission of light, often after excitation of the sample by an appropriate light source or laser beam. Both inorganic and organic analytes can be detected. The electronic spectra of the compounds were taken on a Spectro UV-vis Double beam UVD-3500 spectrometer in the 200-900 nm range at the Department of Applied Chemistry, CUSAT, Kochi, India.

There are three types of electronic transition which can be considered;

1. Transitions involving π , σ , and n electrons
2. Transitions involving charge-transfer electrons
3. Transitions involving d and f electrons

When an atom or molecule absorbs energy, electrons are promoted from their ground state to an excited state. In a molecule, the atoms can rotate and vibrate with respect to each other. These vibrations and rotations also have discrete energy levels, which can be considered as being packed on top of each electronic level.

1.4.5. ^1H NMR spectroscopy

^1H NMR spectra of aroylhydrazones and their metal complexes were recorded using Bruker AV500 FT-NMR Spectrometer with chloroform as the solvent and TMS as internal standard at STIC, CUSAT, Kochi. The NMR spectrum is a plot of the intensity of NMR signals versus the magnetic field (frequency) in reference to TMS. The intensity is measured by the integration of the area under the triangle.

Four types of information can be obtained by interpreting proton NMR spectra.

1) Number of signals

Protons within a compound experience different magnetic environments, which give a separate signal in the NMR spectrum.

2) Position of signals (Chemical shift)

The positions of the signals in an NMR spectrum are based on how far they are from the signal of the reference compound. This information tells us the kind of proton or protons that are responsible for the signal.

3) Integration or intensity of NMR signals

Integration is the area measurement that tells us the relative number of protons that give rise to each signal.

4) Splitting of signals

Splitting of signals is caused by (and therefore tells us the number of) protons bonded to adjacent carbons.

1.4.6. Electron Paramagnetic Resonance (EPR) spectroscopy

Electron spin resonance (ESR) spectroscopy, also known as electron paramagnetic resonance (EPR) spectroscopy discovered by the Russian scientist Zavoisky in 1945, has become one of the most powerful local probes for the study

of condensed matter. It is 'an electronic version' of NMR spectroscopy. This technique utilizes microwave radiation to probe species with unpaired electrons, such as radicals, radical cations, and triplets in the presence of an externally applied static magnetic field. It gives information about the distribution of unpaired electrons in the molecule, which in turn helps in mapping the extent of delocalization of electrons over the ligand. When placed in a magnetic field, the molecules with unpaired electrons undergo transitions between different states. The absorption takes place in the microwave region and the energy of transition E is given by $E = h\nu = g\beta B$, where β is the magnetic moment expressed in Bohr Magnetons, B is the strength of the field and g is the ratio of magnetic moment to angular momentum, known as gyromagnetic ratio [62-65].

These measurements provide the value of magnetic moment. The sub-bands in the absorption bands can explain the nature of the metal-ligand bond in the complex. The ESR measurements require a very small quantity of a sample. It is particularly useful for studying complex formation, where there is no change in the number of electrons of the central metal or ion.

The EPR spectra of the complexes in the polycrystalline state at 298 K and in DMF solution at 77 K were recorded in X band using an ESR-JEOL spectrometer at SAIF, IIT Bombay, India. All the EPR spectra are simulated using the EasySpin 5.0.20 package [66] and the experimental (red) and simulated (blue) best fits are included. In the solid state, variation in the $g_{//}$ and g_{\perp} values indicate that the geometry of the compounds is affected by the nature of the coordinating ligands. The EPR spectra of the complexes in DMF at 77 K gives more information on the geometry of these complexes.

For axial spectra [67], the geometric parameter G was calculated by the equation $G = (g_{//} - 2.0023)/(g_{\perp} - 2.0023)$ represents the exchange interaction between copper(II) centers in the solid polycrystalline complexes. Accordingly, if

G is greater than 4, the exchange interaction may be negligible; however, if G is less than 4, a considerable exchange interaction is indicated in the solid complex.

In-plane sigma bonding parameter α^2 was estimated from the expression [68]

$$\alpha^2 = -A_{||} / 0.036 + (g_{||} - 2.0023) + 3/7(g_{\perp} - 2.0023) + 0.04$$

The following simplified expression were used to calculate the bonding parameters

$$K_{||}^2 = (g_{||} - 2.0023) E_{d-d} / 8\lambda_0,$$

$$K_{\perp}^2 = (g_{\perp} - 2.0023) E_{d-d} / 2\lambda_0$$

$$K_{||}^2 = \alpha^2 \beta^2$$

$$K_{\perp}^2 = \alpha^2 \gamma^2$$

where $K_{||}$ and K_{\perp} are orbital reduction factors and λ_0 represents the one electron spin orbit coupling constant.

Hathaway [69] had pointed out that $K_{||} \approx K_{\perp} \approx 0.77$ for pure sigma bonding, $K_{||} < K_{\perp}$ for in plane π -bonding and $K_{\perp} < K_{||}$ for out-of-plane π -bonding. By comparing the value of in-plane sigma bonding parameter α^2 , the nature of M-L bond is evaluated. The value of α^2 is unity, if the M-L bond is purely ionic and it is completely covalent, if $\alpha^2 = 0.5$. If α^2 values calculated for complexes lie between 0.5 and 1, it means that the complexes under study are partially ionic and partially covalent in nature.

1.4.7. Hirshfeld surface analysis

In the last few years the analysis of molecular crystal structures using tools based on Hirshfeld surfaces has rapidly gained in popularity. The Hirshfeld surface emerged from an attempt to define the space occupied by a molecule in a crystal for the purpose of partitioning the crystal electron density into molecular

fragments. Hirshfeld surfaces were named after F. L Hirshfeld. Hirshfeld surfaces mapped with different properties e.g. d_e , d_{norm} , shape index, curvedness, has proven to be a useful visualization tool for the analysis of intermolecular interactions and the crystal packing behaviour of molecules. The 2D-fingerprint plot provides decomposition of Hirshfeld surfaces into contribution of different intermolecular interactions present in crystal structure. Hence both Hirshfeld surfaces and fingerprint plots facilitates the comparison of intermolecular interactions in building different supramolecular motifs in the crystal structure [70-74].

1.4.8. X-ray crystallography

Single crystal X-ray diffraction is a non-destructive analytical technique which provides detailed information about the internal lattice of crystalline substances, including unit cell dimensions, bond length, bond angles and details of site-ordering. Ideal crystals should be between 150-250 microns in size. Samples are mounted on the tip of a thin glass fibre using an epoxy or cement. This fibre is attached to a brass mounting pin, usually by the use of modelling clay and the pin is then inserted into the goniometer head. The goniometer head and the samples are then fixed to the diffractometer. Then the data is collected and phase problem is solved to find the unique set of phases that can be combined with the structure factors to determine the electron density and therefore, the crystal structure. The trial structure is then solved and refined.

Single-crystal analyses of majority of complexes were performed on a Bruker SMART APEX II CCD diffractometer, equipped with a graphite crystal incident-beam monochromator, and a fine focus sealed tube with Mo $K\alpha$ ($\lambda = 0.71073 \text{ \AA}$) as the X-ray source. The unit cell dimensions were measured and the data collection was performed. Single-crystal X-ray diffraction data of remaining complexes were collected using a Rigaku Oxford Diffraction EOS diffractometer. The crystal was tethered on a Nylon loop and was kept at 173(2) K during data

collection using Cu K α ($\lambda = 1.5418 \text{ \AA}$) radiation as the X-ray source. Bruker SMART software was used for data acquisition and Bruker SAINT software for data integration [75]. Absorption corrections were carried out using SADABS based on Laue symmetry using equivalent reflections [76]. The structure was solved by using SHELXS-97 direct methods and refined by full-matrix least-squares refinement on F^2 using SHELXL-2014/7 [77] as well as the WinGX software package [78]. All non-hydrogen atoms were refined anisotropically and positions of hydrogen atoms on carbon were derived from Fourier difference maps and were placed geometrically with C–H bond distances of 0.93 \AA and refined in the riding model approximation with Uiso(H) set to 1.2 Ueq(C). The structures were plotted using DIAMOND version 3.2g [79] and ORTEP- 3 for windows [78].

1.4.9. Antibacterial activity

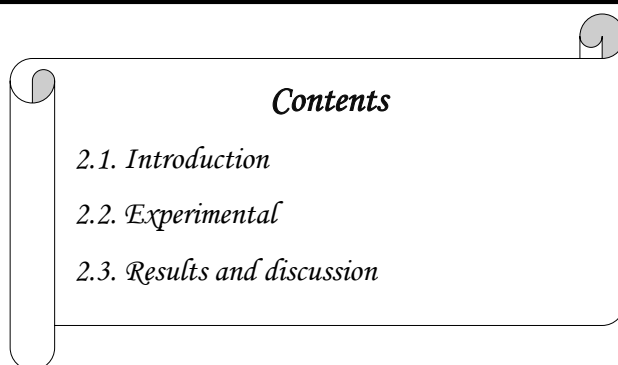
Antibacterial activity studies were done by Agar well diffusion method at the Department of Microbiology, St. Mary's College, Thrissur and at the Department of Biotechnology, Sree Sankara College Kalady.

1.4.10. *In vitro* cytotoxicity studies

In vitro Cytotoxicity studies of complexes were done in tumour cells as well as in normal cells by Trypan Blue Exclusion method at Amala Cancer Research Centre, Thrissur.

Chapter 2

SYNTHESES AND CHARACTERIZATION OF AROYLHYDRAZONES



2.1. Introduction

NNO donor aroylhydrazones derived from 2-benzoylpyridine or di-2-pyridyl ketone are of great importance because of their wide spectrum of biological activity [80,81]. Also the coordinating ability of these ligands towards various metals especially copper ion is interesting. The coordination sites of NNO donor aroylhydrazones are enolate oxygen, azomethine nitrogen and hetero atom present in the carbonyl part. These ligands can form monomer, dimer or polymer with varying coordination geometry. We are interested mainly in the coordination modes of halide and pseudohalide bridged complexes of these ligands [20].

This chapter deals with the syntheses of two aroylhydrazones and various characterization methods including single crystal X-ray diffraction technique. The synthesized hydrazones were 2-benzoylpyridine-3-methoxybenzhydrazone and di-2-pyridyl ketone-3-methoxybenzhydrazone.

2.2. Experimental

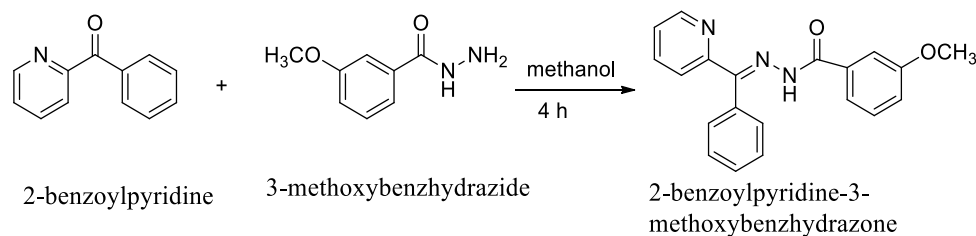
2.2.1. Materials

3-Methoxybenzhydrazide (Alfa Aesar), 2-benzoylpyridine (Sigma Aldrich), di-2-pyridyl ketone (Sigma Aldrich) were used as received. Methanol was dried over fused CaCl_2 and distilled. Other solvents were purified and dried by using standard procedures.

2.2.2. Syntheses of aroylhydrazones

2.2.2.1. Synthesis of 2-benzoylpyridine-3-methoxybenzhydrazone (Hbpm)

2-Benzoylpyridine-3-methoxybenzhydrazone was synthesized by refluxing methanolic solution of 0.183 g (1 mmol) of 2-benzoylpyridine with 0.166 g (1 mmol) of 3-methoxybenzhydrazide (m-anisidine) for about 4 hours [20]. After one week, yellow crystals separated from the mother liquor on cooling and these were washed with methanol, recrystallized from DMF and dried over P_4O_{10} *in vacuo*. The scheme for the reaction is shown below (Scheme 2.1).

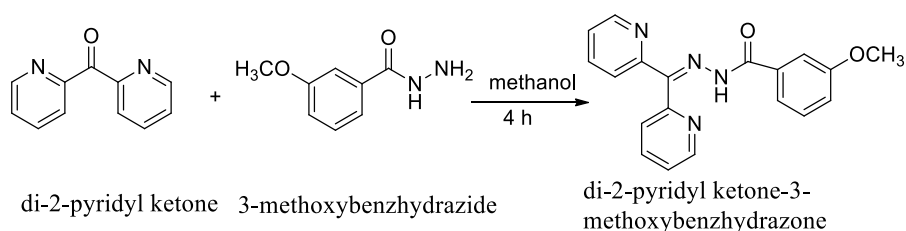


Scheme 2.1. Synthesis of 2-benzoylpyridine-3-methoxybenzhydrazone (Hbpm).

For Hbpm: Yield: 77% (0.254 g). Color: Yellow. Anal. Calc. for $\text{C}_{20}\text{H}_{17}\text{N}_3\text{O}_2$ (M.W.: $331.36 \text{ g mol}^{-1}$) C, 55.95; H, 3.76; N, 9.79%. Found: C, 55.98; H, 3.73; N, 9.75%.

2.2.2.2. Synthesis of di-2-pyridyl ketone-3-methoxybenzhydrazone (Hdkm)

Hdkm was synthesized by refluxing 0.184 g (1 mmol) of di-2-pyridyl ketone in MeOH with 0.166 g (1 mmol) of 3-methoxybenzhydrazide in methanol for about 4 hours. After 2 days, light yellow crystals separated from the mother liquor on cooling and were washed with methanol, and dried over P_4O_{10} *in vacuo* (Scheme 2.2).



Scheme 2.2. Synthesis of di-2-pyridyl ketone-3-methoxybenzhydrazone (Hdkm).

For Hdkm: Yield: 85% (0.282 g). Color: Yellow. Anal. Calc. for $C_{19}H_{16}N_4O_2$ (M.W.: 332.36 g mol^{-1}) C, 68.36; H, 4.85; N, 16.86%. Found: C, 68.41; H, 4.83; N, 16.81%.

2.2.3. Refinement

Single-crystal analysis of Hdkm was performed on a Bruker SMART APEX diffractometer, equipped with a graphite crystal incident-beam monochromator, and a fine focus sealed tube with Mo $K\alpha$ ($\lambda = 0.71073\text{ \AA}$) as the X-ray source. The unit cell dimensions were measured and the data collection was performed at 296(2) K. The single-crystal X-ray diffraction data of Hbpm was collected using a Rigaku Oxford Diffraction EOS diffractometer. The crystal was tethered on a Nylon loop and was kept at 173(2) K during data collection using Cu $K\alpha$ ($\lambda = 1.5418\text{ \AA}$) radiation as the X-ray source. Bruker SMART software was used for data acquisition and Bruker SAINT software for data integration [75]. Absorption corrections were carried out using SADABS based on Laue symmetry using equivalent reflections [76]. The structure was solved by using SHELXS-97 direct methods and refined by full-matrix least-squares refinement on F^2 using SHELXL-2014/7 [77] as well as the

WinGX software package [78]. The structures were plotted using DIAMOND version 3.2g [79] and ORTEP- 3 for windows [78]. All non-hydrogen atoms were refined anisotropically and positions of hydrogen atoms on carbon were derived from Fourier difference maps and were placed geometrically with C–H bond distances of 0.93 Å (0.96 Å for Me) and refined in the riding model approximation with $U_{\text{iso(H)}}$ set to 1.2 $U_{\text{eq(C)}}$ (1.5 $U_{\text{eq(C)}}$ for Me). The hydrogen atoms attached to nitrogen atoms were located from difference Fourier maps.

2.3. Results and discussion

2.3.1. Infrared spectra

The Infrared spectra gave an insight to the structure of the compounds. The characteristic bands of different functional groups provide significant information regarding the structure. The tentative assignments of the significant IR spectral bands of aroylhydrazones are presented in Table 2.1.

Table 2.1. Selected IR spectral assignments (cm^{-1}) of the aroylhydrazones

Compound	$\nu(\text{C}=\text{N})$	$\nu(\text{N}-\text{N})$	$\nu(\text{N}-\text{H})$	$\nu(\text{C}=\text{O})$
Hbpm	1589	1125	3063	1682
Hdkm	1602	1131	3058	1690

The Infrared spectra of aroylhydrazones Hbpm and Hdkm exhibit strong $\nu(\text{C}=\text{O})$ bands at 1682 and 1690 cm^{-1} respectively, which shows the existence of an amido form of the ligands in the solid state [20]. This is again confirmed by the presence of medium bands at 3058 and 3063 cm^{-1} due to N–H vibration. The aroylhydrazone ligands displayed distinct band of C=N at 1591 and 1602 cm^{-1} respectively [82]. The N–N stretching vibrations were found between 1128-1135 cm^{-1} [83].

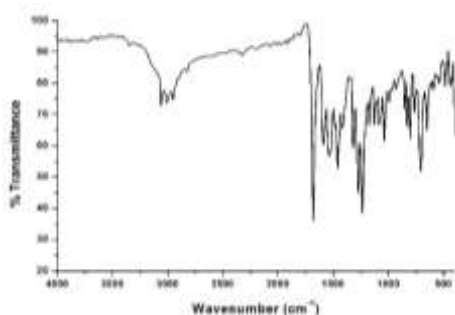


Fig. 2.1. IR Spectrum of Hbpm.

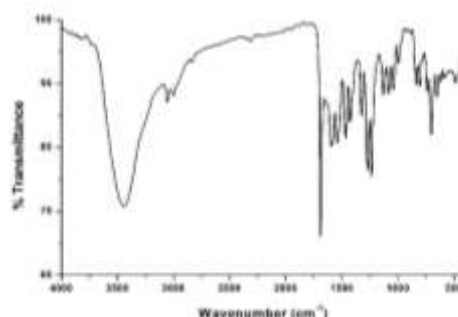


Fig. 2.2. IR Spectrum of Hdkm.

2.3.2. Electronic spectra

The electronic spectra of the prepared aroylhydrazones were taken in DMF solution (10^{-5} M) at room temperature in the 200-900 nm range and the bands are summarized in Table 2.2. The aroylhydrazones show absorption bands in the 270-400 nm range are attributed to π - π^* and n - π^* transitions [84]. The allowed π - π^* transitions exhibit higher intensity over the forbidden n - π^* transitions [85].

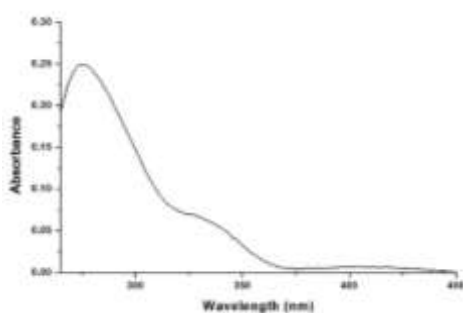


Fig. 2.3. Electronic spectrum of Hbpm.

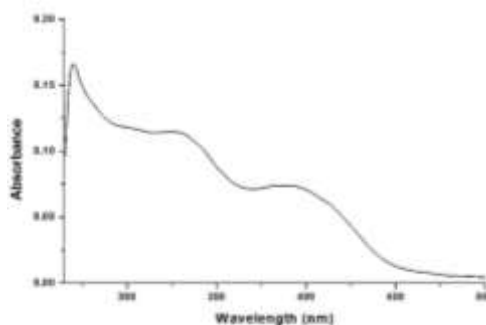


Fig. 2.4. Electronic spectrum of Hdkm.

Table 2.2. Electronic spectral assignments, λ (nm) (ϵ , $M^{-1} cm^{-1}$) of aroylhydrazones

Compound	Intraligand transitions
Hbpm	275 (24870), 330 (6700)
Hdkm	270 (16580), 330 (11370), 395 (7350)

2.3.3. ^1H NMR spectral studies

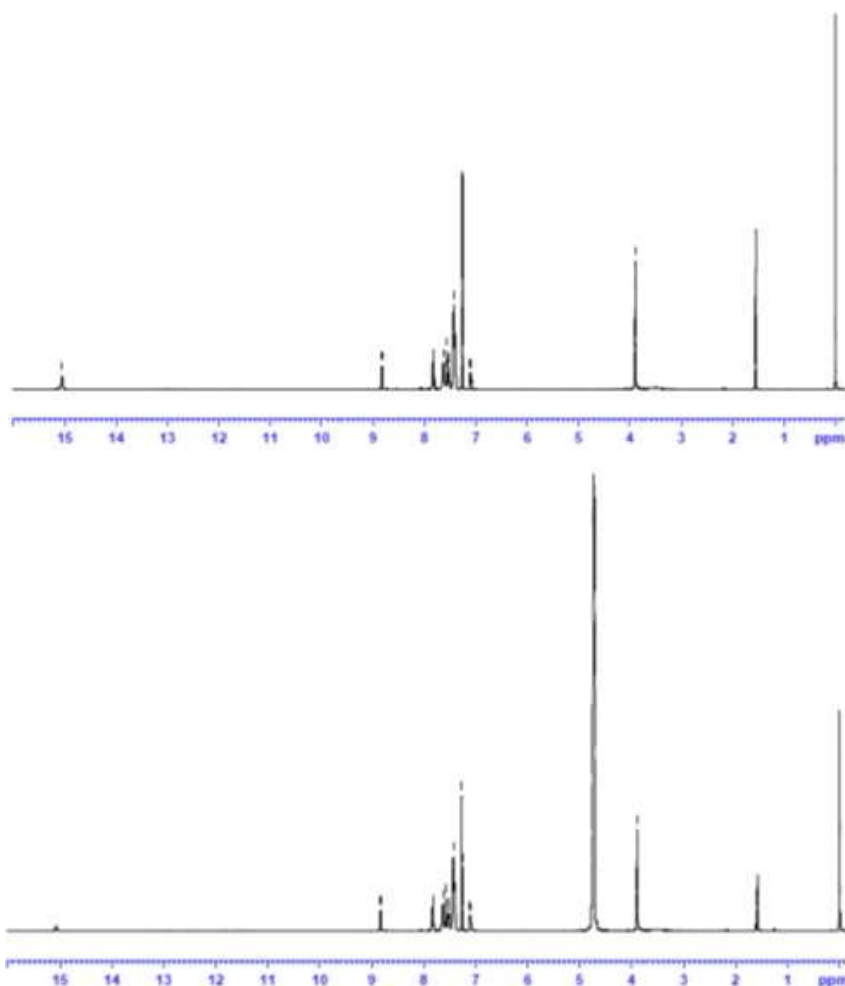


Fig. 2.5. ^1H NMR spectra of Hbpm [bottom: D_2O exchange]

The ^1H NMR spectra of the synthesized aroylhydrazones were recorded using CDCl_3 as solvent and TMS as the internal standard. It gave an idea about the number of different types of hydrogen atoms present in the compound and its electronic environment. Figs. 2.5. and 2.6. show the ^1H NMR spectra of the aroylhydrazones.

In the spectrum of Hbpm, methoxy protons gave a sharp singlet at 3.895 ppm which is integrated as three hydrogen. Multiplets in the range 7.09-7.85 are due to aromatic protons. The proton near to the ring nitrogen appeared as doublet at $\delta=8.83$ ppm. Singlet at 15.05 ppm is attributed to iminolic proton. Upon D₂O exchange this signal is disappeared showing that this proton is readily exchangeable and confirmed the above assignments [86].

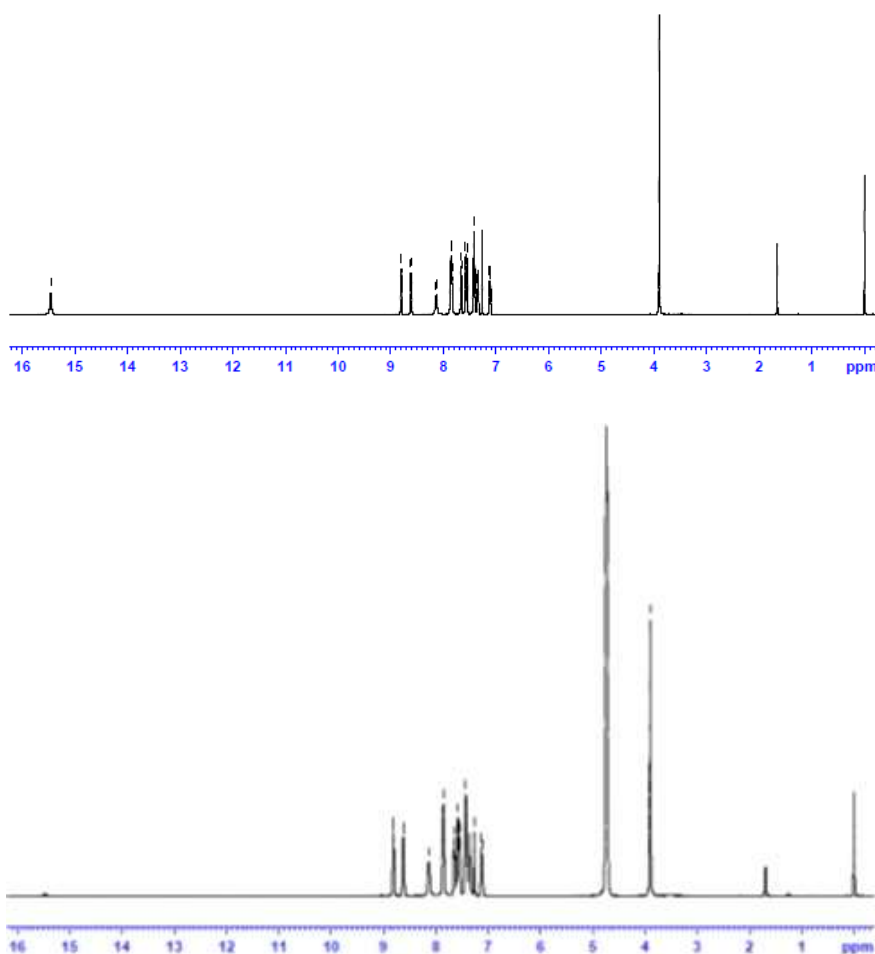


Fig. 2.6. ¹H NMR spectra of Hdkm [bottom: D₂O exchange].

Sharp singlet at 3.899 ppm in the spectrum of Hdkm is due to methoxy proton. Aromatic proton appeared as multiplets in the region 7.1-8.1 ppm. Two doublets at $\delta = 8.8$ and 8.6 ppm are assigned as two similar protons near to the ring nitrogen. A singlet in the downfield region of 15.54 ppm was assigned to the existence of iminolic form of ligand [87]. Here also the assignments were confirmed by D₂O exchange.

2.3.4. Hirshfeld Surface and 2D Fingerprint Plot Analysis

To explore the weak intermolecular interactions and their quantitative contributions towards the crystal packing, Hirshfeld Surfaces and the associated 2D fingerprint plots were generated using Crystal Explorer 17 software [88]. Hirshfeld Surface is defined as the electron density boundary surfaces between the molecules in a crystal and are mapped with different functions (d_{norm} , and shape index) [89]. HS's are drawn transparent to allow the visualization of the compounds.

Normalized contact distance (d_{norm}), ratio encompassing the distances of any surface point to the nearest interior (d_i) and exterior (d_e) atom and the van der Waals radii of the atoms were calculated by using the following equation,

$$d_{\text{norm}} = \frac{d_i - r_i^{\text{vdW}}}{r_i^{\text{vdW}}} + \frac{d_e - r_e^{\text{vdW}}}{r_e^{\text{vdW}}}$$

The values are mapped by using a red-blue-white color scheme: where red region correspond to interactions shorter than r^{vdW} (negative d_{norm} value), blue region correspond to interactions longer than r^{vdW} (positive d_{norm} value) and white region correspond to interactions equal to the r^{vdW} (zero d_{norm} value) [90-92]. Prominent hydrogen bonding interactions are shown by deep red points on the HS.

Bow-tie patterns (orange-blue triangle regions) observed when the surfaces of Hbpm and Hdkm are examined under the shape index function, indicate the

presence of $\pi \cdots \pi$ stacking interactions. The orange concave depressions are indicative of π acceptor regions and the blue convex regions represent C–H donors [93].

The three-dimensional (3D) Hirshfeld surfaces can be resolved into 2D fingerprint plots which help in the quantification of intermolecular interactions in the immediate environment of each molecule in the asymmetric unit [94]. It gave the percentage contribution of each interaction to the Hirshfeld surface area for the various close intermolecular contacts. The FPs are plotted on an XY grid formed by $X = d_i$ and $Y = d_e$ pairs, where the frequency of occurrence of interactions (the number of points with a given (d_e, d_i) pair) are represented by the different colors: blue (low frequency), green (medium) and red (high). The complementary regions are visible in the FPs where one molecule act as donor if $d_i < d_e$ and act as acceptor if $d_i > d_e$. 2D fingerprint plots are displayed by using the translated view with the d_i and d_e scales displayed on the graph axes (ranging from 1.0 to 2.8 Å).

The Hirshfeld surfaces mapped with d_{norm} and shape index for Hbpm and Hdkm are shown in Fig. 2.7. In Hbpm, the most intense red spot indicate a trifurcated hydrogen bonding interaction formed by the H1, H2 and H12 with a common acceptor O1 (Fig. 2.8). Another red spot correspond to intramolecular hydrogen bonding between pyridyl nitrogen and hydrogen atom born by the azomethine nitrogen atom. The two intense red points seen on the surface of Hdkm indicates the high percentage of $O \cdots H$ and $N \cdots H$ interactions (12% and 7.4% respectively).

These two ligands are dominated by the $H \cdots H$ interactions with 45.3% and 42.8% of total HS (Fig. 2.9).

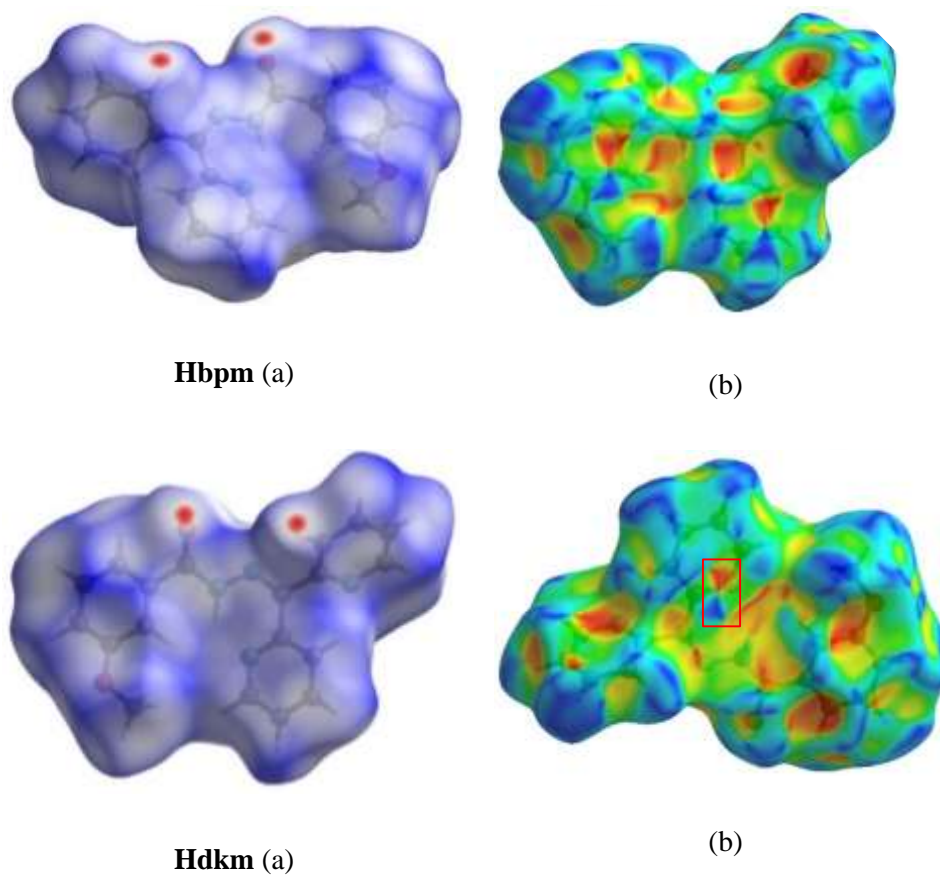
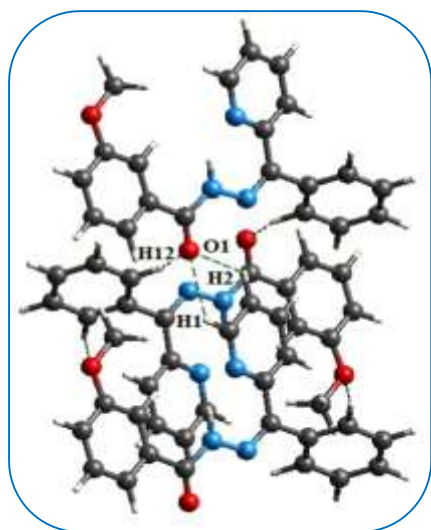
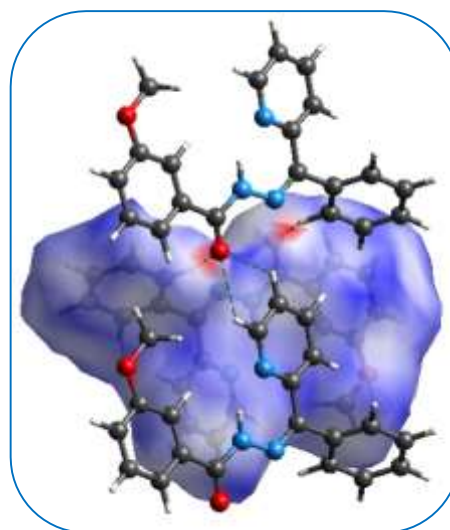


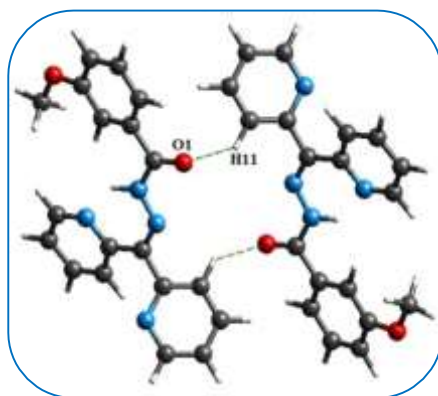
Fig. 2.7. Hirshfeld surfaces for Hbpm and Hdkm mapped with (a) d_{norm} over a fixed color scale of -0.16 (red) to 1.41 \AA (blue) and (b) shape index.



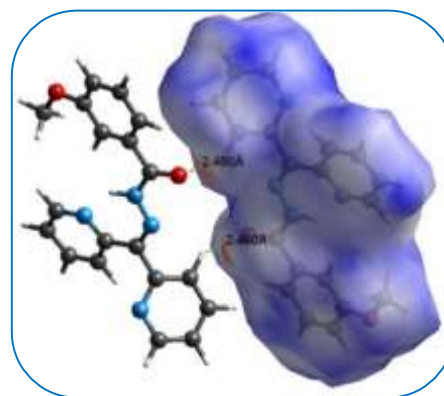
(Hbpm) (a)



(b)



(Hdkm) (a)



(b)

Fig. 2.8. (a) Intermolecular hydrogen bonding interactions present in Hbpm and Hdkm (b) viewing the same short contacts in Hirshfeld surface with external molecules.

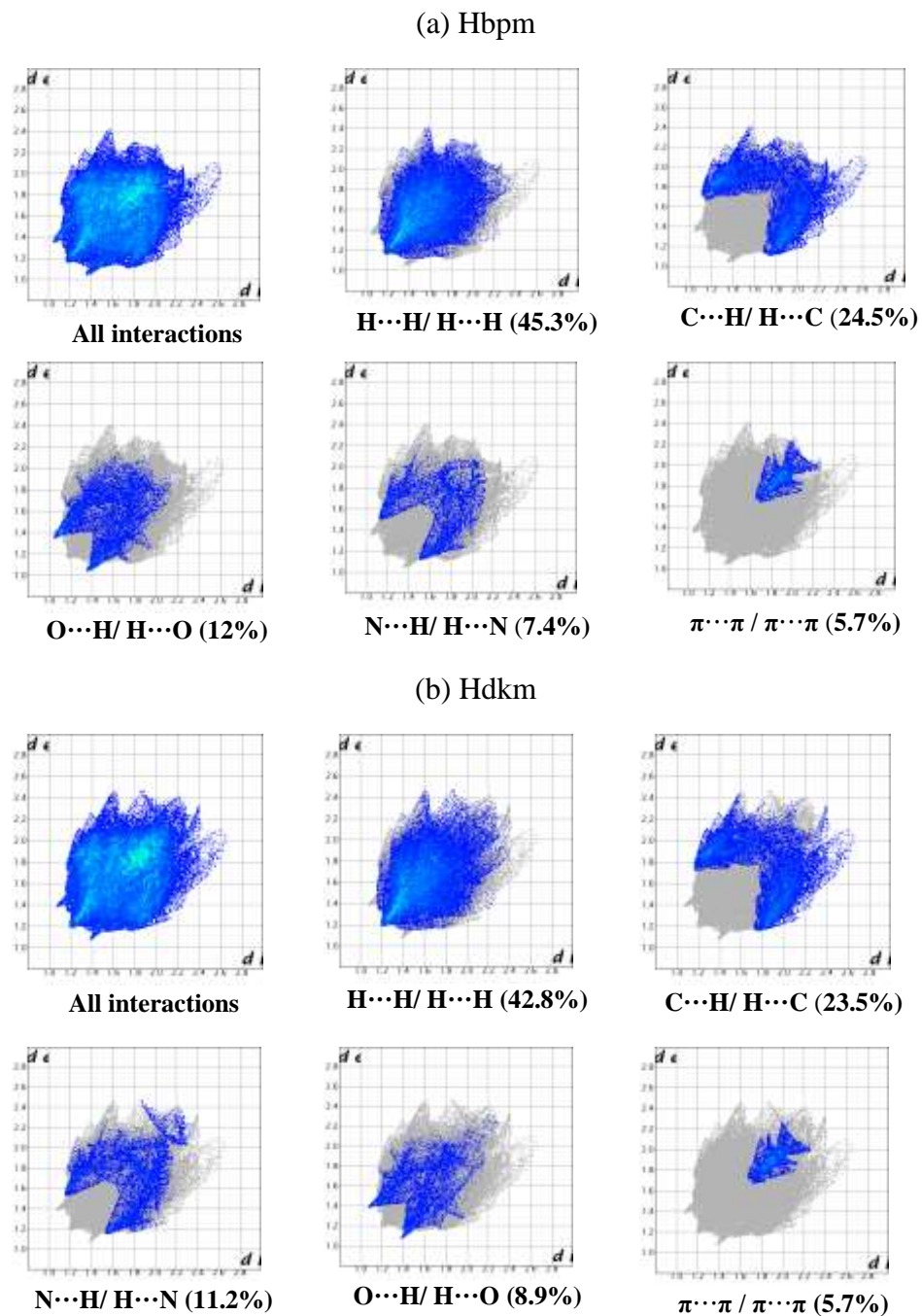


Fig. 2.9. 2D finger print plots with d_e and d_i ranging from 1.0 to 2.8 Å for (a) Hbpm and (b) Hdkm and major decomposition plots.

Table 2.3. Crystallographic data and structure refinement parameters for Hbpm and Hdkm

Parameters	Hbpm	Hdkm
Empirical formula	C ₂₀ H ₁₇ N ₃ O ₂	C ₁₉ H ₁₆ N ₄ O ₂
Formula weight	331.36	332.36
Color, Space group	Yellow, $P\bar{1}$	Yellow, $P\bar{1}$
Crystal system	Triclinic	Triclinic
Cell parameters		
a (Å)	8.0781(8)	8.1944(6)
b (Å)	8.8302(9)	8.8467(6)
c (Å)	11.4011(12)	11.4300(8)
α (°)	82.123(9)	82.081(2)
β (°)	83.907(9)	84.546(2)
γ (°)	84.385(8)	84.828(2)
Volume V (Å ³), Z	798.16(14), 2	814.48(10), 2
Calculated density (ρ) (Mg m ⁻³)	1.379	1.355
Absorption coefficient, μ (mm ⁻¹)	0.736	0.091
F(000)	348	348
Crystal size mm ³	0.29 x 0.24 x 0.22	0.55 x 0.54 x 0.28
θ (°) range for data collection	3.932 to 71.402	3.130 to 31.621
Limiting indices	-9 ≤ h ≤ 8, -10 ≤ k ≤ 8, -14 ≤ l ≤ 12	-12 ≤ h ≤ 12, -13 ≤ k ≤ 13, -16 ≤ l ≤ 16
Reflections collected	4922	36816
Unique Reflections (R _{int})	3090 (0.0310)	5398 (0.0270)
Completeness to θ	67.684, 99.7%	25.242, 98.0%
Absorption correction	Semi-empirical from equivalents	Semi-empirical from equivalents
Maximum and minimum transmission	0.951 and 0.903	0.968 and 0.943
Refinement method	Full-matrix least-squares on F ²	Full-matrix least-squares on F ²
Data / restraints / parameters	3090 / 1 / 232	5398 / 1 / 231
Goodness-of-fit on F ²	0.963	1.013
Final R indices [I > 2 σ (I)]	R ₁ = 0.0473, wR ₂ = 0.1334	R ₁ = 0.0587, wR ₂ = 0.1875
R indices (all data)	R ₁ = 0.0527, wR ₂ = 0.1416	R ₁ = 0.0665, wR ₂ = 0.2006
Largest difference peak and hole (e Å ⁻³)	0.241 and -0.241	0.714 and -0.620

$$R_1 = \frac{\sum ||F_0| - |F_c||}{\sum |F_0|}$$

$$wR_2 = \frac{[\sum w(F_0^2 - F_c^2)^2 / \sum w(F_0^2)^2]^{1/2}}$$

2.3.5. X-ray Crystallography

The crystallographic data along with details of structure solution refinements of the two aroylhydrazones are given in Table 2.3.

2.3.5.1. Crystal structure of 2-benzoylpyridine-3-methoxybenzhydrazone (Hbpm)

The molecular structure of the hydrazone, Hbpm along with the atom numbering scheme is shown in Figure 2.10. Significant bond lengths and bond angles are listed in Table 2.4. The hydrazone, $C_{20}H_{17}N_3O_2$ crystallizes in the triclinic space group $P\bar{1}$. This molecule adopts an *Z* configuration with respect to a C6=N2 bond. The *cis* configurations of C13–N3 and C6–N2 bonds are confirmed by the torsion angle values of $2.0(2)^\circ$ and $4.7(2)^\circ$ corresponding to O1–C13–N3–N2 and C5–C6–N2–N3 moieties respectively. The ligand exists in the amido form in the solid state and is revealed by the C13–O1 bond length of $1.219(17)$ Å (very close to the typical C=O bond length of 1.21 Å) and a bond distance of $1.364(19)$ Å for the C13–N3 bond which is very close to a C–N single bond [95].

Table 2.4. Selected bond lengths (Å) and bond angles ($^\circ$) of Hbpm

Bond lengths (Å)		Bond angles ($^\circ$)	
C1–N1	1.340(19)	C6–N2–N3	118.61(12)
C6–N2	1.292(19)	C13–N3–N2	119.72(11)
N2–N3	1.367(16)	O1–C13–C14	122.17(13)
C13–N3	1.364(19)	N3–C13–C14	114.15(12)
C13–O1	1.219(17)	N2–C6–C5	127.61(13)
C13–C14	1.504(19)		
C14–C15	1.383(2)		
C18–O2	1.368(19)		

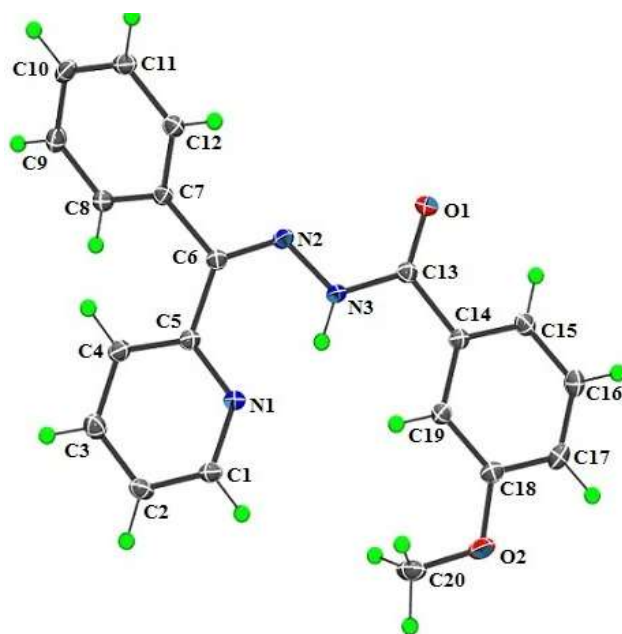


Fig 2.10. ORTEP plot (drawn with 30% thermal ellipsoid) of ligand (Hbpm) along with atom numbering scheme of non-hydrogen atoms.

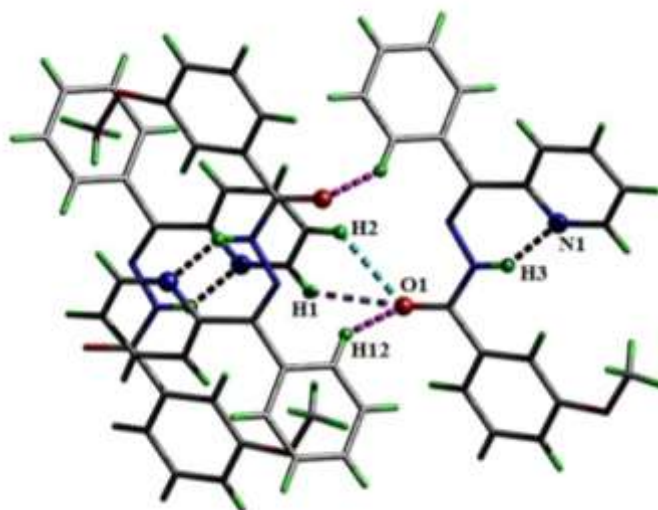


Fig 2.11. Inter and intramolecular hydrogen bonding interactions (dashed lines) in Hbpm.

The hydrogen bonding interactions are listed in Table 2.5. A trifurcated hydrogen bonding interaction is formed by H1, H2 and H12 with a common acceptor O1. Also, an intramolecular hydrogen bond is established between a pyridyl nitrogen N1 and a hydrogen H3 born by the azomethine nitrogen (Fig. 2.11).

Table 2.5. Hydrogen bonding interactions in Hbpm

D–H···A	D–H (Å)	H···A (Å)	D···A (Å)	∠D–H···A (°)
C1–H1···O1 ^a	0.93	2.61	3.240(18)	126
C2–H2···O1	0.93	2.64	3.235(19)	122
N3–H3···N1	0.87(9)	1.92(14)	2.641(17)	138
C12–H12···O1	0.93	2.53	3.261(19)	136

Equivalent position code: a = x, y-1, z.

The two neighbouring molecules are also coupled together by a weak C–H··· π interaction with an H··· π distance of 2.88 Å and a π ··· π stacking interaction between Cg(1) and Cg(3) with a centroid-centroid distance of 3.6529(10) Å, facilitating the packing of the molecule (Fig. 2.12 & Table 2.6).

Table 2.6. Non-bonding interactions in Hbpm

C–H···π interactions			
C–H(I)···Cg(J)	H···Cg (Å)	C···Cg (Å)	∠C–H···Cg (°)
C16–H16···Cg(2) ^a	2.89	3.647(18)	139
π···π interactions			
Cg(I)···Cg(J)	Cg···Cg (Å)	α (°)	β (°)
Cg(1)···Cg(3) ^b	3.653(10)	7.87(7)	22.0

Equivalent position codes: a = 1-x, 2-y, 1-z; b = 1-x, 1-y, 1-z

Cg(1) = N1, C1, C2, C3, C4, C5; Cg(2) = C7, C8, C9, C10, C11, C12; Cg(3) = C14, C15, C16, C17, C18, C19

D, Donor; A, acceptor; Cg, Centroid; α , dihedral angle between planes I & J; β , angle between Cg···Cg and Cg(J) perp.

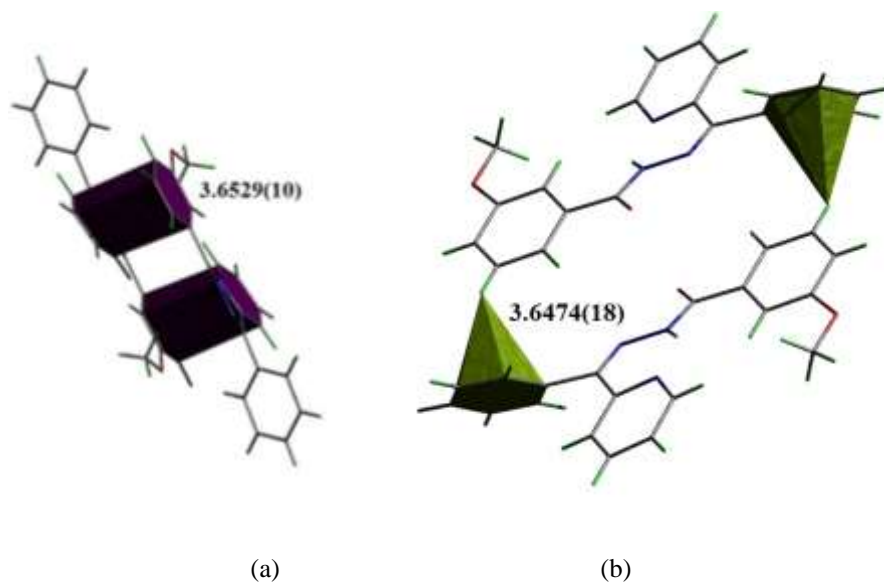


Fig. 2.12. The (a) $\pi \cdots \pi$ and (b) $C-H \cdots \pi$ interaction in Hbpm.

2.3.5.2. Crystal structure of di-2-pyridyl ketone-3-methoxybenzhydrazone (Hdkm)

The molecular structure and the atom numbering scheme of Hdkm is shown in Fig. 2.13 and the important bond distances and bond angles are given in Table 2.7.

Table 2.7. Selected bond lengths (Å) and bond angles (°) of Hdkm

Bond lengths (Å)		Bond angles (°)	
C1–N1	1.338(15)	C6–N3–N4	118.09(9)
C6–N3	1.297(14)	C12–N4–N3	119.48(9)
N3–N4	1.367(16)	O1–C12–C13	121.94(10)
C12–N4	1.364(14)	N4–C12–C13	114.24(9)
C12–O1	1.222(13)	N3–C6–C5	127.79(10)
C12–C13	1.500(15)		
C13–C14	1.389(16)		
C19–O2	1.413(2)		

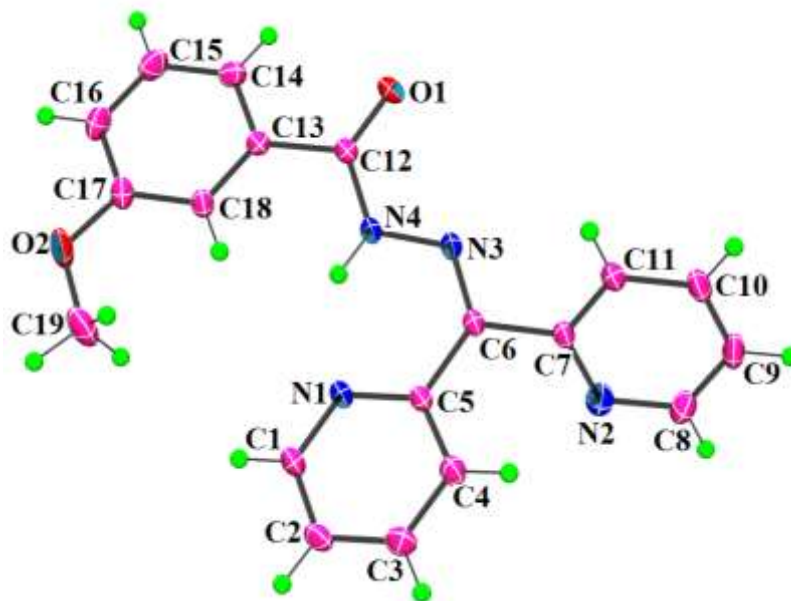


Fig.2.13. ORTEP plot (drawn with 30% thermal ellipsoid) of ligand (Hdkm) along with atom numbering scheme of non-hydrogen atoms.

The hydrazone, $C_{19}H_{16}N_4O_2$ crystallizes in the triclinic space group $P\bar{1}$. This molecule shows a torsion angle value of $177.48(10)^\circ$ corresponding to $N4-N3-C6-C7$ moiety and a value of $4.49(17)^\circ$ corresponding to $N4-N3-C6-C5$ moiety which confirms the *trans* configuration of $N4$ atom with respect to $C7$ atom and the *cis* configuration of $N4$ atom with respect to $C5$ atom. As a result, the *cis* arrangement of $N4$ atom with respect to $N1$ atom favours the $N4-H4 \cdots N1$ intramolecular hydrogen bonding interaction. The existence of amido form of aroylhydrazone in the solid state is unveiled by the $C12-O1$ bond length of $1.222(14) \text{ \AA}$ (very close to the typical $C=O$ bond length of 1.21 \AA) and a bond distance of $1.3643(15) \text{ \AA}$ for the $C12-N4$ bond which is very close to a $C-N$ single bond.

The hydrogen bonding interactions are listed in Table 2.8. One intramolecular hydrogen bonding interaction is present between a pyridyl nitrogen

N1 and the hydrogen H4 attached to azomethine nitrogen N4 with a donor-acceptor distance of 2.462(14) Å and an intermolecular hydrogen bonding between amido oxygen O1 and H11 of pyridyl ring with a donor-acceptor distance of 3.297(17) Å (Fig. 2.14).

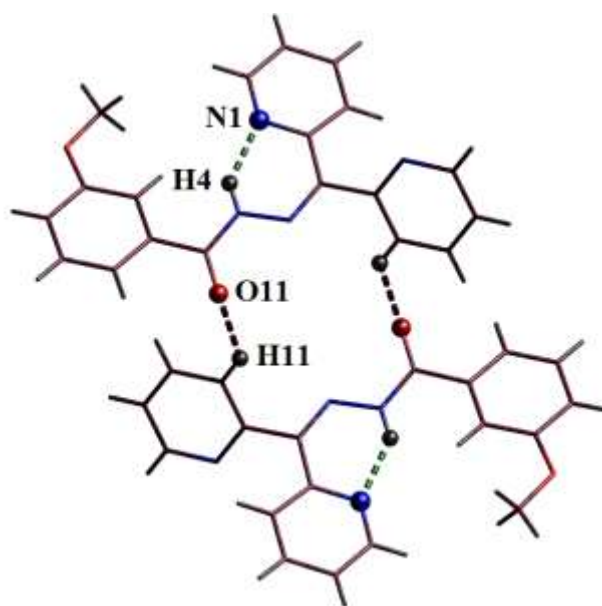


Fig. 2.14. Inter and intramolecular hydrogen bonding interactions (dashed lines) in Hdkm.

Table 2.8. Hydrogen bonding interactions in Hdkm

D–H···A	D–H (Å)	H···A (Å)	D···A (Å)	∠D–H···A (°)
N4–H4···N1	0.872(11)	1.917(13)	2.642(14)	139.6(16)
C11–H11···O1 ^a	0.93	2.57	3.297(17)	136

Equivalent position code: a = -x, -y, 1-z

One C–H··· π interaction between H15 and pyridyl ring Cg(2) with H···Cg distance of 2.96 Å and one π ··· π stacking interaction between pyridyl ring Cg(1) and methoxy ring Cg(3) present in Hdkm are shown in Figs 2.15 and 2.16. C–H··· π and π ··· π interaction parameters are listed in Table 2.9.

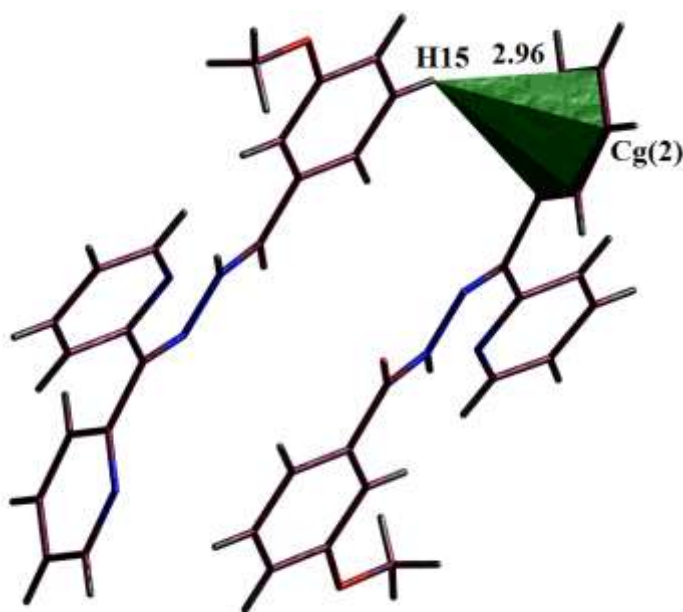
Table 2.9. Non bonding interactions in Hdkm

C–H···π interactions			
C–H(I)···Cg(J)	H···Cg (Å)	C···Cg (Å)	\angleC–H···Cg (°)
C15–H15···Cg(2) ^a	2.96	3.717(17)	140
π···π interactions			
Cg(I)···Cg(J)	Cg···Cg (Å)	α (°)	β (°)
Cg(1)···Cg(3) ^b	3.692(8)	8.40(6)	21.80

Equivalent position codes: a = 1-x, 2-y, 1-z; b = 1-x, 1-y, 1-z

Cg(1) = N1, C1, C2, C3, C4, C5; Cg(2) = N2, C7, C8, C9, C10, C11; Cg(3) = C13, C14, C15, C16, C17, C18

D, Donor; A, acceptor; Cg, Centroid; α , dihedral angle between planes I & J; β , angle between Cg···Cg and Cg(J) perp.

**Fig. 2.15.** Weak C–H··· π interaction in Hdkm.

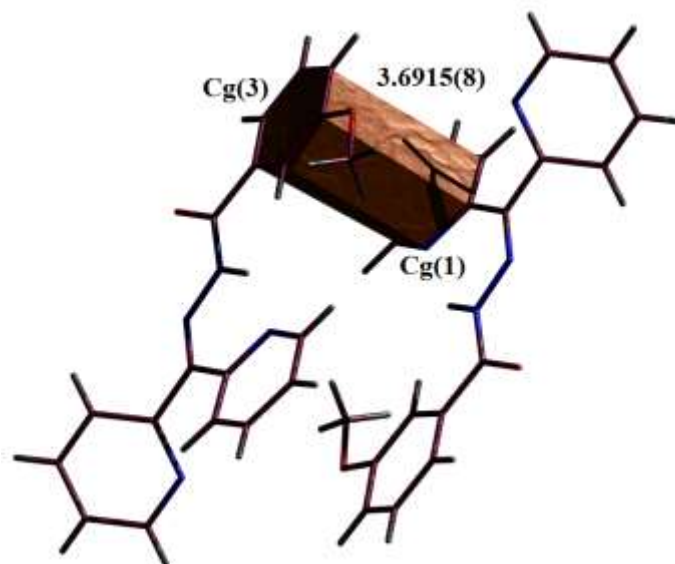
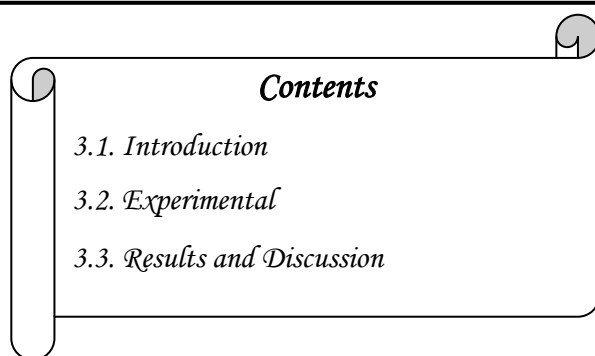


Fig. 2.16. $\pi \cdots \pi$ interaction in Hdkm.

Chapter 3

SYNTHESES AND CHARACTERIZATION OF HALIDE BRIDGED BOX DIMER COPPER(II) COMPLEXES OF AROYLHYDRAZONES



Contents

- 3.1. Introduction*
- 3.2. Experimental*
- 3.3. Results and Discussion*

3.1. Introduction

We were able to isolate three single crystals of halogen bridged copper(II) complexes of two ligand systems, Hbpm and Hdkm, of which two of them were chloride bridged and the other one was a bromide bridged complex [20]. Complexes $[\text{Cu}(\text{bpm})\text{Cl}]_2$ (**1**), $[\text{Cu}(\text{bpm})\text{Br}]_2$ (**2**) and $[\text{Cu}(\text{dkm})\text{Br}]_2$ (**3**) are halogen bridged box dimers having monoclinic lattice with $P2_1/n$ symmetry. They have distorted square pyramidal geometry with Addison parameter values of 0.16, 0.155 and 0.05 respectively [96]. The synthesis, spectral characterization, Hirshfeld surface analysis, 2D fingerprint plot analysis and SCXRD are discussed here.

3.2. Experimental

3.2.1. Materials

Copper(II) chloride dihydrate and copper(II) bromide dihydrate were purchased from Sigma-Aldrich. All the reagents and solvents used were of Analar grade and were used as received.

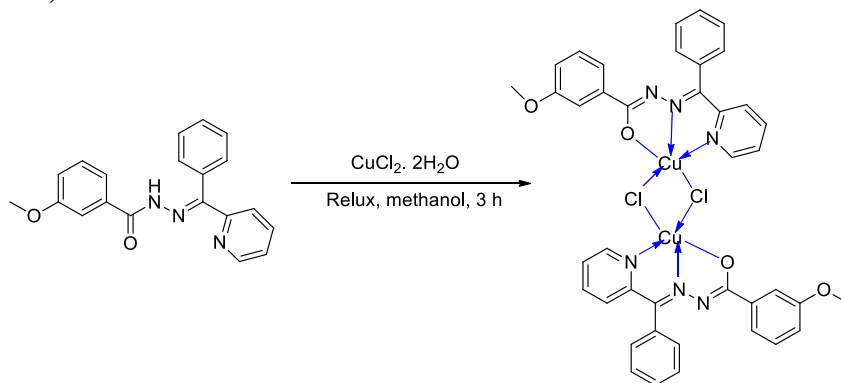
3.2.2. Syntheses of copper(II) complexes

3.2.2.1. Synthesis of [Cu(bpm)Cl]₂ (1)

Methanolic solutions of hydrazone, Hbpm (0.331 g, 1 mmol) and copper(II) chloride dihydrate (0.170 g, 1 mmol) were mixed and refluxed for three hours. The resulting green colored solution was allowed to stand for slow evaporation at room temperature. Green needle crystals suitable for SCXRD were obtained from the mother liquor next day. The crystals were then filtered off, washed with methanol and dried over P₄O₁₀ *in vacuo* (Scheme 3.1) [20].

For [Cu(bpm)Cl]₂ (1): Yield: 85% (0.742 g). Color: Green. Anal. Calc. for C₄₀H₃₂Cl₂Cu₂N₆O₄ (M.W.: 858.72 g mol⁻¹) C, 55.95; H, 3.76; N, 9.79%. Found: C, 55.98; H, 3.73; N, 9.75%.

λ_M (DMF): 6.8 mho cm² mol⁻¹.



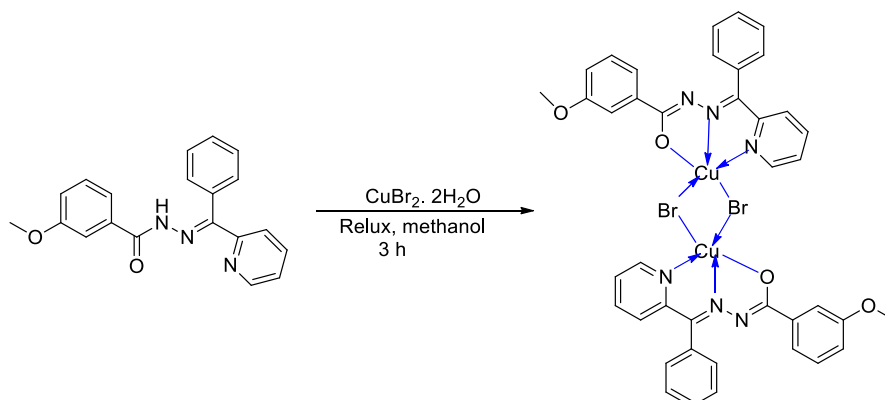
Scheme 3.1. Synthesis of [Cu(bpm)Cl]₂ (1).

3.2.2.2. Synthesis of [Cu(bpm)Br]₂ (2)

Methanolic solutions of hydrazone, Hbpm (0.331 g, 1 mmol) and copper(II) bromide (0.223 g, 1 mmol) were mixed and refluxed for three hours. The resulting green colored solution was allowed to stand for slow evaporation at room temperature. Green needle crystals were obtained from the mother liquor within 3 days. The crystals were then filtered off, washed with methanol and dried over P₄O₁₀ *in vacuo* (Scheme 3.2) [20].

For [Cu(bpm)Br]₂ (2): Yield: 85.4% (0.733 g). Color: Green. Anal. Calc. for C₄₀H₃₂Br₂Cu₂N₆O₄ (M.W.: 947.62 g mol⁻¹) C, 50.70; H, 3.40; N, 8.87%. Found: C, 50.90; H, 3.43; N, 8.85%.

λ_M (DMF): 15 mho cm² mol⁻¹.



Scheme 3. 2. Synthesis of [Cu(bpm)Br]₂ (2).

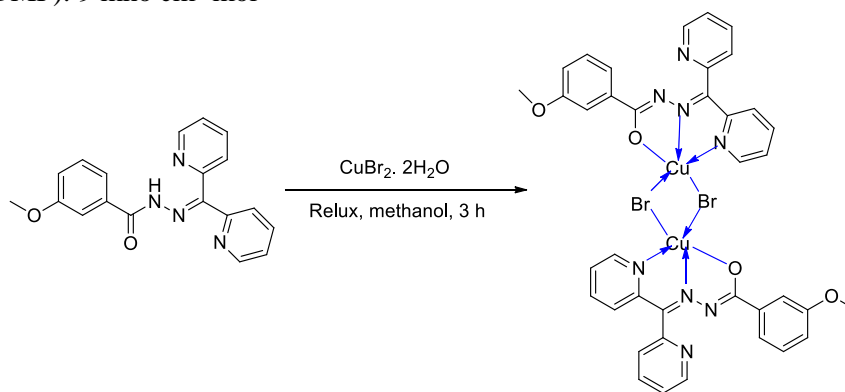
3.2.2.3. Synthesis of [Cu(dkm)Br]₂ (3).

Methanolic solutions of copper(II) bromide (0.223 g, 1 mmol) and aroylhydrazone, Hdkm (0.332 g, 1 mmol) were mixed and refluxed for three hours. The green colored solution obtained was allowed for slow evaporation at room temperature. Green needle shaped crystals were obtained from the mother liquor

within 3 days. The crystals were then filtered off, washed with methanol and dried over P_4O_{10} *in vacuo* (Scheme 3.3).

For $[Cu(dkm)Br]_2$ (**3**): Yield: 85% (0.807 g). Color: Green. Anal. Calc. for $C_{38}H_{30}Br_2Cu_2N_8O_4$ (M.W.: 949.6 g mol⁻¹) C, 48.06; H, 3.18; N, 11.80%. Found: C, 48.10; H, 3.13; N, 11.78%.

λ_M (DMF): 9 mho cm² mol⁻¹



Scheme 3.3. Synthesis of $[Cu(dkm)Br]_2$ (**3**).

3.3. Results and discussion

3.3.1. Infrared spectra

The tentative assignments of the significant IR spectral bands of copper(II) complexes of Hbpm and Hdkm are presented in Table 3.1. The spectra are shown in Figs. 3.1-3.3. The spectrum of Hbpm exhibits a strong $\nu(C=O)$ band at 1682 cm⁻¹, which shows the existence of an amido form of the ligand in the solid state [20]. Absence of this band in complexes **1** and **2** confirms the enolization as a result of complexation. Also, this ligand displayed distinct bands at 3058, 1599, 1128 cm⁻¹ corresponding to $\nu(N-H)$, $\nu(C=N)$ and $\nu(N-N)$, respectively [97,98]. The azomethine $\nu(C=N)$ band of Hbpm appearing at 1599 cm⁻¹ is shifted to lower frequency in the range 1592-1595 cm⁻¹ for complexes **1** and **2** confirming the coordination *via* azomethine nitrogen and the appearance of new $\nu(C=N)$ bands at

1559, 1562 and 1557 cm^{-1} respectively, indicates the iminolization. The absence of a band at 3058 cm^{-1} in the complexes shows the loss of a hydrogen atom from the amide group on complexation.

Also the ligand Hdkm exhibits a characteristic C=O band at 1690 cm^{-1} , confirming the existence of amido form in the solid state. In $[\text{Cu}(\text{dkm})\text{Br}]_2$ (**3**), this band disappeared and a new band appeared at 1366 cm^{-1} due to $\nu(\text{C}-\text{O})$ confirming complexation [99]. Moreover azomethine $\nu(\text{C}=\text{N})$ band is shifted to lower frequency and a new C=N band appeared at 1562 cm^{-1} .

Table 3.1. IR spectral assignments (cm^{-1}) of Hbpm, Hdkm and its copper(II) complexes

Compound	$\nu(\text{N}-\text{H})$	$\nu(\text{C}=\text{O}) / \nu(\text{C}-\text{O})$	$\nu(\text{C}=\text{N})$	$\nu(\text{C}=\text{N})^a$
Hbpm	3058	1682	1599	---
$[\text{Cu}(\text{bpm})\text{Cl}]_2$ (1)	---	1366	1593	1559
$[\text{Cu}(\text{bpm})\text{Br}]_2$ (2)	---	1366	1592	1562
Hdkm	3058	1690	1602	---
$[\text{Cu}(\text{dkm})\text{Br}]_2$ (3)	---	1366	1590	1562

^a newly formed C=N bond

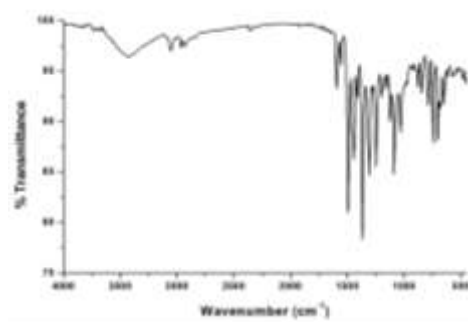
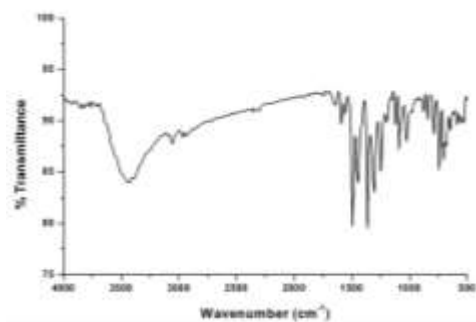


Fig. 3.1. IR Spectrum of $[\text{Cu}(\text{bpm})\text{Cl}]_2$ (**1**). **Fig. 3.2.** IR Spectrum of $[\text{Cu}(\text{bpm})\text{Br}]_2$ (**2**).

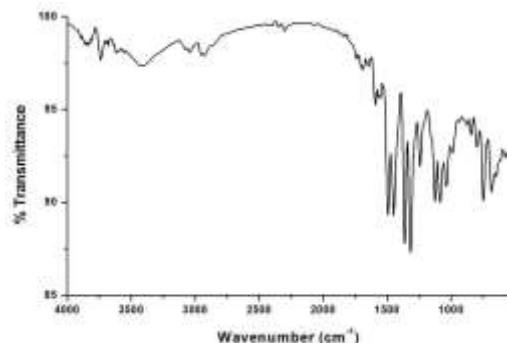


Fig. 3.3. IR Spectrum of $[\text{Cu}(\text{dkm})\text{Br}]_2$ (**3**).

3.3.2. Electronic spectra

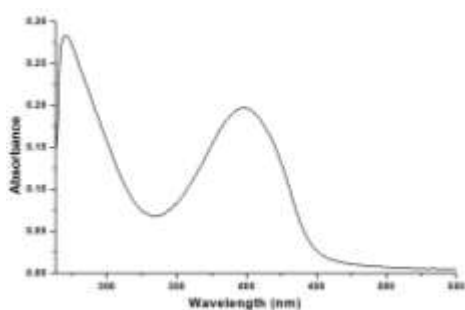
The electronic spectra of the copper(II) complexes were recorded in DMF solution at room temperature. The data are summarised in Table 3.2 and the spectra are shown in Figs. 3.4 - 3.6.

The copper(II) ion with d^9 electronic configuration shows a distorted square pyramidal geometry in these three complexes as proven by the single crystal XRD studies. For all the three compounds, an intense band was observed in the high energy 400 nm region comprising of transitions from coordinating atoms of aroylhydrazone to the metal centre which was absent in the ligand and was attributed to LMCT transitions [100,20]. The intraligand transition ($n \rightarrow \pi^*$ and $\pi \rightarrow \pi^*$) for the compounds were found at 271, 269 and 266 nm respectively for complexes **1-3**. These transitions slightly shifted during complexation.

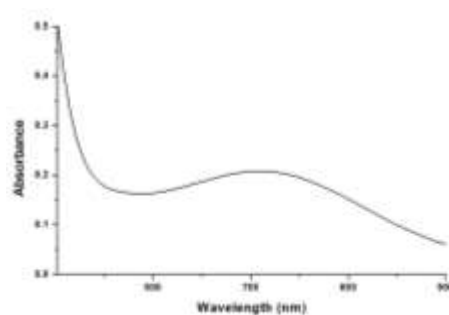
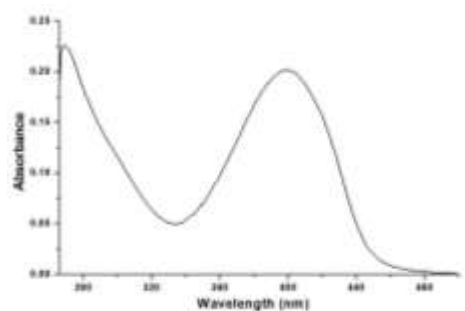
For obtaining dd spectra of these copper(II) complexes, spectra were recorded in 10^{-3} M DMF solution. The absorptions at low energy 691-707 nm region correspond to $d-d$ transitions [101].

Table 3.2. Electronic spectral assignments, λ_{\max} (nm) (ϵ , $M^{-1} \text{ cm}^{-1}$) of copper(II) complexes **1**, **2** and **3**

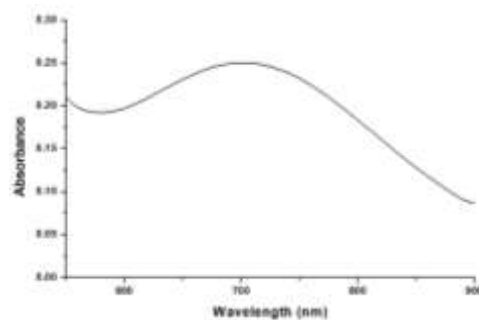
Compound	<i>d-d</i>	LMCT	Intraligand transitions
Hbpm	---	---	275 (24870), 330 (6700)
[Cu(bpm)Cl] ₂ (1)	707 (210)	399 (19650)	271 (28370)
[Cu(bpm)Br] ₂ (2)	706 (250)	400 (20170)	269 (22520)
Hdkm	---	---	270 (16580), 330 (11370), 395 (7350)
[Cu(dkm)Br] ₂ (3)	691 (265)	401 (73230)	273 (96790)



(a) LMCT and intraligand transitions

(b) *d-d***Fig. 3.4.** Electronic spectra of [Cu(bpm)Cl]₂ (**1**).

(a) LMCT and intraligand transitions

(b) *d-d***Fig. 3.5.** Electronic spectra of [Cu(bpm)Br]₂ (**2**).

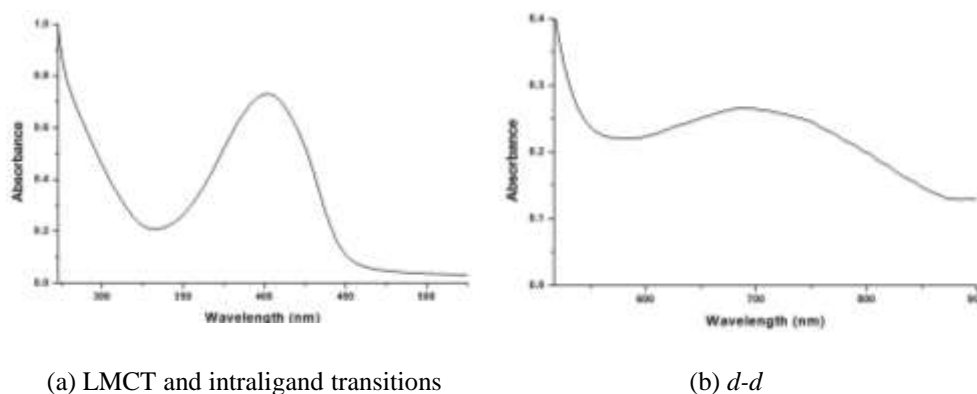


Fig. 3.6. Electronic spectra of $[\text{Cu}(\text{dkm})\text{Br}]_2$ (**3**).

3.3.4. Electron paramagnetic resonance spectra

The EPR spectra of the complexes in the polycrystalline state at 298 K and in DMF solution at 77 K were recorded in X band using an ESR-JEOL spectrometer. All the EPR spectra are simulated using the EasySpin 5.0.20 package [66] and the experimental (red) and simulated (blue) best fits are included. The EPR spectral and bonding parameters of the copper(II) complexes are presented in Table 3.3. The EPR spectra of the complexes are shown in Figs. 3.7-3.9. In the solid state, variation in the g_{\parallel} and g_{\perp} values indicate that the geometry of the compounds are affected by the nature of the coordinating ligands. The EPR spectra of the complexes in DMF at 77 K gives more information on the geometry of these complexes [102].

Complex $[\text{Cu}(\text{bpm})\text{Cl}]_2$ (**1**) exhibits one broad singlet at $g_{\text{iso}} = 2.03$ in the polycrystalline state at 298 K arising from dipolar broadening and enhanced spin lattice relaxation [103]. At 77 K in DMF solution, the compound shows an axial spectrum with well-defined four hyperfine lines ($g_{\parallel} = 2.23$, $g_{\perp} = 2.06$, $A_{\parallel} = 185 \times 10^{-4} \text{ cm}^{-1}$) in the parallel region as expected due to interaction of the electronic spin

with the nuclear spin ($I = 3/2$) of the copper. Hyperfine lines are expected, but not observed in the perpendicular region of the spectrum (Fig. 3.7, Table 3.3) [104].

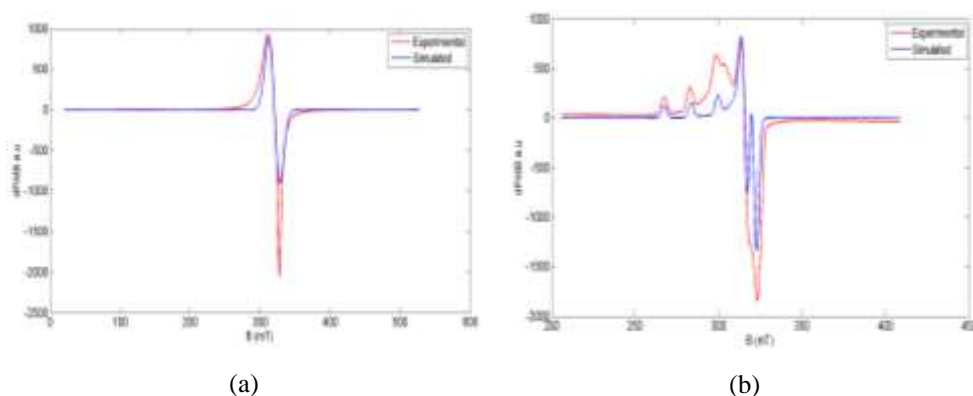


Fig. 3.7. EPR spectra of complex **1** in (a) polycrystalline state at 298 K and (b) DMF solution at 77 K.

For $[\text{Cu}(\text{bpm})\text{Br}]_2$ (**2**), EPR spectrum with axial values g_{\parallel} (2.20) $>$ g_{\perp} (2.075) was observed in the polycrystalline state (298 K) [105]. In DMF solution at 77 K, it has four hyperfine lines in the parallel region with $g_{\parallel} = 2.274$ and $g_{\perp} = 2.06$, characteristic of an axial spectrum while no hyperfine lines are observed in the perpendicular region (Fig 3.8, Table 3.3). The majority of Cu(II) complexes show EPR spectra with the usual g values $g_{\parallel} > g_{\perp} > 2.0023$ [106-108].

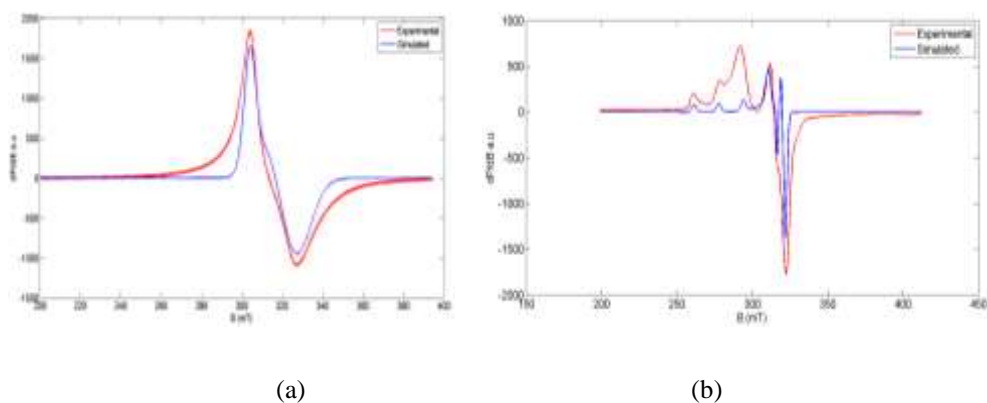


Fig. 3.8. EPR spectra of complex **2** in (a) polycrystalline state at 298 K and (b) DMF solution at 77 K.

Complex $[\text{Cu}(\text{dkm})\text{Br}]_2$ (**3**) displays isotropic spectra at $g_{\text{iso}} = 2.150$ in its polycrystalline state. The same complex in DMF solution at 77 K also shows a well resolved axial spectrum with hyperfine splitting in the parallel region with $g_{\parallel} = 2.295$, $g_{\perp} = 2.070$, $A_{\parallel} = 210 \times 10^{-4} \text{ cm}^{-1}$ and $A_{\perp} = 28.9 \times 10^{-4} \text{ cm}^{-1}$ (Fig. 3.9, Table 3.3).

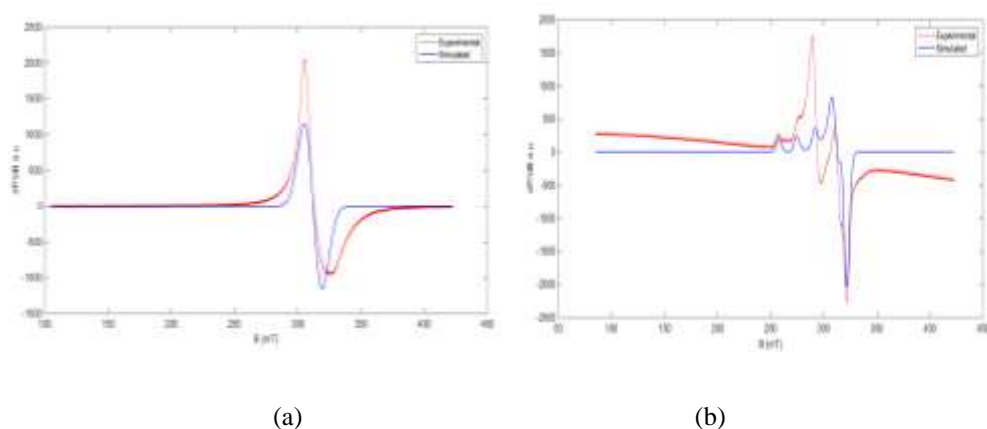


Fig. 3.9. EPR spectra of complex **3** in (a) polycrystalline state at 298 K and (b) DMF solution at 77 K.

For these pentacoordinate complexes in DMF at 77 K, the fact that g_{\parallel} is greater than g_{\perp} suggests a distorted square pyramidal structure consistent with SCXRD analysis and rules out the possibility of a trigonal bipyramidal structure [109].

For axial spectra, the geometric parameter G was calculated by the equation $G = (g_{\parallel} - 2.0023)/(g_{\perp} - 2.0023)$ representing the exchange interaction between copper(II) centers in the solid polycrystalline complexes. Accordingly, if G is greater than 4, the exchange interaction may be negligible; however, if G is less than 4, a considerable exchange interaction is indicated in the solid complex [110]. For complex **3**, G value is slightly less than 4 indicating exchange interaction.

In-plane sigma bonding parameter α^2 was estimated from the expression [15]

$$\alpha^2 = -A_{\parallel} / 0.036 + (g_{\parallel} - 2.0023) + 3/7(g_{\perp} - 2.0023) + 0.04$$

The following simplified expression were used to calculate the bonding parameters

$$K_{\parallel}^2 = (g_{\parallel} - 2.0023) E_{d-d} / 8\lambda_0,$$

$$K_{\perp}^2 = (g_{\perp} - 2.0023) E_{d-d} / 2\lambda_0$$

$$K_{\parallel}^2 = \alpha^2 \beta^2$$

$$K_{\perp}^2 = \alpha^2 \gamma^2$$

where K_{\parallel} and K_{\perp} are orbital reduction factors and λ_0 represents the one electron spin orbit coupling constant.

Hathaway [15] has pointed out that $K_{\parallel} \approx K_{\perp} \approx 0.77$ for pure sigma bonding, $K_{\parallel} < K_{\perp}$ for in plane π -bonding and $K_{\perp} < K_{\parallel}$ for out-of-plane π -bonding. For complex **1**, it is observed that $K_{\parallel} < K_{\perp}$ shows significant in plane π -bonding.

$K_{\perp} < K_{\parallel}$ for complex **2** indicates significant out-of-plane π -bonding in the complex. By comparing the value of in-plane sigma bonding parameter α^2 , the nature of M-L bond is evaluated. The value of α^2 is unity, if the M-L bond is purely ionic and it is completely covalent, if $\alpha^2 = 0.5$. Here α^2 values calculated for complexes **1** and **2** lie between 0.5 and 1, it means that the complexes under study are partially ionic and partially covalent in nature [111].

Table 3.3. Spin Hamiltonian and bonding parameters of copper(II) complexes **1**, **2** and **3**.

Parameters	[Cu(bpm)Cl] ₂ (1)	[Cu(bpm)Br] ₂ (2)	[Cu(dkm)Br] ₂ (3)
Polycrystalline state at 298K			
g_{\parallel}	--	2.20	--
g_{\perp}	--	2.075	--
g_{iso}	2.03	2.1166	2.150
G	--	2.7194	--
DMF solution (77 K)			
g_{\parallel}	2.23	2.274	2.295
g_{\perp}	2.06	2.06	2.070
g_{avg}	2.116	2.1313	2.145
A_{\parallel}	185	197	210
A_{\perp}	---	18	28.9
α^2	0.8065	0.8843	0.944
β^2	0.9318	0.9266	0.7997
γ^2	0.9381	0.8540	0.8145
K_{\parallel}	0.7515	0.7552	0.7997
K_{\perp}	0.7566	0.7552	0.7692
f	120.5	115.4	109.3

A values in 10^{-4} cm^{-1}

3.3.4. Hirshfeld Surface and 2D Fingerprint Plot Analysis

The intermolecular interactions present in complexes **1-3** are quantified using Hirshfeld surface analysis. They are mapped using (a) d_{norm} and (b) shape index which are shown in Figs. 3.10 and 3.11. The surfaces are kept transparent during mapping for the visualization of various interactions. The red spots on the surfaces of d_{norm} plot for complexes **1-3** depicts prominent intermolecular hydrogen bonding interactions (Fig. 3.12 (a & b)). While the red concave region on the surface around the acceptor atom and a blue convex region around the donor H-atom in the shape index plot depict C–H $\cdots\pi$ interaction [112].

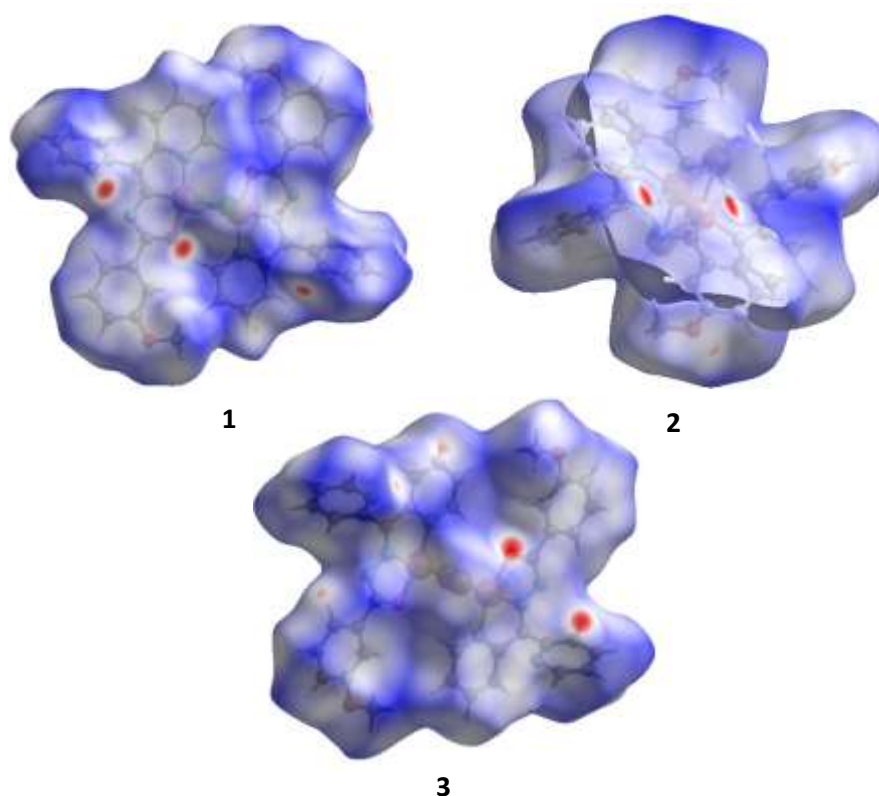


Fig. 3.10. Hirshfeld surfaces for **1**, **2** and **3** mapped with d_{norm} over a fixed color scale of -0.16 (red) to 1.41 \AA (blue).

Bow-tie patterns observed when viewed under shape index function for complexes **1-3** indicating the presence of $\pi \cdots \pi$ contacts (Fig. 3.11) [113].

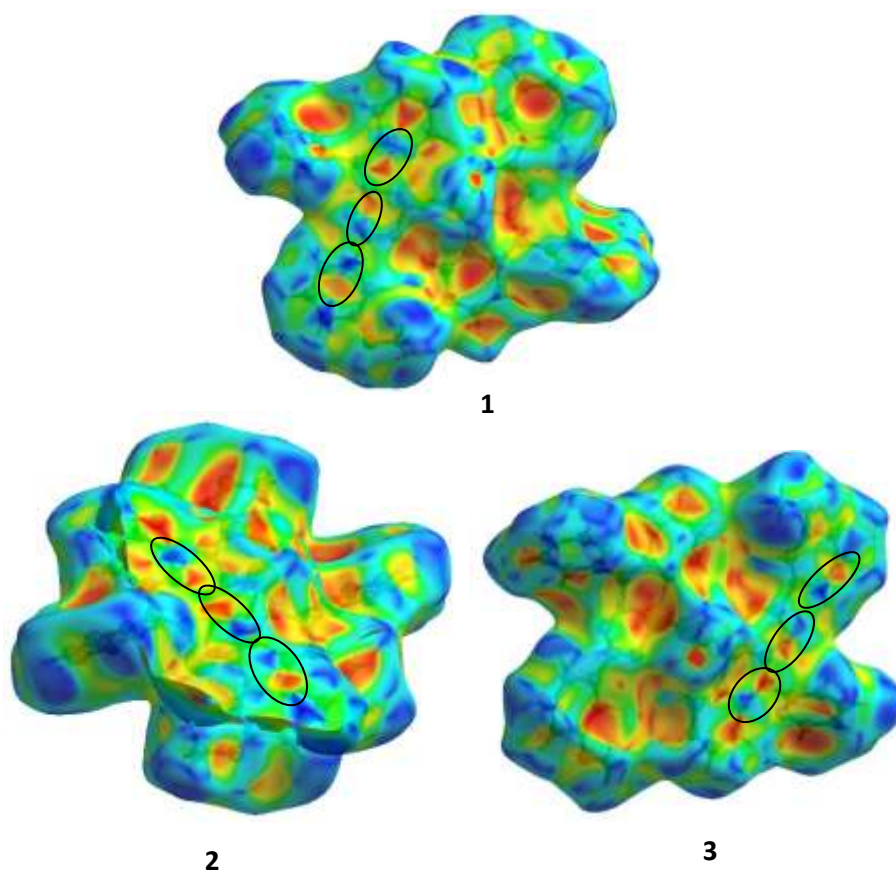


Fig. 3.11. ‘Bow-tie’ pattern (marked by black circles) on the HS’s of **1**, **2** and **3** indicating the relative percentage of $\pi \cdots \pi$ interactions.

Further, intercontacts are plotted using 2D fingerprint plot analysis as shown in Fig. 3.13. $\pi \cdots \pi$ interaction seen in complexes **1**, **2** and **3** are 4.7, 4.1 and 4.9 % respectively. All the three complexes are dominated by H \cdots H interaction [114].

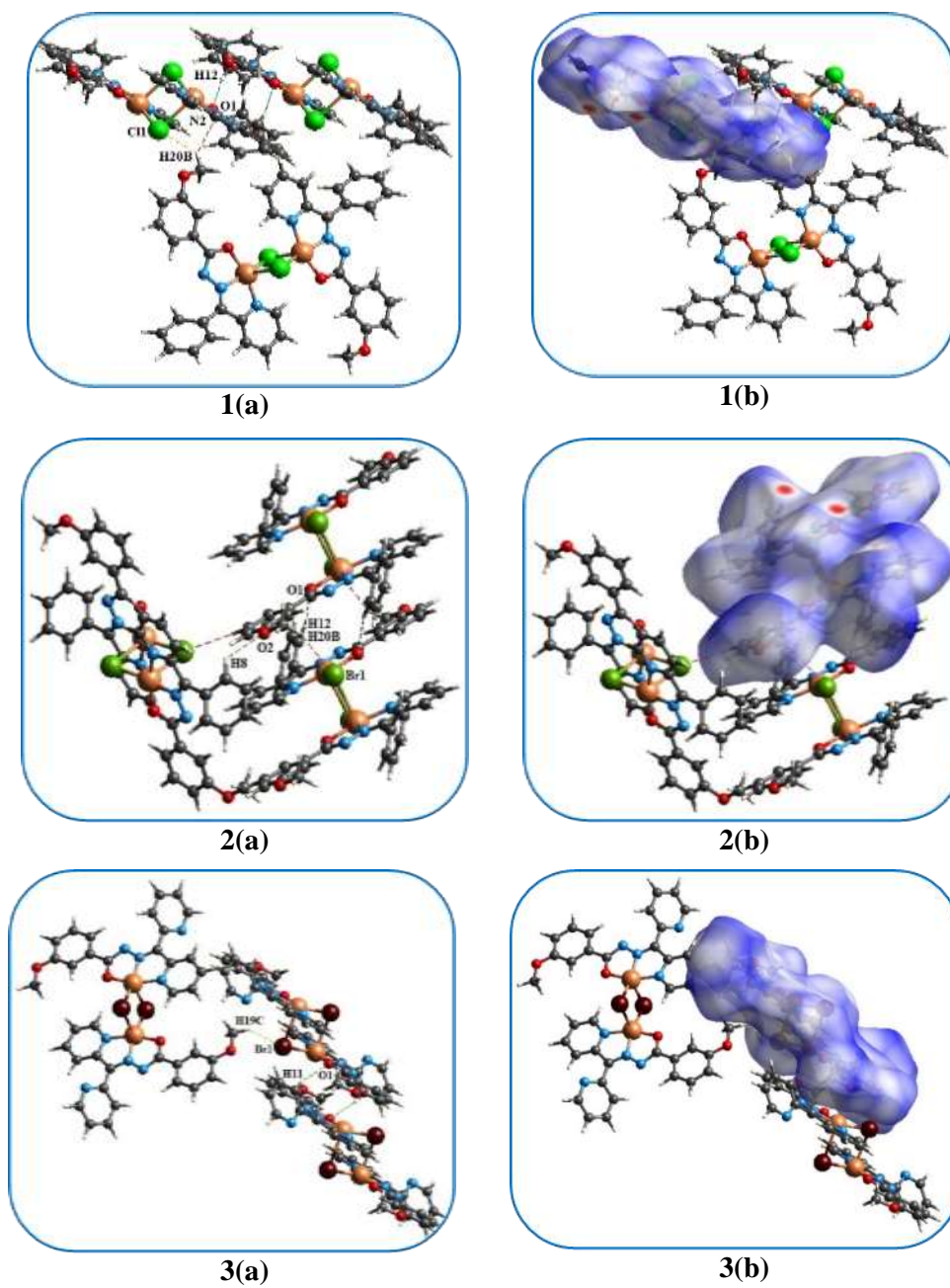
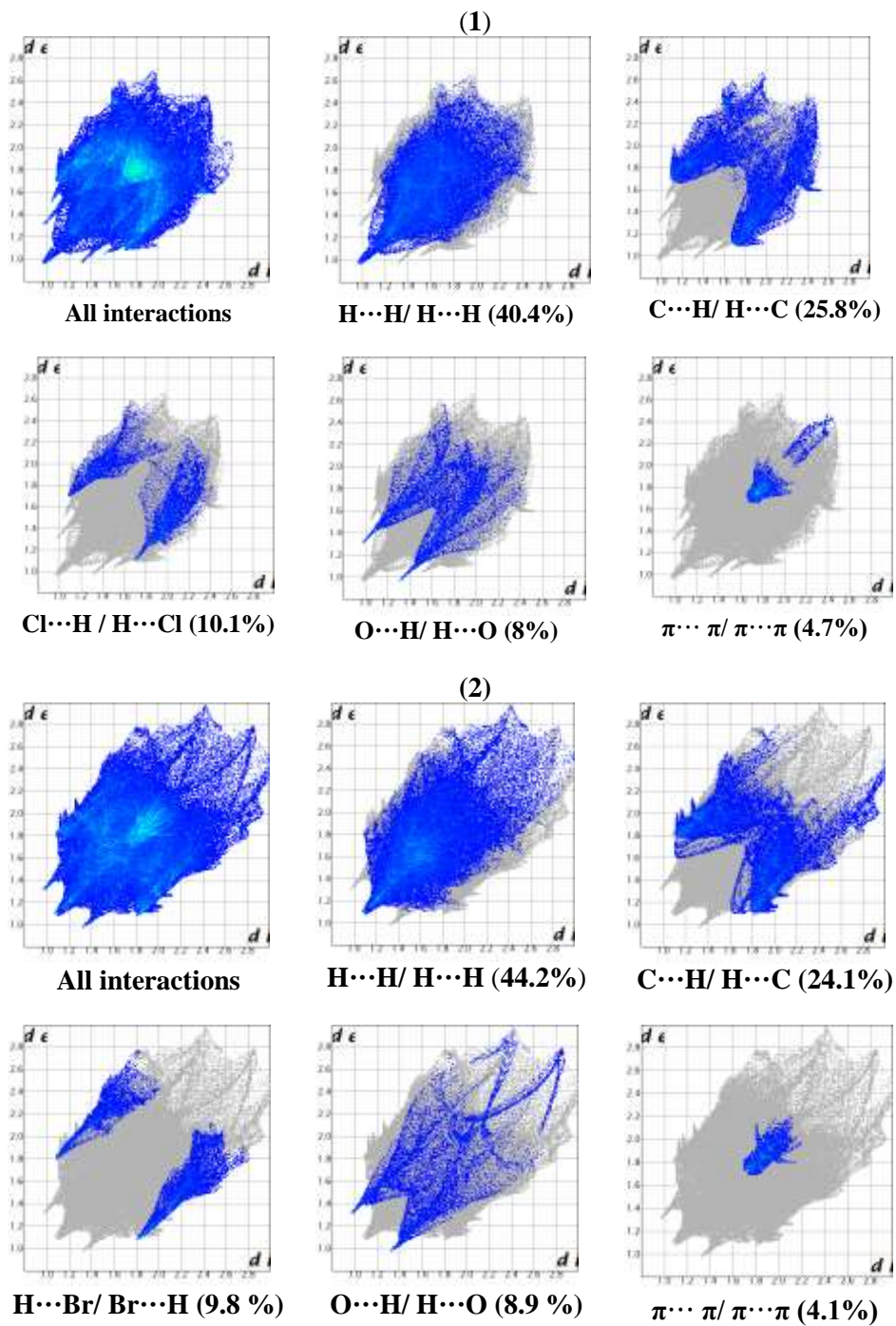


Fig. 3.12. (a) Intermolecular hydrogen bonding interactions present in **1**, **2** and **3**, (b) viewing the same short contacts in Hirshfeld surface with external molecules



(3)

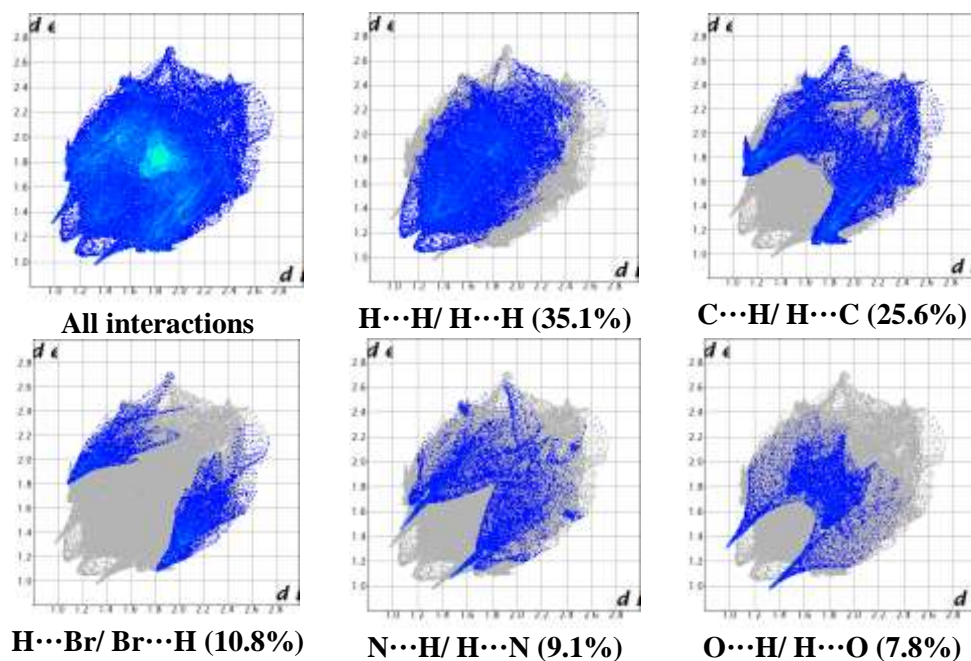


Fig. 3.13. 2 D finger print plots with d_e and d_i ranging from 1.0 to 2.8 Å for complexes **1**, **2** and **3** and major decomposition plots.

3.3.5 X-ray crystallography

3.3.5.1 Crystal structure description of $[\text{Cu}(\text{bpm})\text{Cl}]_2$ (**1**) and $[\text{Cu}(\text{bpm})\text{Br}]_2$ (**2**)

The molecular structure of $[\text{Cu}(\text{bpm})\text{Cl}]_2$ (**1**) and $[\text{Cu}(\text{bpm})\text{Br}]_2$ (**2**) along with the atom numbering scheme are depicted in Figures 3.14 and 3.15 and selected bond lengths (Å) and bond angles ($^\circ$) are shown in Table 3.5. The Crystallographic data and structure refinement parameters for **1** and **2** are collated in Table 3.4.

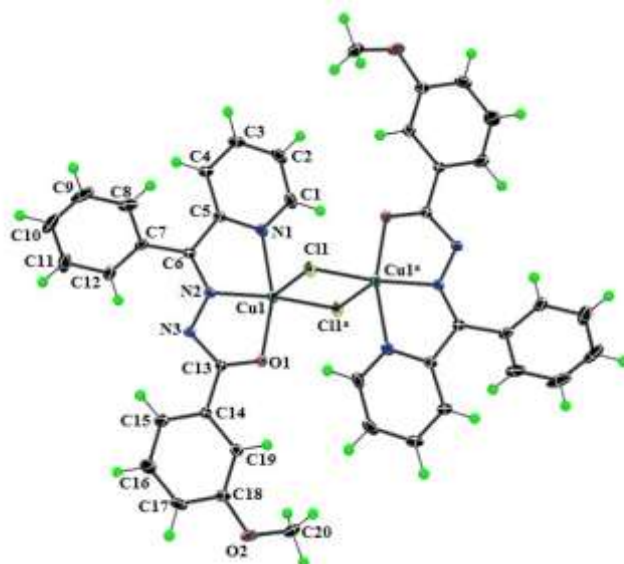


Fig. 3.14. ORTEP plot (drawn with 30% thermal ellipsoid) of [Cu(bpm)Cl]₂ (1) along with atom numbering scheme of non-hydrogen atoms.

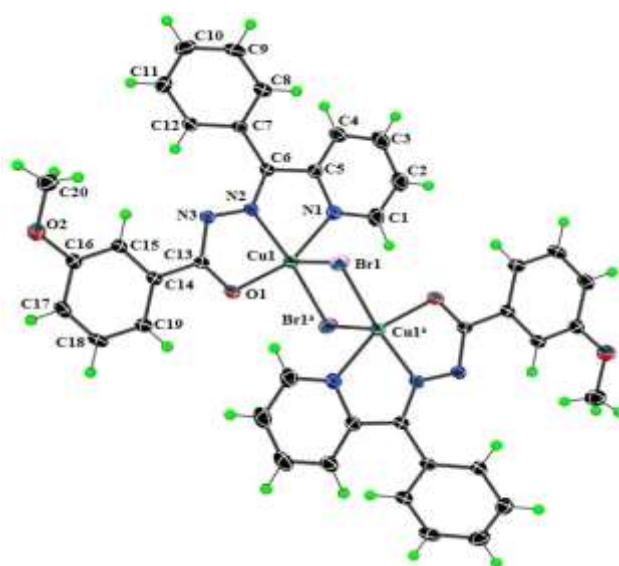


Fig. 3.15. ORTEP plot (drawn with 30% thermal ellipsoid) of [Cu(bpm)Br]₂ (2) along with atom numbering scheme of non-hydrogen atoms.

Table 3.4. Crystallographic data and structure refinement parameters for **1** and **2**.

Parameters	[Cu(bpm)Cl] ₂ (1)	[Cu(bpm)Br] ₂ (1)
Empirical formula	C ₄₀ H ₃₂ Cl ₂ Cu ₂ N ₆ O ₄	C ₄₀ H ₃₂ Br ₂ Cu ₂ N ₆ O ₄
Formula weight	858.72	947.62
Color	Green	Green
Crystal system	Monoclinic	Monoclinic
Space group	<i>P</i> 2 ₁ / <i>n</i>	<i>P</i> 2 ₁ / <i>n</i>
Cell parameters		
a (Å)	8.7184(4)	9.1239(8)
b (Å)	15.4599(2)	14.5939(15)
c (Å)	13.5827(3)	14.4342(15)
α (°)	90	90
β (°)	99.909(2)	96.776(4)
γ (°)	90	90
Volume V (Å ³), Z	1803.44(10), 2	1908.5(3), 2
Calculated density (ρ) (Mg m ⁻³)	1.581	1.649
Absorption coefficient, μ (mm ⁻¹)	3.248	3.258
F(000)	876	948
Crystal size mm ³	0.38 x 0.08 x 0.07	0.30 x 0.08 x 0.06
θ (°) range for data collection	4.370 to 71.328	2.798 to 28.506
Limiting indices	-10 ≤ h ≤ 7, -18 ≤ k ≤ 18, -16 ≤ l ≤ 12	-12 ≤ h ≤ 10, -19 ≤ k ≤ 19, -19 ≤ l ≤ 18
Reflections collected	7275	33984
Unique Reflections (R _{int})	3504 (0.0296)	4841 (0.0319)
Completeness to θ	67.684 96.7%	25.242 99.9%
Absorption correction	Semi-empirical from equivalents	Semi-empirical from equivalents
Maximum and minimum transmission	0.782 and 0.739	0.521 and 0.391
Refinement method	Full-matrix least-squares on F ²	Full-matrix least-squares on F ²
Data / restraints / parameters	3319 / 0 / 245	4841 / 0 / 244
Goodness-of-fit on F ²	0.716	1.023
Final R indices [I > 2σ (I)]	R ₁ = 0.0350, wR ₂ = 0.0979	R ₁ = 0.0279, wR ₂ = 0.0757
R indices (all data)	R ₁ = 0.0376, wR ₂ = 0.1025	R ₁ = 0.0463, wR ₂ = 0.0842
Largest difference peak and hole (e Å ⁻³)	0.331 and -0.573	0.364 and -0.303

$$R_1 = \frac{\sum ||F_o| - |F_c||}{\sum |F_o|}$$

$$wR_2 = \frac{[\sum w(F_o^2 - F_c^2)^2 / \sum w(F_o^2)^2]^{1/2}}$$

Chlorine bridged box dimer copper(II) complex $[\text{Cu}(\text{bpm})\text{Cl}]_2$ (**1**) got crystallized in monoclinic lattice with $P2_1/n$ space group. The complex contains a C_2 axis which is perpendicular to the $\text{Cu1}-\text{Cl1}-\text{Cu1}^a-\text{Cl1}^a$ plane. The coordination sites of metal atom are satisfied by the pyridyl nitrogen, azomethine nitrogen and enolate oxygen atoms of monoanionic tridentate aroylhydrazone. Two fused five membered metallo chelate rings $\text{Cg}(2)$ (comprised of atoms Cu1 , O1 , C13 , N3 , N2) and $\text{Cg}(3)$ are formed by the complexation. Comparison of bond distances $\text{Cu1}-\text{Cl1}$ (2.243 Å), $\text{Cu1}-\text{Cl1}^a$ (2.716 Å), $\text{Cu1}^a-\text{Cl1}$ (2.243 Å) and $\text{Cu1}^a-\text{Cl1}^a$ (2.716 Å) support the bridging dinuclear structure of complex **1**. The extent of distortion in this pentacoordinate complex is calculated by Addison parameter (τ) value. Addison parameter is calculated by the equation, $\tau = (\beta - \alpha)/60$ [115], where $\beta > \alpha$ are the two largest valence angles around the central metal atom. τ values are zero and unity for perfect square pyramidal and trigonal bipyramidal geometries respectively. Copper atoms Cu1 and Cu1^a adopted a distorted square pyramidal geometry (τ value = 0.16). O1 , N1 , N2 donor atoms of aroylhydrazone and the chloride ion Cl1 occupied the basal plane of the square pyramid and the chlorine atom of the adjoining monomer resides an axial position. The $\text{Cu}\cdots\text{Cu}$ non-bonded distance in this dimer complex is approximately 3.369 Å. $\text{Cu1}-\text{Cl1}^a$ distance (axial metal-halogen distance = 2.716 Å) is longer than the $\text{Cu1}-\text{Cl1}$ distance (equatorial metal-halogen distance = 2.243 Å). Different bond angles around the metal atom ($\text{Cl1}^a-\text{Cu1}-\text{N1}$ (89.53°), $\text{N1}-\text{Cu1}-\text{N2}$ (80.39°), $\text{N2}-\text{Cu1}-\text{O1}$ (79.59°) and $\text{O1}-\text{Cu1}-\text{Cl1}^a$ (93.72°) revealed the distortion from the square pyramid geometry. There is significant elongation of the $\text{C13}-\text{O1}$ bond from 1.2185(18) Å to 1.276(2) Å for complex **1** and 1.279 Å for complex **2** with an accompanying reduction in the $\text{C13}-\text{N3}$ bond from 1.3653(19) Å to 1.335(3) Å for complex **1** and 1.328 Å for complex **2** respectively, when compared with free aroylhydrazones already discussed in Chapter 2. It is an evidence for enolization.

Table 3.5. Selected bond lengths and bond angles of [Cu(bpm)Cl]₂ (**1**) and [Cu(bpm)Br]₂ (**2**).

[Cu(bpm)Cl] ₂ (1)		[Cu(bpm)Br] ₂ (2)	
Bond lengths (Å)			
Cu1–N2	1.937(16)	N1–Cu1	2.008(2)
Cu1–O1	1.964(14)	N2–Cu1	1.926(18)
Cu1–N1	2.008(18)	O1–Cu1	1.954(15)
Cu1–Cl1	2.243(6)	Cu1–Br1	2.362(4)
Cu1–Cl1 ^a	2.716(6)	Cu1–Br1 ^a	2.869(4)
Cl1–Cu1 ^a	2.716(6)	Br1–Cu1 ^a	2.869(4)
N1–C5	1.351(3)	N1–C5	1.347(3)
N2–C6	1.297(3)	N2–C6	1.284(3)
N3–N2	1.366(2)	N3–N2	1.361(2)
N3–C13	1.335(3)	N3–C13	1.328(3)
O1–C13	1.276(2)	O1–C13	1.279(3)
Bond angles (°)			
N2–Cu1–O1	79.59(6)	N2–Cu1–O1	79.68(7)
N2–Cu1–N1	80.39(7)	N2–Cu1–N1	80.06(7)
O1–Cu1–N1	159.97(7)	O1–Cu1–N1	159.47(7)
N2–Cu1–Cl1	164.68(5)	N2–Cu1–Br1	168.80(5)
O1–Cu1–Cl1	98.66(4)	O1–Cu1–Br1	97.45(5)
N1–Cu1–Cl1	100.74(6)	N1–Cu1–Br1	101.81(5)
N2–Cu1–Cl1 ^a	100.32(5)	N2–Cu1–Br1 ^a	92.40(5)
O1–Cu1–Cl1 ^a	93.72(5)	O1–Cu1–Br1 ^a	91.11(5)
N1–Cu1–Cl1 ^a	89.53(6)	N1–Cu1–Br1 ^a	93.03(6)
Cl1–Cu1–Cl1 ^a	94.97(2)	Br1–Cu1–Br1 ^a	98.50(12)
a = -x, -y, 1-z		a = 1-x, 2-y, -z	

The interaction parameters are collated in Table 3.6. In complex **1**, a bifurcated, 3 center-2-electron hydrogen bond is observed between a chlorine, Cl1 (acceptor) and H1 and H20B of the donor atoms C1 and C20 (methoxy carbon), respectively [116]. Hydrogen H20B of the methoxy carbon interacts with N2 and H12 from the enolate oxygen O1 (Fig. 3.16).

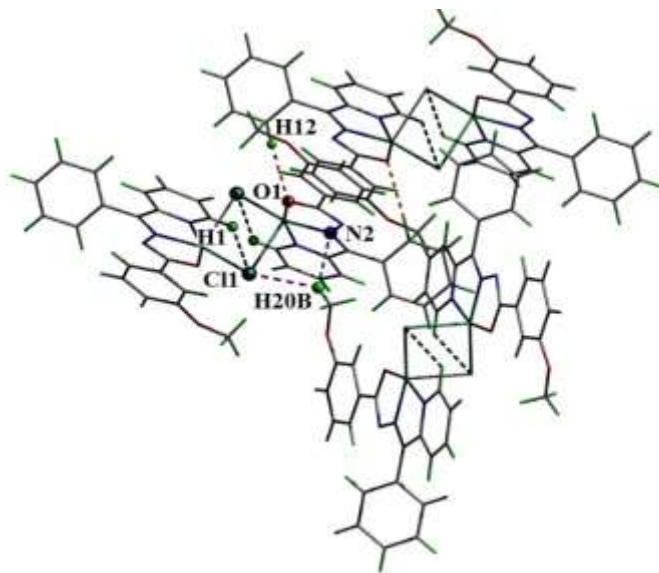


Fig. 3.16. Packing diagram showing hydrogen bonding (dashed lines) in complex **1**.

Table 3.6. Hydrogen bonding interactions in **1** and **2**

D–H···A	D–H (Å)	H···A (Å)	D···A (Å)	∠D–H···A (°)
[Cu(bpm)Cl]₂ (1)				
C20–H20B···C11 ^a	0.98	2.89	3.683(3)	138
C20–H20B···N2 ^b	0.98	2.66	3.467(3)	139
C1–H1···C11	0.95	2.90	3.443(3)	117
C12–H12···O1	0.95	2.44	3.363(3)	164
[Cu(bpm)Br]₂ (2)				
C1–H1···Br1	0.93	3.00	3.548(3)	119
C20–H20B···Br1 ^c	0.96	3.05	3.942(3)	155
C8–H8···O2	0.93	2.60	3.246(3)	127
C12–H12···N3	0.93	2.61	2.933(3)	101
C12–H12···O1	0.93	2.46	3.374(3)	167
C15–H15···N3	0.93	2.43	2.752(3)	100

Equivalent position codes: a = $x+1/2, -y-1/2, z-1/2$; b = $-x+1/2, y-1/2, -z+1/2$; c = $-x+2, -y+2, -z$

Table 3.7. Non-bonding interactions in **1** and **2**

C–H⋯π interactions				
[Cu(bpm)Cl]₂ (1)				
C–H(I)⋯Cg(J)	H⋯Cg (Å)	C⋯Cg (Å)	\angleC–H⋯Cg (°)	
C1–H1⋯Cg(1) ^a	2.90	3.199(3)	100	
C10–H10⋯Cg(6) ^b	2.73	3.543(4)	144	
C20–H20B⋯Cg(2) ^c	2.95	3.806(3)	147	
[Cu(bpm)Br]₂ (2)				
C2–H2⋯Cg(5) ^d	2.85	3.600(3)	139	
C20–H20A⋯Cg(5) ^e	2.76	3.605(3)	147	
π⋯π interactions				
[Cu(bpm)Cl]₂ (1)				
Cg(I)⋯Cg(J)	Cg⋯Cg (Å)	α (°)	β (°)	γ (°)
Cg(2)⋯Cg(2) ^f	3.593(10)	0	18.28	18.28
Cg(3)⋯Cg(6) ^f	3.560(13)	2.53(11)	16.21	15.69
Cg(4)⋯Cg(6) ^f	3.631(15)	3.12(12)	19.72	21.87
[Cu(bpm)Br]₂ (2)				
Cg(2)⋯Cg(2) ^g	3.878(11)	0.03(8)	24.1	24.1
Cg(3)⋯Cg(6) ^g	3.632(13)	5.77(10)	10.4	10.4
Cg(4)⋯Cg(6) ^g	3.884(14)	7.90(12)	22.8	22.5

Equivalent position codes: a = x, y, z; b = 1/2+x, 1/2-y, 1/2+z; c = 1/2-x, -1/2+y, 1/2-z; d = 3/2-x, 1/2+y, 1/2-z; e = 5/2-x, -1/2+y, 1/2-z; f = 1-x, -y, 1-z; g = 2-x, 2-y, -z

[CuL¹Cl]₂ (**1**): Cg(1) = Cu1, Cl1, Cu1^a, Cl1^a; Cg(2) = Cu1, O1, C13, N3, N2; Cg(3) = Cu1, N1, C5, C6, N2; Cg(4) = N1, C1, C2, C3, C4, C5; Cg(5) = C7, C8, C9, C10, C11, C12; Cg(6) = C14, C15, C16, C17, C18, C19

[CuL¹Br]₂ (**2**): Cg(1) = Br1, Cu1, Br1^a, Cl1^a; Cg(2) = Cu1, O1, C13, N3, N2; Cg(3) = Cu1, N1, C5, C6, N2; Cg(4) = N1, C1, C2, C3, C4, C5; Cg(5) = C7, C8, C9, C10, C11; Cg(6) = C14, C15, C16, C17, C18, C19

D, Donor; A, acceptor; Cg, Centroid.

Analysis of the short ring interaction indicates that the newly formed Cg(1) consists of Cu1, C11, Cu1^a and C11^a interacts with metallocycle Cg(4) (pyridyl ring of the ligand). Also, aromatic ring Cg(2) interacts face to face with each other at a distance of 3.5927(10) Å. Cg(6) of one molecule interacts with both Cg(3) (comprising of atoms Cu1, N1, C5, C6, N2) and Cg(4) (comprising of atoms N1, C1, C2, C3, C4 and C5) of a neighbouring molecule with centroid-centroid distances of 3.560(13) Å and 3.631(15) Å, respectively (Fig. 3.17).

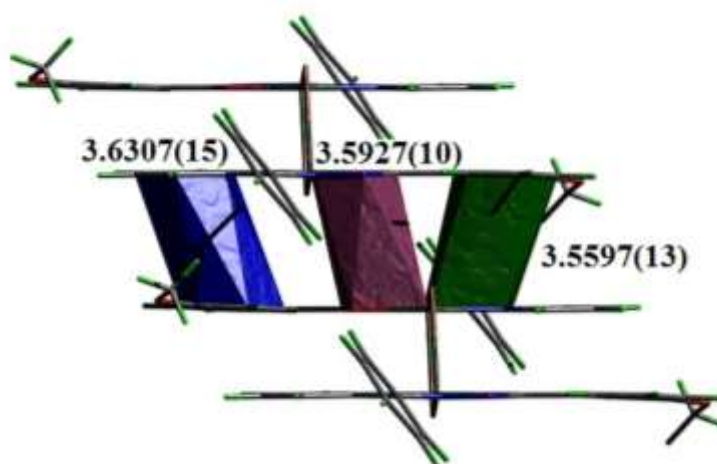


Fig. 3.17. The $\pi \cdots \pi$ interactions in complex 1.

Three weak C–H $\cdots\pi$ interactions (Fig. 3.18) are present in the molecule. Hydrogens H10 and H20B attached to the respective carbon atoms C10 and C20 interact with Cg(6) (comprised of atoms C14, C15, C16, C17, C18 and C19) and Cg(2) (comprised of atoms Cu1, O1, C13, N3 and N2). Another weak interaction is formed between C1–H1 and a halogen bearing a four membered aromatic ring Cg(1) with an H $\cdots\pi$ distance of 2.90 Å (Table 3.7).

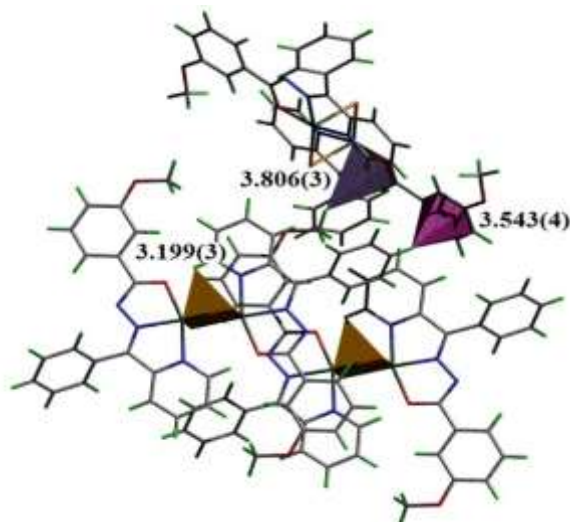


Fig. 3.18. Weak C–H··· π interaction in complex **1**.

The geometry of complex **2** is similar to that of complex **1** except for the fact that the Cu···Cu separation is 3.436 Å and the Addison parameter is 0.155. The axial/apical metal-bromine distance is 2.362/2.869 Å. The packing of the molecule in complex **2** includes hydrogen bonding, weak C–H··· π and π ··· π stacking interactions. A bifurcated intramolecular hydrogen bond exists between N3 (acceptor) and H12 and H15 of donor atoms C12 and C15 with D···A distances of 2.933 and 2.752 Å, respectively. Bromine atom Br1 is involved in two intermolecular interactions with H1 and H20B, thus forming a bifurcated three center hydrogen bond [117]. Two intermolecular hydrogen bonding interactions, C8–H8···O2 and C12–H12···O1, are also present in the lattice of complex **2** with D···A distances of 3.246 and 3.374 Å, respectively (Fig. 3.19 & Table 3.6).

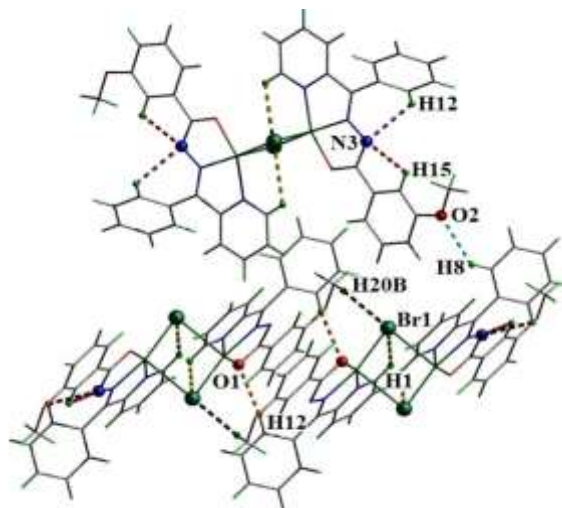


Figure 3.19. Hydrogen bonding (dashed lines) in complex 2.

The five membered ring Cg(5) (comprised of atoms C7, C8, C9, C10, C11 and C12) is involved in weak C–H··· π interactions with H2 and H20A of carbon atoms C2 and C20 (methoxy carbon) at H···Cg distances of 2.85 and 2.76 Å, respectively (Fig. 3.20 & Table 3.7).

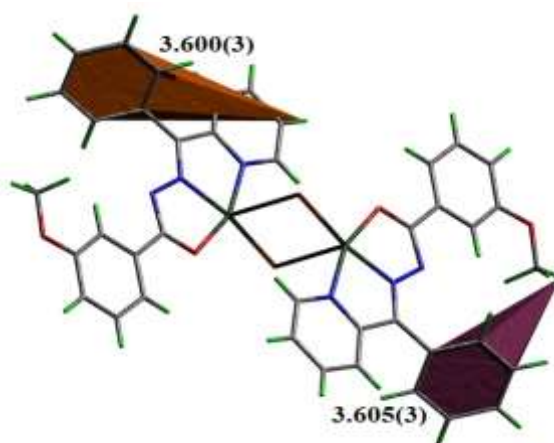


Fig. 3.20. Weak C–H··· π interaction in complex 2.

Metallocycle Cg(2) interacts face to face with each other with a centroid-centroid distance of 3.8780 Å. The six-membered aromatic ring Cg(6) interacts both with the five-membered chelate ring Cg(3) and six-membered pyridine ring Cg(4) at a distance of 3.6316 and 3.8843 Å (Fig. 3.21 & Table 3.7).

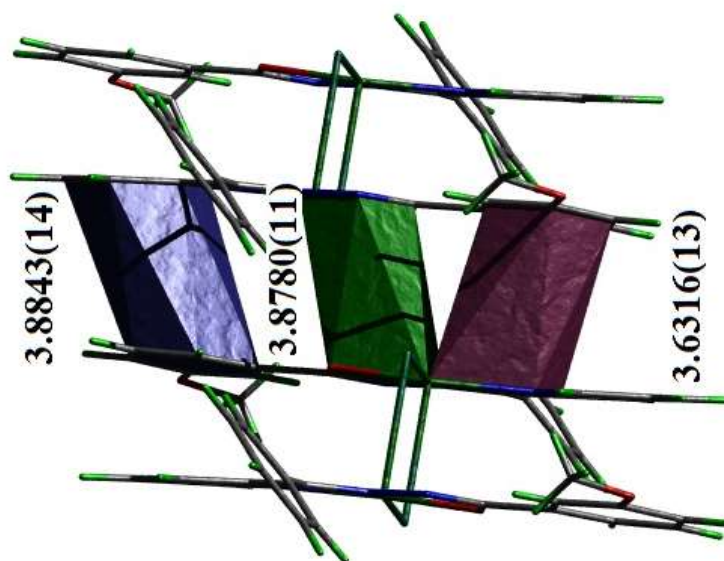


Fig. 3.21. The $\pi \cdots \pi$ interactions in complex **2**.

3.3.5. Crystal structure of [Cu(dkm)Br]₂ (**3**)

Green needle shaped crystals of [Cu(dkm)Br]₂ were obtained by slow evaporation of the mother liquor. Molecular structure of (**3**) along with the atom numbering scheme is depicted in Fig. 3.22 and relevant interatomic distances (Å) and bond angles (°) are listed in Table 3.9. The Crystallographic data and structure refinement parameters for **3** is tabulated in Table 3.8.

Table 3.8. Crystal data and structural refinement parameters of Cu(dkm)Br]₂ (3)

Compound	[Cu(dkm)Br] ₂ (3)
Empirical formula	C ₃₈ H ₃₀ Br ₂ Cu ₂ N ₈ O ₄
Formula weight	949.60
Color	Green
Crystal system	Monoclinic
Space group	<i>P2₁/n</i>
Cell parameters	
a (Å)	8.6984(18)
b (Å)	15.604(4)
c (Å)	13.522(3)
α (°)	90
β (°)	97.126(8)
γ (°)	90
Volume V (Å ³)	1821.2(7)
Z	2
Calculated density (ρ) (Mg m ⁻³)	1.732
Absorption coefficient, μ (mm ⁻¹)	3.416
F(000)	948
Crystal size mm ³	0.30 x 0.25 x 0.20
θ (°) range for data collection	2.611 to 28.412
Limiting indices	-7 ≤ h ≤ 11, -20 ≤ k ≤ 20, -18 ≤ l ≤ 18
Reflections collected	14328
Unique Reflections (R _{int})	4579 (0.1631)
Completeness to θ	25.242 98.9%
Absorption correction	Semi-empirical from equivalents
Maximum and minimum transmission	0.509 and 0.363
Refinement method	Full-matrix least-squares on F ²
Data / restraints / parameters	4246 / 0 / 245
Goodness-of-fit on F ²	1.013
Final R indices [I > 2σ (I)]	R ₁ = 0.0743, wR ₂ = 0.1659
R indices (all data)	R ₁ = 0.1312, wR ₂ = 0.2031
Largest difference peak and hole (e Å ⁻³)	1.662 and -1.466

$$R_1 = \frac{\sum ||F_o| - |F_c||}{\sum |F_o|}$$

$$wR_2 = \left[\frac{\sum w(F_o^2 - F_c^2)^2}{\sum w(F_o^2)^2} \right]^{1/2}$$

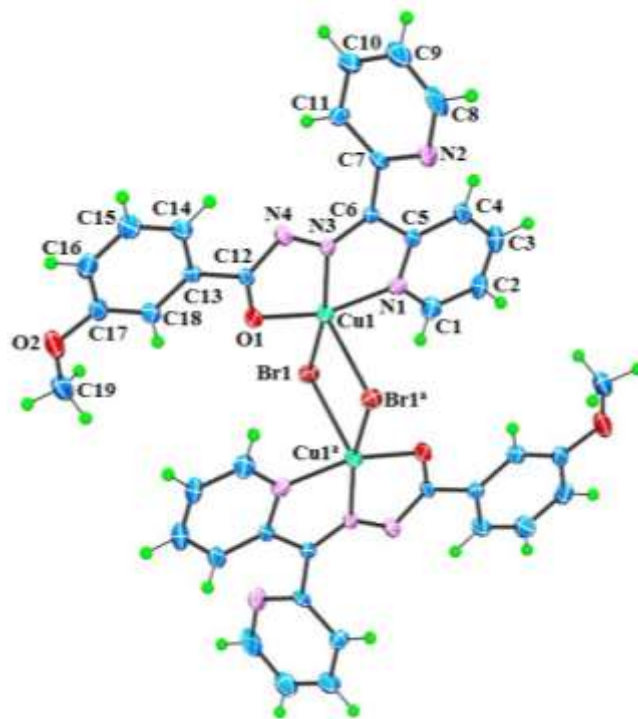


Fig. 3.22. ORTEP plot (drawn with 30% thermal ellipsoid) of $[\text{Cu}(\text{dkm})\text{Br}]_2$ (**3**) along with atom numbering scheme of non-hydrogen atoms.

Table 3.9. Selected bond lengths and bond angles of $[\text{Cu}(\text{dkm})\text{Br}]_2$ (**3**)

Bond lengths (Å)		Bond angles (°)	
Cu1–N3	1.937(5)	N3–Cu1–O1	78.89(19)
Cu1–O1	1.958(4)	N3–Cu1–N1	81.1(2)
Cu1–N1	1.986(6)	O1–Cu1–N1	159.9(2)
Cu1–Br1	2.3861(12)	N3–Cu1–Br1	163.41(15)
Cu1–Br1 ^a	2.8219(13)	Br–1–Cu1–Br1 ^a	96.71(3)

$$a = -x+1, -y, -z$$

The bromine bridged copper(II) box dimer complex **2** got crystallized in a monoclinic lattice with $P2_1/n$ symmetry and possess a C_2 axis perpendicular to the $Cu1-Br1-Cu1^a-Br1^a$ plane. Each Cu(II) center is coordinated by the tridentate monoanionic hydrazone ligand *via* the enolate oxygen, azomethine nitrogen and pyridyl nitrogen. Two pentagonal metallo-chelate rings Cg(2) (Cu1, O1, C12, N4, N3) and Cg(3) (Cu1, N1, C5, C6, N3) with chelate bite angles of $78.89(19)^\circ$ and $81.1(2)^\circ$ respectively are formed by coordination. The remaining two coordination sites are occupied by the bridging bromide anions. Both metal centres Cu1 and $Cu1^a$ displays a distorted square pyramidal geometry with an Addison parameter (τ) value of 0.05, whose basal plane contains the atoms N1, N3, O1 and Br1. The elongated apical position is occupied by a second bromide anion $Cu1-Br1^a = 2.822 \text{ \AA}$. The double bromide bridge gives rise to a $Cu \cdots Cu$ separation distance of approximately 3.476 \AA within the dimeric moiety. The axial metal-bromine distance, $Cu1-Br1^a = 2.822 \text{ \AA}$, is longer than the equatorial metal-bromine distance, $Cu1-Br1 = 2.386 \text{ \AA}$. Most of the angles including central copper atoms like $Br1-Cu1-N1$ (100.56°), $N1-Cu1-N3$ (81.06°), $N3-Cu1-O1$ (78.88°) and $O1-Cu1-Br1$ (98.52°) are widely different from 90° and 180° , suggesting significant distortion from square pyramidal geometry [118]. C12-O1 bond lengthened from $1.2217(14) \text{ \AA}$ to $1.269(8) \text{ \AA}$ and C12-N4 bond reduced from $1.3643(15) \text{ \AA}$ to $1.338(8) \text{ \AA}$ upon complexation which is an evidence for enolization.

A bifurcated hydrogen bonding is established between Br1 and H19C borne on methyl carbon and the H1 atom [119]. Also two intramolecular and one intermolecular hydrogen bonding interactions are present in complex **3** (Fig. 3.23. and Table 3.10). Two $C-H \cdots \pi$ interactions present in complex **3** are shown in Fig. 3.24 (Table 3.10).

Table 3.10. Hydrogen bonding and non-bonding interactions in **3**

Hydrogen bonding interactions				
D–H···A	D–H (Å)	H···A (Å)	D···A (Å)	∠D–H···A (°)
C4–H4···N2	0.93	2.47	3.017(9)	118
C11–H11···O1 ^a	0.93	2.46	3.349(9)	160
C14–H14···N4	0.93	2.47	2.794(9)	100
C1–H···Br1	0.93	2.98	3.530(8)	119
C19–H19C···Br1 ^b	0.96	3.00	3.530(8)	136
C–H···π interactions				
C–H(I)···Cg(J)	H···Cg (Å)	C···Cg (Å)	∠C–H···Cg (°)	
C1–H···Cg(1) ^c	2.92	3.222(7)	101	
C9–H9···Cg(6) ^d	2.73	3.537(10)	146	
π···π interactions				
Cg(I)···Cg(J)	Cg···Cg (Å)	α (°)	β (°)	
Cg(2)···Cg(2) ^a	3.582(3)	0	15.56	
Cg(3)···Cg(6) ^a	3.628(4)	4.6(3)	18.27	
Cg(4)···Cg(6) ^a	3.649(4)	3.9(3)	19.23	

Equivalent position codes: a = -x,-y,-z; b = x-1/2,-y-1/2, z+1/2; c = x-1/2, -y-1/2, z+1/2; d = -1/2+x, 1/2-y,-1/2+z;

Cg(2) = Cu1, O1, C12, N4, N3; Cg(3) = Cu1, N1, C5, C6, N3; Cg(4) = N1, C1, C2, C3, C4, C5; Cg(6) = C13, C14, C15, C16, C17, C18

D, Donor; A, acceptor; Cg, Centroid.

There is a face to face interaction between Cg(2) with π ··· π distance of 3.582(3) Å. Metallocycle Cg(6) interact both with Cg(3) and Cg(4) with centroid-centroid distance of 3.628(4) and 3.649(4) Å respectively (Fig. 3.25& Table 3.10).

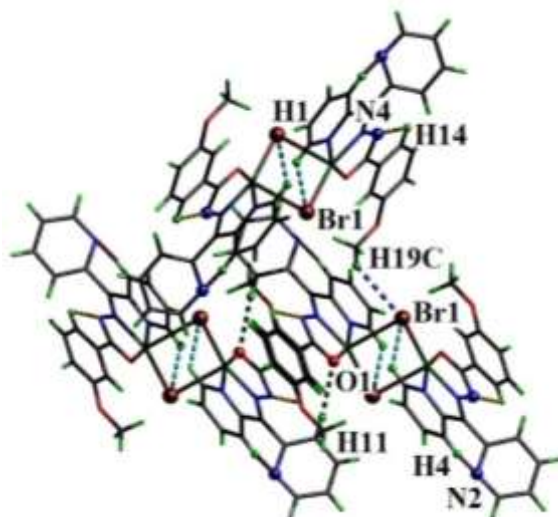


Fig. 3.23. Inter and intramolecular hydrogen bonding interactions in compound **3**.

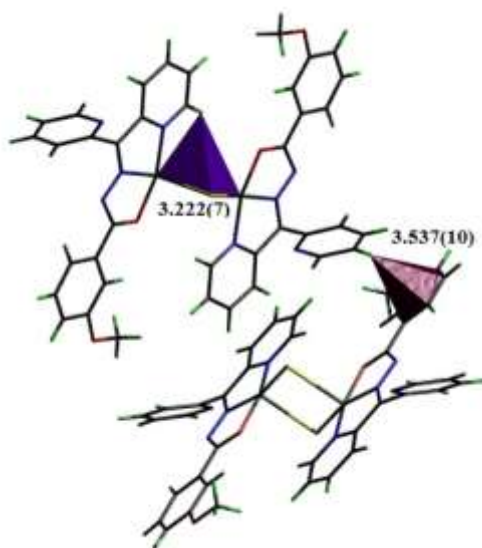


Fig. 3.24. C-H... π interactions in compound **3**.

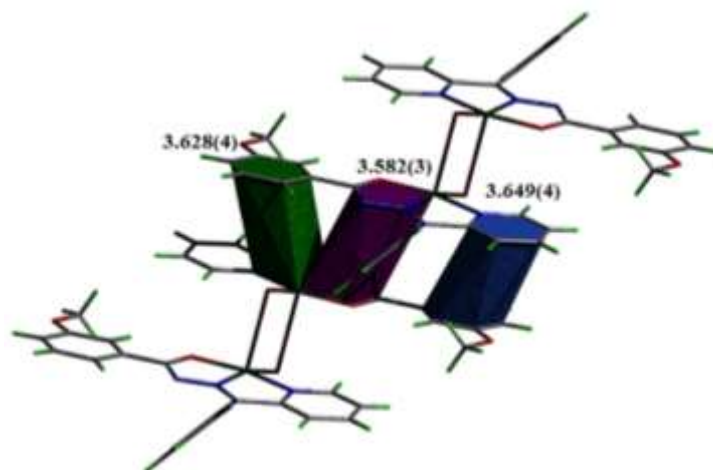
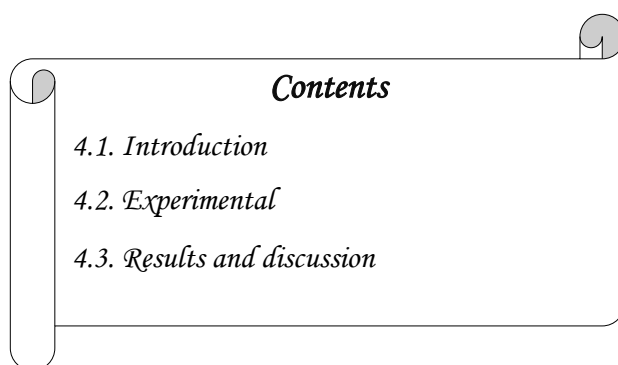


Fig. 3.25. $\pi \cdots \pi$ interactions in compound 3.

Chapter 4

SYNTHESES AND CHARACTERIZATION OF COPPER(II) AND NICKEL(II) COMPLEXES OF AROYLHYDRAZONES CONTAINING PSEUOHALIDES AS COLIGANDS



Contents

- 4.1. Introduction*
- 4.2. Experimental*
- 4.3. Results and discussion*

4.1. Introduction

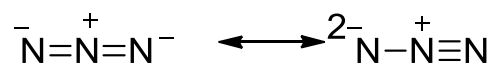
Here we discuss the syntheses and characterization of copper(II) and nickel(II) complexes of aroylhydrazones containing pseudohalides as coligands. Two pseudohalides, azide and thiocyanate are used as coligands. Complexes $[\text{Cu}(\text{bpm})\text{N}_3]_2$ (**4**), $[\text{Cu}(\text{dkm})\text{N}_3]_2$ (**5**) and $[\text{Ni}(\text{dkm})\text{N}_3]_2$ (**6**) are azide bridged box dimer complexes whereas complex $[\text{Cu}(\text{bpm})(\text{SCN})]_n$ (**7**) is a thiocyanate bridged one dimensional polymer. The design and syntheses of pseudohalide bridged copper(II) complexes have been an attractive area of research [120-123]. Structural and magnetic properties of double *end-on* ($\mu_{1,1}\text{-N}_3$) azido-bridged dimeric complexes have been most widely studied [134-126]. Also thiocyanate anion is a versatile bridging group [127,128]. To obtain discrete one dimensional, two

dimensional or three dimensional systems these pseudohalides are excellent ligand systems.

4.1.1. The pseudohalogens - azide (N_3^-) and thiocyanate (SCN^-)

4.1.1.1. Azide anion

N_3^- is a linear triatomic anion that is isoelectronic with CO_2 and is shown by two resonance structures;



The flexidentate azide ligand (N_3^-) shows its versatility and efficiency in metal complexes either as terminal monodentate or as bridging-bi, -tri and -tetradentate linker. Complexes containing terminal monodentate azido ligand in mononuclear or polynuclear complexes which exist in different geometries [129]. Different coordination modes of azide ion are given in Fig. 4.1. As a bridging bidentate ligand, azide binds the metal *via end-on* and *end-to-end* mode [130]. Two types of *end-on* coordination modes are: (a) single $\mu_{1,1}$: *end-on* (Fig. 4b) and (b) double $\mu_{1,1}$: *end-on* (Fig. 4c). We have reported a double *end-on* azide bridged box dimer copper(II) complex of 2-benzoylpyridine 3-methoxybenzhydrazone [20]. Double *end-on* bridging may be symmetric [131] or asymmetric [132]. The *end-to-end* coordination modes are also of two types: (a) single *end-to-end* (Fig. 4d) and (b) double *end-to-end* (Fig. 4e) [133-136]. Only a few examples of trinuclear systems with azido bridges are reported in the literature and the possible coordination modes are $\mu_{1,1,1}\text{-N}_3$ (Fig. 4f) and $\mu_{1,1,3}\text{-N}_3$ (Fig. 4g), respectively [137-139]. A variety of structural types exhibited by tetranuclear systems namely metallocrowns, linear arrays, cubanes and defective cubanes [140-142]. Also, unprecedented azido coordination modes like $\mu_{1,1,3,3}\text{-N}_3$ (Fig. 4i) and $\mu_{1,1,1,3,3,3}\text{-N}_3$ (Fig. 4j) have been reported [143].

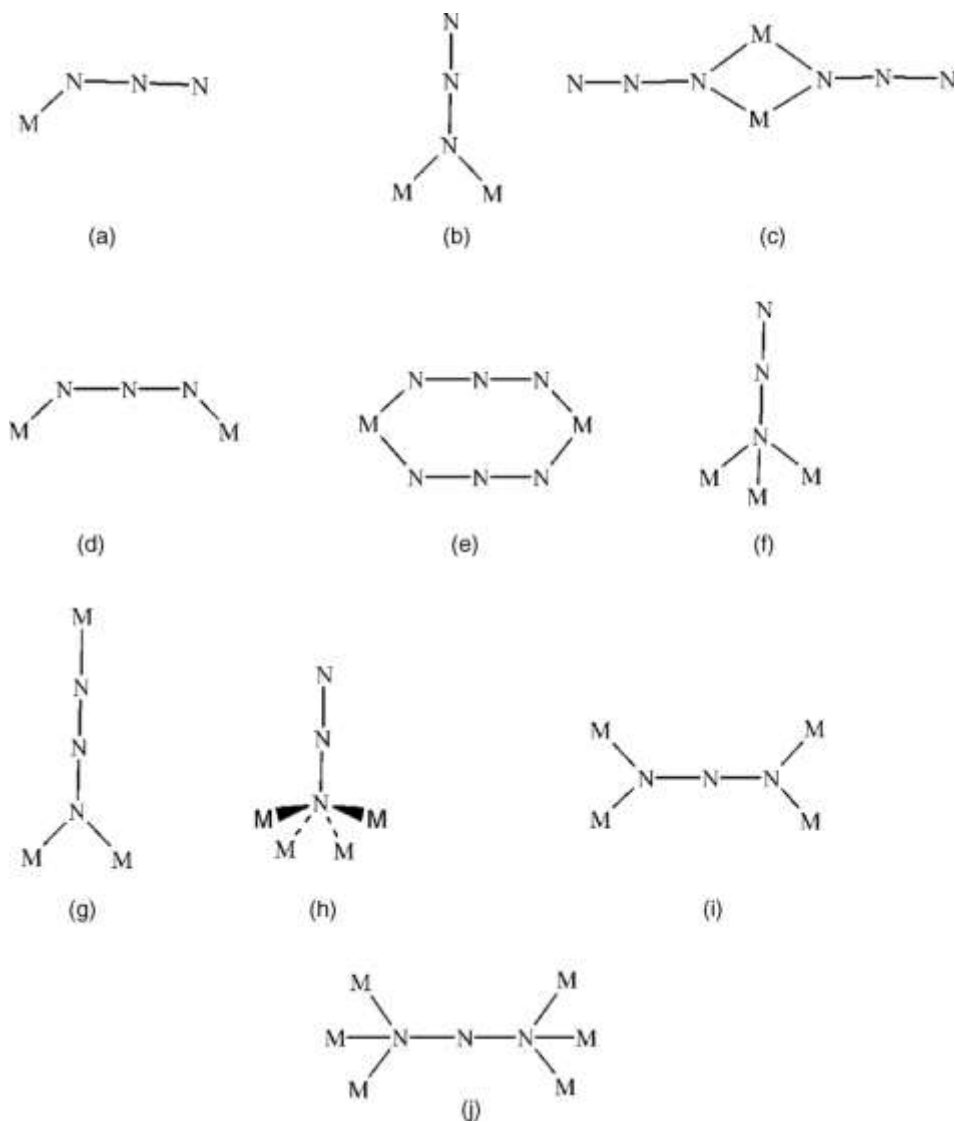


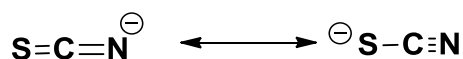
Fig. 4.1. Different coordination modes of azide ion

Degree of coordination of azide ion depends on the requirement of the complex as a whole. In binuclear complexes, the factors influencing whether the azide coordinates as an *end-on* bridge to form a four membered ring or *end-to-end* bridge to form an eight membered ring are not fully understood. When the N_3^- anion acts as bridging ligand, normally the *end-to-end* 1,3-coordination mode gives

antiferromagnetic coupling, while the *end-on* 1,1-mode gives ferromagnetic coupling, but for very large M– $\mu_{1,3}$ -N₃–M bond angles the magnetic coupling may be reversed [144]. We have interested in a box dimer complex in which azide coordinate as double *end-on* bridge to form a complex with short metal-metal bond.

4.1.1.2. Thiocyanate anion

Thiocyanate is a linear ambidentate ligand capable of forming a wide variety of complexes having 1-D, 2-D and 3-D polymeric structures [145,146]. It shares its negative charge approximately equally between nitrogen and sulfur and it is analogues to cyanate ion, OCN⁻. Resonance structure of thiocyanate ion is given below.



Thiocyanate can act as terminal or bridging ligand. For the SCN⁻ anion the bridging mode usually involves a 1,3-coordination mode with both nitrogen and sulfur atom bound to the metal ions. In the recent years, the study of polynuclear Cu(II) complexes of thiocyanate have obtained considerable attention.

4.2. Experimental

4.2.1. Materials

Copper(II) chloride dihydrate, nickel perchlorate hexahydrate, NaN₃ and KSCN were purchased from Sigma-Aldrich. All the reagents and solvents used were of Analar grade and were used as received.

Caution! Azido compounds are potentially explosive. Although no problems were encountered in the present study, it should be prepared only in small quantities and handled with care.

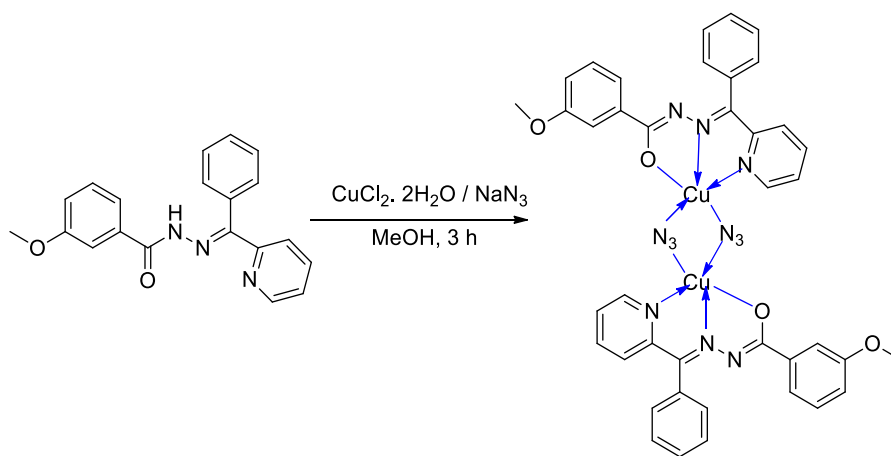
4.2.2. Syntheses of azide bridged complexes

4.2.2.1. Synthesis of [Cu(bpm)N₃]₂ (**4**)

Copper chloride dihydrate (0.170 g, 1 mmol) dissolved in methanol was added to a methanolic solution of aroylhydrazone, Hbpm (0.331 g, 1 mmol). The mixture was refluxed for three hours. To the resulting green solution, sodium azide (0.130 g, 2 mmol) in hot methanol was added. Slow evaporation of the solution yielded green needle shaped crystals and were separated, washed with ether and dried over P₄O₁₀ *in vacuo* (Scheme 4.1) [20].

For [Cu(bpm)N₃]₂ (**4**) Yield: 79% (0.688 g). Color: Green. Anal. Calc. for C₄₀H₃₂Cu₂N₁₂O₄ (M.W.: 871.85 g mol⁻¹) C, 55.10; H, 3.70; N, 19.28%. Found: C, 55.43; H, 3.43; N, 19.28%.

λ_M (DMF): 3 mho cm² mol⁻¹.



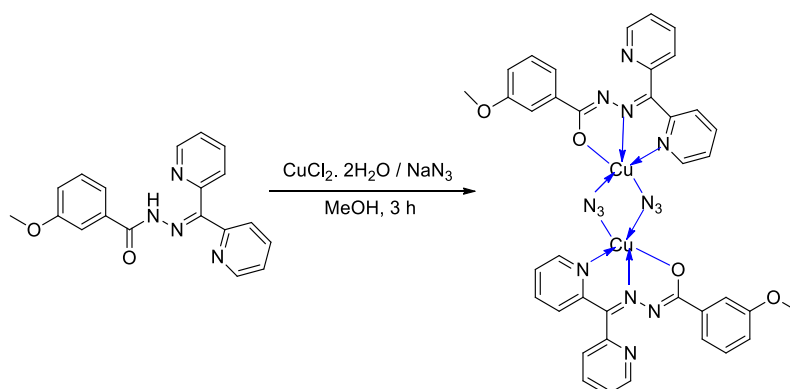
Scheme 4.1. Synthesis of [Cu(bpm)N₃]₂ (**4**).

4.2.2.2. Synthesis of [Cu(dkm)N₃]₂ (5)

[Cu(dkm)N₃]₂ (5) was prepared by the addition of the methanolic solutions of NaN₃ (0.130 g, 2 mmol), to the reaction mixture of Hdkm (0.332 g, 1 mmol) and copper chloride dihydrate (0.170 g, 1 mmol) in methanol. The resulting solution was refluxed for 3 hours and left overnight. The dark green solid was collected and recrystallized from DMF within one week and dried over P₄O₁₀ *in vacuo* (Scheme 4.2).

For [Cu(dkm)N₃]₂ (5) Yield: 74% (0.646 g). Color: Green. Anal. Calc. for C₃₈H₃₀Cu₂N₁₄O₄ (M.W.: 873.86 g mol⁻¹) C, 52.23; H, 3.46; N, 22.44%. Found: C, 52.25; H, 3.43; N, 22.48%.

λ_M (DMF): 6 mho cm² mol⁻¹.



Scheme 4.2. Synthesis of [Cu(dkm)N₃]₂ (5).

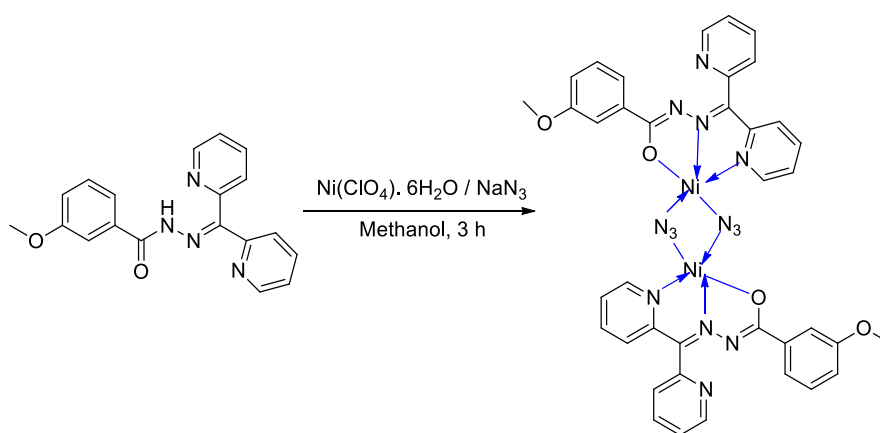
4.2.2.3. Synthesis of [Ni(dkm)N₃]₂ (6)

[Ni(dkm)N₃]₂ (6) was prepared by the addition of the methanolic solutions of NaN₃ (0.130 g, 2 mmol), to the reaction mixture of Hdkm (0.332 g, 1 mmol) and nickel(II) perchlorate hexahydrate (0.365 g, 1 mmol) in methanol. The resulting solution was refluxed for 3 hours and left overnight. The dark green precipitate

was collected and recrystallized from DMF within ten days and dried over P_4O_{10} *in vacuo* (Scheme 4.3).

For $[Ni(dkm)N_3]_2$ (**6**) Yield: 76% (0.656 g). Color: Green. Anal. Calc. for $C_{38}H_{30}Cu_2N_{14}O_4$ (M.W.: $864.14 \text{ g mol}^{-1}$) C, 52.82; H, 3.50; N, 22.69%. Found: C, 52.85; H, 3.53; N, 22.658%.

λ_M (DMF): $8 \text{ mho cm}^2 \text{ mol}^{-1}$.



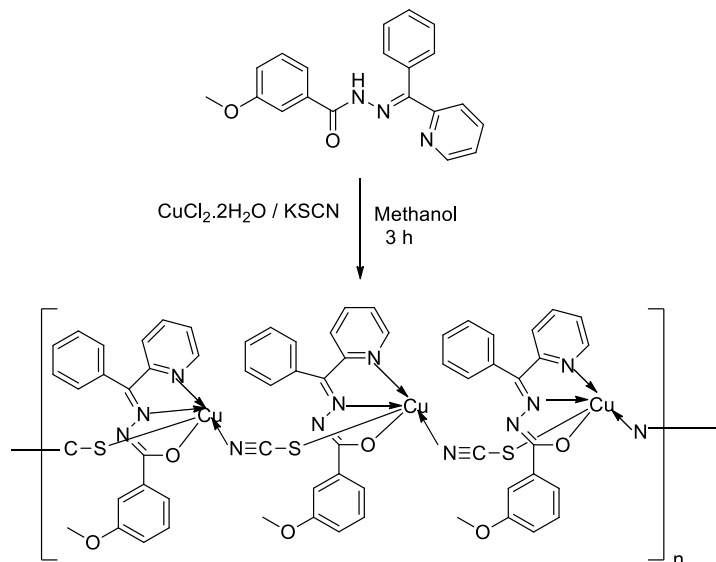
Scheme 4.3. Synthesis of $[Ni(dkm)N_3]_2$ (**6**).

4.2.2.4. Synthesis of $[Cu(bpm)NCS]_n$ (**7**)

Methanolic solutions of KSCN (0.198 g, 2 mmol) was added to the reaction mixture of Hbpm (0.331 g, 1 mmol) and copper(II) chloride dihydrate (0.170 g, 1 mmol) in methanol. The resulting solution was refluxed for 3 hours and left overnight. The green needle crystals obtained were separated and dried over P_4O_{10} *in vacuo* (Scheme 4.4).

For $[Cu(bpm)NCS]_n$ (**7**) Yield: 76% (0.343 g). Color: Green. Anal. Calc. for $C_{21}H_{16}CuN_4O_2S$ (M.W.: $451.99 \text{ g mol}^{-1}$) C, 55.80; H, 3.57; N, 12.40%. Found: C, 55.85; H, 3.54; N, 12.458%.

λ_M (DMF): $13 \text{ mho cm}^2 \text{ mol}^{-1}$.



Scheme 4.4. Synthesis of $[\text{Cu}(\text{bpm})\text{NCS}]_n$ (**7**).

4.3. Results and discussion

4.3.1. Infrared spectra

The most important IR spectral bands along with their tentative assignments are listed in Table 4.1. and the spectra are shown in Fig. 4.1- 4.4. Spectra of pseudohalide bridged complexes are compared with that of the respective ligands to monitor the changes on complexation. Free ligands Hbpm and Hdkm show characteristic C=O band at 1682 and 1690 cm^{-1} respectively which are absent in the complexes and the presence of new band in the region 1366-1370 cm^{-1} shows the coordination *via* iminolate form. A band observed in the 3058-3063 cm^{-1} region in free ligands has been disappeared and a new C=N band appeared on complexation.

Azide bridged box dimer complexes **4-6** showed characteristic sharp band due to asymmetric bridging mode of azido anion at 2050, 2045 and 2046 cm^{-1} respectively [20,147,148]. The thiocyanato bridged polymer complex **7** showed a

sharp single peak at 2109 cm^{-1} , which characterizes the presence of bridging SCN^- anion, bridging $[\text{M}-\text{NCS}-\text{M}']$ complexes exhibits $\nu(\text{CN})$ well above 2100 cm^{-1} [21,149-153].

Table 4.1. IR spectra of Hbpm, Hdkm and its complexes in cm^{-1}

Compound	$\nu(\text{N-H})$	$\nu(\text{C=O})/$ $\nu(\text{C-O})$	$\nu(\text{C=N})$	$\nu(\text{C=N})^a$	$\nu(\text{N}_3)/$ $\nu(\text{SCN})$
Hbpm	3063	1682	1589	---	---
Hdkm	3058	1690	1602	---	---
$[\text{Cu}(\text{bpm})\text{N}_3]_2$ (4)	---	1366	1593	1559	2050
$[\text{Cu}(\text{dkm})\text{N}_3]_2$ (5)	---	1366	1590	1562	2045
$[\text{Ni}(\text{dkm})\text{N}_3]_2$ (6)	---	1366	1590	1557	2046
$[\text{Cu}(\text{bpm})\text{NCS}]_n$ (7)	---	1624	1594	1562	2109

^a newly formed C=N bond

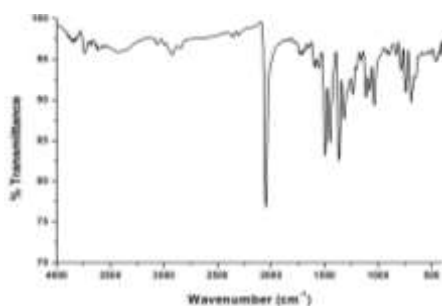


Fig. 4.1. IR spectrum of complex 4.

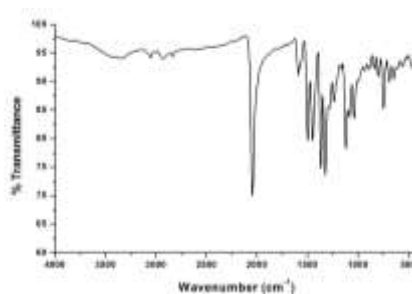


Fig. 4.2. IR spectrum of complex 5.

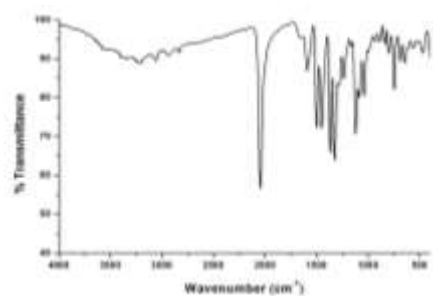


Fig. 4.3. IR spectrum of complex 6.

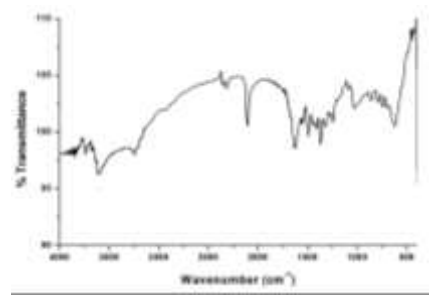


Fig. 4.4. IR spectrum of complex 7.

4.3.2. Electronic spectra

Electronic spectra of the compounds were taken in DMF solution (1×10^{-5} M) at room temperature. For obtaining *d-d* bands of the copper(II) and nickel(II) complexes, spectra were recorded in 10^{-3} M solution. The λ_{max} (nm) values of complexes **4-7** were tabulated in Table 4.2 and the spectra were shown in Fig. 4.5-4.8. For all the compounds intraligand transitions were observed in the range 255–344 nm which can be assigned to $\pi \rightarrow \pi^*$ and $n \rightarrow \pi^*$ transitions. Charge transfer bands for all the compounds were found in the 399-401 nm region. The appearance of band in the vicinity of 400 nm for complexes **4-6** should be considered as $\mu_{-1,1} \text{N}_3^- \rightarrow \text{M(II)}$ charge transfer transitions [11,154]. Also complex **7** showed LMCT band at 401 nm. The *d-d* bands for Cu(II) complexes were observed as broad bands in the 644-648 nm range which is characteristic of Cu(II) complexes with square pyramidal geometry consistent with SCXRD analysis. This was due to the single electron residing in the $d_{x^2-y^2}$ ground state. Also complex [Ni(bpm)N₃]₂ (**6**) showed *d-d* band near 690 nm.

Table 4.2. Electronic spectral assignments, λ_{max} (nm) (ϵ , $\text{M}^{-1} \text{cm}^{-1}$) of complexes **4-7**

Compound	<i>d-d</i>	LMCT	Intraligand transitions
[Cu(bpm)N ₃] ₂ (4)	646 (470)	399 (21800)	273 (65670)
[Cu(dkm)N ₃] ₂ (5)	648 (230)	398 (53620)	275 (70100)
[Ni(bpm)N ₃] ₂ (6)	645 (230)	398 (48160)	344 (99520)
[Cu(bpm)NCS] _n (7)	672 (180)	400 (63330)	275 (79830)

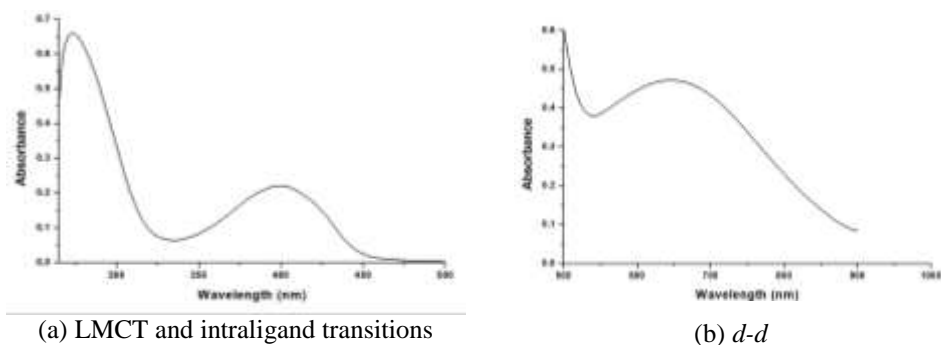


Fig. 4.5. Electronic spectra of complex 4.

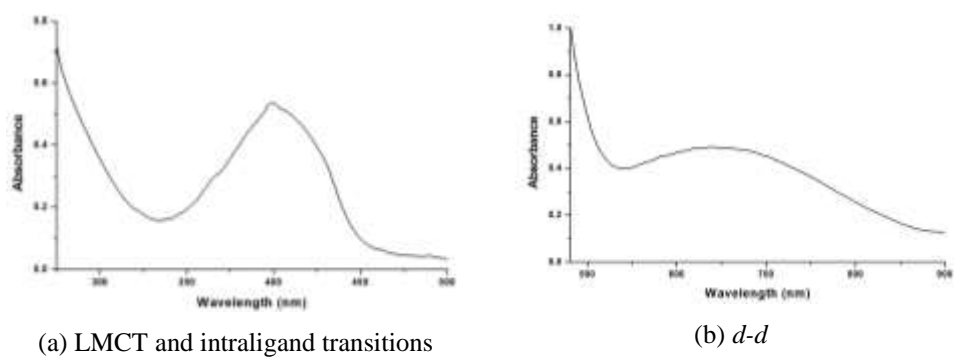


Fig. 4.6. Electronic spectra of complex 5.

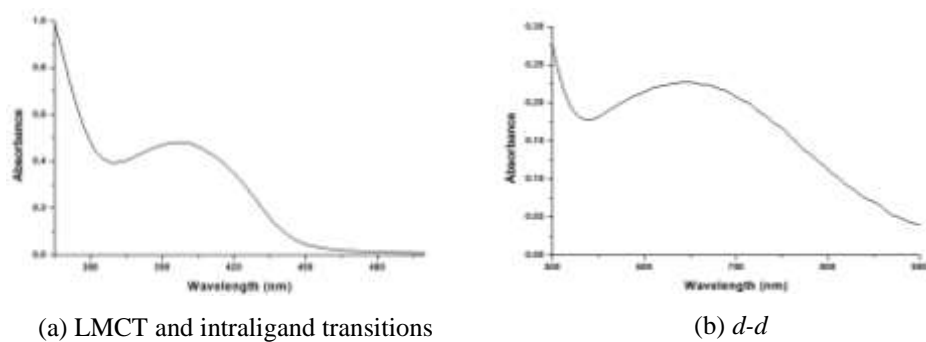


Fig. 4.7. Electronic spectra of complex 6.

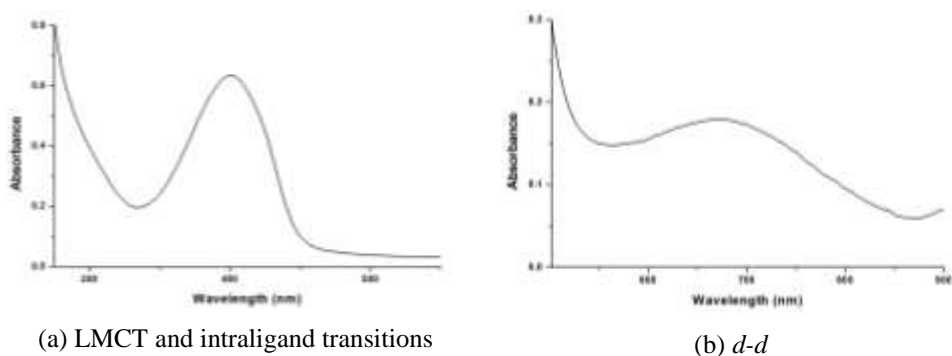


Fig. 4.8. Electronic spectra of complex **7**.

4.3.3. Electron paramagnetic resonance spectra

EPR spectra gave an information about the geometry and electronic environment of paramagnetic metal(II) complexes. The power of EPR lies in the fact that in a way similar to NMR it can yield direct structural information at microscopic and macroscopic scales. Often, information unavailable from other spectroscopies, such as X-ray or molecular spectroscopy, can be obtained directly from EPR.

The EPR spectra of the complexes in the polycrystalline state at 298 K and in DMF solution at 77 K were recorded in X band using an ESR-JEOL spectrometer. All the EPR spectra were simulated using the EasySpin 5.0.20 package [66] and the experimental (red) and simulated (blue) best fits are included. The EPR spectral and bonding parameters of the copper(II) complexes are listed in Table 4.3. In the solid state, variation in the g_{\parallel} and g_{\perp} values indicate that the geometry of the compounds is affected by the nature of the coordinating ligands. The EPR spectra of the complexes in DMF solution at 77 K gave more information on the geometry of these complexes.

Table 4.3. Spin Hamiltonian and bonding parameters of copper(II) complexes **4**, **5** and **7**

Parameters	4	5	7
Polycrystalline state at 298 K			
g_{\parallel}	2.133	2.225	2.20
g_{\perp}	2.035	2.050	2.039
g_{iso}	2.0676	2.1083	2.0927
G	3.9969	4.6688	5.3869
DMF solution (77 K)			
g_{\parallel}	2.36	2.256	2.265
g_{\perp}	2.14	2.06	2.06
g_{avg}	2.2133	2.1253	2.1266
A_{\parallel}	227	189.5	199
A_{\perp}	-	-	-
α^2	1.0865	0.8453	0.8816
β^2	0.8415	0.9095	0.8714
γ^2	1.0442	0.8454	0.8582
K_{\parallel}	0.9143	0.7688	0.7682
K_{\perp}	1.1345	0.7459	0.7566
f	104	119	113

A values in 10^{-4} cm^{-1}

The spectrum of complex $[\text{Cu}(\text{bpm})\text{N}_3]_2$ (**4**) in polycrystalline state at 298 K displayed an axial features with $g_{\parallel} = 2.133$ and $g_{\perp} = 2.035$. In DMF solution at 77 K, it showed an axial spectrum with well resolved hyperfine lines in the parallel region with $g_{\parallel} = 2.36$ and $g_{\perp} = 2.14$ (Fig.4.9). As $g_{\parallel} > g_{\perp} > 2.0023$, a square pyramidal geometry can be assigned and rules out the possibility of a trigonal bipyramidal structure which would be expected to have $g_{\perp} > g_{\parallel}$ [155,156].

Complexes **5** and **7** show axial spectra in polycrystalline state at 298 K with $g_{\parallel} = 2.225$ and $g_{\perp} = 2.050$ for complex **5** & $g_{\parallel} = 2.20$ and $g_{\perp} = 2.039$ for complex **7** respectively. Also in DMF solution at 77 K both complexes **5** and **7** display axial spectra with hyperfine lines in the parallel region but no hyperfine lines in the perpendicular region (Figs. 4.10 & 4.11) [157,158].

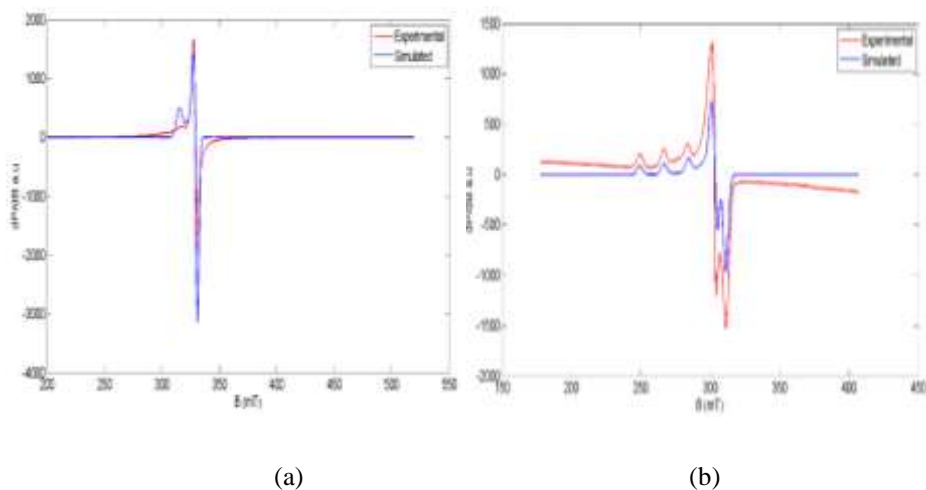


Fig. 4.9. EPR spectra of complex **4** in (a) polycrystalline state at 298 K and (b) DMF solution at 77 K.

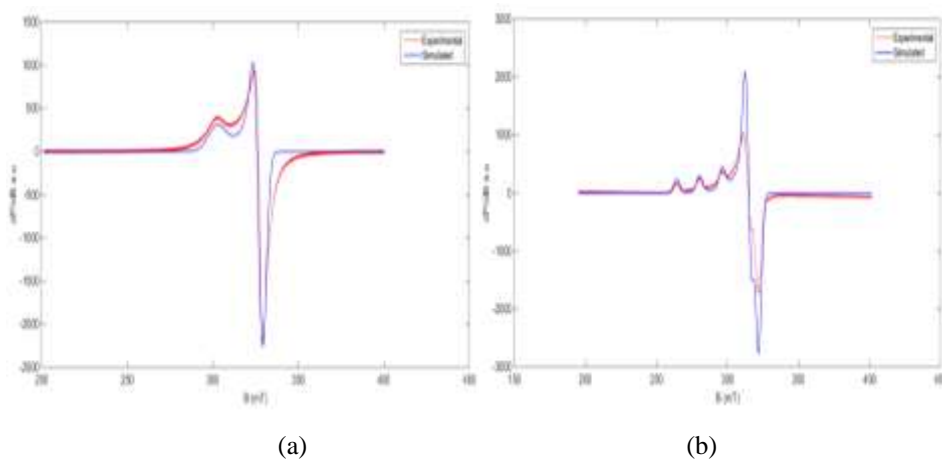


Fig. 4.10. EPR spectra of complex **5** in (a) polycrystalline state at 298 K and (b) DMF solution at 77 K.

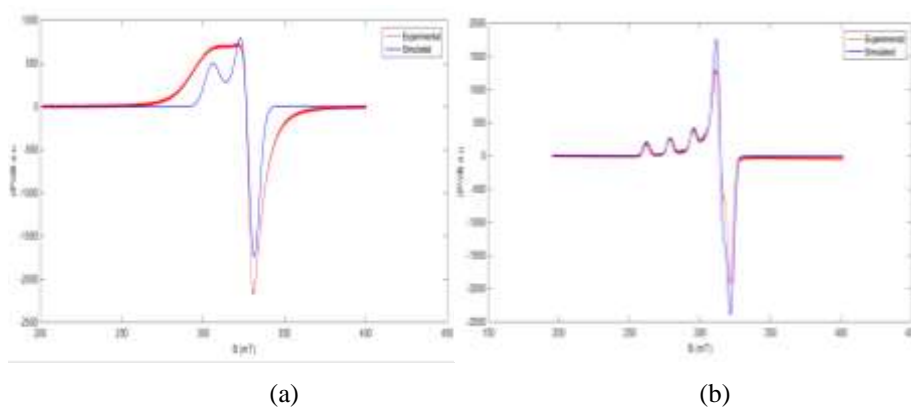


Fig. 4.11. EPR spectra of complex **7** in (a) polycrystalline state at 298 K and (b) DMF solution at 77 K.

For axial spectra [15], the geometric parameter G was calculated by the equation $G = (g_{\parallel} - 2.0023)/(g_{\perp} - 2.0023)$ and G represents the exchange interaction between copper(II) centers in the solid polycrystalline complexes. Accordingly, if G is greater than 4, the exchange interaction may be negligible; however, if G is less than 4, a considerable exchange interaction is indicated in the solid complex. For complex **4**, G value is slightly less than 4 indicating the presence of exchange interaction. The high value of G for complex **7** showed negligible exchange interaction.

The EPR parameters g_{\parallel} , g_{\perp} , A_{\parallel} and the energies of $d-d$ transitions were used to evaluate the bonding parameters α^2 , β^2 and γ^2 which may be regarded as measures of the covalency in the in-plane σ -bonds, in-plane π -bonds and out-of-plane π -bonds.

In-plane sigma bonding parameter α^2 was estimated from the expression [16]

$$\alpha^2 = -A_{\parallel} / 0.036 + (g_{\parallel} - 2.0023) + 3/7(g_{\perp} - 2.0023) + 0.04$$

The following simplified expression were used to calculate the bonding parameters

$$K_{\parallel}^2 = (g_{\parallel} - 2.0023) E_{d-d} / 8\lambda_0,$$

$$K_{\perp}^2 = (g_{\perp} - 2.0023) E_{d-d} / 2\lambda_0$$

$$K_{\parallel}^2 = \alpha^2 \beta^2$$

$$K_{\perp}^2 = \alpha^2 \gamma^2$$

where K_{\parallel} and K_{\perp} are orbital reduction factors and λ_0 represents the one electron spin orbit coupling constant.

Hathaway [17] has pointed out that $K_{\parallel} \approx K_{\perp} \approx 0.77$ for pure sigma bonding, $K_{\parallel} < K_{\perp}$ for in plane π -bonding and $K_{\perp} < K_{\parallel}$ for out-of-plane π -bonding. For complex **1**, it is observed that $K_{\parallel} < K_{\perp}$ shows significant in plane π -bonding. $K_{\perp} < K_{\parallel}$ for complex **2** indicates significant out-of-plane π -bonding in the complex [159]. By comparing the value of in-plane sigma bonding parameter α^2 , the nature of M-L bond is evaluated. The value of α^2 is unity, if the M-L bond is purely ionic and it is completely covalent, if $\alpha^2 = 0.5$. Here α^2 values calculated for complexes **5** and **7** lie between 0.5 and 1, it means that the complexes under study are partially ionic and partially covalent in nature.

The index of tetragonal distortion f is calculated as $f = g_{\parallel} / A_{\parallel}$, whose value may vary from 105 to 135 for small to medium distortion and depends on the nature of the coordinated atom. Small distortion was found in the case of compound **4** where f has a value of 103 and medium distortion for complex **5** ($f = 119$).

4.3.4. Hirshfeld Surface Analysis

Hirshfeld surface analysis have been done using Crystal explorer 17 software to analyse the presence of intermolecular interactions. Hirshfeld surfaces

for complexes **4**, **5**, **6** and **7** were mapped over d_{norm} (Fig. 4.12) and shape index function (Fig. 4.13). The d_{norm} surface is the normalized function of d_i and d_e , with white, red and blue coloured surfaces. Deep red points on the surfaces of these complexes indicate prominent hydrogen bonding interactions [160].

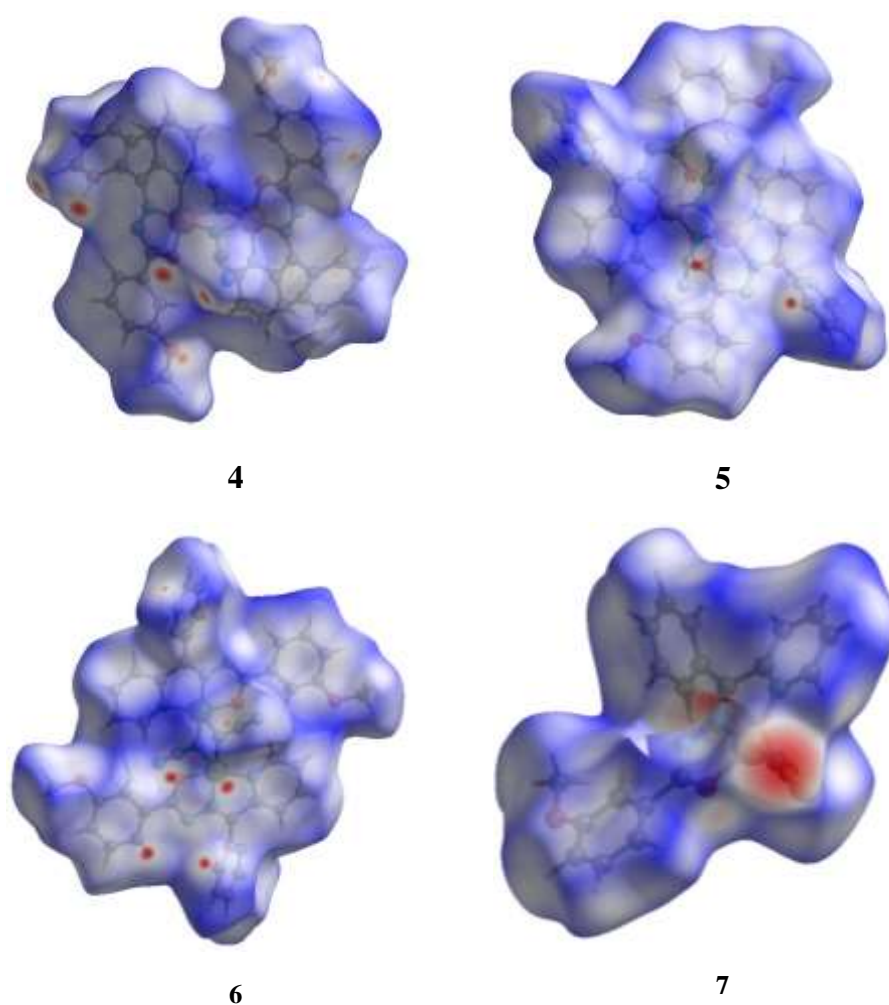


Fig. 4.12. Hirshfeld surfaces for complexes **4**, **5**, **6** and **7** mapped with d_{norm} .

The shape index plot of complexes **4-7** give a red concave region around the π acceptor atom a blue convex region around the donor H-atom [161].

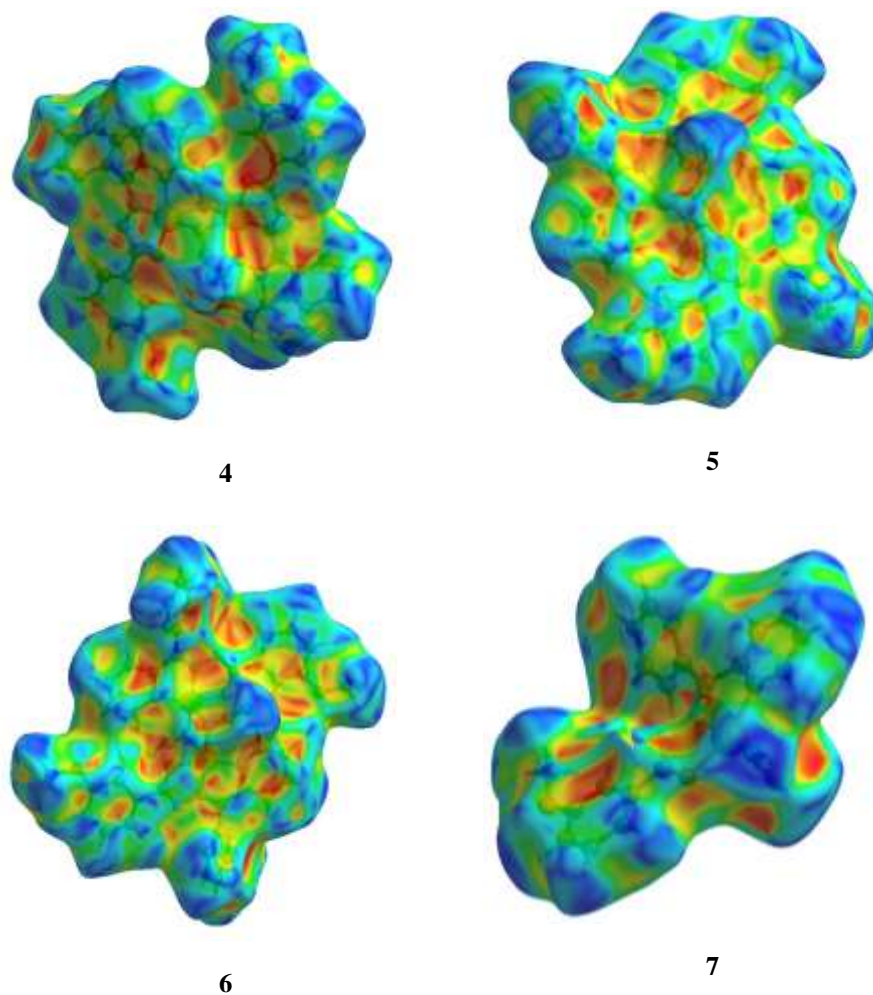


Fig. 4.13. Hirshfeld surfaces for complexes **4**, **5**, **6** and **7** mapped with shape index.

The intermolecular hydrogen bonding interactions in complexes **4**, **6** and **7** are visualized using Crystal explorer and also viewed with external molecule (Fig. 4.14).

From 2D fingerprint plot analysis, it is shown that all the complexes are dominated by H \cdots H interaction.

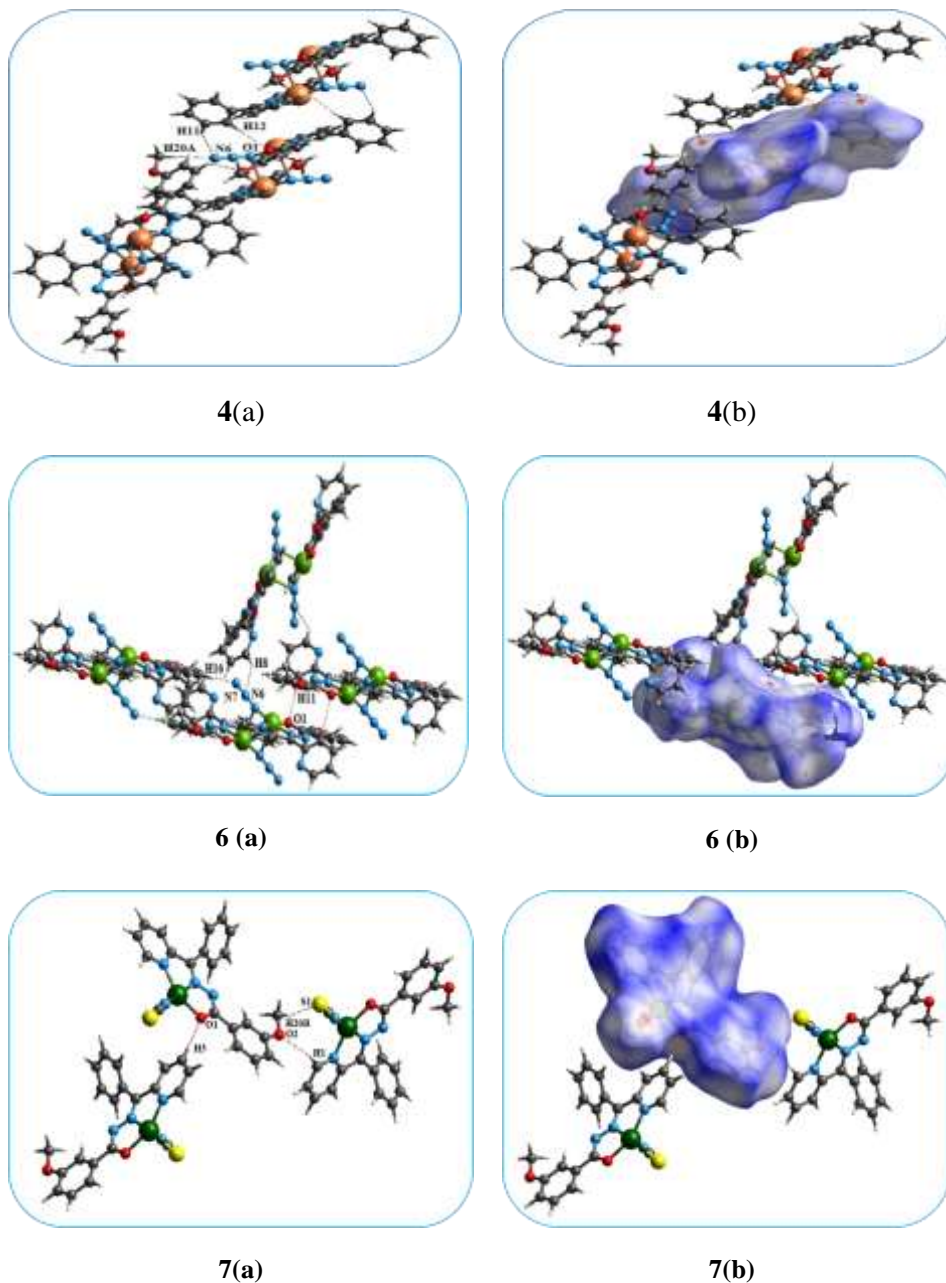


Fig. 4.14. (a) Intermolecular hydrogen bonding interactions present in **4**, **6** and **7**, (b) viewing the same short contacts in Hirshfeld surface with external molecules.

4.3.5. X-ray crystallography

Table 4.4. Crystal data and structural refinement parameters of [Cu(bpm)N₃]₂ (4) and [Cu(dkm)N₃]₂ (5).

Parameters	[Cu(bpm)N ₃] ₂ (4)	[Cu(dkm)N ₃] ₂ (5)
Empirical formula	C ₄₀ H ₃₂ Cu ₂ N ₁₂ O ₄	C ₃₈ H ₃₀ Cu ₂ N ₁₄ O ₄
Formula weight	871.88	873.86
Color	Green	Green
Crystal system	Monoclinic	Monoclinic
Space group	<i>P</i> 2 ₁ / <i>n</i>	<i>P</i> 2 ₁ / <i>n</i>
Cell parameters		
a (Å)	8.9943(5)	9.5946(9)
b (Å)	19.5918(13)	9.0226(7)
c (Å)	10.8382(8)	21.746(2)
α (°)	90	90
β (°)	98.305(2)	98.763(4)
γ (°)	90	90
Volume V (Å ³), Z	1889.8(2), 2	1860.6(3), 2
Calculated density (ρ) (Mg m ⁻³)	1.532	1.560
Absorption coefficient, μ (mm ⁻¹)	1.186	1.206
F(000)	892	892
Crystal size mm ³	0.30 x 0.20 x 0.20	0.30 x 0.20 x 0.20
θ (°) range for data collection	2.514 to 28.340	2.948 to 28.324
Limiting indices	-12 ≤ h ≤ 7 -26 ≤ k ≤ 25 -14 ≤ l ≤ 14	-12 ≤ h ≤ 12 -12 ≤ k ≤ 7 -28 ≤ l ≤ 26
Reflections collected	15287	14939
Unique Reflections (R _{int})	4709 (0.0331)	4635 (0.0276)
Completeness to θ	25.242 99.8%	25.242 99.9%
Absorption correction	Semi-empirical from equivalents	Semi-empirical from equivalents
Maximum and minimum transmission	0.784 and 0.750	0.521 and 0.391
Refinement method	Full-matrix least-squares on F ²	Full-matrix least-squares on F ²
Data / restraints / parameters	4595 / 0 / 264	4541 / 0 / 263
Goodness-of-fit on F ²	0.916	0.762
Final R indices [I > 2σ (I)]	R ₁ = 0.0342, wR ₂ = 0.0999	R ₁ = 0.0332, wR ₂ = 0.0985
R indices (all data)	R ₁ = 0.0497, wR ₂ = 0.1127	R ₁ = 0.0483, wR ₂ = 0.1139
Largest difference peak and hole (e Å ⁻³)	0.426 and -0.253	0.312 and -0.333

$$R_1 = \frac{\sum ||F_o| - |F_c||}{\sum |F_o|}$$

$$wR_2 = \frac{[\sum w(F_o^2 - F_c^2)^2]}{\sum w(F_o^2)^2}^{1/2}$$

4.3.5.1. General features in the crystal structures of [Cu(bpm)N₃]₂ (**4**) and [Cu(dkm)N₃]₂ (**5**)

Compounds **4** and **5** are azide bridged box dimer copper(II) complexes crystallized in the monoclinic, *P*2₁/*n* space group. The asymmetric unit is formed by one half of the molecule and the other half is related by a centre of inversion in the Cu1–N4–Cu1^a–N4^a/Cu1–N5–Cu1^a–N5^a ring resulting in a centrosymmetric closely associated crystallographically equivalent molecules bridged *via* nitrogen atoms. Crystal data and structure refinement parameters of complexes [Cu(bpm)N₃]₂ (**4**) and [Cu(dkm)N₃]₂ (**5**) are given in Table 4.4. The molecular structures are presented in Figures 4.15 and 4.16 along with the atom numbering scheme and selected bond lengths (Å) and bond angles (°) are shown in Table 4.5.

X-ray diffraction study revealed that they are centrosymmetric dimers in which the central copper(II) atom has a pentacoordinated geometry. The coordination modes are satisfied by tridentate monoanionic aroylhydrazone ligand using its azomethine nitrogen N2 in **4** and N3 in **5**, enolate oxygen O1 and pyridyl nitrogen N1 and two azido anions. Both azido anions are *end-on* bridging with the metal atom and this leads to a smaller Cu...Cu non-bonding distance of 3.242(4) Å (complex **4**) and 3.1979(5) Å (complex **5**) compared with the distances in halide bridged complexes **1** (3.369 Å) and **2** (3.436 Å) already discussed in Chapter 3. The bridging pseudohalide is quasi-linear with N–N–N angle of 175.53 in **4** and 177.2° in **5** and are asymmetric with respect to its basal-apical bond lengths. Basal-apical bond lengths are 1.975/2.516 Å in **4** and 1.958/2.417 Å in **5** and a metalloplane (Cu₂N₂) is formed due to di-μ_{1,1}-azido bridging results in a parallelogram with angle summation of 360°. Therefore the mode of *end-on* azido bridging is asymmetric in terms of the coordination position it occupies [20,162]. This is one of the consequences of Jahn-Teller distortion in a d⁹ copper (II) system. The bond distances in the azido complex **4** follow the order metal-axial azido nitrogen (2.516 Å) > metal-pyridyl nitrogen (2.009 Å) > metal-enolate oxygen

(1.945 Å) = metal-equatorial azido nitrogen (1.945 Å) > metal-azomethine nitrogen (1.932 Å). Complex **5** follows the similar order except metal-enolate oxygen distance is greater than the metal-equatorial azido nitrogen distance.

4.3.5.2. Crystal structure of [Cu(bpm)N₃]₂ (**4**)

Green single crystals of complex **4** suitable for SCXRD was obtained by the slow evaporation of mother liquor. N1, N2 and O1 atoms of aroylhydrazone and N4 atom of bridging azide occupied the basal plane of the square pyramid. The other azide atom N4^a of adjacent monomer occupies the axial position. The metal centre deviates from the least squares plane by a distance of 0.0489 Å towards the axial N4^a atom and the azomethine nitrogen N2 deviates the most (0.0108 Å) amongst other donor atoms from the plane. The chelate bite angles around the copper centre summate to 395.86 ° reveal the magnitude of distortion from the square pyramidal geometry. Addison parameter calculations gave a τ value 0.27 which highlight the distorted square pyramidal geometry [163] and also substantiated by the bond angles around the central copper(II) metal with the coordinating atoms. As a result of complexation, two fused five-membered metallocycles Cg(2) (Cu1, O1, C13, N3 and N2) and Cg(3) (Cu1, N1, C5, C6 and N2) are formed.

Ring puckering analysis [164] shows that two pairs of fused five-membered chelate rings Cg(2) and Cg(3) around the copper(II) centre are puckered. Cg(2) develops an envelope conformation [165] with puckering parameters $Q(2) = 0.0833(14)$ Å and $\psi(2) = 352.7(13)$. Metallocycle Cg(3) is twisted on C6–N2 with puckering parameters $Q(2) = 0.0885(19)$ and $\psi(2) = 132.0(13)$. The puckering is also calculated by pseudorotation parameters P and τ [166] and it was found that $P = 153.2(11)^\circ$, $\tau(m) = 7.4(1)^\circ$ for reference bond Cu1–O1 for Cg(2) and $P = 284.8(6)^\circ$, $\tau(m) = 10.4(1)^\circ$ for reference bond Cu1–N1 for Cg(3).

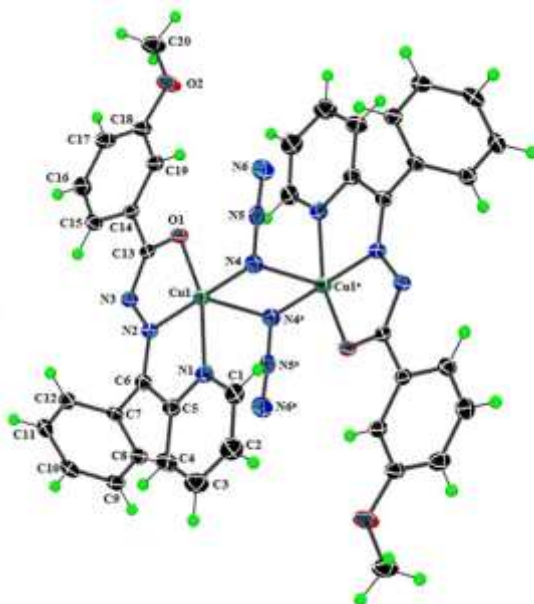


Fig. 4.15. ORTEP plot (drawn with 30% thermal ellipsoid) of $[\text{Cu}(\text{bpm})\text{N}_3]_2$ (**4**) along with atom numbering scheme of non-hydrogen atoms.

4.3.5.3. Crystal structure of $[\text{Cu}(\text{dkm})\text{N}_3]_2$ (**5**)

Crystal structure of complex **5** is too similar to that of complex **4**. Complex **5** gave a τ value of 0.17 which highlight the distortion from the perfect square pyramidal geometry. The atoms N1, N3 and O1 of aroylhydrazone and N5 atom of azide define a square plane of the distorted square planar geometry in which the axial position is satisfied by the N5^a atom of the nearby unit *via* $\mu_{1,1}$ -bridging. Also the Cu(II) atom displaced by 0.1062 Å from the square plane. Selected bond lengths (Å) and bond angles (°) are given in Table 4.5.

The crystal packing in complex **4** is supported by hydrogen bonding, weak N–N $\cdots\pi$ and $\pi\cdots\pi$ stacking interactions.

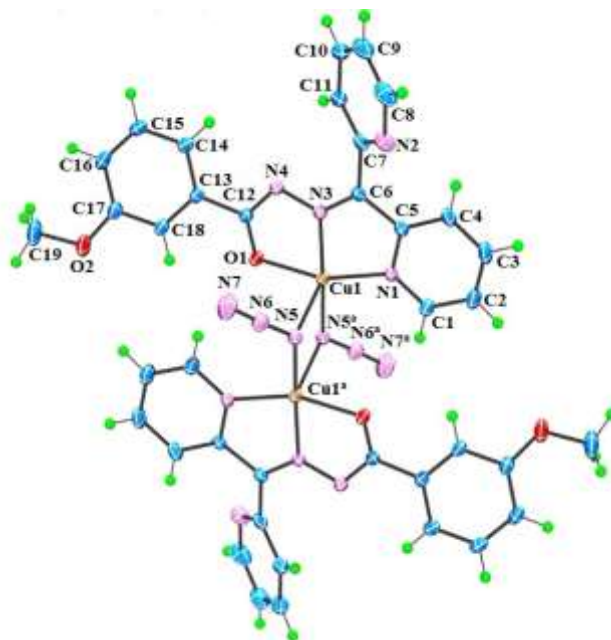


Fig. 4.16. ORTEP plot (drawn with 30% thermal ellipsoid) of [Cu(dkm)N₃]₂ (**5**) along with atom numbering scheme of non-hydrogen atoms.

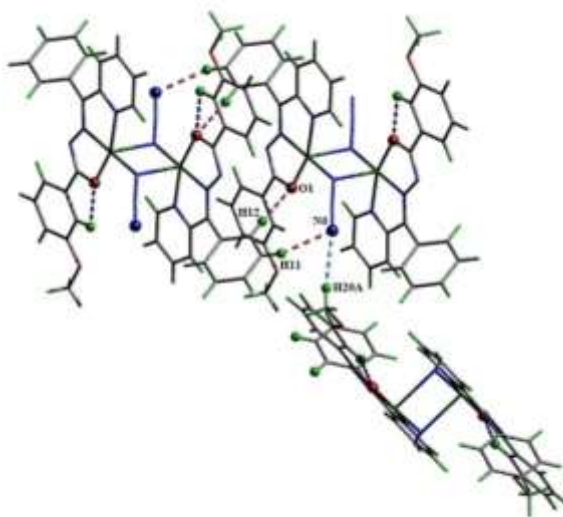


Fig. 4.17. Hydrogen bonding interaction (dashed lines) in complex **4**.

Table 4.5. Selected bond lengths and bond angles of **4** and **5**

[Cu(bpm)N ₃] ₂ (4)		[Cu(dkm)N ₃] ₂ (5)	
Bond lengths (Å)			
N1–Cu1	2.009(18)	N1–Cu1	2.017(18)
N2–Cu1	1.932(18)	N3–Cu1	1.938(17)
O1–Cu1	1.946(14)	O1–Cu1	1.985(15)
N4–Cu1	1.945(19)	N5–Cu1	1.959(19)
N4 ^a –Cu1	2.516(19)	N5 ^a –Cu1	2.417(19)
N4–N5	1.198(3)	N5–N6	1.197(3)
N5–N6	1.141(3)	N6–N7	1.146(3)
C13–N3	1.331(3)	C12–N4	1.336(3)
C13–O1	1.288(3)	C12–O1	1.285(2)
Bond angles (°)			
N2–Cu1–O1	80.46(6)	N3–Cu1–O1	79.50(7)
N2–Cu1–N4	177.13(7)	N3–Cu1–N5	170.14(8)
O1–Cu1–N4	101.12(7)	O1–Cu1–N5	95.30(7)
N2–Cu1–N1	80.56(7)	N3–Cu1–N1	80.30(7)
O1–Cu1–N1	160.78(7)	O1–Cu1–N1	159.66(7)
N4–Cu1–N1	97.72(7)	N5–Cu1–N1	104.33(8)
N4–Cu1–N4 ^a	87.69(7)	N5–Cu1–N5 ^a	86.67(7)
a = -x, -y, 1-z		a = 1-x, 2-y, -z	

Table 4.6 Hydrogen bonding interactions in [Cu(bpm)N₃]₂ (**4**) and [Cu(dkm)N₃]₂ (**5**)

Hydrogen bonding interactions				
D–H···A	D–H (Å)	H···A (Å)	D···A (Å)	∠D–H···A (°)
[Cu(bpm)N₃]₂ (4)				
C20–H20A···N6 ^a	0.96	2.67	3.623(4)	171
C11–H11···N6	0.93	2.58	3.392(4)	146
C12–H12···O1	0.93	2.53	3.433(3)	164
[Cu(dkm)N₃]₂ (5)				
C1–H1···N6	0.93	2.59	3.243(3)	127
C4–H4···N2	0.93	2.51	3.034(3)	116

Equivalent position codes: a = x+1/2, -y+1/2, z+1/2

D, Donor; A, acceptor; Cg, Centroid; α, dihedral angle between planes I & J; β, angle between Cg···Cg and Cg(J)perp.

A bifurcated, 3c-2e hydrogen bond is seen in the complex between an azido nitrogen N6 (acceptor) and H11 and H20A of carbon atoms C11 and C20 with D···A distances of 3.392(4) and 2.769 Å, respectively. Another interaction is between enolate oxygen O1 and H12 attached to carbon C12 (Fig. 4.18 & Table 4.6).

One N–N··· π interaction is observed between the five-membered Cg(3) ring and N(6) of an azido group with N···Cg distance of 3.284(3) Å (Fig. 4.18 & Table 4.7).

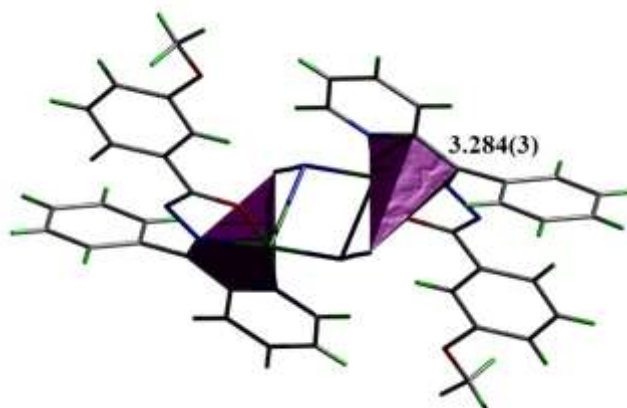


Fig. 4.18. Weak N–N··· π interaction in complex **4**.

Crystal packing in complex **4** is also stabilised by π ··· π stacking interactions. Face to face π interactions exist between the five membered metallocycles Cg(2) and also between six membered rings Cg(5) with slippage parameter of 1.604 and 1.332 Å respectively. Six membered aromatic ring Cg(6) interact both with Cg(3) and Cg(4) with Cg···Cg distance of 3.924(12) and 3.864(14) Å respectively. Four π ··· π stacking interactions in complex **4** are shown in Fig. 4.19 (Table 4.7).

Table 4.7. Non-bonding interactions in **4** and **5**

$\pi \cdots \pi$ interactions				
[Cu(bpm)N₃]₂ (4)				
Cg(I)⋯Cg(J)	Cg⋯Cg (Å)	α (°)	β (°)	γ (°)
Cg(2) Cg(2) ^a	3.7921(10)	0	25.02	25.02
Cg(3) Cg(6) ^a	3.9237(12)	9.48(10)	19.97	29.03
Cg(4) Cg(6) ^a	3.8638(14)	6.90(11)	19.31	21.42
Cg(5) Cg(5) ^b	3.6133(13)	0	21.63	21.63
[Cu(dkm)N₃]₂ (5)				
Cg(2)⋯Cg(2) ^c	3.9335(10)	0	32.24	32.24
Cg(3)⋯Cg(6) ^c	3.4644(12)	11.39(9)	2.16	13.51
Cg(6)⋯Cg(6) ^d	3.6076(13)	0	16.46	16.46
N–N⋯π interactions				
[Cu(bpm)N₃]₂ (4)				
Y–X(I)⋯Cg(J)	X⋯Cg (Å)	Y⋯Cg (Å)	\angleY–X⋯Cg (°)	
N5–N6⋯Cg(3) ^e	3.284(3)	2.991(2)	65.22(15)	
[Cu(dkm)N₃]₂ (5)				
N6–N7⋯Cg(2) ^f	3.645(3)	3.199(2)	58.49(15)	
C–H⋯π interactions				
[Cu(dkm)N₃]₂ (5)				
C–H(I)⋯Cg(J)	H⋯Cg (Å)	C⋯Cg (Å)	\angleC–H⋯Cg (°)	
C3–H3⋯Cg(5) ^g	2.89	3.640(3)	139	
Ring-metal interaction				
[Cu(dkm)N₃]₂ (5)				
Me(I)⋯Cg(J)	Me⋯Cg(Å)	Me(J)	β (°)	
Cu1⋯Cg(6) ^c	3.906	3.029	39.17	

Equivalent position codes: a = 2-x, -y, -z; b = 2-x, -y, 1-z; c = 1-x, 1-y, 2-z; d = -x, 1-y, 2-z; e = 1-x, -y, -z; f = 1-x, 2-y, 2-z; g = 3/2-x, 1/2+y, 3/2-z.

[Cu(bpm)N₃]₂ (**4**): Cg(2) = Cu1, O1, C13, N3, N2; Cg(3) = Cu1, N1, C5, C6, N2; Cg(4) = N1, C1, C2, C3, C4, C5; Cg(5) = C7, C8, C9, C10, C11, C12; Cg(6) = C14, C15, C16, C17, C18, C19.

[Cu(dkm)N₃]₂ (**5**): Cg(2) = Cu1, O1, C12, N4, N3; Cg(3) = Cu1, N1, C5, C6, N3; Cg(5) = N2, C7, C11, C10, C9, C8; Cg(6) = C13, C14, C15, C16, C17, C18.

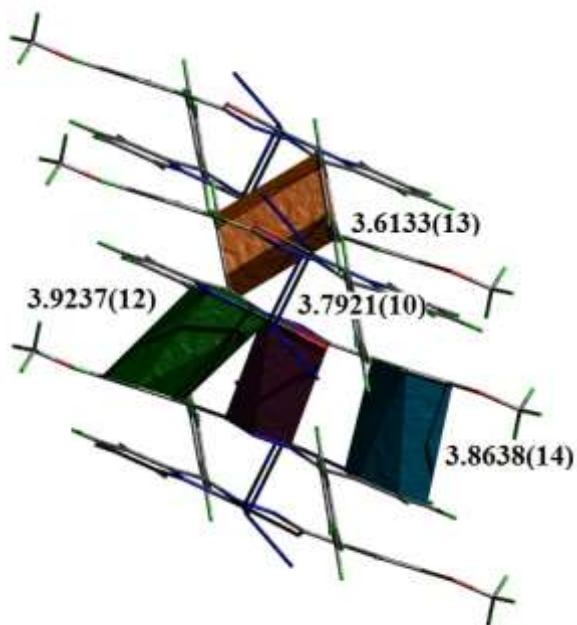


Fig. 4.19. The $\pi \cdots \pi$ interactions in complex **4**.

Diving into the hydrogen bonding interactions, we experience two intramolecular interactions in complex **5**. The hydrogen atoms H1 and H4 attached to carbon atoms C1 and C4 are involved in hydrogen bonding with azide nitrogen N6 and pyridyl nitrogen N2 with D \cdots A distances of 3.243(3) and 3.034(3) Å respectively (Fig. 4.20 & Table 4.6).

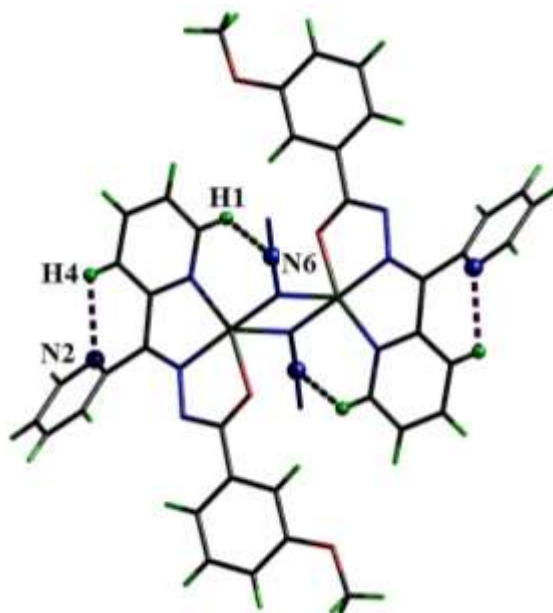


Fig. 4.20. Hydrogen bonding interaction (dashed lines) in complex **5**.

The C–H \cdots π interaction C3–H3 \cdots Cg(5) and metal \cdots π interaction Cu1 \cdots Cg(6) present in complex **5** are shown in Fig. 4.21 (a) & (b) (Table 4.7).

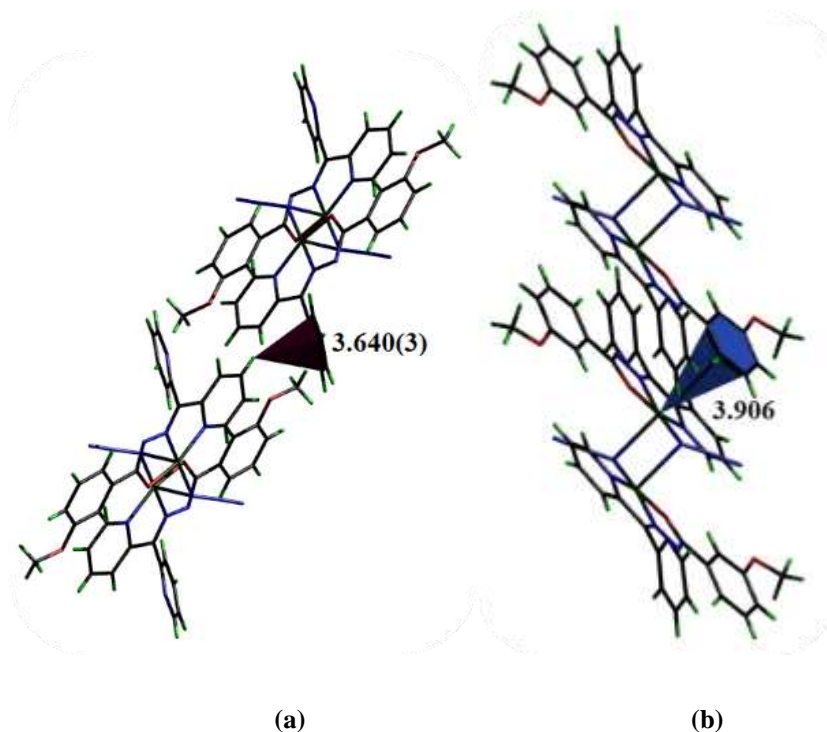


Fig. 4.21. (a) C–H $\cdots\pi$ and (b) metal $\cdots\pi$ interaction in complex **5**.

Five membered metallocycle Cg(2) (comprised of atoms Cu1, O1, C12, N4 and N3) interact face to face with each other and also with six membered aromatic ring Cg(6) (comprised of atoms C13, C14, C15, C16, C17 and C18) with Cg \cdots Cg distances of 3.934(10) and 3.608(13) respectively (Fig. 4.22 & Table 4.7).

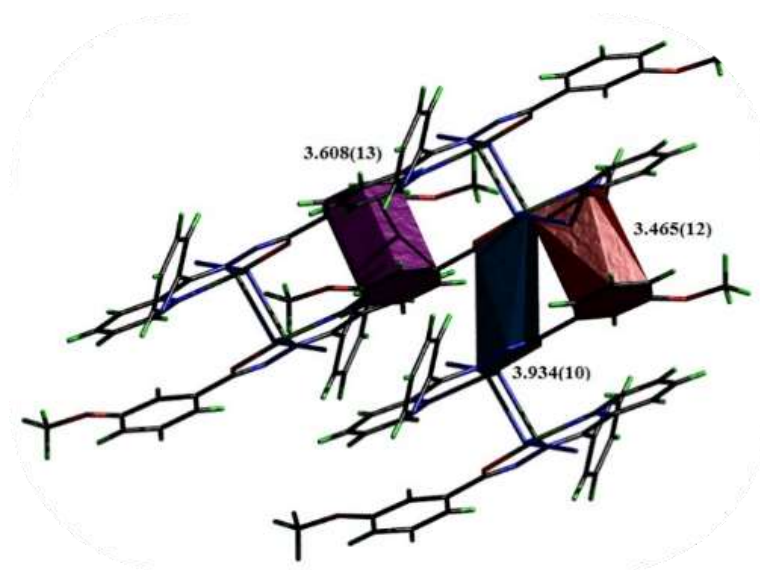


Fig. 4.22. The $\pi\cdots\pi$ interactions in complex **5**.

The N(7) atom of bridging azido group forming an intrachain interaction N(6)–N(7)··· π with N(7)··· π distance of 3.645(3) Å (Fig. 4.23 & Table 4.7).

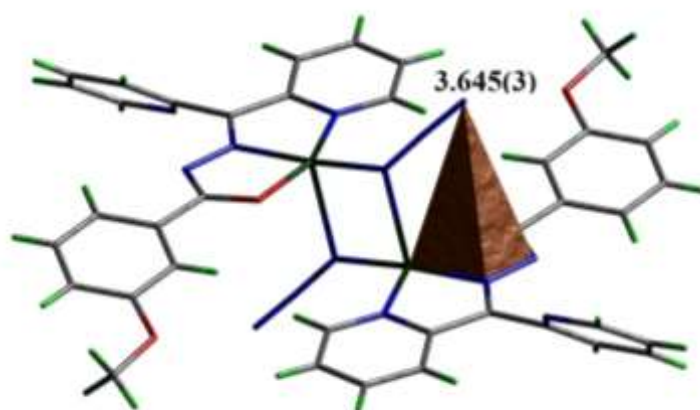


Fig. 4.23. The N–N··· π interaction in complex **5**.

4.3.5.4. Crystal structure of [Ni(dkm)N₃]₂ (6)**Table 4.8.** Crystal data and structural refinement parameters of [Cu(bpm)N₃]₂ (6) and [Cu(dkm)N₃]₂ (7)

Parameters	[Ni(dkm)N ₃] ₂ (6)	[Cu(bpm)NCS] _n (7)
Empirical formula	C ₃₈ H ₃₀ N ₁₄ Ni ₂ O ₄	C ₂₁ H ₁₆ CuN ₄ O ₂ S
Formula weight	864.14	451.98
Color	Green	Green
Crystal system	Monoclinic	Orthorhombic
Space group	<i>P</i> 2 ₁ / <i>n</i>	<i>P</i> <i>n</i> <i>a</i> 21
Cell parameters		
a (Å)	9.5695(10),	21.1308(15)
b (Å)	9.0296(9)	16.0989(14)
c (Å)	21.697(2)	5.6842(4)
α (°)	90	90
β (°)	99.094(4)	90
γ (°)	90	90
Volume V (Å ³), Z	1851.3(3), 2	1933.7(3), 4
Calculated density (ρ) (Mg m ⁻³)	1.550	1.553
Absorption coefficient, μ (mm ⁻¹)	1.080	1.263
F(000)	888	924
Crystal size mm ³	0.53 x 0.45 x 0.25	0.30 x 0.20 x 0.20
θ (°) range for data collection	2.950 to 33.308	2.708 to 28.404
Limiting indices	-14 ≤ h ≤ 12 -12 ≤ k ≤ 12 -33 ≤ l ≤ 29	-28 ≤ h ≤ 28 -21 ≤ k ≤ 18 -7 ≤ l ≤ 7
Reflections collected	39418	15306
Unique Reflections (R _{int})	7157 (0.0645)	4866 (0.0417)
Completeness to θ	25.242 98.6%	25.242 99.8%
Absorption correction	Semi-empirical from equivalents	Semi-empirical from equivalents
Maximum and minimum transmission	0.964 and 0.941	0.786 and 0.703
Refinement method	Full-matrix least-squares on F ²	Full-matrix least-squares on F ²
Data / restraints / parameters	5006 / 0 / 262	4716 / 1 / 263
Goodness-of-fit on F ²	1.130	0.953
Final R indices [I > 2σ (I)]	R ₁ = 0.0392, wR ₂ = 0.0617	R ₁ = 0.0389, wR ₂ = 0.0759
R indices (all data)	R ₁ = 0.0792, wR ₂ = 0.0710	R ₁ = 0.0591, wR ₂ = 0.0827
Largest difference peak and hole (e Å ⁻³)	0.641 and -0.806	0.293 and -0.439
$R_1 = \frac{\sum F_o - F_c }{\sum F_o } \quad wR_2 = \frac{[\sum w(F_o^2 - F_c^2)^2]}{\sum w(F_o^2)^2}]^{1/2}$		

The crystal structure of complex **6** is very similar to complex **5**, main difference is it is a nickel(II) complex. Crystal data and refinement parameters are given in Table 4.8. and the ORTEP diagram is shown in Fig. 4.24. Selected bond lengths (Å) and and bond angles (°) are given in Table 4.9.

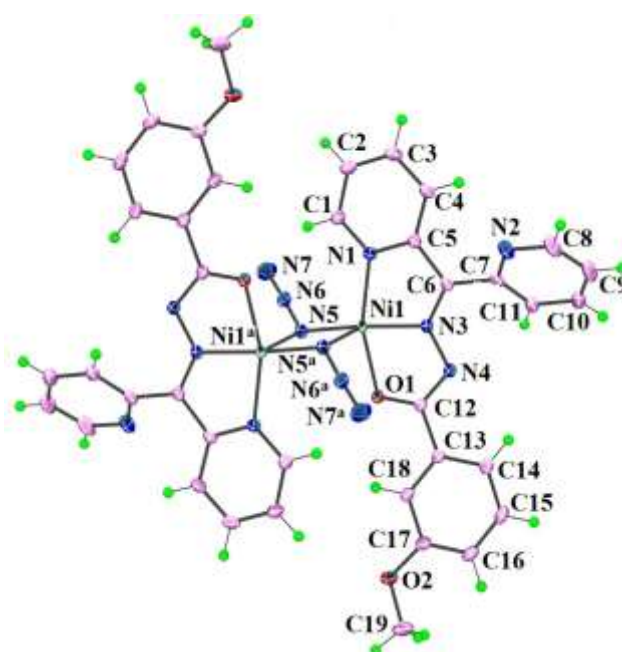


Fig. 4.24. ORTEP plot (drawn with 30% thermal ellipsoid) of $[\text{Ni}(\text{dkm})\text{N}_3]_2$ (**6**) along with atom numbering scheme of non-hydrogen atoms.

The green needle shaped complex $[\text{Ni}(\text{dkm})\text{N}_3]_2$ (**6**) crystallized in monoclinic $P21/n$ symmetry. The basal plane of the square pyramid is satisfied by the donor atoms of aroylhydrazone (pyridyl nitrogen N1, azomethine nitrogen N3 and enolate oxygen O1) and N5 of the azido group. The equatorial plane is satisfied by the nitrogen atom N5^a of the second azido group. These both azido anions are involved in *end-on* bridging. The tridentate aroylhydrazone forms two fused five membered metallocycles with chelate bite angles of 80.44(6) and 79.44(6)° respectively. The bridging Ni–N bond lengths are significantly different with values 1.9583(15)/2.4096(15) for basal/apical bonds. The azido groups are

quasi-linear with N–N–N bond angle of 177.4(2). Also the metal centre deviates from the least squares plane by a distance of 0.0868 Å. Moreover, the different angles around the metal centre summate to 359.4°. The τ value of 0.167 show a distorted square pyramidal geometry.

Table 4.9. Selected bond lengths and bond angles of **6**

Bond lengths (Å)		Bond angles (°)	
[Ni(dkm)N ₃] ₂ (6)		[Ni(dkm)N ₃] ₂ (6)	
N1–Ni1	2.0185(16)	N3– Ni1–O1	79.44(6)
N3–Ni1	1.9324(15)	N3– Ni1–N5	169.79(6)
O1–Ni1	1.9871(13)	O1– Ni1–N5	95.07(6)
N5–Ni1	1.9583(15)	N3– Ni1–N1	80.44(6)
N5 ^a –Ni1	2.4096(15)	O1–Ni1–N1	159.74(6)
N5–N6	1.205(2)	N5–Ni1–N1	104.45(6)
N6–N7	1.149(3)	N5– Ni1–N5 ^a	86.59(6)
N4–C12	1.336(2)		
O1–C12	1.282(2)		

Table 4.10. Hydrogen bonding interactions in [Ni(dkm)N₃]₂ (**6**) and [Cu(bpm)SCN]_n (**7**)

Hydrogen bonding interactions				
D–H···A	D–H (Å)	H···A (Å)	D···A (Å)	∠D–H···A (°)
[Ni(dkm)N ₃] ₂ (6)				
C1–H1···N6	0.95	2.57	3.236(3)	127.1
C4–H4···N2	0.95	2.50	3.034(3)	115.8
C8–H8···N6 ^a	0.95	2.69	3.471(3)	139.4
C11–H11···O1 ^b	0.95	2.64	3.588(3)	173.9
C16–H16···N7 ^c	0.95	2.62	3.341(3)	132.7
[Cu(bpm)SCN] _n (7)				
C1–H1···O2 ^d	0.93	2.64	3.444(5)	144.8
C3–H3···O1 ^e	0.93	2.53	3.385(6)	154
C20–H20B···S1 ^f	0.96	3.02	3.954(5)	165.9

Equivalent position codes : a = $x+1/2, -y+1/2, z+1/2$; b = $-x+1, -y+1, -z+1$; c = $x+1, y+1, z$; d = $x+1/2, -y+3/2, z+1$; e = $3/2-x, 1/2+y, -1/2+z$; f = $x-1/2, -y+3/2, z-1$.

D, Donor; A, acceptor; Cg, Centroid; α , dihedral angle between planes I & J; β , angle between Cg···Cg and Cg(J) perp.

Three intramolecular hydrogen bonds C(11)–H(11)···N(4), C(1)–H(1)···N(6) and C(4)–H(4)···N(2) generate $S_2^2(6)$ ring motifs. The N7 atom of azide act as acceptor in C(16)–H(16)···N(7) intermolecular hydrogen bonding interaction (Fig. 4.25). The hydrogen bonding interactions are listed in Table 4.10.

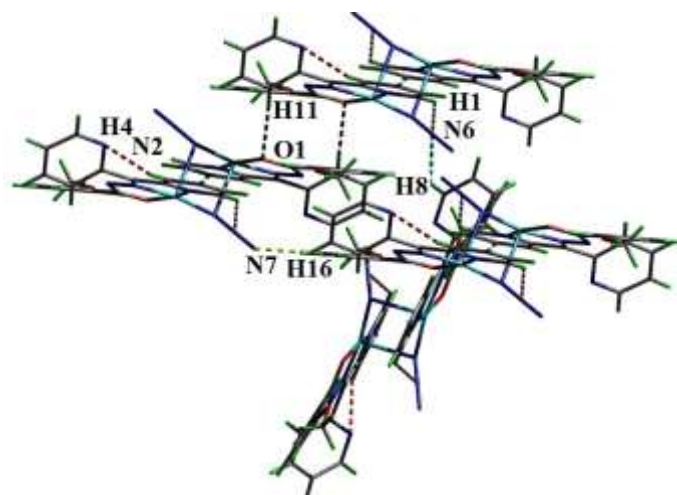


Fig. 4.25. Hydrogen bonding interaction (dashed lines) in complex **6**.

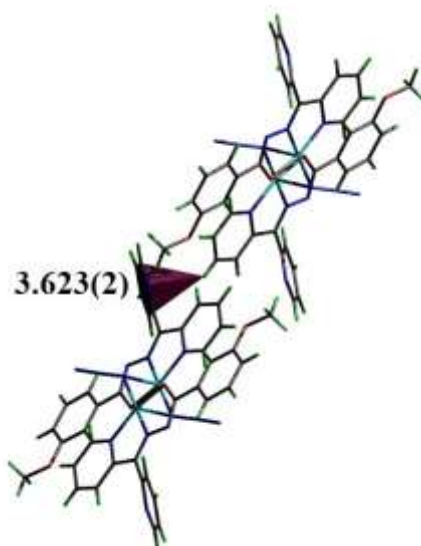


Fig. 4.26. Weak C–H···π interaction in complex **6**.

Table 4.11. Non-bonding interactions in **6**

$\pi \cdots \pi$ interactions				
Cg(I)⋯Cg(J)	Cg⋯Cg (Å)	α (°)	β (°)	γ (°)
Cg(2)⋯Cg(2) ^a	3.9383(9)	0.02(7)	32.7	32.7
Cg(3)⋯Cg(6) ^a	3.4532(11)	11.39(9)	2.3	14.0
Cg(6)⋯Cg(6) ^b	3.5926(12)	0.00(9)	16.2	16.2
N–N⋯π interactions				
Y–X(I)⋯Cg(J)	X⋯Cg (Å)	Y⋯Cg (Å)	\angleY–X⋯Cg (°)	
N(6)–N(7)⋯Cg(2) ^c	3.647(2)	3.1932(17)	58.11(13)	
C–H⋯π interactions				
C–H(I)⋯Cg(J)	H⋯Cg (Å)	C⋯Cg (Å)	\angleC–H⋯Cg (°)	
C(3)–H(3)⋯Cg(5) ^d	2.86	3.623(2)	138	
Ring-metal interaction				
Me(I)⋯Cg(J)	Me⋯Cg(Å)	Me(J)	β (°)	
Ni(1)⋯Cg(6) ^a	3.902	-3.004	39.65	

Equivalent position codes: a = 1-x, 1-y, 1-z; b = 2-x, 1-y, 1-z; c = 1-x,-y,1-z; d = 1/2-x,-1/2+y,3/2-z.

[Ni(dkm)N₃]₂ (**6**): Cg(2) = Ni1, O1, C12, N4, N3; Cg(3) = Ni1, N1, C5, C6, N3; Cg5 = N2, C7, C11, C10, C9, C8; Cg6 = C13, C14, C15, C16, C17, C18.

Non-bonding interaction parameters for complex **6** are arranged in Table 4.11. As seen in complex **5**, one C–H⋯ π , one ring-metal, three $\pi \cdots \pi$ and one N–N⋯ π interactions are present in complex **6**.

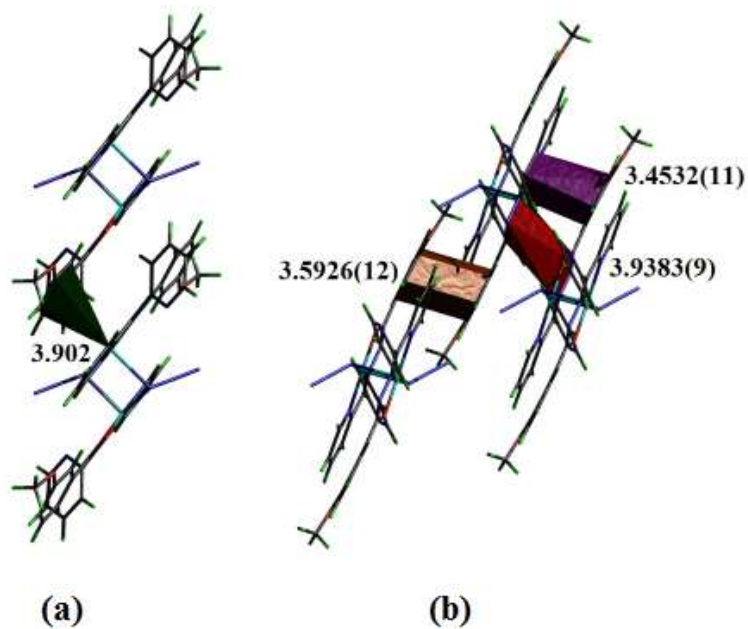


Fig. 4.27. (a) Ring-metal interaction (b) $\pi \cdots \pi$ interaction in complex **6**.

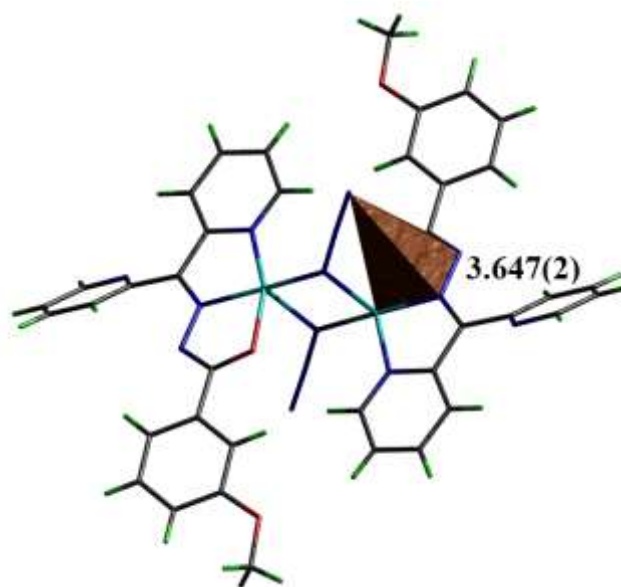


Fig. 4.28. (a) N-N $\cdots\pi$ interaction in complex **6**.

4.3.5.5. Crystal structure of [CuL¹NCS]_n (7)

The compound crystallises in the orthorhombic space group *Pna2*₁. The asymmetric unit of the complex is shown in Fig. 4.29. The crystal structure of complex [CuL¹NCS]_n (7) is an infinite 1D polymeric chain of Cu(II) with aroylhydrazone [167]. The tridentate monoanionic NNO donor aroylhydrazone and the nitrogen N4 of thiocyanate occupies the axial position of square plane and the sulfur atom of adjacent thiocyanate housing the axial position of square pyramidal geometry. Each thiocyanate function as a *cis*- $\mu_{1,3}$ bridge which reveal the ambidenticity of the thiocyanate coligand and links adjacent units into a 1D chain (Fig.4. 30). The coordination geometry of copper(II) metal is thus distorted square pyramidal. The bond dimensions of the complex is comparable to those in similar systems [168]. Selected bond lengths and bond angles are tabulated in Table 4.12. The intrachain Cu–Cu separation in the polymeric chain is 5.684 Å. The Jahn-Teller distortion about copper(II) centre is revealed by the axial elongation of bond length around the metal ion, Cu1–S1= 2.6548(14) and Cu1–N4 = 1.931(3) Å. The thiocyanate coligand is almost linear with a bond angle of 179.1(4)° [169].

The extent of distortion for the pentacoordinated complex is given by Addison parameter, $\tau = 0.157$ and the least squares plane calculation shows a high deviation of the metal centre by a distance of 0.2362 Å. Two chelate bite angles around the metal centre are 79.62 and 80.03°.

Ring puckering analysis shows that five membered chelate ring Cg(2) (comprised of atoms Cu1, N1, C5, C6 and N2) is puckered with puckering parameters $Q(2) = 0.098(3)$ Å and $\psi(2) = 35(2)$ ° and develops an *E* conformation.

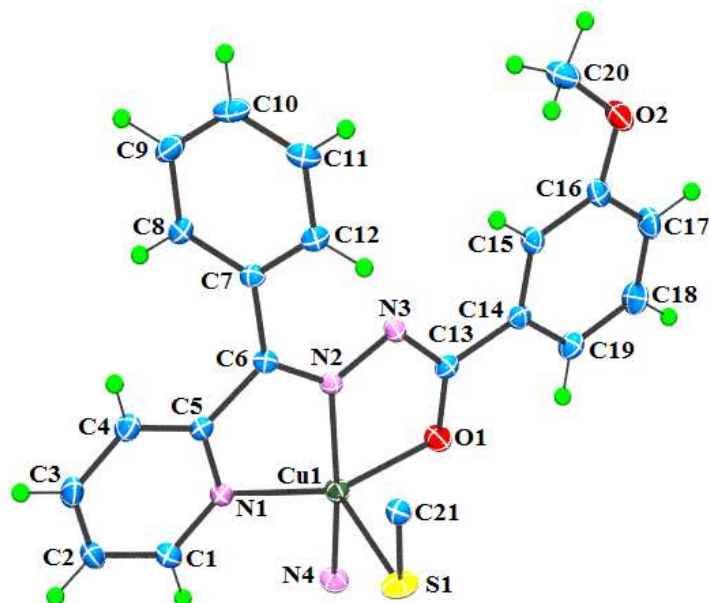


Fig. 4.29. ORTEP plot (drawn with 30% thermal ellipsoid) of asymmetric unit of $[\text{CuL}^1\text{NCS}]_n$ (**7**) along with atom numbering scheme of non-hydrogen atoms.

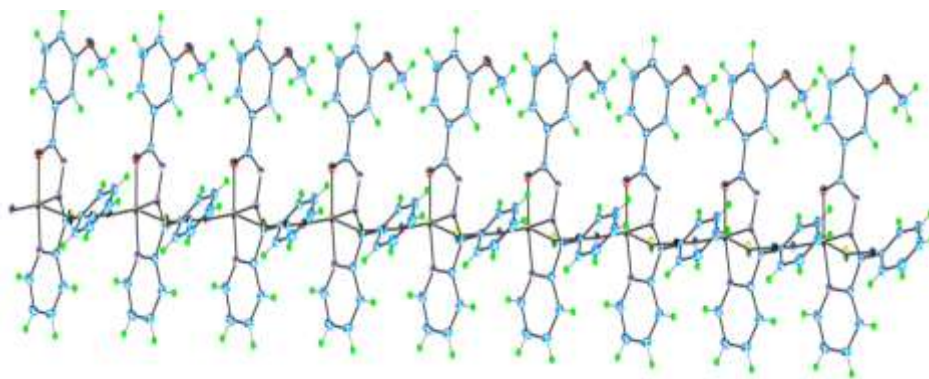
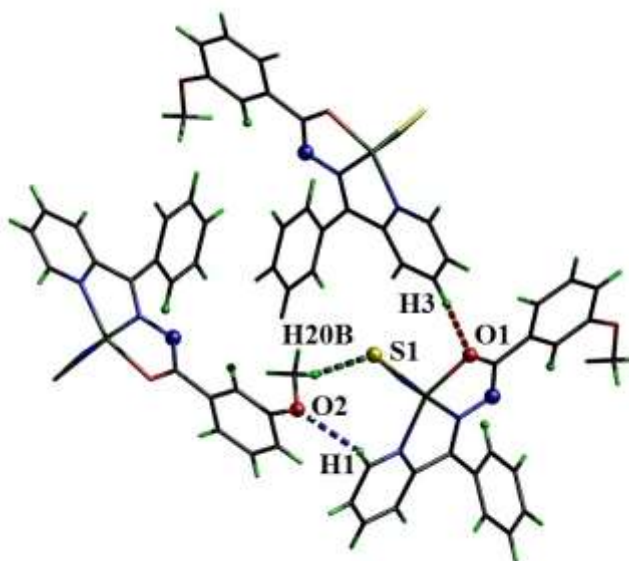


Fig. 4.30. ORTEP plot (drawn with 30% thermal ellipsoid) of 1D polymer chain of $[\text{CuL}^1\text{NCS}]_n$ (**7**).

Table 4.12. Selected bond lengths and bond angles of [Cu(bpm)SCN]_n (**7**)

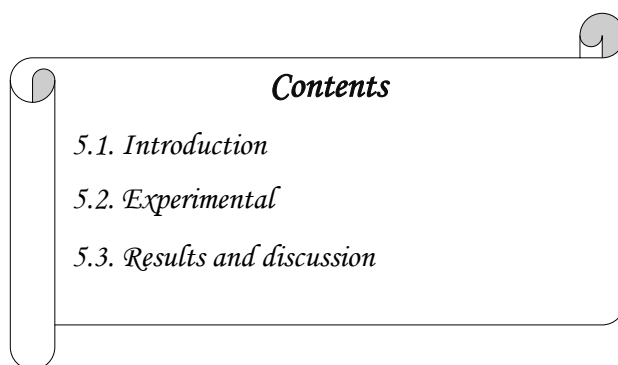
Bond lengths (Å)		Bond angles (°)	
N1–Cu1	2.030(3)	N3–Ni1–O1	79.44(6)
N2–Cu1	1.926(3)	O1–Cu1–N1	156.67(12)
O1–Cu1	1.996(3)	S1–Cu1–N1	97.84(10)
N4–Cu1	1.930(3)	S1–Cu1–O1	96.29(10)
S1–Cu1	2.655(13)	O1–Cu1–N4	98.00(14)
N2–N3	1.371(4)	O1–Cu1–N2	79.62(13)
N3–C13	1.320(5)	N2–Cu1–N4	166.13(15)
O1–C13	1.277(5)	N1–Cu1–N2	80.04(14)

The crystal packing in complex **7** is stabilised by three intermolecular hydrogen bonding interactions like .C(1)–H(1)···O(2), C(3)–H(3)···O(1) and C(20)–H(20B)···S(1) with D···A distances of 3.444(5), 3.385(6) and 3.954(5) Å respectively (Table 4.10).

**Fig. 4.31.** Hydrogen bonding interaction (dashed lines) in complex **7**.

Chapter 5

SYNTHESES AND CHARACTERIZATION OF BISLIGATED COMPLEXES OF AROYLHYDRAZONES



5.1. Introduction

Unlike previous chapters, we have six single crystals of bisligated transition metal complexes of aroylhydrazones in the present chapter. Complexes [Cu(bpm)₂] (**8**) and [Cu(dkm)(Hdkm)](ClO₄)-0.8H₂O (**9**) are bisligated copper(II) complexes; [Ni(bpm)₂] (**10**) and [Ni(bpm)₂] (**11**) are bisligated nickel(II) complexes; [Co(bpm)₂(ClO₄)] (**12**) is bisligated cobalt(III) and last one is bisligated zinc(II) complex [Zn(bpm)₂] (**13**). They were characterized by various physico-chemical methods and the intermolecular interactions are quantified using Hirshfeld Surface Analysis.

5.2. Experimental

5.2.1. Materials

$\text{Cu}(\text{NO}_3)_2 \cdot 3\text{H}_2\text{O}$, $\text{Cu}(\text{ClO}_4)_2 \cdot 6\text{H}_2\text{O}$, $\text{NiCl}_2 \cdot 6\text{H}_2\text{O}$, $\text{Ni}(\text{OAc})_2 \cdot 4\text{H}_2\text{O}$, $\text{Ni}(\text{ClO}_4)_2 \cdot 6\text{H}_2\text{O}$, $\text{Co}(\text{ClO}_4)_2 \cdot 6\text{H}_2\text{O}$, $\text{Zn}(\text{OAc})_2 \cdot 2\text{H}_2\text{O}$ were purchased from Sigma-Aldrich. All the reagents and solvents used were of Analar grade and were used as received.

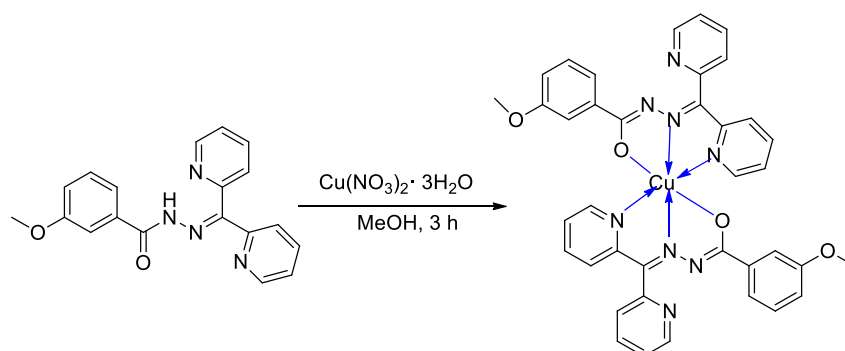
5.2.2. Syntheses of bisligated copper(II) complexes

5.2.2.1. Synthesis of $[\text{Cu}(\text{dkm})_2]$ (8)

Copper nitrate trihydrate (0.241 g, 1 mmol) in methanolic solution was added to a methanolic solution of aroylhydrazone, Hdkm (0.332 g, 1 mmol) and the mixture was refluxed for three hours. Slow evaporation of the solution yielded green needle shaped crystals and were separated, washed with ether and dried over P_4O_{10} *in vacuo* (Scheme 5.1).

For $[\text{Cu}(\text{dkm})_2]$ (8) Yield: 89% (0.646 g). Color: Green. Anal. Calc. for $\text{C}_{38}\text{H}_{30}\text{CuN}_8\text{O}_4$ (M.W.: $726.25 \text{ g mol}^{-1}$) C, 62.84; H, 4.16; N, 15.43%. Found: C, 62.88; H, 4.13; N, 15.48%.

λ_M (DMF): $7 \text{ mho cm}^2 \text{ mol}^{-1}$.



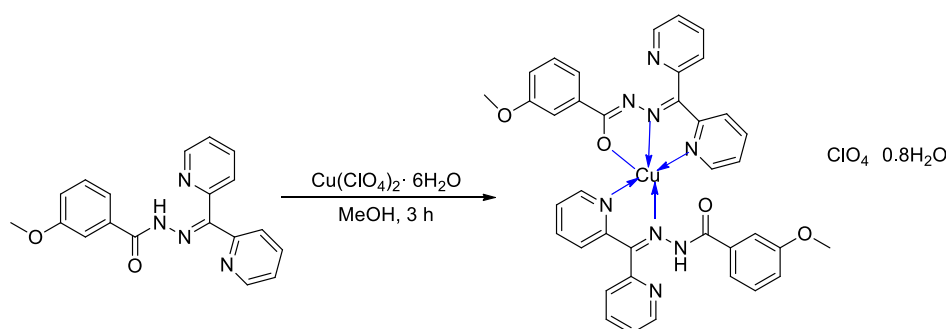
Scheme 5.1. Synthesis of $[\text{Cu}(\text{dkm})_2]$ (8).

5.2.2.2. Synthesis of [Cu(dkm)(Hdkm)](ClO₄)·0.8H₂O (9).

[Cu(dkm)(Hdkm)](ClO₄)·0.8H₂O (9) was prepared by the addition of the methanolic solution of Hdkm (0.332 g, 1 mmol) and copper perchlorate hexahydrate (0.370 g, 1 mmol) in methanol. The resulting solution was refluxed for 3 hours and left overnight. The dark green solid was collected and recrystallized from DMF within one week and dried over P₄O₁₀ *in vacuo* (Scheme 5.2).

For [Cu(dkm)(Hdkm)](ClO₄)·0.8H₂O (9) Yield: 77% (0.646 g). Color: Green.
Anal. Calc. for C₄₀H_{34.61}ClCuN₆O_{8.80} (M.W.: 839.11 g mol⁻¹) C, 54.03; H, 3.94; N, 13.27%. Found: C, 54.00; H, 3.93; N, 13.28%.

λ_M (DMF): 58 mho cm² mol⁻¹.

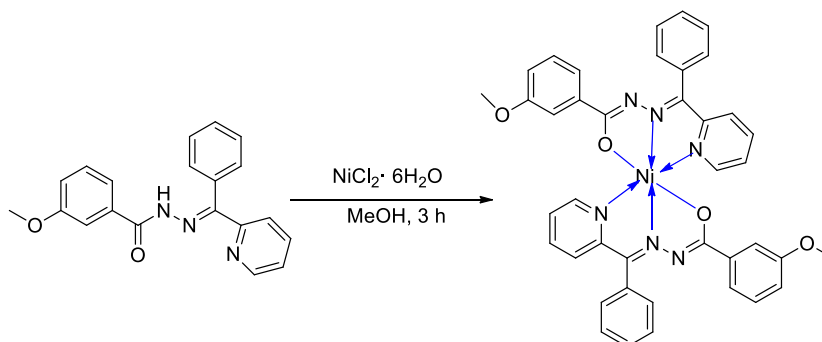


Scheme 5.2. Synthesis of [Cu(dkm)(Hdkm)](ClO₄)·0.8H₂O (9).

5.2.2.3. Synthesis of [Ni(bpm)₂] (10)

[Ni(bpm)₂] (10) was prepared by the addition of Hbpm (0.331 g, 1 mmol) and nickel(II) chloride hexahydrate (0.238 g, 1 mmol) in methanol. The resulting solution was refluxed for 3 hours and the green precipitate was collected and recrystallized from DMF and dried over P₄O₁₀ *in vacuo* (Scheme 5.3).

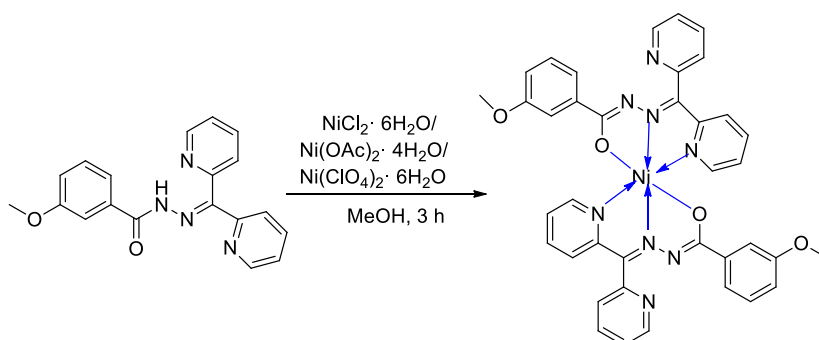
For [Ni(bpm)₂] (**10**) Yield: 73% (0.525 g). Color: Green. Anal. Calc. for C₄₀H₃₂N₆NiO₄ (M.W.: 719.41 g mol⁻¹) C, 66.78; H, 4.48; N, 11.68%. Found: C, 66.75; H, 4.43; N, 11.65%; λ_M (DMF): 5 mho cm² mol⁻¹.



Scheme 5.3. Synthesis of [Ni(bpm)₂] (**10**).

5.2.2.4. Synthesis of [Ni(dkm)₂] (**11**)

Methanolic solutions of Hdkm (0.332 g, 1 mmol) and nickel(II) chloride hexahydrate (0.238 g, 1 mmol) were mixed and the resulting solution was refluxed for 3 hours and left overnight. The green needle crystals obtained were separated and dried over P₄O₁₀ *in vacuo* (Scheme 5.4). We have prepared complexes using nickel acetate and nickel nickel perchlorate salts also, but we got same crystal structure for all the three cases.



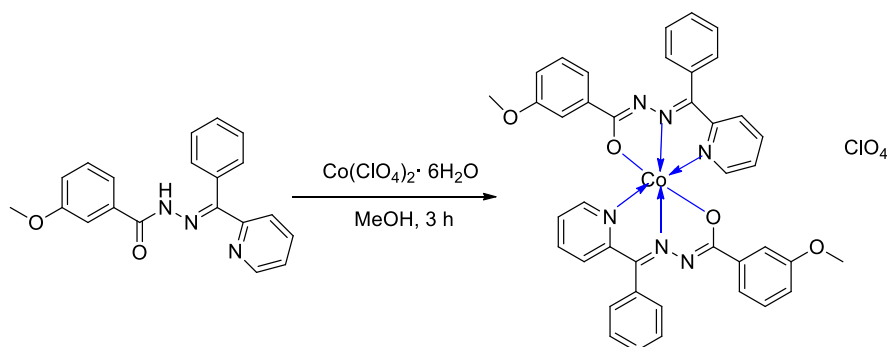
Scheme 5.4. Synthesis of [Ni(dkm)₂] (**11**).

For [Ni(dkm)₂] (**11**) Yield: 75% (0.541 g). Color: Green. Anal. Calc. for C₃₈H₃₀N₈NiO₄ (M.W.: 721.39 g mol⁻¹) C, 63.27; H, 4.19; N, 15.53 %. Found: C, 63.25; H, 4.17; N, 15.58%.

λ_M (DMF): 9 mho cm² mol⁻¹.

5.2.2.5. Synthesis of [Co(bpm)₂](ClO₄) (**12**)

Methanolic solution of cobalt perchlorate hexahydrate (0.366 g, 1 mmol) was added to the methanolic solution of Hbpm (0.331 g, 1 mmol) and the resulting solution was refluxed for 3 hours. The green needle crystals obtained were separated and dried over P₄O₁₀ *in vacuo* (Scheme 5.5).



Scheme 5.5. Synthesis of [Co(bpm)₂](ClO₄) (**12**).

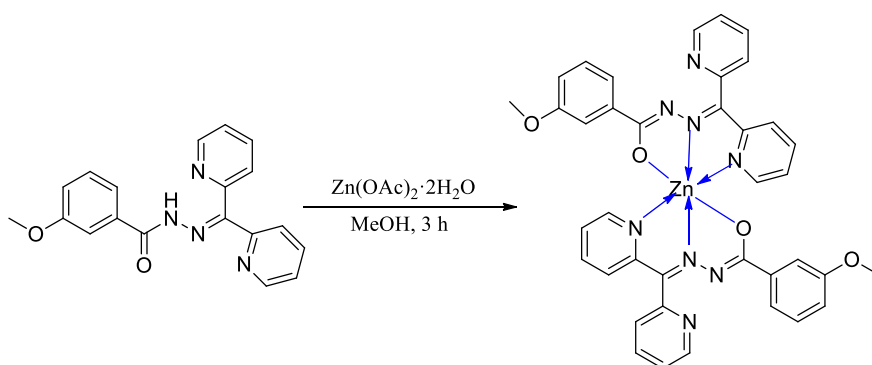
For [Co(bpm)₂](ClO₄) (**12**) Yield: 79% (0.647 g). Color: Green. Anal. Calc. for C₄₀H₃₂ClCoN₆O₈ (M.W.: 819.10 g mol⁻¹) C, 58.65; H, 3.94; N, 4.33 %. Found: C, 58.65; H, 4.37; N, 4.35%.

λ_M (DMF): 48 mho cm² mol⁻¹.

5.2.2.6. Synthesis of [Zn(bpm)₂] (**13**)

Methanolic solutions of Hbpm (0.331 g, 1 mmol) and zinc(II) acetate dihydrate (0.219 g, 1 mmol) were mixed and the resulting solution was refluxed for

3 hours and kept for two days. The yellow block shaped crystals obtained was separated and dried over P_4O_{10} *in vacuo* (Scheme 5.6).



Scheme 5.6. Synthesis of $[Zn(bpm)_2]$ (**13**).

For $[Zn(bpm)_2]$ (**13**) Yield: 72% (0.522 g). Color: Yellow. Anal. Calc. for $C_{40}H_{31}N_6O_4Zn$ (M.W.: $725.10 \text{ g mol}^{-1}$) C, 62.69; H, 4.15; N, 15.39 %. Found: C, 62.65; H, 4.17; N, 15.38%.

λ_M (DMF): $5 \text{ mho cm}^2 \text{ mol}^{-1}$.

5.3. Results and discussion

5.3.1. Infrared spectra

The significant infrared spectral bands along with their tentative assignments are listed in Table 5.1. and the spectra are shown in Figs. 5.1.- 5.6. Strong bands due to $\nu(C=O)$ and $\nu(N-H)$ in aroylhydrazones are absent in complexes $Cu(dkm)_2$ (**8**), $Ni(bpm)_2$ (**10**), $Ni(dkm)_2$ (**11**), $[Co(bpm)_2](ClO_4)$ (**12**) and $Zn(bpm)_2$ (**13**), and a new band due to $\nu(C-O)$ are observed in the $1358\text{-}1370 \text{ cm}^{-1}$ region suggesting the coordination of aroylhydrazone to the metal centre *via* imininolic form on complexation [170-172]. But complex **9** showed bands at 1370 and 1684 cm^{-1} due to $\nu(C-O)$ and $\nu(C=O)$ in which one aroylhydrazone is coordinated to the metal in an amido form and another is coordinated in an imininolic

form [173]. Spectra of complexes are compared with that of the respective ligands to monitor the changes on complexation [20]. Azomethine band observed in the 1589-1602 cm^{-1} region in free ligands are shifted to lower frequency in complexes and a new $\nu(\text{C}=\text{N})$ band appeared in the 1591-1597 cm^{-1} region proves the imonolization of aroylhydrazone in these complexes.

Table 5.1. IR spectral assignments of Hbpm and Hdkm and its complexes in cm^{-1}

Compound	$\nu(\text{N-H})$	$\nu(\text{C=O})/$ $\nu(\text{C-O})$	$\nu(\text{C=N})$	$\nu(\text{C=N})^a$
Hbpm	3063	1682	1589	-
Hdkm	3058	1690	1602	-
[Cu(dkm) ₂] (8)	-	1370	1498	1597
[Cu(dkm)(Hdkm)](ClO ₄)·H ₂ O (9)	-	1684, 1370	1503	1597
[Ni(bpm) ₂] (10)	-	1364	1498	1591
[Ni(dkm) ₂] (11)	-	1358	1503	1591
[Co(bpm) ₂](ClO ₄) (12)	-	1360	1494	1595
[Zn(bpm) ₂] (13)	-	1362	1505	1596

^a newly formed C=N bond

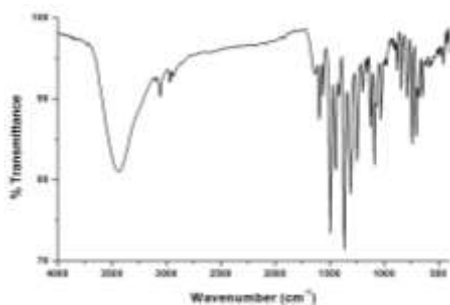


Fig. 5.1. IR Spectrum of complex **8**.

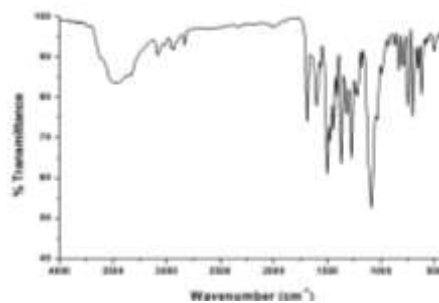


Fig. 5.2. IR Spectrum of complex **9**.

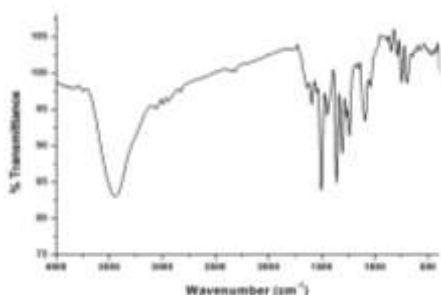


Fig. 5.3. IR Spectrum of complex 10.

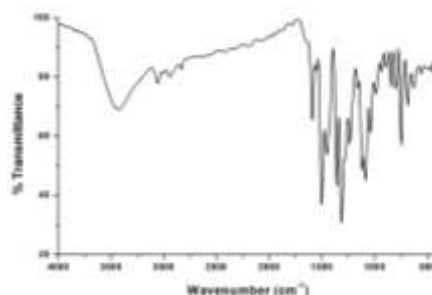


Fig. 5.4. IR Spectrum of complex 11.

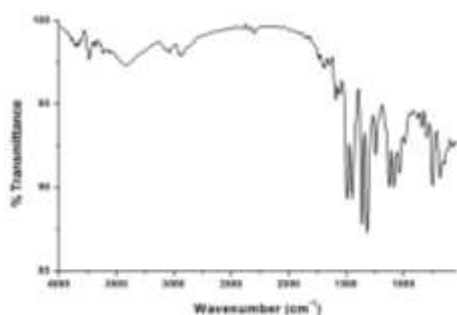


Fig. 5.5. IR Spectrum of complex 12.

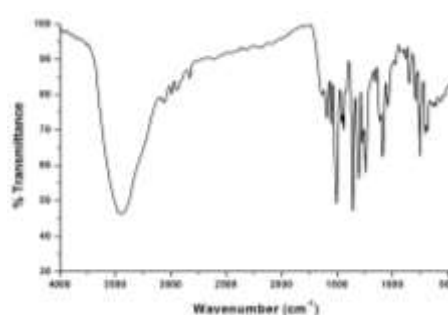


Fig. 5.6. IR Spectrum of complex 13.

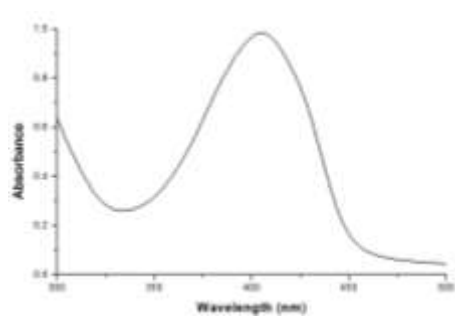
5.3.2. Electronic spectra

Electronic spectra of the compounds were taken in DMF solution (1×10^{-5} M) at room temperature and the spectral assignments are summarized in Table 5.2. For obtaining *d-d* bands of the complexes, spectra were recorded in 10^{-3} M solution and the spectra are shown in Figs. 5.7-5.10. Intraligand transitions were observed in the range 275–349 nm for all the compounds which can be assigned to $\pi \rightarrow \pi^*$ and $n \rightarrow \pi^*$ transitions. Ligand to metal charge transfer transitions were observed in the 392-412 nm range. The *d-d* bands were obtained only for copper complexes **8** and **9** [174]. *d-d* bands were expected for the Ni(II) complexes also, but unfortunately we could not locate any bands probably due to masking of high

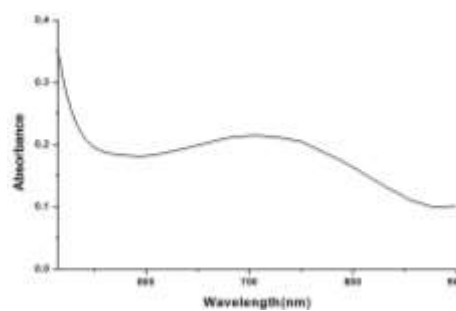
intensity charge transfer bands [175,176]. Compound **13** being a zinc(II) complex, no *d-d* bands are observed since they have a closed shell d^{10} configuration.

Table 5.2. Electronic spectral assignments, λ_{\max} (nm) of complexes **8-13**

Compound	<i>d-d</i>	LMCT	Intraligand transitions
[Cu(dkm) ₂] (8)	702 (210)	404 (98300)	299 (63050)
[Cu(dkm)(Hdkm)](ClO ₄)·H ₂ O (9)	676 (11810)	398 (35730)	349 (975)
[Ni(bpm) ₂] (10)	--	406 (84890)	314 (45660)
[Ni(dkm) ₂] (11)	--	401 (20970)	300 (9430)
[Co(bpm) ₂](ClO ₄) (12)	--	412 (60060)	268 (79670)
[Zn(bpm) ₂] (13)	--	392 (91840)	298 (35990)

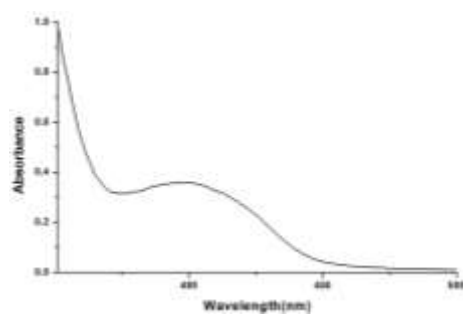


(a) LMCT and intraligand transitions

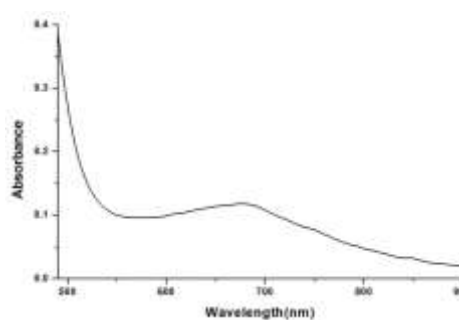


(b) *d-d*

Fig. 5.7. Electronic spectra of complex **8**.



(a) LMCT and intraligand transitions



(b) *d-d*

Fig. 5.8. Electronic spectra of complex **9**.

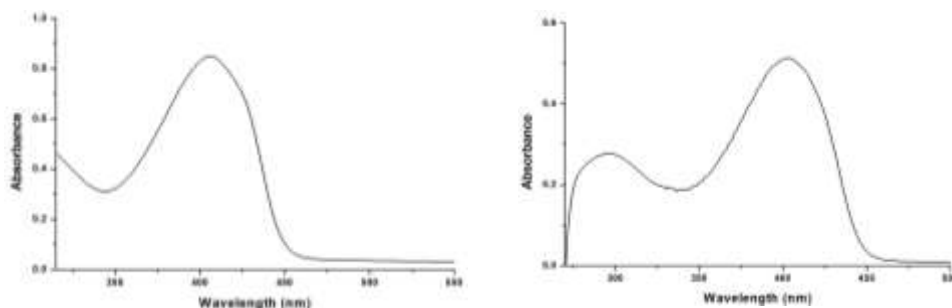


Fig. 5.9. Electronic spectra of (a) complex **10** and (b) complex **11**.

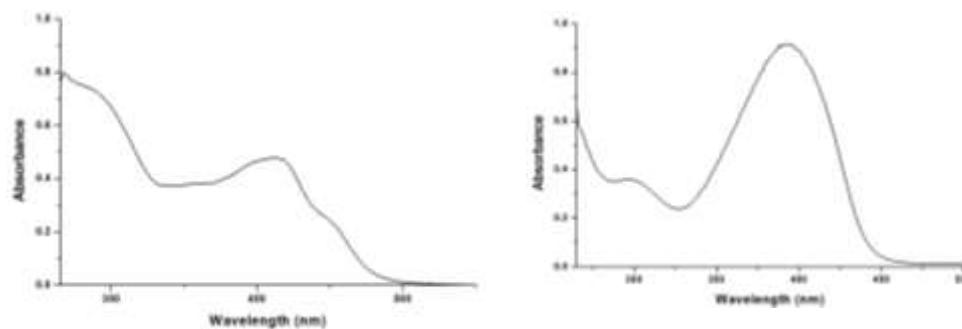


Fig. 5.10. Electronic spectra of (a) complex **12** and (b) complex **13**.

5.3.3. Electron paramagnetic resonance spectra

The EPR spectra of the copper(II) complexes **8** and **9** in the polycrystalline state at 298 K and in DMF solution at 77 K were recorded in X band using an ESR-JEOL spectrometer. All the EPR spectra are simulated using the EasySpin 5.0.20 package [66] and the experimental (red) and simulated (blue) best fits are included. The spin Hamiltonian parameters of the copper(II) complexes calculated are listed in Table 5.3.

At 298 K, complex **8** show an axial spectrum with $g_{\parallel} = 2.160$ and $g_{\perp} = 2.053$ with no hyperfine lines [177]. In DMF solution at 77 K, complex **8** displayed an axial spectrum having four hyperfine lines in the parallel region with $g_{\parallel} = 2.258$, $g_{\perp} = 2.069$ and $A_{\parallel} = 195 \times 10^{-4} \text{ cm}^{-1}$ [178]. However the perpendicular region is devoid of any hyperfine lines (Fig. 5.11). Calculated G value for the complex is 3.111 which is less than four indicating the possibility of exchange interaction. The index of tetragonal distortion f is calculated as $f = g_{\parallel}/A_{\parallel}$, whose value is 116 (medium distortion) and depends on the nature of the coordinated atom [179].

Table 5.3. Spin Hamiltonian and bonding parameters of copper(II) complexes **8** and **9**

Parameters	8	9
Polycrystalline state at 298 K		
g_{\parallel}	2.160	-
g_{\perp}	2.053	-
g_{iso}	2.089	-
G	3.111	-
DMF solution (77 K)		
g_{\parallel}	2.258	2.280
g_{\perp}	2.069	2.067
g_{avg}	2.195	2.209
A_{\parallel}	195	209
α^2	0.8654	0.9273
β^2	0.8871	0.8517
γ^2	0.9062	0.8223
K_{\parallel}	0.7677	0.7898
K_{\perp}	0.7842	0.7625
f	116	109

A values in 10^{-4} cm^{-1}

We were not able to simulate the experimental plot of complex **9** in polycrystalline state at 298 K, as it contains so many peaks. But in DMF solution at 77 K it showed an axial spectrum with $g_{\parallel} = 2.280$, $g_{\perp} = 2.067$, but no hyperfine

lines in the perpendicular region (Fig. 5.12). Four hyperfine lines in the parallel region ($A_{\parallel} = 209 \times 10^{-4} \text{ cm}^{-1}$) are due to the interaction of the odd electron with nuclear spin ($I = 3/2$ for ^{65}Cu). Small distortion was found for complex **9** since its $f = 109$ [180].

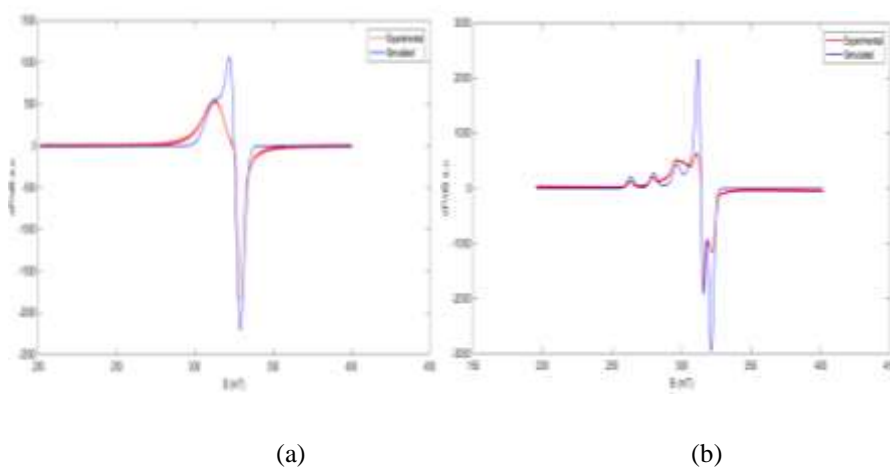


Fig. 5.11. EPR spectra of complex **8** in (a) polycrystalline state at 298 K and (b) DMF solution at 77 K.

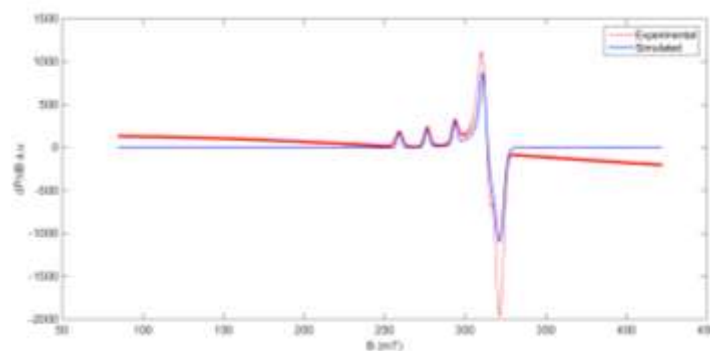
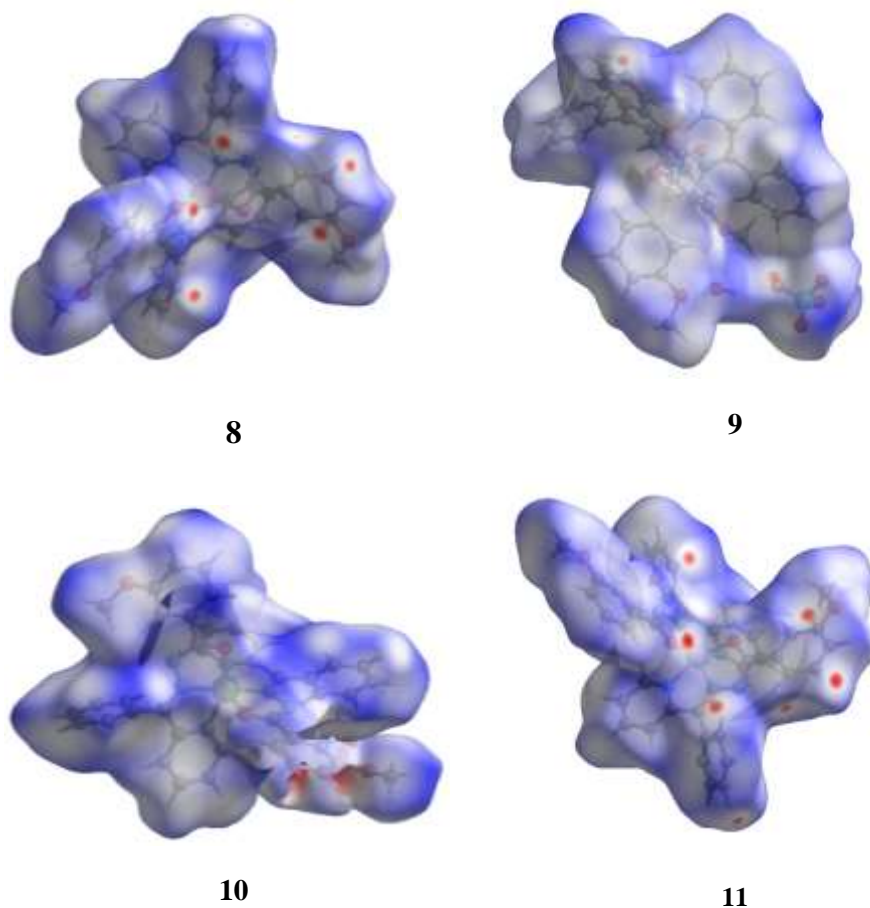


Fig. 5.12. EPR spectra of complex **9** in DMF solution at 77 K.

5.3.4. Hirshfeld Surface Analysis

To explore weak intermolecular interactions, Hirshfeld surface analyses were carried out using Crystal explorer 17 software and were mapped over d_{norm} (Fig. 5.13) and shape index function (Fig. 5.14) for complexes **8**, **9**, **10**, **11**, **12** and **13**. Hirshfeld surfaces are produced through the partitioning of space within a crystal where the ratio of promolecule to procrystal electron density is equal to 0.5, generating continuous, non-overlapping surfaces. They are widely used to visualize and study the significance of weak interactions in the molecular packing [181,182]. Deep red points on the surface of these complexes represent prominent hydrogen bonding interactions.



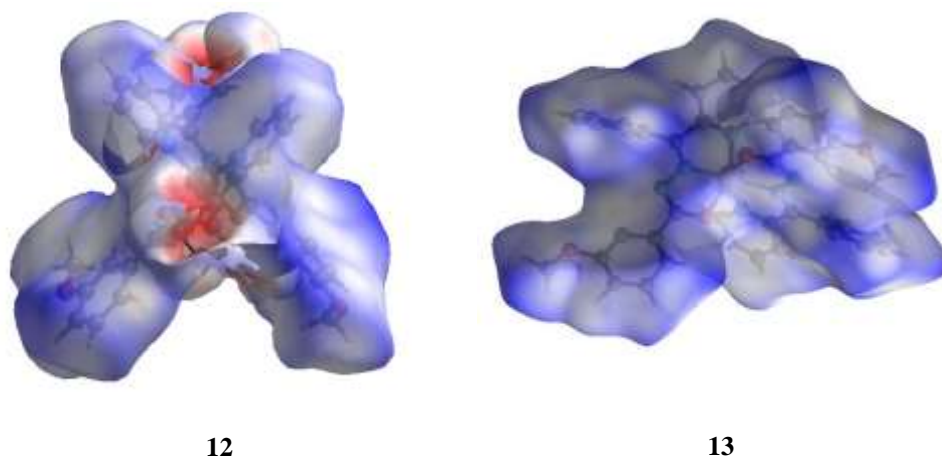
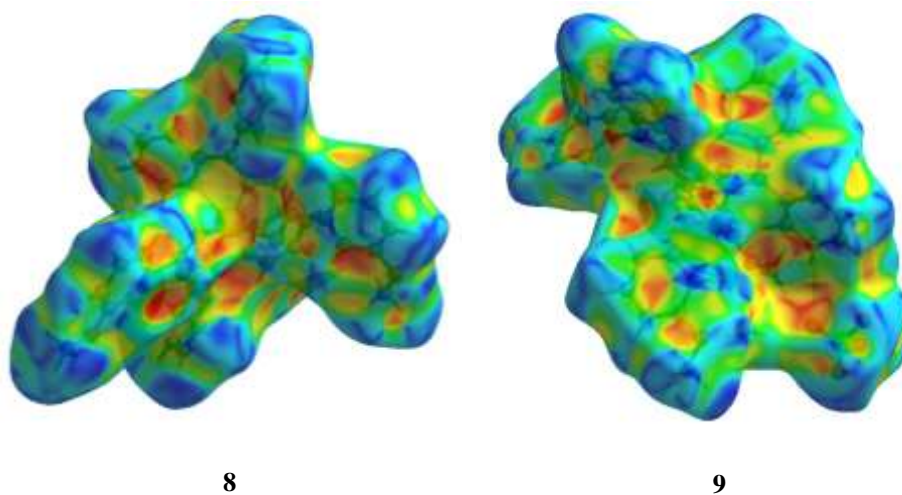


Fig. 5.13. Hirshfeld surfaces for complexes **8**, **9**, **10**, **11**, **12** and **13** mapped with d_{norm} .

The shape index plot of complexes **8-13** gave a red concave region around the π acceptor atom, a blue convex region around the donor H-atom and is shown in Fig. 5.14 [183].



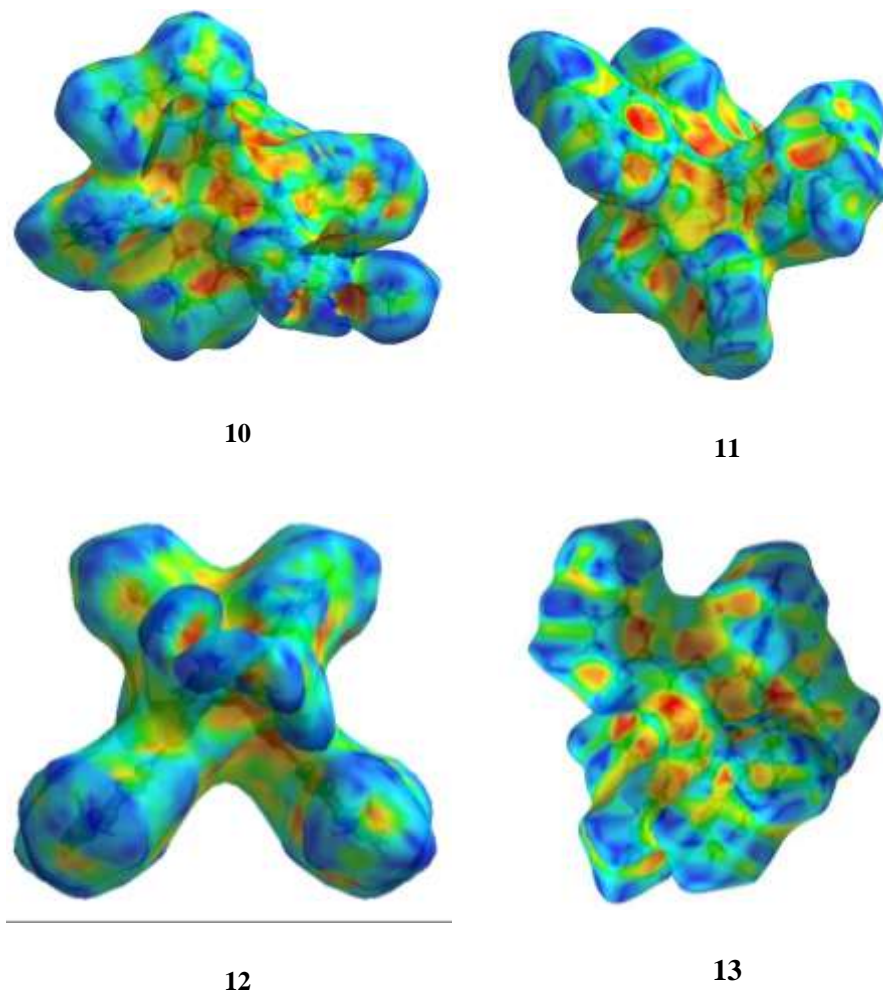
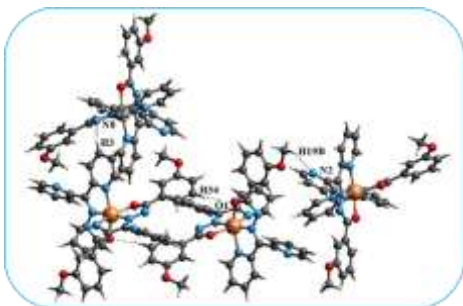


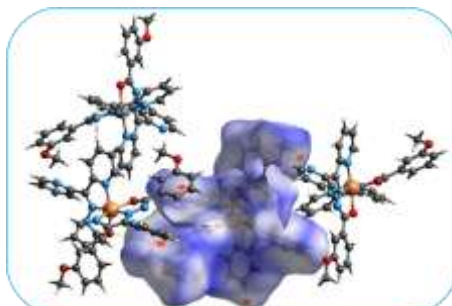
Fig. 5.14. Hirshfeld surfaces for complexes **8**, **9**, **10**, **11** and **12** mapped with shape index.

The intermolecular hydrogen bonding interactions in complexes **8**, **9**, **11** and **12** were visualized using Crystal explorer and also viewed with external molecule (Fig. 5.15).

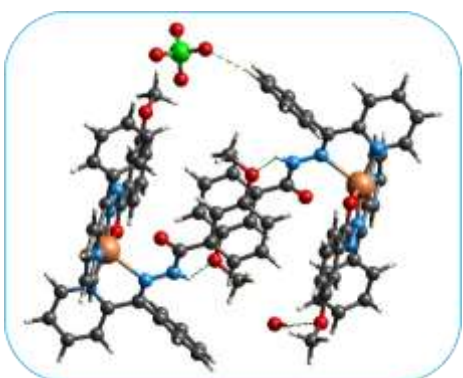
Here also H···H interaction % is high in all the six complexes.



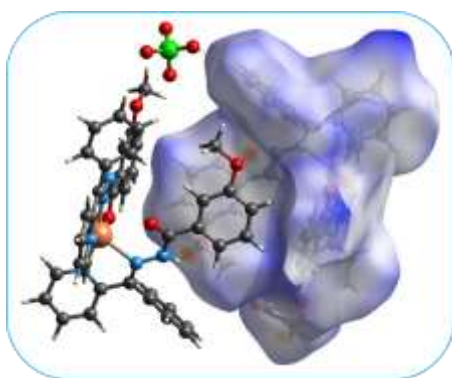
8 (a)



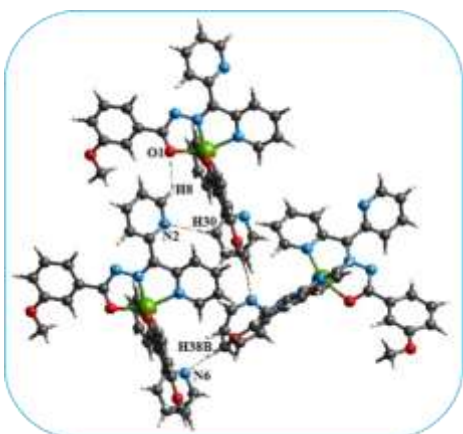
8 (b)



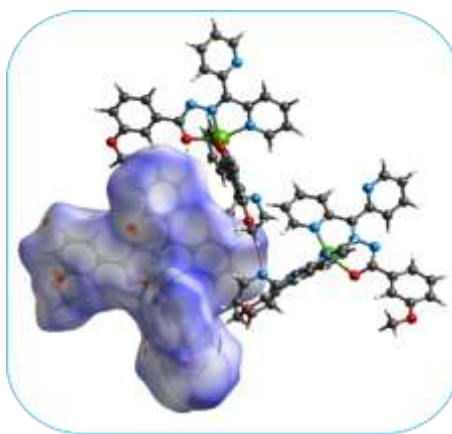
9 (a)



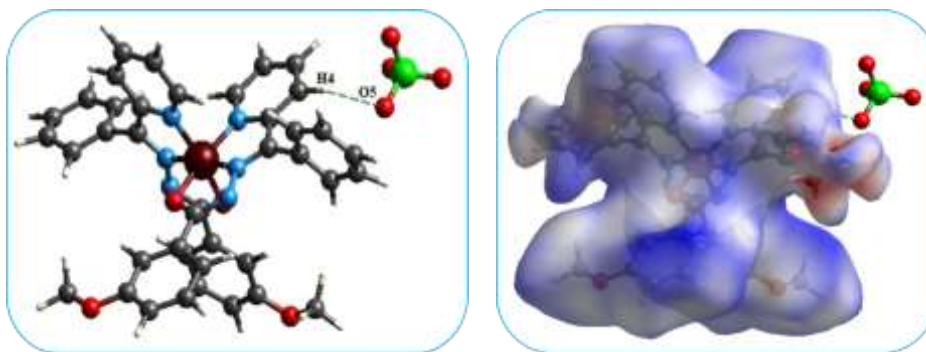
9 (b)



11 (a)



11 (b)



12 (a)

12 (b)

Fig. 5.15. (a) Intermolecular hydrogen bonding interactions present in **8**, **9**, **11** and **12** (b) viewing the same short contacts in Hirshfeld surface with external molecules.

5.3.5. X-ray crystallography

5.3.5.1. Crystal structure of $[\text{Cu}(\text{dkm})_2]$ (**8**)

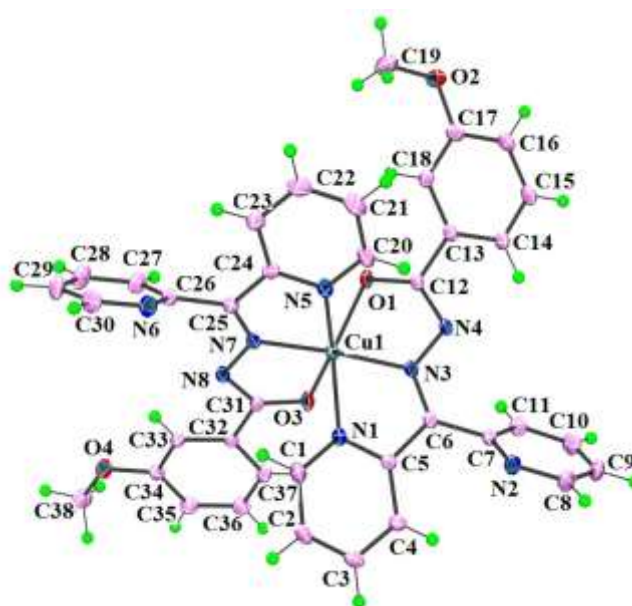


Fig. 5.16. ORTEP plot (drawn with 30% thermal ellipsoid) of $[\text{Cu}(\text{dkm})_2]$ (**8**) along with atom numbering scheme of non-hydrogen atoms.

Table 5.4. Crystal data and structural refinement parameters of [Cu(dkm)₂] (**8**) and [Cu(bpm)(Hbpm)](ClO₄)·0.8H₂O (**9**)

Parameters	[Cu(dkm) ₂] (8)	[Cu(bpm)(Hbpm)](ClO ₄)·0.8H ₂ O (9)
Empirical formula	C ₃₈ H ₃₀ CuN ₈ O ₄	C ₄₀ H _{34.61} ClCuN ₆ O _{8.80}
Formula weight	726.24	839.11
Color	Green	Green
Crystal system	Monoclinic	Monoclinic
Space group	<i>P</i> 2 ₁ / <i>c</i>	<i>P</i> 2 ₁ / <i>n</i>
Cell parameters		
a (Å)	14.813(6)	13.4723(12)
b (Å)	10.028(4)	14.5010(12)
c (Å)	22.808(9)	20.5611(18)
α (°)	90	90
β (°)	91.771(11)	108.237(2)
γ (°)	90	90
Volume V (Å ³), Z	3386(2), 4	3815.1(6), 4
Calculated density (ρ) (Mg m ⁻³)	1.424	1.461
Absorption coefficient, μ (mm ⁻¹)	0.700	0.707
F(000)	1500	1732
Crystal size mm ³	0.53 x 0.50 x 0.23	0.41 x 0.29 x 0.22
θ (°) range for data collection	3.010 to 29.006	2.997 to 26.826
Limiting indices	-19 ≤ h ≤ 20 -13 ≤ k ≤ 13 -30 ≤ l ≤ 31	-17 ≤ h ≤ 17 -18 ≤ k ≤ 18 -26 ≤ l ≤ 26
Reflections collected	61247	115171
Unique Reflections (R _{int})	9010 (0.0365)	8171 (0.0326)
Completeness to θ	25.242 98.9 %	25.242 99.6 %
Absorption correction	Semi-empirical from equivalents	Semi-empirical from equivalents
Maximum and minimum transmission	0.870 and 0.865	0.875 and 0.860
Refinement method	Full-matrix least-squares on F ²	Full-matrix least-squares on F ²
Data / restraints / parameters	8494 / 0 / 462	8113 / 1605 / 805
Goodness-of-fit on F ²	1.044	1.027
Final R indices [I > 2σ (I)]	R ₁ = 0.0323, wR ₂ = 0.0850	R ₁ = 0.0383, wR ₂ = 0.1012
R indices (all data)	R ₁ = 0.0409, wR ₂ = 0.0904	R ₁ = 0.0442, wR ₂ = 0.1061
Largest difference peak and hole (e Å ⁻³)	0.338 and -0.595	0.439 and -0.343
$R_1 = \frac{\sum F_o - F_c }{\sum F_o } \quad wR_2 = \frac{[\sum w(F_o^2 - F_c^2)^2 / \sum w(F_o^2)^2]^{1/2}}{\sum w(F_o^2)^2}^{1/2}$		

The molecular structure of complex [Cu(dkm)₂] (**8**) along with atom numbering scheme is shown in Fig. 5.16 and the significant bond lengths and bond angles are given in Table 5.5. Crystal data and structural refinement parameters of complexes [Cu(dkm)₂] (**8**) and [Cu(bpm)(Hbpm)](ClO₄)·0.8H₂O (**9**) are given in Table 5.4.

Complex [Cu(dkm)₂] (**8**) got crystallized in monoclinic space group *P*2₁/*c*. The coordination geometry of the bisligated copper(II) complex is distorted octahedral with an N₄O₂ chromophore in which both the ligands are coordinated to the copper ion in a monoanionic tridentate mode *via* enolate oxygens (O1 and O3), azomethine nitrogens (N3 and N7) and pyridine nitrogens (N1 and N5) [184,185]. The configuration of coordinating atoms around central copper atom is *trans*-N(3,7)-*cis*-N(1,5)-*cis*-O(1,3). The *trans* azomethine nitrogen atoms N3 and N7 are not much farther from 180 ° as shown from its N3–Cu1–N7 bond angle of 175.69°. Comparing the C12–O1 (1.222 Å) and C12–N4 (1.364 Å) bond lengths of aroylhydrazone (Hdkm) already discussed in Chapter 2 with the bond lengths of complexes and found that the values are affected by complexation, i.e, C12–O1 (1.268(17) Å) and C31–O3 (1.256 (18) Å) bonds show single bond character and C12–N4 (1.340 (18) Å) and C31–N8 (1.347 (19) Å) bonds show double bond character on complexation.

Four fused five membered metallocycles are formed as a result of coordination of two aroylhydrazone units, imposing large distortions on the ideally octahedral coordinate angles. The two aroylhydrazone moieties are not aligned perpendicular to each other as it is shown from the dihedral angle of 76.15° between both bicyclic chelate rings.

Table 5.5. Selected bond lengths and bond angles of [Cu(dkm)₂] (**8**) and [Cu(bpm)(Hbpm)](ClO₄)·0.8H₂O (**9**).

[Cu(dkm) ₂] (8)		[Cu(bpm)(Hbpm)](ClO ₄)·0.8H ₂ O (9)	
Bond lengths (Å)			
Cu1–N1	2.118(15)	Cu1–N1	1.980(17)
Cu1–N3	1.942(13)	Cu1–N2	1.923(2)
Cu1–O1	2.048(12)	Cu1–N4	1.992(17)
Cu1–N5	2.254(15)	Cu1–N5	2.299(17)
Cu1–N7	1.966(13)	Cu1–O1	1.952(17)
Cu1–O3	2.186(13)	C13–O1	1.279(3)
C12–O1	1.268(17)	C33–O3	1.212(3)
C12–N4	1.364(18)	N3–C13	1.339(3)
N3–N4	1.374(17)	N6–C33	1.373(3)
N7–N8	1.368(16)	N2–N3	1.374(2)
C31–O3	1.255(18)	N5–N6	1.360(2)
C31–N8	1.347(19)		
Bond angles (°)			
O1–Cu1–O3	99.19(5)	N2–Cu1–O1	80.32(8)
N1–Cu1–N5	100.83(6)	N2–Cu1–N1	80.59(8)
N3–Cu1–N7	175.69(5)	O1–Cu1–N1	160.91(7)
O1–Cu1–N5	86.89(6)	O1–Cu1–N4	98.27(7)
N4–Cu1–N5	77.66(10)	N1–Cu1–N5	102.93(6)
N1–Cu1–N4	96.04(9)	N4–Cu1–N5	75.17(7)
N1–Cu1–N2	78.10(10)	N2–Cu1–N4	160.35(15)
O1–Cu1–N3	78.25(5)	N4–Cu1–N1	99.67(7)
O3–Cu1–N1	83.81(6)	N2–Cu1–N5	124.13(14)
O1–Cu1–N1	156.88(5)	O1–Cu1–N5	87.92(8)
O3–Cu1–N5	153.07(4)		

Ring puckering analyses and least square plane calculations show that these four fused five membered chelate rings Cg(1), Cg(2), Cg(3) and Cg(4) are puckered. Cg(1) (Cu1, O1, C12, N4 and N3) and Cg(2) (Cu1, O3, C31, N8 and N7) are puckered with puckering parameters $Q(2) = 0.098 \text{ \AA}$, $\psi(2) = 354.14^\circ$ for Cg(1), $Q(2) = 0.143$, $\psi(2) = 5.95^\circ$ for Cg(2) and develops an envelope

conformation. Metallocycle Cg(3) (Cu1, N1, C5, C6 and N3) and Cg(4) (Cu1, N5, C24, C25 and N7) are puckered with puckering parameters $Q(2) = 0.066\text{\AA}$, $\psi(2) = 75.28^\circ$ for Cg(1), $Q(2) = 0.223$, $\psi(2) = 29.45^\circ$ for Cg(2) and develops an envelope conformation.

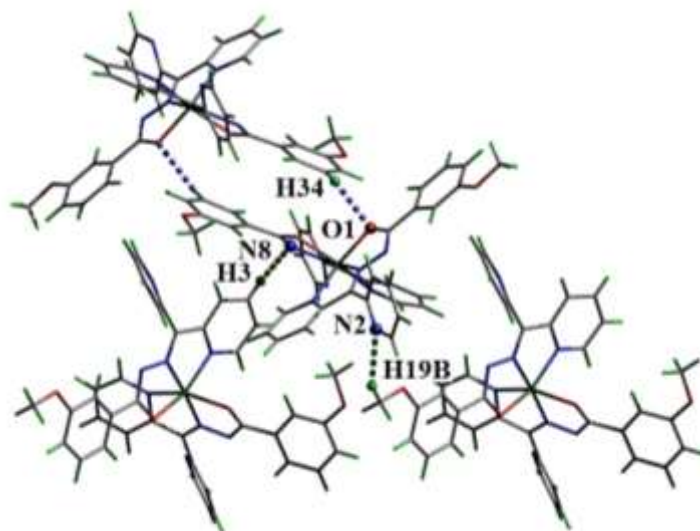


Fig 5.17. Intermolecular hydrogen bonding interactions (dashed lines) in $[\text{Cu}(\text{dkm})_2]$ (**8**).

Table 5.6. Hydrogen bonding interactions in $[\text{Cu}(\text{dkm})_2]$ (**8**) and $[\text{Cu}(\text{bpm})(\text{Hbpm})](\text{ClO}_4)\cdot 0.8\text{H}_2\text{O}$ (**9**)

Hydrogen bonding interactions				
D–H···A	D–H (Å)	H···A (Å)	D···A (Å)	$\angle\text{D–H}\cdots\text{A}$ (°)
$[\text{Cu}(\text{dkm})_2]$ (8)				
C3–H3···N8 ^a	0.95	2.58	3.346	138
C19–H19B···N2 ^a	0.95	2.58	3.807	148
C34–H34···O1 ^b	0.95	2.59	3.373	140
$[\text{Cu}(\text{bpm})(\text{Hbpm})](\text{ClO}_4)\cdot 0.8\text{H}_2\text{O}$ (9)				
N6–H6···O4 ^b	0.93	2.64	3.444(5)	144.8
O9–H9A···O2 ^c	0.93	2.53	3.385(6)	154
C30–H30···O5 ^b	0.96	3.02	3.954(5)	165.9

Equivalent position codes: a = 1-x, -1/2+y, 1/2-z; b = 1-x, 1-y, 1-z; c = x, y, z; D, Donor; A, acceptor.

No classic hydrogen bond was found in the crystal structure of complex **8**. Three intermolecular hydrogen bonding interactions are present in this compound. One is between pyridyl nitrogen N2 and methoxy hydrogen H19B, another is between enolate oxygen O1 and hydrogen H34 attached to carbon C34 and the last one is between azomethine nitrogen N8 and hydrogen H3 and these interactions are shown in Fig. 5.17 (Table 5.6).

Table 5.7. Non-bonding interactions in **8** and **9**

$\pi \cdots \pi$ interactions				
Cg(I) \cdots Cg(J)	Cg \cdots Cg (Å)	α (°)	β (°)	γ (°)
[Cu(dkm) ₂] (8)				
Cg(1) \cdots Cg(7) ^a	3.893	61.849	28.74	56.97
Cg(2) \cdots Cg(5) ^b	3.958	65.440	33.86	70.22
$C-H \cdots \pi$ interactions				
[Cu(bpm)(Hbpm)](ClO ₄) \cdot 0.8H ₂ O (9)				
C-H(I) \cdots Cg(J)	H \cdots Cg (Å)	C \cdots Cg (Å)	$\angle C-H \cdots Cg$ (°)	
C3-H3 \cdots Cg(18) ^c	2.51	3.394(2)	156	

Equivalent position codes: a = x, y, z; b = 1-x, 1/2+y, 1/2-z; c = 3/2-x, -1/2+y, 3/2-z.

[Cu(dkm)₂] (**8**): Cg(1) = Cu1, O1, C12, N4, N3; Cg(2) = Cu1, O3, C31, N8, N7; Cg(5) = N1, C1, C2, C3, C4, C5; Cg(7) = N5, C20, C21, C22, C23, C24.

The centroid Cg(1) in complex **8** is involved in $\pi \cdots \pi$ interaction with Cg(5) and the chelate ring Cg(2) is with the pyridyl ring Cg(5) with Cg \cdots Cg distances of 3.892 and 3.958 Å respectively (Fig. 5.18) (Table 5.7).

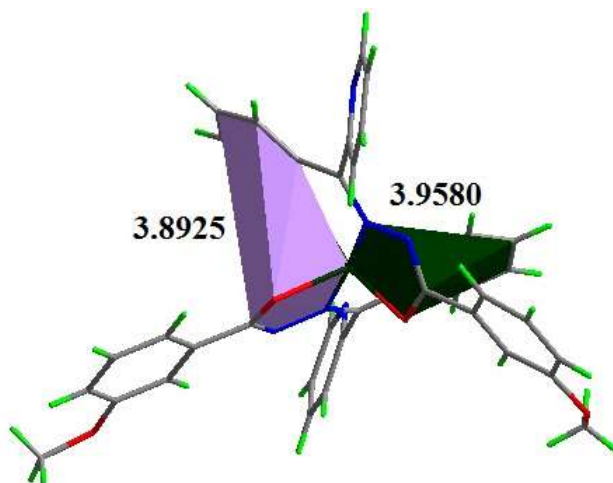


Fig. 5.18. The $\pi \cdots \pi$ interaction in $[\text{Cu}(\text{dkm})_2]$ (**8**).

5.3.5.2. Crystal structure of $[\text{Cu}(\text{bpm})(\text{Hbpm})](\text{ClO}_4) \cdot 0.8\text{H}_2\text{O}$ (**9**)

The molecular structure of complex **9** is shown in Fig. 5.19. and the selected bond lengths and bond angles are shown in Table 5.5. In this monomeric copper(II) complex, two arylhydrazone units are coordinated, one in monoanionic tridentate mode and another in neutral bidentate mode [186]. One perchlorate anion act as counter ion and one solvent water molecule is present outside the coordination sphere. From the comparison of C13–O1 (1.279(3) Å) and C33–O3 (1.212 (3) Å) bond distances it is clear that one arylhydrazone bonds in amido form and another in iminolic form to the metal [187]. IR values also support this coordination. Here the complex is pentacoordinated using two pyridyl nitrogens (N1 and N4), two azomethine nitrogens (N2 and N5) and one enolate oxygen (O1). Addison parameter (τ) value of 0.0093 ($\tau = (\beta - \alpha)/60$) indicate slight distortion from perfect square square pyramidal geometry (for perfect square pyramidal and trigonal bipyramidal geometries the values of τ are zero and unity respectively). Comparison of bond lengths of coordinating atoms show that the metal-axial nitrogen distance (Cu1–N5 = 2.299 Å (17) is longer than metal-equatorial bond

distances (Cu1–N1 = 1.980(17), Cu1–N2 = 1.923(18), Cu1–N4 = 1.992(17), Cu1–O1 = 1.952(17) Å) and hence the basal plane of the square pyramid is satisfied by the atoms N1, N2, N4 and O1. The azomethine nitrogen N5 of the neutral aroylhydrazone occupies the axial position.

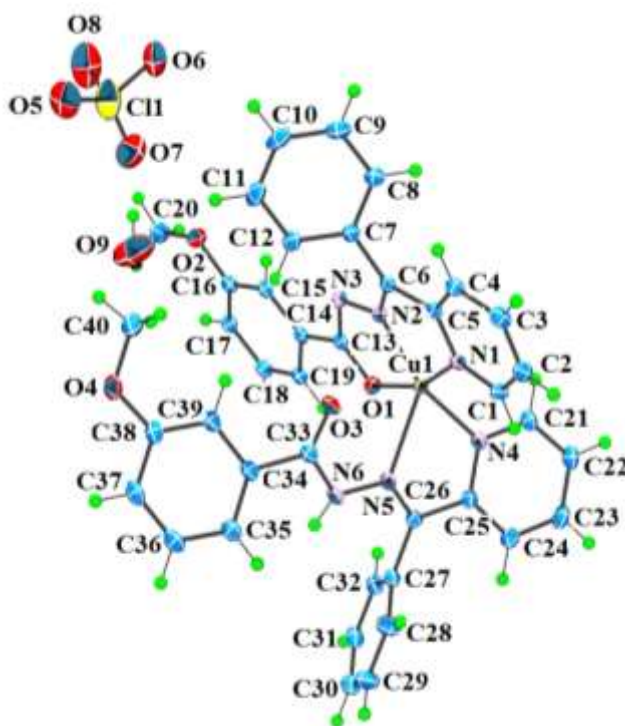


Fig. 5.19. ORTEP plot (drawn with 30% thermal ellipsoid) of [Cu(bpm)(Hbpm)](ClO₄)·0.8H₂O (**9**) along with atom numbering scheme of non-hydrogen atoms.

Ring puckering analyses and least square plane calculations show that five membered chelate rings Cg(7) is puckered (comprised of atoms Cu1, N4, C25, C26 and N5) with puckering parameters $Q(2) = 0.222(18)$ Å, $\psi(2) = 143.1(5)^\circ$ and develops an envelope conformation. The puckering is also calculated by pseudorotation parameters P and τ and it was found that $P = 292.6(3)^\circ$, $\tau (m) = 22.5(1)^\circ$ for reference bond Cu1–N4.

The C30–H30···O5 hydrogen bond connects oxygen O5 of counter ion perchlorate with hydrogen H30 attached to carbon C30 with D···A distance of 3.389(9) Å. The methoxy oxygen atom O2 form a hydrogen bond O9–H9A···O2 with solvent water molecule and another methoxy oxygen O4 is involved in hydrogen bonding interaction with the hydrogen atom H6 of the uncoordinated azomethine nitrogen N6 (Fig. 5.20). Also the complex is stabilized by one C–H··· π interaction (Fig. 5.21).

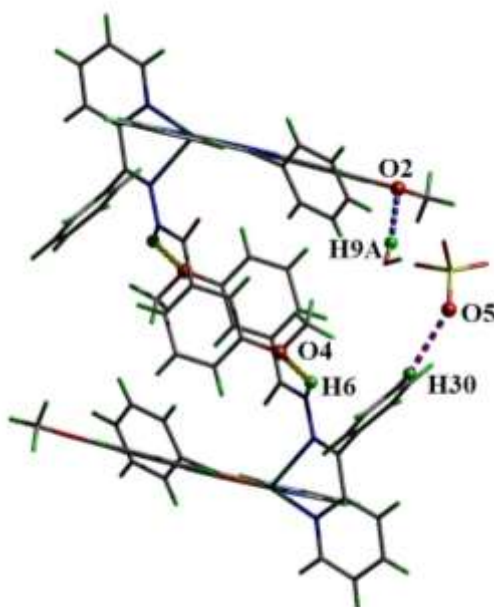


Fig 5.20. Hydrogen bonding interactions (dashed lines) in [Cu(bpm)(Hbpm)](ClO₄)·0.8H₂O (**9**).

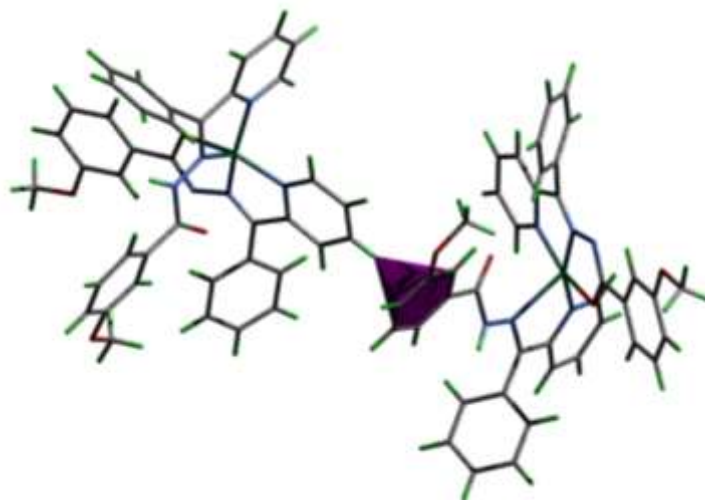


Fig. 5.21. The C–H··· π interaction in [Cu(bpm)(Hbpm)](ClO₄) · 0.8H₂O (**9**).

5.3.5.3. General features in the crystal structures of [Ni(bpm)₂] (**10**) and [Ni(dkm)₂] (**11**)

The crystal data and refinement parameters of [Ni(bpm)₂] (**10**) and [Ni(dkm)₂] (**11**) are given Table 5.8. and the respective *ORTEP* plots are shown in Figs.5.22 and 5.23. Selected bond lengths and bond angles are given in Table 5.9. Both the complexes got crystallized in monoclinic lattice with *P*2₁/*c* space group and the coordination geometry around the metal ion is distorted octahedral which can be described with an NiN₄O₂ chromophore. The hexacoordination of nickel(II) centre is satisfied by two monoanionic aroylhydrazone units using its pyridyl nitrogens (N1, N4 in **10** and N1, N5 in **11**), azomethine nitrogens (N2, N5 in **10** and N3, N7 in **11**) and iminolate oxygen atoms (O1 and O3) [188].

The configuration of donor atoms is *trans*- N(2,5)-*cis*-N(1,4)-*cis*-O(1,3) in **10** and *trans*- N(3,7)-*cis*-N(1,5)-*cis*-O(1,3) in **11**. The azomethine nitrogen atoms are *trans* in both complexes as shown from its bond angle of 178.17° (**10**) in **10** and 175.82° (**11**) in **11**. The coordination of aroylhydrazone units in monoanionic

iminolic form is evident from the C–O (C13–O1 = 1.269(3) and C33–O3 = 1.268(3) Å in **10**, C12–O1 = 1.267(14) C31–O3 = 1.269(14) Å in **11**) and C–N (C13–N3 = 1.336(3) and C33–N6 = 1.333(3) Å in **10**, C12–N4 = 1.346(15) C31–N8 = 1.344(15) Å in **11**) bond length values.

The intraligand bite angles are in the range 77.23(9)–78.10(10)° in **10** and 77.18(4)–78.52(4)° in **11**. Four metalochelate rings are formed by the coordination of two monoanionic arylhydrazone ligands. The angle between two bicyclic rings formed by the arylhydrazone with the metal ion is 84.59° (almost perpendicular) for complex **10** and 77.31° for **11**.

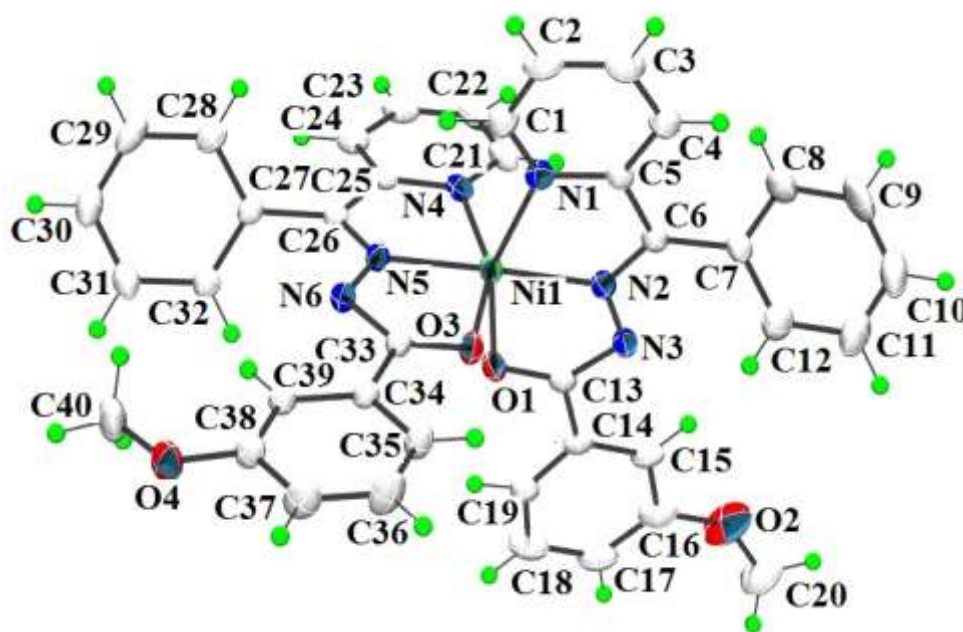


Fig. 5.22. ORTEP plot (drawn with 30% thermal ellipsoid) of [Ni(bpm)₂] (**10**) along with atom numbering scheme of non-hydrogen atoms.

Table 5.8. Crystal data and structural refinement parameters of [Ni(bpm)₂] (**10**) and [Ni(dkm)₂] (**11**)

Parameters	[Ni(bpm) ₂] (10)	[Ni(dkm) ₂] (11)
Empirical formula	C ₄₀ H ₃₂ N ₆ NiO ₄	C ₃₈ H ₃₀ N ₈ NiO ₄
Formula weight	719.41	721.41
Color	Green	Green
Crystal system	Monoclinic	Monoclinic
Space group	<i>P</i> 2 ₁ / <i>c</i>	<i>P</i> 2 ₁ / <i>c</i>
Cell parameters		
a (Å)	13.6662(14)	14.5181(16)
b (Å)	16.0640(16)	10.0442(11)
c (Å)	16.1741(14)	23.008(3)
α (°)	90	90
β (°)	102.170(3)	91.370(4)
γ (°)	90	90
Volume V (Å ³), Z	3471.0(6), 4	3354.2(6), 4
Calculated density (ρ) (Mg m ⁻³)	1.377	1.429
Absorption coefficient, μ (mm ⁻¹)	0.610	0.634
F(000)	1496	1496
Crystal size mm ³	0.25 x 0.15 x 0.10	0.35 x 0.20 x 0.15
θ (°) range for data collection	2.872 to 26.586	3.017 to 28.433
Limiting indices	-17 ≤ h ≤ 17 -20 ≤ k ≤ 20 -20 ≤ l ≤ 18	-19 ≤ h ≤ 19 -13 ≤ k ≤ 13 -30 ≤ l ≤ 29
Reflections collected	87657	68845
Unique Reflections (R _{int})	7269 (0.1716)	8404 (0.0377)
Completeness to θ	25 99.9%	25.242 99.8%
Absorption correction	Semi-empirical from equivalents	Semi-empirical from equivalents
Maximum and minimum transmission	0.780 and 0.624	0.521 and 0.391
Refinement method	Full-matrix least-squares on F ²	Full-matrix least-squares on F ²
Data / restraints / parameters	7152 / 321 / 527	8404 / 0 / 462
Goodness-of-fit on F ²	1.045	1.025
Final R indices [I > 2σ (I)]	R ₁ = 0.0577, wR ₂ = 0.0927	R ₁ = 0.0291, wR ₂ = 0.0770
R indices (all data)	R ₁ = 0.1148, wR ₂ = 0.1073	R ₁ = 0.0360, wR ₂ = 0.0804
Largest difference peak and hole (e Å ⁻³)	0.252 and -0.345	0.300 and -0.623
$R_1 = \sum F_o - F_c / \sum F_o \quad wR_2 = [\sum w(F_o^2 - F_c^2)^2 / \sum w(F_o^2)^2]^{1/2}$		

Table 5.9. Selected bond lengths and bond angles of [Ni(bpm)₂] (**10**) and [Ni(dkm)₂] (**11**).

[Ni(bpm) ₂] (10)		[Ni(dkm) ₂] (11)	
Bond lengths (Å)			
Ni1–N1	2.099(3)	Ni1–N1	2.111(11)
Ni1–N2	1.979(2)	Ni1–N3	1.976(11)
Ni1–O1	2.086(2)	Ni1–O1	2.083(10)
Ni1–N4	2.096(2)	Ni1–N5	2.099(13)
Ni1–N5	1.972(2)	Ni1–N7	1.985(11)
Ni1–O3	2.087(2)	Ni1–O3	2.061(10)
C13–O1	1.269(4)	C12–O1	1.267(15)
C33–O3	1.268(3)	C31–O3	1.269(15)
C13–N3	1.336(3)	C12–N4	1.346(15)
C33–N6	1.333(3)	C31–N8	1.344(15)
N2–N3	1.362(3)	N3–N4	1.366(15)
N5–N6	1.364(3)	N7–N8	1.370(14)
Bond angles (°)			
O1–Ni1–O3	94.89(8)	O1–Ni1–O3	97.30(4)
O3–Ni1–N5	77.67(9)	O3–Ni1–N7	77.18(4)
N4–Ni1–N5	77.66(10)	N5–Ni1–N7	78.52(4)
N1–Ni1–N4	96.04(9)	O1–Ni1–N5	84.60(4)
N1–Ni1–N2	78.10(10)	N1–Ni1–N3	78.33(4)
N2–Ni1–N5	178.17(10)	N3–Ni1–N7	175.82(4)
O1–Ni1–N2	77.23(9)	O1–Ni1–N3	77.34(4)
O3–Ni1–N1	89.76(9)	O3–Ni1–N1	86.58(4)
O1–Ni1–N1	155.33(8)	O1–Ni1–N1	155.67(4)
O3–Ni1–N4	155.34(8)	O3–Ni1–N5	155.29(4)

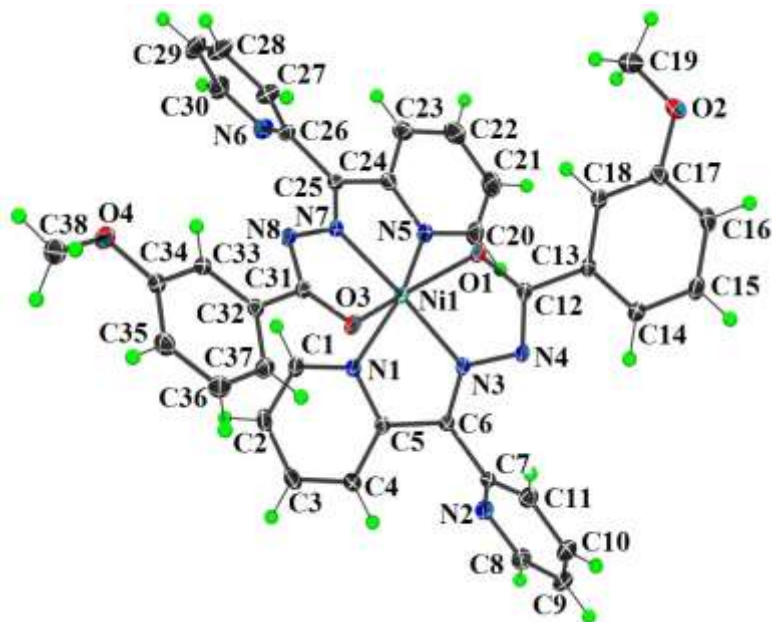


Fig. 5.23. ORTEP plot (drawn with 30% thermal ellipsoid) of $[\text{Ni}(\text{dkm})_2]$ (**11**) along with atom numbering scheme of non-hydrogen atoms.

5.10. Hydrogen bonding interactions in $[\text{Ni}(\text{dkm})_2]$ (**11**)

Hydrogen bonding interactions

D–H···A	D–H (Å)	H···A (Å)	D···A (Å)	$\angle\text{D–H}\cdots\text{A}$ (°)
C4–H4···N2	0.95	2.57	3.051(18)	111.8
C8–H8···O1 ^a	0.95	2.63	3.386(18)	136.9
C23–H23···N6	0.95	2.69	3.162(2)	111.6
C30–H30···N2 ^b	0.95	2.64	3.580(2)	172.0
C38–H38B···N6 ^c	0.98	2.59	3.451(2)	147.2

Equivalent position codes: a = $x, y-1, z$; b = $x, y+1, z$; c = $-x, y+1/2, -z+1/2$.

D, Donor; A, acceptor.

Table 5.11. Non-bonding interactions in $[\text{Ni}(\text{dkm})_2]$ (**11**)

$\pi\cdots\pi$ interactions				
Cg(I)···Cg(J)	Cg···Cg (Å)	α (°)	β (°)	γ (°)
Cg(1)···Cg(7) ^a	3.953(9)	65.12(6)	34.9	69.1
Cg(2)···Cg(5) ^a	3.834(8)	66.95(6)	29.00	60.8

Equivalent position codes: a = x, y, z .

[Ni(dkm)₂] (**11**): Cg(1) = Cu1, O1, C12, N4, N3; Cg(2) = Cu1, O3, C31, N8, N7; Cg(5) = N1, C1, C2, C3, C4, C5; Cg(7) = N5, C20, C21, C22, C23, C24.

The crystal packing of the complex **11** was stabilised by hydrogen bonding interactions and $\pi \cdots \pi$ interactions. Pyridyl nitrogen N2 is involved in bifurcated hydrogen bonding interaction with the hydrogens H4 and H30 attached to carbons C4 and C30. Also another pyridyl nitrogen N6 is involved in bifurcated hydrogen bond with hydrogen H38B attached to methoxy carbon and H23. Iminolic oxygen O1 forms a C8–H8 \cdots O1 hydrogen bond with donor acceptor distance of 3.386(18) Å (Fig. 5.24, Table 5.10). The $\pi \cdots \pi$ stacking interactions Cg(1) \cdots Cg(7) and Cg(2) \cdots Cg(5) with Cg \cdots Cg distances 3.953(9) and 3.834(8) Å respectively reinforces crystal structure cohesion in molecular packing in the crystal lattice (Fig. 5.25, Table 5.11).

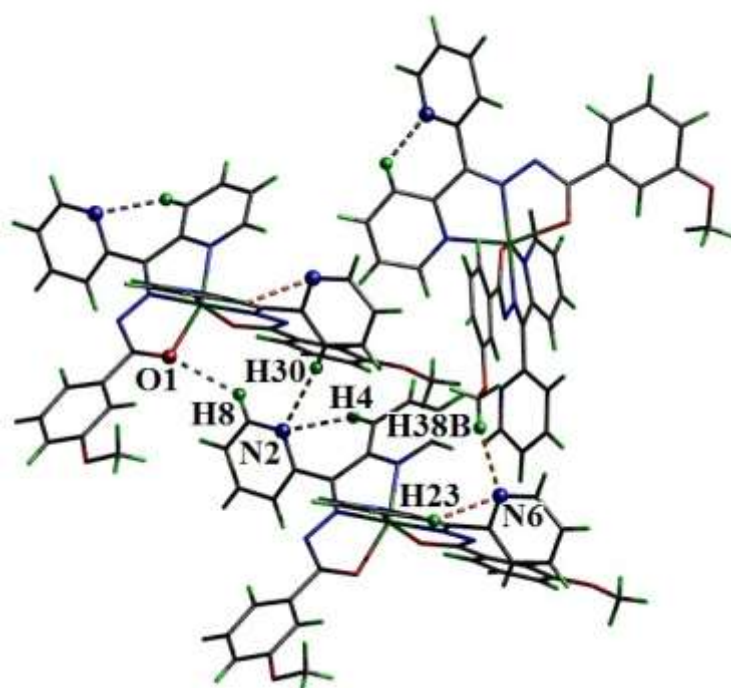


Fig 5.24. Hydrogen bonding interactions (dashed lines) in [Ni(dkm)₂] (**11**).

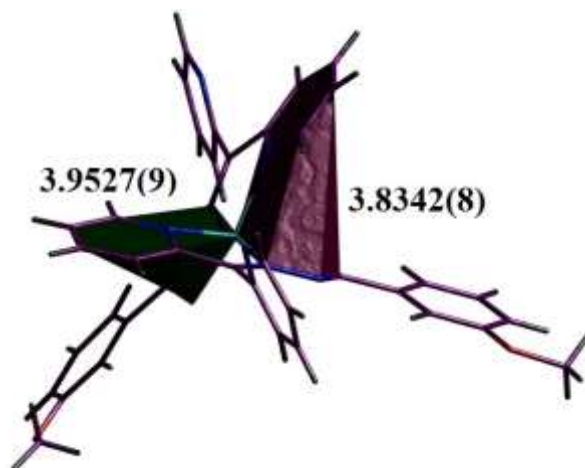


Fig. 5.25. The $\pi \cdots \pi$ interaction in [Ni(dkm)₂] (11).

5.3.5.4. Crystal structure of [Co(bpm)₂]ClO₄ (12)

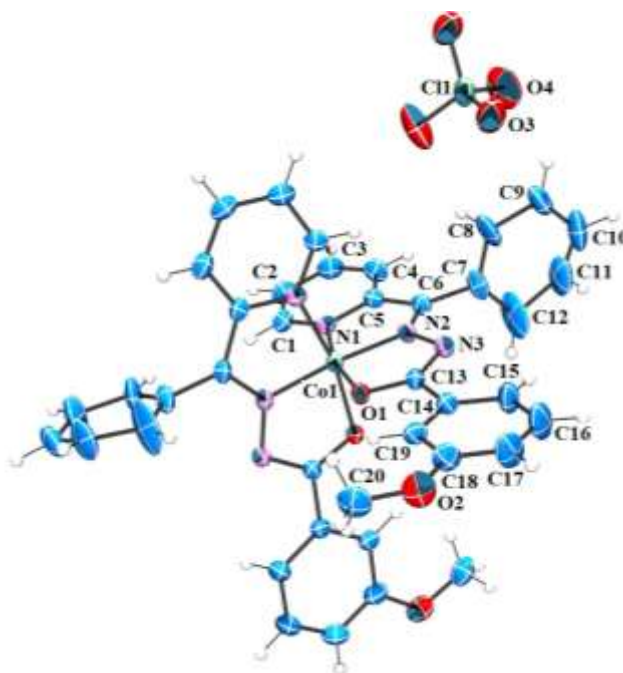


Fig. 5.26. ORTEP plot (drawn with 30% thermal ellipsoid) of [Co(bpm)₂]ClO₄ (12) along with atom numbering scheme of non-hydrogen atoms.

Table 5.12. Crystal data and structural refinement parameters of [Co(bpm)₂](ClO₄) (12) and [Zn(bpm)₂] (13)

Parameters	[Co(bpm) ₂](ClO ₄) (12)	[Zn(bpm) ₂] (13)
Empirical formula	C ₄₀ H ₃₂ ClCo N ₆ O ₈	C ₄₀ H ₃₁ N ₆ O ₄ Zn
Formula weight	819.10	725.10
Color	Brown	Yellow
Crystal system	Orthorhombic,	Monoclinic
Space group	<i>Pcca</i>	<i>P2₁/c</i>
Cell parameters		
a (Å)	17.4984(18)	13.8052(11)
b (Å)	11.2127(12)	16.1534(12)
c (Å)	19.240(2)	16.3833(11)
α (°)	90	90
β (°)	90	101.598(3)
γ (°)	90	90
Volume V (Å ³), Z	3775.0(7), 4	3578.9(5), 4
Calculated density (ρ) (Mg m ⁻³)	1.441	1.346
Absorption coefficient, μ (mm ⁻¹)	0.588	0.736
F(000)	1688	1500
Crystal size mm ³	0.40 x 0.35 x 0.30	0.50 x 0.25 x 0.20
θ (°) range for data collection	1.816 to 28.408	2.497 to 28.232
Limiting indices	-20 ≤ h ≤ 23 -14 ≤ k ≤ 15 -25 ≤ l ≤ 25	-18 ≤ h ≤ 18 -20 ≤ k ≤ 18 -17 ≤ l ≤ 21
Reflections collected	56119	28531
Unique Reflections (R _{int})	4744 (0.0378)	8846 (0.0334)
Completeness to θ	25.242 100.0 %	25.242 99.8 %
Absorption correction	Semi-empirical from equivalents	Semi-empirical from equivalents
Maximum and minimum transmission	0.843 and 0.799	0.863 and 0.802
Refinement method	Full-matrix least-squares on F ²	Full-matrix least-squares on F ²
Data / restraints / parameters	4744 / 12 / 271	8846 / 3 / 468
Goodness-of-fit on F ²	1.074	0.881
Final R indices [I > 2σ (I)]	R ₁ = 0.0564, wR ₂ = 0.1517	R ₁ = 0.0426, wR ₂ = 0.1204
R indices (all data)	R ₁ = 0.0906, wR ₂ = 0.1930	R ₁ = 0.0778, wR ₂ = 0.1488
Largest difference peak and hole (e Å ⁻³)	0.589 and -0.413	0.536 and -0.425
$R_1 = \sum F_o - F_c / \sum F_o $ $wR_2 = [\sum w(F_o^2 - F_c^2)^2 / \sum w(F_o^2)^2]^{1/2}$		

Crystal data and structural refinement parameters of complexes [Co(bpm)₂](ClO₄) (**12**) and [Zn(bpm)₂] (**13**) are given in Table 5.12. Coordination geometry of cobalt atom is distorted octahedral with an N₄O₂ chromophore. Complex [Co(bpm)₂](ClO₄) (**12**) got crystallized in orthorhombic centrosymmetric space group *Pcca* and the molecular structure is shown in Fig. 5.26. The asymmetric unit of bisligated Co(III) complex contains half of cationic complex with perchlorate ion acting as a counter ion. The selected bond lengths and bond angles are presented in Table 5.13 [87]. The hexacoordination around the cobalt(III) centre is satisfied by the NNO donor atoms of two aroylhydrazone units in iminolic form. The C13–O1(1.299(2) Å) and C13–N3(1.364 (15) Å) bond lengths show the coordination in iminolic form during complexation. The chelate bite angles around the metal centre (82.83(12)–83.79(14)°) reveal the magnitude of distortion from the octahedral geometry. The coordinating atoms form a *trans*-N(2,2^b)-*cis*-N(1,1^b)-*cis*-O(1,1^b) configuration around the cobalt ion [188].

Ring puckering analysis shows that six membered aromatic ring Cg(6) (comprised of atoms C7, C8, C9, C10, C11 and C12) is puckered with puckering amplitude $Q = 0.11(2)$ Å, $\theta = 135(11)^\circ$ and $\psi = 77(16)^\circ$.

The crystal packing in **12** is supported only by hydrogen bonding interaction whereas in complex **13**, it is supported by C–H... π and π ... π stacking interactions. In complex **12**, C16–H16...O3 hydrogen bond with D...A distance of 3.246(8) Å connect between hydrogen H16 of aroylhydrazone and the oxygen O3 of counter ion perchlorate (Fig. 5.27 & Table 5.14).

Table 5.13. Selected bond lengths and bond angles of [Co(bpm)₂]ClO₄ (**12**) and [Zn(bpm)₂] (**13**).

Bond lengths (Å)			
[Co(bpm) ₂]ClO ₄ (12)		[Zn(bpm) ₂] (13)	
Co1–O1	1.886(2)	Zn1–O1	2.121(17)
Co1–N1	1.914(2)	Zn1–O3	2.132(18)
Co1–N2	1.846(2)	Zn1–N1	2.234(2)
C13–O1	1.299(2)	Zn1–N2	2.060(2)
C13–N3	1.329(4)	Zn1–N4	2.228(2)
N2–N3	1.364(5)	Zn1–N5	2.060(2)
Cl1–O3	1.458(2)	C13–O1	1.267(3)
Cl1–O4	1.367(2)	C33–O3	1.269(3)
Bond angles (°)			
O1–Co1–N2	82.83(12)	O1–Zn1–N1	150.35(7)
N1–Co1–N2	83.79(14)	N2–Zn1–N1	74.57(7)
O1–Co1–O1 ^a	89.49(9)	O1–Zn1–N2	75.86(7)
O1–Co1–N2 ^a	92.96(9)	O3–Zn1–N5	75.31(7)
O1 ^a –Ni1–N1	91.56(9)	N4–Zn1–N5	75.33(7)
O1–Co1–N1	166.61(16)	O3–Zn1–N4	150.63(7)
N2–Co1–N2 ^a	174.12(10)	N2–Zn1–N5	178.33(8)
N1–Co1–N2 ^a	100.40(10)	O1–Zn1–O3	98.15(7)
		N1–Zn1–N4	94.88(7)

a = 1-x, y, 3/2-z

Table 5.14 Hydrogen bonding interaction in **12**

Hydrogen bonding interaction				
D–H···A	D–H (Å)	H···A (Å)	D···A (Å)	∠D–H···A (°)
C(16)–H(16)···O(3) ^a	0.93	2.55	3.246(8)	131

Equivalent position code: a = 1-x, -1+y, 3/2-z

5.3.5.5. Crystal structure of [Zn(bpm)₂] (**13**)

The molecular structure of complex **13** is shown in Fig. 5.28 and the selected bond lengths and bond angles are listed in Table 5.13. The compound crystallizes in monoclinic *P2₁/c* space group. [Zn(bpm)₂] (**13**) is a monomeric complex, with each aroylhydrazone unit coordinating to the Zn(II) centre in a

tridentate monoanionic enolate form, giving a distorted octahedral environment with an N_4O_2 chromophore [189]. The distortion from the ideal octahedral geometry is revealed from the marked deviation of all angles subtended at the Zn(II) centre made by the donor atoms of aroylhydrazone. Four fused five membered metallocycles are formed on complexation and the chelate bite angles are in the range $74.57(7)$ - $75.86(7)^\circ$ which is more acute compared with other complexes reported earlier in this chapter. The azomethine nitrogen atoms N2 and N5 occupy *trans* positions with N2–Zn1–N5 bond angle of $178.33(8)^\circ$ and the configuration of coordinating atoms around the Zn centre are *trans*-N(2,5)-*cis*-N(1,4)-*cis*-O(1,3).

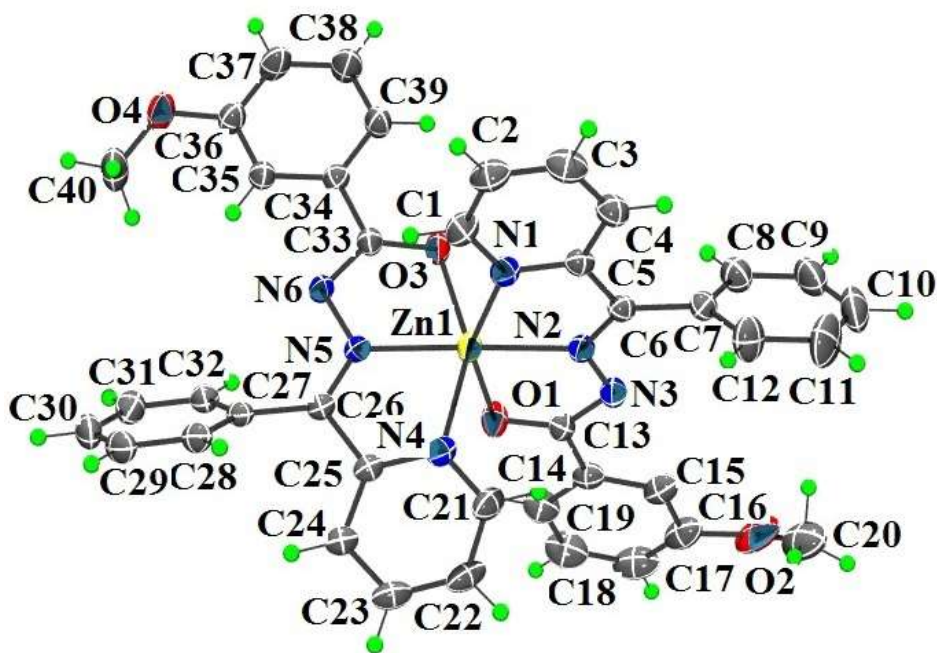


Fig. 5.28. ORTEP plot (drawn with 30% thermal ellipsoid) of $[Zn(bpm)_2]$ (13) along with atom numbering scheme of non-hydrogen atoms.

Ring puckering analysis shows that five membered chelate ring Cg(3) (comprised of atoms Zn1, N1, C5, C6 and N2) is puckered with puckering parameters $Q(2) = 0.121(18) \text{ \AA}$ and $\psi(2) = 200.0(10)^\circ$ and develops a twisted conformation [190]. The pseudorotation parameters P and τ are $P = 8.2(9)^\circ$, τ (m) = $10.8(1)^\circ$ for reference bond Zn1–N1.

A C–H $\cdots\pi$ interaction is observed in complex **13** between the six-membered Cg(8) ring and H40B of a methoxy carbon (Fig. 5.29) and a face to face $\pi\cdots\pi$ stacking interaction between pyridyl rings Cg(5) at a distance of $3.989(15) \text{ \AA}$ (Fig. 5.30). Non-bonding interactions in complex **13** are listed in Table 5.15.

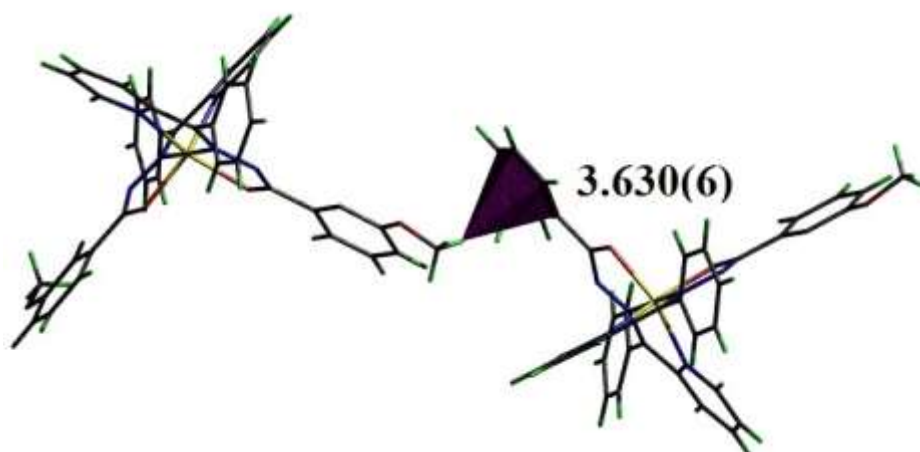


Fig. 5.29. The C–H $\cdots\pi$ interaction in complex **13**.

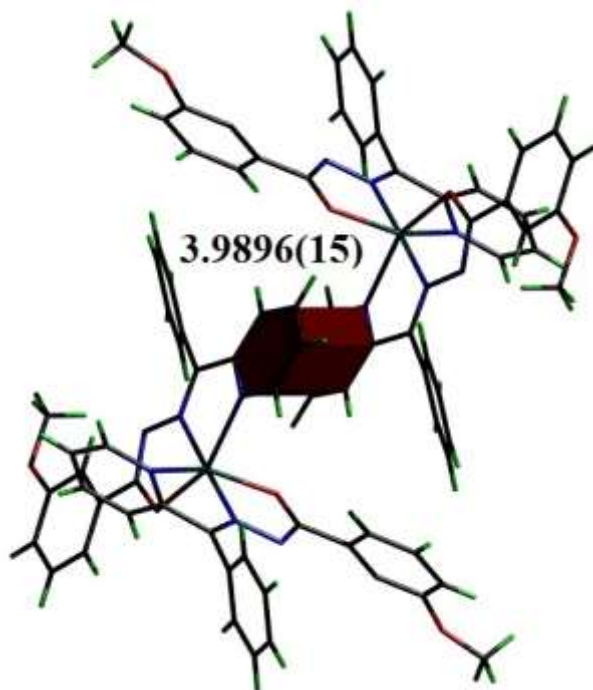


Fig. 5.30. The $\pi \cdots \pi$ interaction in complex **13**.

Table 5.15. Non-bonding interactions in **13**

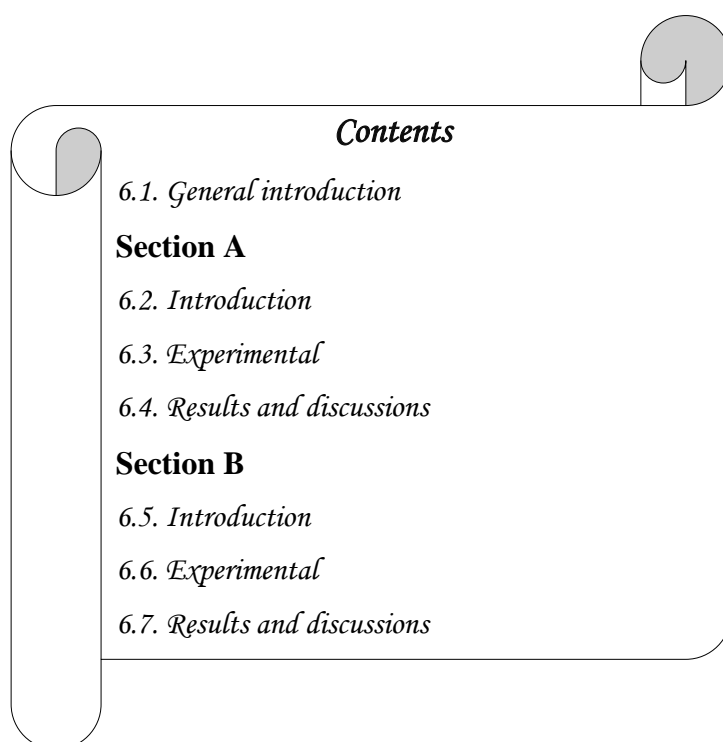
$\pi \cdots \pi$ interaction				
Cg(I)⋯Cg(J)	Cg⋯Cg (Å)	α (°)	β (°)	γ (°)
Cg(5)⋯Cg(5) ^a	3.989(15)	0	32.90	32.90
C–H⋯π interaction				
C–H(I)⋯Cg(J)	H⋯Cg (Å)	C⋯Cg (Å)	\angleC–H⋯Cg (°)	
C(40)–H(40B)⋯Cg(8) ^b	2.77	3.630(6)	150	

Equivalent position codes: a = 1-x, -y, -z; b = 1+x, 1/2-y, 1/2+z.

[Zn(bpm)₂] (**13**): Cg(5) = N1, C5, C6, C7, C8, C9; Cg(8) = C14, C15, C16, C17, C18, C19.

Chapter 6

ANTIBACTERIAL AND CYTOTOXICITY STUDIES OF SELECTED COMPLEXES



Contents

- 6.1. General introduction*
- Section A**
- 6.2. Introduction*
- 6.3. Experimental*
- 6.4. Results and discussions*
- Section B**
- 6.5. Introduction*
- 6.6. Experimental*
- 6.7. Results and discussions*

6.1. General Introduction

This chapter is divided into two sections based on the biological applications, antibacterial activity and cytotoxicity studies of selected complexes.

Section A deals with the antibacterial activities of complexes against both Gram(+) and Gram(-) bacterial stains. The Gram(+) bacteria used were *Staphylococcus aureus* and *Bacillus cereus* and Gram(-) bacteria were *Escherichia coli* and *Pseudomonas aeruginosa*. The antibacterial activity of the complexes has been investigated by Agar well diffusion method [191-193].

Section B deals with *in vitro* cytotoxicity studies of selected complexes in tumour cells as well as in normal cells by Trypan blue exclusion method [194-197].

Section A

ANTIBACTERIAL ACTIVITY

6.2. Introduction

Bacteria are microscopic organisms with a large domain of prokaryotic type. Typically a few micrometers in length, bacteria have a number of shapes, ranging from spheres to rods. Danish Physician Christian Grams, discovered the differential staining technique known as Gram staining, which differentiates the bacteria into two groups “Gram positive” and “Gram negative” [198,199]. Gram-positive bacteria stain purple because their cell walls are rich in peptidoglycan, while Gram negative bacteria, which lose the crystal violet, are counter-stained by saffranin and hence appear red in colour.

During an infection, “bacterial cells grow and divide, replicating repeatedly to reach large numbers”. In order to do so, bacteria “must synthesize or take up many types of biomolecules” causing cell deaths and disruption of cell function of the host organisms. Bacteria could also promote infection and disease by producing toxins that can exert their effects directly on a target cell or by disabling the immune system [200].

Antimicrobial activity is the process of killing or inhibiting the disease causing microbes. They may be anti-bacterial, anti-fungal or antiviral. Antibacterial activity of the complexes were tested *in vitro* against both Gram(+) and Gram(-) bacterial stains. In the present study of antimicrobial activity, two Gram-positive and two Gram-negative bacteria are selected.

(1) *Staphylococcus aureus*

They are Gram positive, round-shaped, non-motile, arranged in grape-like clusters; they grow on nutrient agar and produce colonies, which are golden yellow, white or lemon yellow in colour; frequently found in the upper respiratory tract and on the skin.

The word *staphylococcus* is derived from the Greek language (Gr. Staphylo= bunch of grapes; Coccus = a grain or berry) while the species name is derived from latin language (L; aureus = golden) [201]. They are capable of growth both aerobically and anaerobically. *Staphylococcus* is differentiated from micrococcus and another genus of the same family by its ability to utilize glucose, mannitol and pyruvate anaerobically.

(2) *Bacillus cereus* (*B. cereus*)

They are Gram-positive, rod-shaped, spore-forming bacterium that occurs naturally in many kinds of foods. It is the cause of “fried rice syndrome” as the bacteria are classically contracted from fried rice dishes that have been sitting at room temperature for hours.

(3) *Escherichia coli* (*E. coli*)

They are Gram-negative rods, motile with peritrichate flagella or nonmotile. They are commonly found in the lower intestine of warm-blooded organisms (endotherms).

Escherichia in 1885 discovered *Escherichia coli* which grows massively in fresh fecal matter under aerobic conditions for 3 days, but its numbers decline slowly afterwards [202]. They are commonly seen in coccobacillary form, which do not form any spore and have 4 to 8 paritrichate flagella, are sluggishly motile, are facultative anaerobes and grow in laboratory media. Most *E. coli* strains are harmless, but some serotypes can cause serious food poisoning in their hosts, and are occasionally responsible for product recalls due to food contamination.

(4) *Pseudomonas aeruginosa* (*P. aeruginosa*)

Pseudomonas is a Gram-negative, rod-shaped, asporogenous, and monoflagellated bacterium that can cause disease in plants and animals. It has a pearlescent appearance and grape-like or tortilla-like odour. Primary habitat of *P. aeruginosa* is human and animal gastro- intestinal tract, water, sewage, soil and vegetation. They are mostly related with hospital infections and post burn infections. They also cause infections of middle ear, eyes and urinary tracts. It is also associated with diarrhoea, pneumonia and osteomyelitis. Due to drug resistant nature of *P. aeruginosa*, it causes infection in patients receiving long term antibiotic therapy for wounds, burns and cystic fibrosis and other illness.

Various techniques for evaluating antimicrobial activity are

- i) Agar disc-diffusion method[203-206]
- ii) Agar well diffusion method
- iii) Agar Diffusion[207]
- iv) Broth Dilution method[208]
- v) Agar Dilution method [209]
- vi) Bioluminescence assay [210]
- vii) Cytofluorometric method [211].

6.2.1. Mode of action

Antimicrobial drugs interfere chemically with the synthesis function of vital components of microorganisms. The cellular structure and functions of eukaryotic cells of the human body. These differences provide us with selective toxicity of chemotherapeutic agents against bacteria. Antimicrobial drugs may either kill microorganisms outright or simply prevent their growth. There are various ways in which these agents exhibit their antimicrobial activity. They may inhibit

- Protein synthesis or ribosome function
- Bacterial nucleic acid synthesis
- Cell-wall synthesis
- Folate metabolism
- Enzymatic activity
- Cytoplasmic membrane function [212-214].

6.3. Experimental

6.3.1. Materials and Methods

6.3.1.1. Bacterial cultures used

Two Gram positive bacteria; *Staphylococcus* (MTCCNO 3103), *Bacillus* (MTCCNO 869) *sp* and two Gram negative bacteria; *Escherichia coli* (MTCCNO 68) and *Pseudomonas* (MTCCNO 2642) *sp*. were used in this study. The pure cultures were purchased from Microbial Type Culture Collection and Gene Bank, Institute of Microbial Technology, Chandigarh, India.

6.3.1.2. Media used

Nutrient Broth

(HiMedia Laboratories Pvt Ltd, Mumbai)

Peptic digest of animal tissue : 5 g

Sodium chloride	: 5 g
Yeast extract	: 1.5 g
Distilled water	: 1000 ml (pH – 7.4)

Nutrient Agar

(HiMedia Laboratories Pvt Ltd, Mumbai)

Peptic digest of animal tissue	: 5 g
Sodium chloride	: 5 g
Yeast extract	: 1.5 g
Distilled water	: 1000 ml (pH – 7.4)
Agar	: 15 g

6.3.2. Well Diffusion Method

Antibacterial test was carried out by well diffusion method with some modifications. The bacterial cultures (mentioned above) were maintained in nutrient broth. Each culture was uniformly distributed on Nutrient agar plates using sterile swabs. Wells of 3 mm diameter were cut on the surface of Nutrient agar plates at a distance of 2 cm using sterile well borer. DMSO (2 %) was used to dissolve the complex, which was found to have no adverse effect on the bacterial cultures. Complexes of different concentrations [100, 250, 500, 1000 & 1500 µg/ml] were added on each disc with a micropipette. Well with DMSO but, without complex was used as control. Then the plates were incubated at 37 °C for 24 hrs. After incubation, zone diameter was measured.

6.4. Results and discussions

The antibacterial activity of the two aroylhydrazones and their selected complexes were tested against two Gram-positive and two Gram-negative bacterial strains by agar well diffusion method and the zone of inhibition (mm) are presented

in Tables 6.1. and 6.2. The graphical representation of antibacterial activity of compounds against bacterial strains are shown in Figs. 6.1- 6.9.

Table 6.1. Antibacterial activity of aroylhydrazone **Hbpm** and its complexes **1**, **2**, **4** and **9**

Bacteria	Compound ($\mu\text{g/ml}$)	Hbpm	Zone diameter (mm)			
			1	2	4	9
	DMSO	-	-	-	-	-
<i>E.coli</i>	100	-	-	-	-	-
	250	-	-	-	-	-
	500	-	-	-	-	-
	1000	-	-	-	-	-
	1500	-	-	-	-	-
<i>Pseudomonas</i>	100	-	-	-	-	-
	250	-	-	-	-	-
	500	-	-	-	-	-
	1000	-	-	-	-	-
	1500	-	-	-	-	-
<i>Staphylococcus</i>	100	8	18	14	15	14
	250	9	20	17	15	16
	500	10	23	18	15	17
	1000	12	26	19	15	19
	1500	13	27	20	15	20
<i>Bacillus</i>	100	-	-	7	11	7
	250	-	-	8	12	10
	500	-	-	12	13	13
	1000	-	-	15	14	15
	1500	-	-	17	15	17

Table 6.2. Antibacterial activity of aroylhydrazone **Hdkm** and its complexes **3**, **5** and **8**

Bacteria	Compound ($\mu\text{g/ml}$)	Zone diameter (mm)			
		Hdpm	3	5	8
	DMSO	-	-	-	-
<i>E.coli</i>	100	-	-	-	-
	250	-	-	-	-
	500	-	-	-	-
	1000	-	-	-	-
	1500	-	-	-	-
<i>Pseudomonas</i>	100	-	-	-	-
	250	-	-	-	-
	500	-	-	-	-
	1000	-	-	-	-
	1500	-	-	-	-
<i>Staphylococcus</i>	100	11	15	20	18
	250	12	17	21	20
	500	15	20	23	22
	1000	16	23	25	26
	1500	17	25	26	28
<i>Bacillus</i>	100	9	16	12	13
	250	11	22	15	15
	500	12	23	17	17
	1000	13	26	21	21
	1500	15	26	23	24

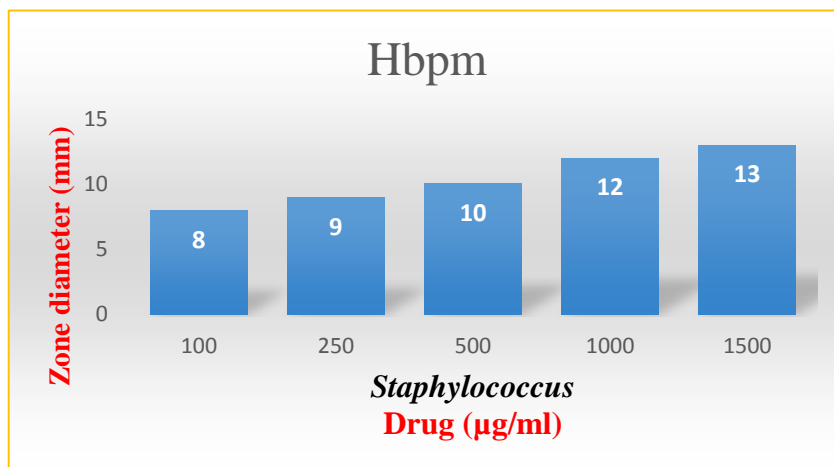


Fig. 6.1. Graphical representation of antibacterial activity of Hbpm against *Staphylococcus aureus*.

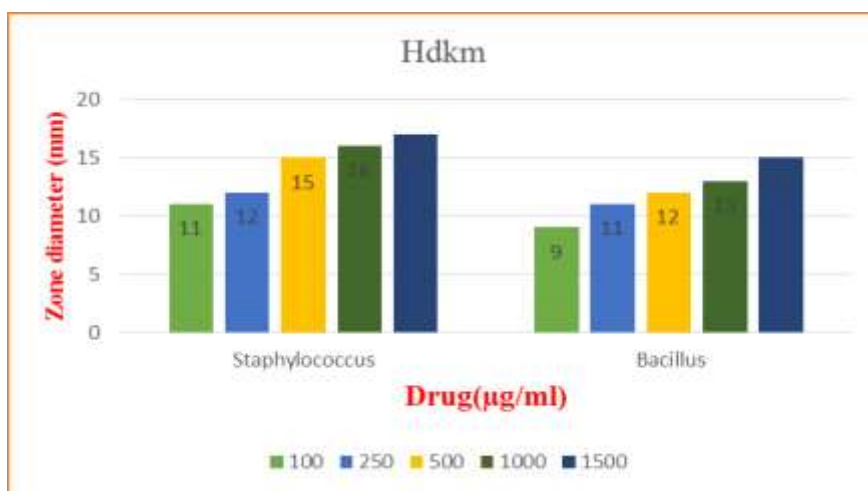


Fig. 6.2. Graphical representation of antibacterial activity of Hdkm against *Staphylococcus aureus* and *Bacillus cereus*.

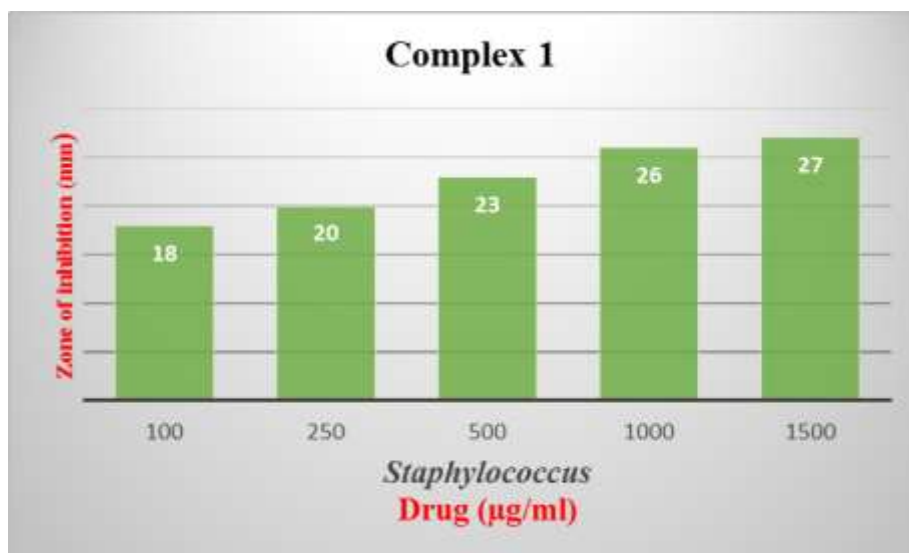


Fig. 6.3. Graphical representation of antibacterial activity of complex 1 against *Staphylococcus aureus*.

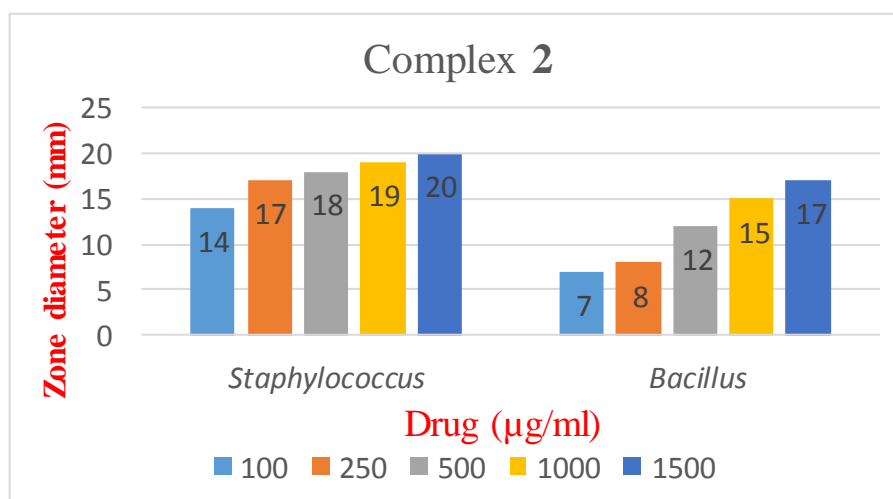


Fig. 6.4. Graphical representation of antibacterial activity of complex 2 against *Staphylococcus aureus* and *Bacillus cereus*.

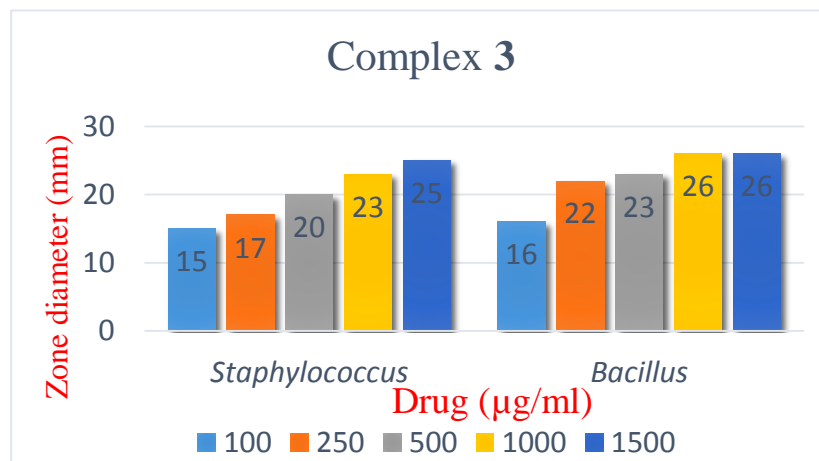


Fig. 6.5. Graphical representation of antibacterial activity of complex 3 against *Staphylococcus aureus* and *Bacillus cereus*.

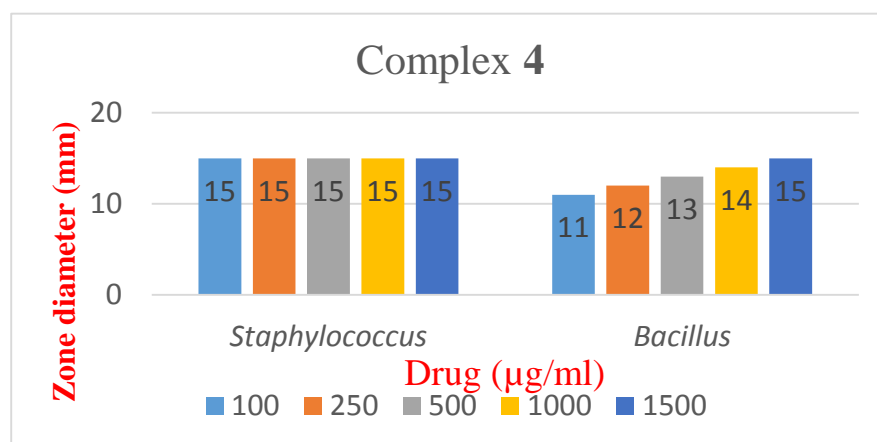


Fig. 6.6. Graphical representation of antibacterial activity of complex 4 against *Staphylococcus aureus* and *Bacillus cereus*.

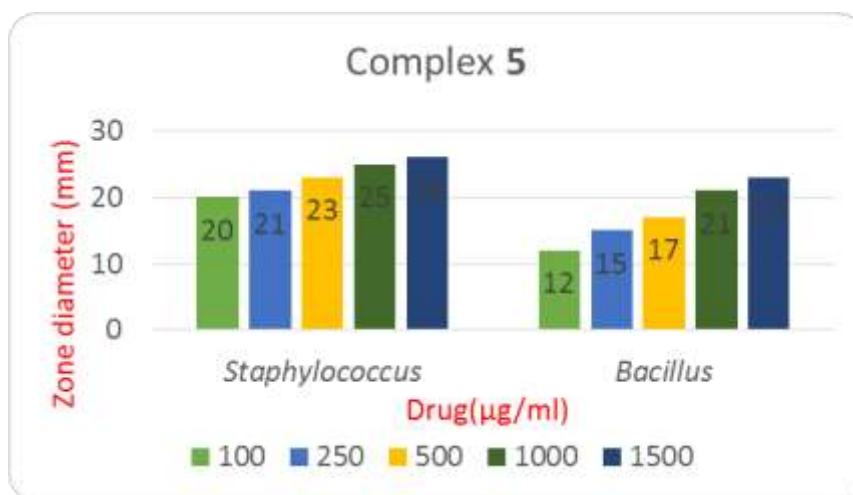


Fig. 6.7. Graphical representation of antibacterial activity of complex 5 against *Staphylococcus aureus* and *Bacillus cereus*.

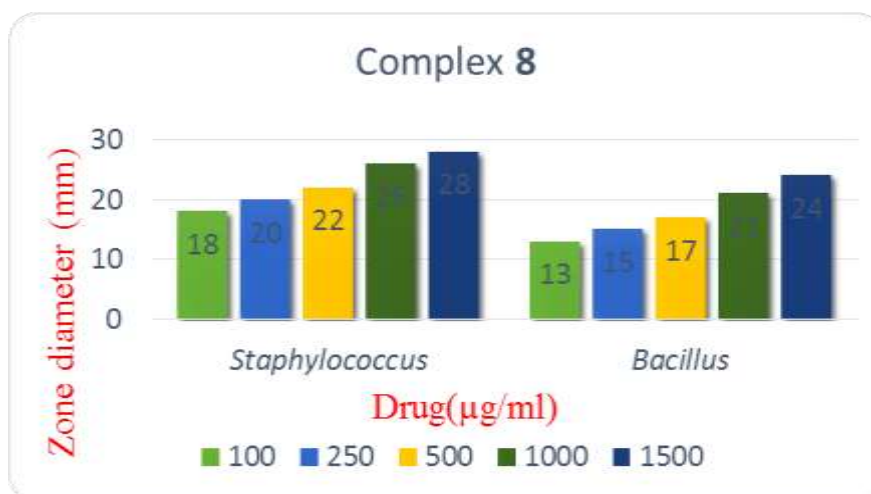


Fig. 6.8. Graphical representation of antibacterial activity of complex 8 against *Staphylococcus aureus* and *Bacillus cereus*.

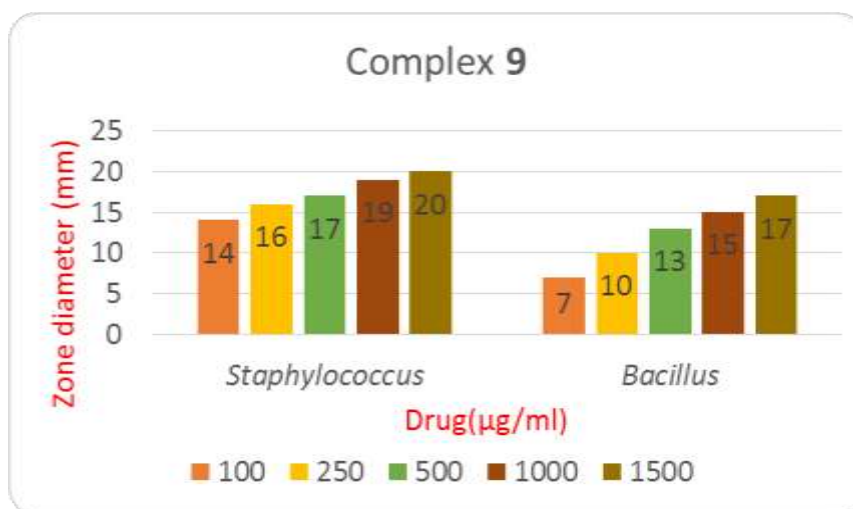


Fig. 6.9. Graphical representation of antibacterial activity of complex 9 against *Staphylococcus aureus* and *Bacillus cereus*.

The antibacterial effects were tested against two stains each of Gram positive and Gram negative bacteria by well diffusion method. After incubation the diameter of zone of inhibition was measured. All the compounds are inactive against gram-negative bacterial stains. Among the complexes of aroylhydrazones (Hbpm), the complex $[\text{Cu}(\text{bpm})_2]$ (**1**) exhibited higher activity against *Staphylococcus aureus* and this complex is inactive against all other bacterial stains. The best result was obtained for complex $[\text{Cu}(\text{dkm})_2]$ (**8**), i.e., 28 mm at 1500 µg/ml against *Staphylococcus aureus* among the two sets of aroylhydrazones. A comparative study of the aroylhydrazones and their metal complexes indicate that complexes showed higher antibacterial activity than their corresponding aroylhydrazones. Compounds showed antibacterial activity against the tested strains of bacteria in a dose dependent manner. It is known that chelation tends to make ligands act as more powerful and potent bacterial agents [215]. Such increased activity of the complexes can be explained on the basis of the Overtone concept of the permeability [216,217] and Tweedy Chelation theory [218-220].

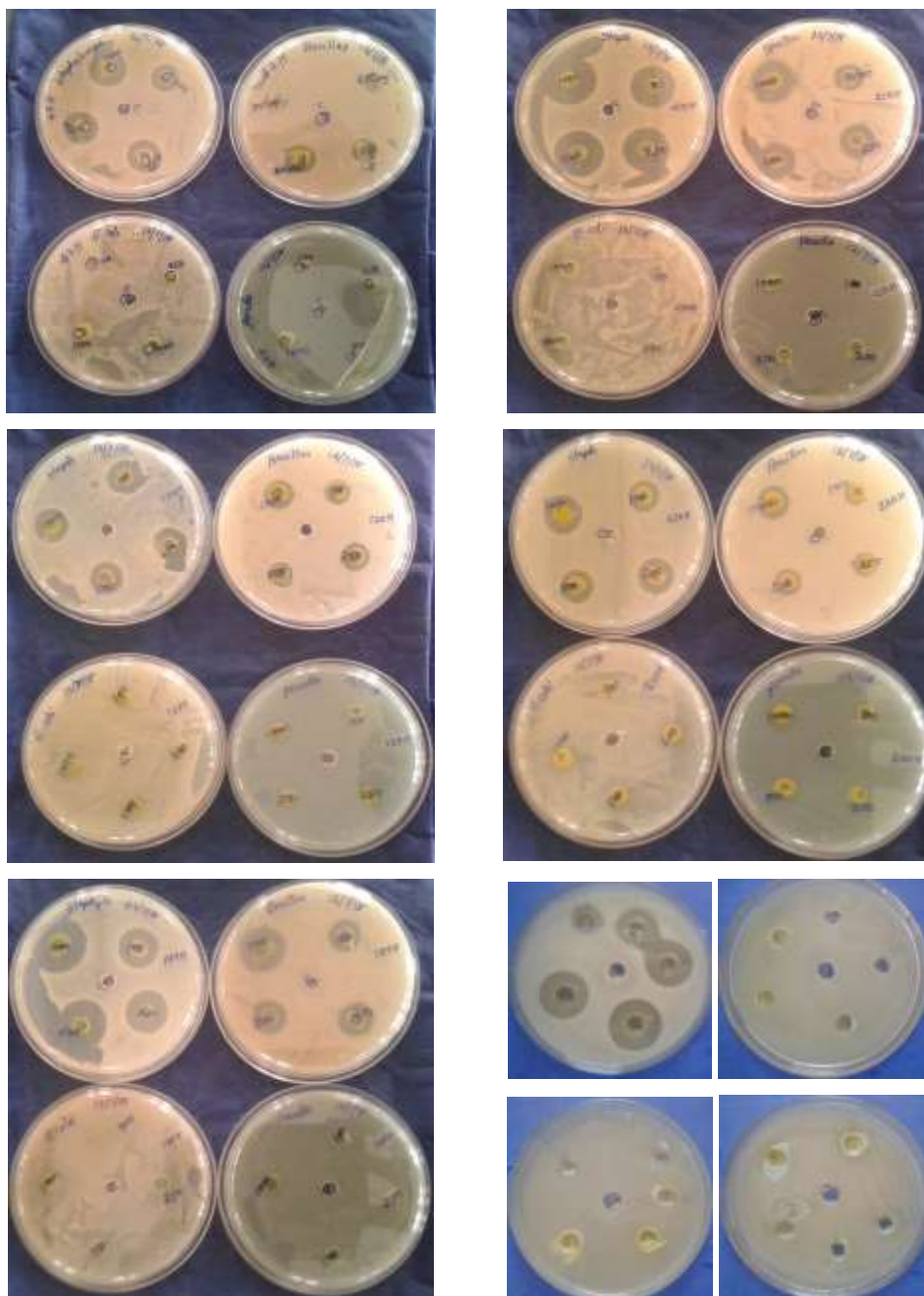


Fig. 6.10. Photograph showing antibacterial activity of various complexes

Overtone concept of cell permeability states that the lipid membrane that surrounds the cell favours the passage of only the lipid-soluble materials due to which liposolubility is an important factor, which controls the antimicrobial activity.

On chelation, the polarity of the metal ion will be reduced to a greater extent due to the overlap of the ligand orbital and partial sharing of the positive charge of the metal ion with donor groups. Also, it increases the delocalization of π -electrons over the whole chelate ring and enhances the lipophilicity of the complexes [221]. This increased lipophilicity enhances the penetration of the complexes into lipid membranes and blocking of the metal binding sites in the enzymes of microorganisms. These complexes also disturb the respiration process of the cell and thus blocks the synthesis of the proteins that restricts further growth of the organism [222].

Furthermore, the mode of action of the compound may involve formation of a hydrogen bond through the azomethine group with the active centre of cell constituents, resulting in interference with normal cell process.

The antibacterial activity of the ligand pyridine-2-carboxaldehyde 4-hydroxybenzoylhydrazone and its two azide bridged copper(II) complexes were evaluated against the bacteria *Entrobacter facealis*, *Staphylococcus aureus*, *Entrobacter aerogenes*, *Escherichia coli*, *Klebsiella pneumonia* and *Proteus mirabilis*, with the complexes demonstrating enhanced activity relatively to the free aroylhydrazone [122]. Fekri *et al*, synthesized three copper(II) complexes of 2-hydroxybenzaldehyde benzhydrazone and the antibacterial activity result showed that they have better activity towards Gram positive bacteria than towards Gram negative bacteria. The reason for this may probably be due to the difference of the cell membrane structure, where the outer membrane of Gram negative bacteria can reduce the damage from the complexes. This means that the external membrane of

Gram negative bacteria may play a preventive role for the antibacterial effect of this complexes [223].

Section B

CYTOTOXICITY STUDY

6.5. Introduction

Aroylhydrazones and their complexes exhibit a wide variety of properties, *e.g.* antimicrobial, antitumour, DNA binding and magnetism and therefore represent attractive materials in chemistry and medicine [224,225]. To improve the efficiency and overcome the side effects of already known chemotherapeutic agents, numerous transition metal complexes have been synthesized and tested for cytotoxicity studies [226-228]. Cytotoxicity studies of two hydrazones, 4-nitrobenzhydrazide and 2-acetylpyridine benzhydrazide by MTT assay, suggested that they significantly reduce the cell viability of breast cancer cell lines (MCF7) and human prostate adenocarcinoma (DU145) in a dose dependent manner [229]. *In vitro* cytotoxicity of benzhydrazone-related ligands and their copper(II) complexes against THP-1 and HepG2 cells demonstrated that the complexes are significantly more cytotoxic than the corresponding ligands [230].

Cell viability and cytotoxicity assays are used for drug screening and cytotoxicity tests of chemicals. They are based on various cell functions such as enzyme activity, cell membrane permeability, cell adherence, ATP production, co-enzyme production, and nucleotide uptake activity. Cytotoxicity is the quality of being toxic to cells. Examples of toxic agents are an immune cell or some types of venom. Researchers can look for cytotoxic compounds in developing a therapeutic that targets rapidly dividing cancer cells. To measure cell viability, researchers established methods such as Trypan blue exclusion method, Colony Formation

method, Crystal Violet method, Tritium-Labeled Thymidine Uptake method, MTT and WST methods [231,232].

6.6. Experimental

6.6.1. *In vitro* cytotoxicity study - Trypan Blue Exclusion Method

It is used to determine the number of viable cells present in a cell suspension. Trypan Blue is a widely used assay for staining dead cells. It is based on the principle that live cells possess intact cell membranes that exclude trypan blue, whereas dead cells do not. In this method, cell viability must be determined by counting the unstained cells with a microscope or other instruments. A viable cell will have a clear cytoplasm whereas a nonviable cell will have a blue cytoplasm.

The test compounds were studied for short term *in vitro* cytotoxicity using Dalton's Lymphoma Ascites (DLA) cells. The tumour cells aspirated from the peritoneal cavity of tumour bearing mice were washed thrice with normal saline or PBS (Phosphate buffered saline). Viable cell suspension (1×10^6 cells in 0.1 ml) was added to tubes containing various concentrations of the test compounds and the volume was made up to 1 ml using phosphate buffered saline. Control tube contained only cell suspension. These assay mixture were incubated for 3 hours at 37 °C. Further cell suspension was mixed with 0.1 ml of 1% trypan blue and kept for 2-3 minutes and loaded on a haemocytometer. Dead cells take up the blue colour of trypan blue while live cells do not take up the dye. The number of stained and unstained cells were counted separately. % cytotoxicity was calculated using the equation

$$\% \text{ cytotoxicity} = \frac{\text{No. of dead cells}}{\text{No. of live cells} + \text{No. of dead cells}} \times 100$$

Before the % cytotoxicity of compounds are tested using tumour cells, the % cytotoxicity of compounds are tested using normal rat spleen cells.

The test compound was studied for short term *in vitro* cytotoxicity using rat spleen cells. For this rat was sacrificed using carbon dioxide anaesthesia and the spleen tissue was dissected out. It was then smashed to single cell suspension in RPMI (Rosewell Park Memorial Institute) complete medium containing antibiotics and filtered using mesh cloth. The collected cells were washed thrice and suspended in known volume of RPMI complete medium containing antibiotics and counted. Viable cell suspension (1×10^6 cells in 0.1 ml) was added to tubes containing various concentrations of the test compound and the volume was made upto 1 mL using RPMI media. Control tubes contained only cell suspension (without additives). These tubes were incubated for 3 h at 37°C. At the end of incubation cell suspension in the tubes were mixed with 0.1 mL 1% trypan blue and kept for 2-3 minute and loaded on a haemocytometer. Dead cells take up the blue colour of trypan blue while live cells do not take up the dye. The number of stained cells were counted separately. The % cytotoxicity was calculated by using the above formula.

6.7. Results and discussions

The % cytotoxicity of two aroylhydrazones and their selected complexes are given in Tables 6.3 and 6.4 and the graphical representation of % cytotoxicity is shown in Figs. 6.10 and 6.11.

Table 6.3. % cytotoxicity results of Hbpm and its complexes **1, 2, 4** and **12**

Drug concentration (µg/ml)	% cytotoxicity				
	Hbpm	1	2	4	12
200	52	82	74	100	56
100	32	62	52	78	42
50	20	42	35	60	30
20	8	30	12	52	12
10	0	18	10	40	8

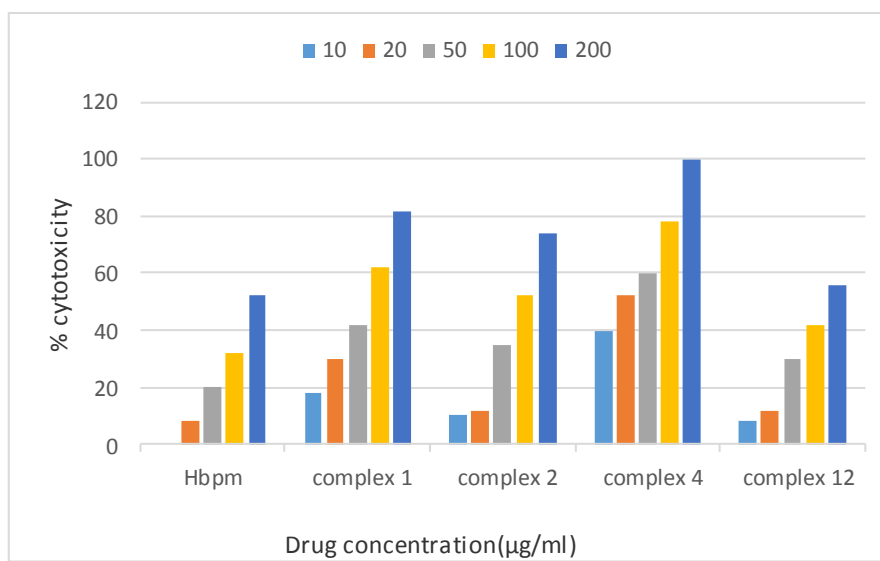
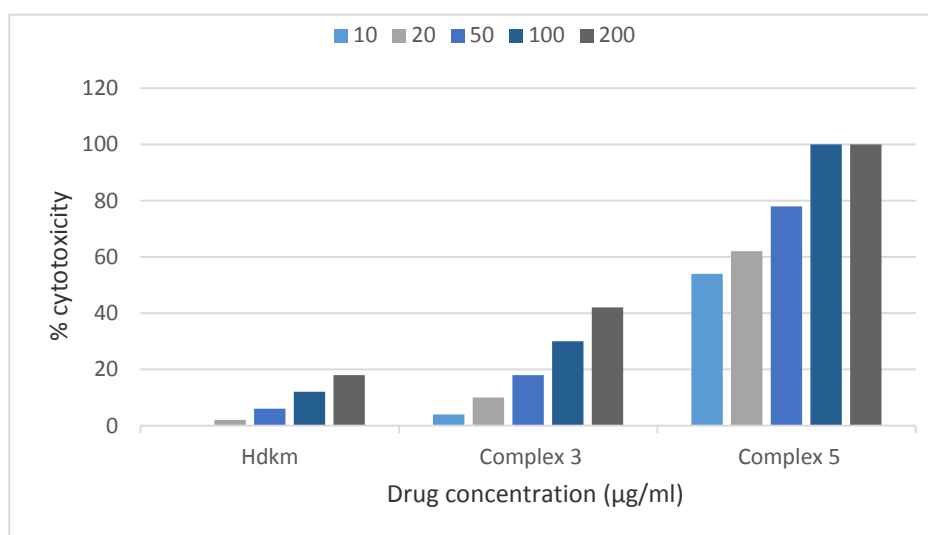


Fig. 6.10. Graphical representation of % cytotoxicity of Hbpm and its complexes **1, 2, 4** and **12**.

Table 6.4. % cytotoxicity results of Hbpm and its complexes **3** and **5**

Drug concentration ($\mu\text{g/ml}$)	% cytotoxicity		
	Hdkm	3	5
200	18	42	100
100	12	30	100
50	6	18	78
20	2	10	62
10	0	4	54

**Fig. 6.11.** Graphical representation of % cytotoxicity of Hdkm and its complexes **3** and **5**.

The results of % cytotoxicity studies of compounds showed that as compared to free ligands, complexes have better cytotoxicity. The ligands Hbpm and Hdkm show % cytotoxicity of 52 and 18% at 200 $\mu\text{g/ml}$ concentration.

Among all the tested compounds, complex $[\text{Cu}(\text{dkm})\text{N}_3]_2$ (**5**) has highest activity *i.e.*, at 100 and 200 $\mu\text{g}/\text{ml}$ it shows 100% cytotoxicity. Chloride bridged complex $[\text{Cu}(\text{bpm})\text{Cl}]_2$ (**1**) has high activity (82%) than bromide bridged one $[\text{Cu}(\text{bpm})\text{Br}]_2$ (**2**) (74%). Two azide bridged complexes $[\text{Cu}(\text{bpm})\text{N}_3]_2$ (**4**) and $[\text{Cu}(\text{dkm})\text{N}_3]_2$ (**5**) have 100% cytotoxicity at 200 $\mu\text{g}/\text{ml}$, higher than halide bridged complex. The chelation of the benzhydrazone ligand with the Cu(II) ion is considered responsible for the observed cytotoxic effect.

The % cytotoxicity of compounds were also tested in normal cells and the results showed that they are non-toxic in nature.

Chapter 7

SUMMARY AND CONCLUSION

Aroylhydrazones have attracted considerable attention due to their wide spectrum of activities in the biological, medicinal, catalytic and polymerisation fields. Biological and medicinal activities include antimicrobial, antioxidant, anticancer, antitubercular and DNA binding. They are resourceful compounds which can act as potential multifunctional ligands with interesting coordination modes in either neutral, monoanionic, dianionic or tetraanionic forms bearing unusual coordination numbers. Among the various transition metals, dinuclear copper(II) complexes are gaining more importance because of their relevance in biological fields. Copper exhibits rich coordination chemistry with complexes and has its own footprint in both magnetic susceptibility and EPR. Copper(II) complexes of diverse drugs have been the subject of a large number of research studies due to its synergic activity with the drug. The design and synthesis of halide/pseudohalide bridged dinuclear copper(II) complexes of hydrazones have been an attractive area of research. Copper(II) complexes of 2-acetylpyridine and 2-benzylpyridine derived hydrazones are known to act as an effective strategy for antimicrobial activity improvement. Furthermore, metal complexes of aroylhydrazones have shown *in vitro* cytotoxic activity.

Summary of the thesis

The thesis is divided into seven chapters.

Chapter 1

This chapter gives an idea about the general introduction of aroylhydrazones derived by the condensation of aldehydes/ketones with hydrazides. Coordinating properties, coordination diversity and objectives of the present work are discussed here. Various physicochemical techniques like IR, UV, EPR, elemental analysis, Hirshfeld Surface Analysis and SCXRD employed for the characterization of aroylhydrazones and their complexes, biological applications like antibacterial activity and cytotoxicity are also discussed in this chapter.

Chapter 2

Chapter 2 describes the syntheses and characterization of two aroylhydrazones 2-benzoylpyridine-3-methoxybenzhydrazone and di-2-pyridyl ketone-3-methoxybenzhydrazone. The characteristic C=O and N–H peaks in the aroylhydrazones give significant information regarding the existence of amido form of the ligand. Electronic spectra show absorption band due to π - π^* and n - π^* transitions. Number of different types of hydrogen atoms present in the compound and its electronic environment are obtained from ^1H NMR spectra. X-ray crystallography showed that both crystals exist in the triclinic crystal system with $P\bar{1}$ space group. Torsion angles C5–C6–N2–N3 and N2–N3–C13–O1 are $4.7(2)^\circ$ and $2.1(2)^\circ$ which support the *cis* configurations of the C(6)–N(2) and C(13)–N(3) bonds in Hbpm. Pyridine rings in the aroylhydrazones are favourable for forming intermolecular hydrogen bonding with azomethine N atom. Hirshfeld surfaces for aroylhydrazones are mapped with d_{norm} and shape index. 2D fingerprint plot

analysis help in quantification of the intermolecular interactions. These decomposition analyses will allow one to assess each interaction discretely that is otherwise overlapped in the full finger print plots. The non-directional H...H contacts are one of the major contributors to the overall interaction.

Chapter 3

Chapter 3 deals with the syntheses and characterization of three single crystals of halogen bridged copper(II) complexes of two aroylhydrazones, Hbpm and Hdkm, of which two of them are chloride bridged and the other one is a bromide bridged complex. They are characterized by IR, electronic and EPR spectra, HS analysis and SCXRD technique. Complexes [Cu(bpm)Cl]₂ (**1**), [Cu(bpm)Br]₂ (**2**) and [Cu(dkm)Br]₂ (**3**) are halogen bridged box dimer copper(II) complexes having monoclinic lattice with *P*2₁/*n* symmetry. They have distorted square pyramidal geometry with Addison parameter values of 0.16, 0.155 and 0.05 respectively. In all the three complexes, the basal plane contains planar N, N, O aroylhydrazone ligand and the halogen atom. The halogen atom of the nearby monomer engages an axial position forming a dimer with Cu...Cu separation of approximately 3.369, 3.436 and 3.4760 Å for complexes **1**, **2** and **3** respectively. The apical metal-halogen distance is longer than the equatorial metal-halogen distance. All the three copper(II) complexes show similar binding modes having $g_{\parallel} > g_{\perp} > 2.0023$ values and it shows that a single electron resides in the $d_{x^2-y^2}$ ground state. Intermolecular contacts present in them are shown by Hirshfeld surface analysis.

Chapter 4

Chapter 4 discusses the syntheses and characterization of copper(II) and nickel(II) complexes of aroylhydrazones containing pseudohalides as coligands. Two pseudohalides, azide and thiocyanate are used as coligands. Complexes

[Cu(bpm)N₃]₂ (**4**), [Cu(dkm)N₃]₂ (**5**) and [Ni(dkm)N₃]₂ (**6**) are azide bridged box dimer complexes whereas complex [Cu(bpm)(SCN)]_n (**7**) is a thiocyanate bridged one dimensional polymer. Azide bridged complexes **4**, **5** and **6** showed characteristic azide bridging peak at 2045 cm⁻¹. Bridging [M–NCS–M'] complex **7** exhibits ν(CN) well above 2100 cm⁻¹. Complexes **4-7** showed *d-d* bands in the 646-691 nm range. SCXRD analysis showed that compounds **4-6** crystallize in monoclinic lattice with *P2₁/n* symmetry while compound **7** crystallizes in orthorhombic lattice with *Pna21* symmetry. Addison parameter calculations give τ values 0.27, 0.174, 0.167 and 0.157 respectively which highlight the distorted square pyramidal geometry and also substantiated by the bond angles around the central metal with the coordinating atoms. For complexes **4-6**, the basal plane of the square pyramid is satisfied by the donor atoms of aroylhydrazone and N atom of azide. The N atom of adjacent monomer occupies the axial position. EPR plots showed that copper(II) complexes **4**, **5** and **7** display axial spectra. In the case of all the complexes, the non-directional H···H contacts are one of the major contributors to the overall interaction.

Chapter 5

Chapter 5 portrays syntheses and characterization of six bisligated transition metal complexes of copper(II), nickel(II), cobalt(III) and zinc(II). The synthesized compounds are physico-chemically characterized by CHN analysis, molar conductivity and spectroscopic techniques like IR, UV and EPR. The molecular structure of the complexes have been resolved using single crystal XRD studies. XRD studies reveal that in all complexes except complex **9**, the tridentate aroylhydrazone coordinates to the metal center *via* pyridine nitrogen, azomethine nitrogen and iminolate oxygen and found to possess distorted octahedral geometry. In complex **9**, one aroylhydrazone is coordinated to the metal *via* tridentate monoanionic form whereas another is coordinated *via* bidentate neutral form and one perchlorate anion is present outside the coordination sphere.

Chapter 6

In this chapter antibacterial activity and cytotoxicity studies of selected complexes are discussed. The antibacterial activities of the complexes have been screened *in vitro* against both Gram(+) and Gram(-) bacterial stains. The Gram(+) bacteria used are *Staphylococcus aureus* and *Bacillus cereus* and Gram(-) bacteria are *Escherichia coli* and *Pseudomonas aeruginosa*. The antibacterial activity of the complexes has been investigated by Agar well diffusion method. Complexes showed good antibacterial activity compared to free ligands in a dose dependent manner. The highest activity was shown by complex [Cu(dkm)₂] (**8**). No inhibition zone was formed in the case of Gram(-) bacterial stains.

In vitro cytotoxicity of the complexes have been tested by Trypan blue exclusion method. The results of % cytotoxicity studies of compounds showed that as compared to free ligands, complexes have better cytotoxicity. The ligands Hbpm and Hdkm showed % cytotoxicity of 52 and 18% at 200 µg/ml concentration. Among all the tested compounds, complex [Cu(dkm)N₃]₂ (**5**) has high activity *i.e.*, at 100 and 200 µg/ml it shows 100% cytotoxicity. Chloride bridged complex [Cu(bpm)Cl]₂ (**1**) has high activity (82%) than bromide bridged one [Cu(bpm)Br]₂ (**2**) (74%). Two azide bridged complexes [Cu(bpm)N₃]₂ (**4**) and [Cu(dkm)N₃]₂ (**5**) have 100% cytotoxicity at 200 µg/ml, higher than halide bridged complex **1**. The chelation of the benzhydrazone ligand with the Cu(II) ion is considered responsible for the observed cytotoxic effect.

The % cytotoxicity of compounds are also tested in normal cells and the results showed that they are non-toxic in nature.

Chapter 7

Chapter 7 explains the conclusion and future aspects of our work. We have successfully isolated single crystals of two similar aroylhydrazones 2-benzoylpyridine-3-methoxybenzhydrazone (Hbpm) and di-2-pyridyl ketone-3-methoxybenzhydrazone (Hdkm) and their complexes. Three halide bridged box dimer copper(II) complexes, four pseudohalide bridged complexes and six bisligated complexes of copper(II), nickel(II), cobalt(III) and zinc(II) complexes are prepared using these two aroylhydrazones, Hbpm and Hdkm. All the bridged box dimer complexes show distorted square pyramidal geometry with monoclinic space group. Hirshfeld Surface Analysis of all prepared complexes were done using Crystal Explorer 17 software. Antibacterial activity of selected complexes have been done and showing better activity compared to free ligands in a dose dependent manner. Cytotoxicity studies of complexes shows high % cytotoxicity. Among all the tested compounds, complex $[\text{CuL}^2\text{N}_3]_2$ (**5**) has high activity *i.e.*, at 100 and 200 $\mu\text{g/ml}$ it shows 100% cytotoxicity.

Future Outlook

- Synthesize more NNO donor ligands
- Syntheses of acetate, thiocyanate and dicyanamide bridged complexes of copper(II) and nickel(II)
- Antifungal and antiviral activity studies
- Study of structural and magnetic properties of double *end-on* azido-bridged dimeric copper(II) complexes
- A theoretical study of the synthesized compounds to get an idea about the HOMO and LUMO molecular orbitals
- *In vivo* cytotoxicity studies of synthesized compounds
- Electrostatic Potential (ESP) analysis will give an in-depth insight into the inherent electronic differences in the structure of the synthesized compounds.

References

- [1] E. J. Corey, D. Enders, *Tetrahedron Lett.* **1976**, *17*, 11.
- [2] N. P. Belskaya, W. Dehaen, V.A. Bakulev, *Arch. Org. Chem.* **2010**, *1*, 275.
- [3] E. Corey, *Tetrahedron Lett.* **1976**, *17*, 3.
- [4] A. J. Xavier, M. Thakur, J. M. Marie, *J. Chem. Pharm. Res.* **2012**, *4*, 986.
- [5] L. Yueqin, Y. Zhiwei, Z. Minya, L. Yun, H. Jing, W. Xuehong, L. Zhengfeng, *RSC Adv.* **2017**, *7*, 41527.
- [6] S. Mondal, C. Das, B. Ghosh, B. Pakhira, A. J. Blake, M. G. B. Drew, S. K. Chattopadhyay, *Polyhedron* **2014**, *80*, 272.
- [7] N. Mohan, S. Muthurani, R. Ramesh, *J. Organomet. Chem.* **2016**, *807*, 45.
- [8] A. A. R. Despaigne, F. B. D. Costa, O. E. Piro, E. E. Castellano, S. R. W. Louro, H. Beraldo, *Polyhedron* **2012**, *38*, 285.
- [9] A. A. R. Despaigne, J. G. Da Silva, A. C. M. Carmo, O. E. Piro, E. E. Castellano, H. Beraldo, *Inorg. Chim. Acta* **2009**, *362*, 2117.
- [10] S.S. Sreejith, A. Nair, V. A. Smolenski, J. P. Jasinski, M. R. P. Kurup, *Inorg. Chim. Acta* **2018**, *469*, 264.
- [11] B. Samanta, J. Chakraborty, S. Shit, S.R. Batten, P. Jensen, J. D. Masuda, S. Mitra, *Inorg. Chim. Acta* **2007**, *360*, 2471.
- [12] G. N. Babu, A. R. B. Rao, Srinivas Keesara, S. Pal, *J. Organomet. Chem.* **2017**, *848*, 243.
- [13] N. A. Mangalama, S. Sivakumara, M. R. P. Kurup, E. Suresh,

- Spectrochim. Acta A* **2010**, 75, 686.
- [14] Bibitha Joseph, *Studies on Transition Metal Chelates of Some Tridentate Aroylhydrazones*, Ph. D Thesis, CUSAT, **2014**,139.
- [15] F. A. Mautner, F. R. Louka, T. Le Guet, S. S. Massoud, *J. Mol. Struct.* **2009**, 919, 203.
- [16] F. A. Mautner, F. R. Louka, A. A. Gallo, M. R. Saber, N. B. Burham, J. H. Albering, S. S. Massoud, *Transition Met. Chem.* **2010**, 35, 613.
- [17] M. Wriedt, C. Näther, *Eur. J. Inorg. Chem.* **2011**, 2, 228.
- [18] J. Boeckmann, C. C. Näther, *Polyhedron* **2012**, 31, 587.
- [19] K. Das, T. N. Mandal, S. Roy, A. Jana, S. Konar, C.-M. Liu, A. K. Barik, S. K. Kar, *Polyhedron* **2011**, 30, 715.
- [20] M. M. Fousiamol, M. Sithambaresan, V. A. Smolenski, J. P. Jasinski, M. R. P. Kurup, *Polyhedron* **2018**, 141, 60.
- [21] K. Das, A. Datta, C. Sinha, J.-H. Huang, E. Garribba, C.-S. Hsiao, C.-L. Hsu, *Chem. Open* **2012**, 1, 80.
- [22] Z.-X. Miao, M.-X. Li, M. Shao, H.-J. Liu, *Inorg. Chem. Commun.* **2007**, 10, 1117.
- [23] F. C. Liu, Y. F. Zeng, J. P. Zhao, B. W. Hu, X. H. Bu, J. Ribas, S. R. Batten, *Inorg. Chem. Commun.* **2007**, 10, 129.
- [24] Y. F. Zeng, F. C. Liu, J. P. Zhao, S. Cai, X. H. Bu, J. Ribas, *Chem. Commun.* **2006**, 21, 2227.
- [25] Q. F. Yang, Z. G. Gu, C. H. Li, J. Q. Tao, J. L. Zuo, X. Z. You, *Inorg. Chim. Acta* **2007**, 360, 2875.
- [26] A. Escuer, M. Font-Bardia, S. S. Massoud, F. A. Mautner, E. Penalba, X. Solans, R. Vicente, *New J. Chem.* **2004**, 28, 681.

- [27] G. Ambrosi, P. Dapporto, M. Formica, V. Fusi, L. Giorgi, A. Guerri, P. Paoli, R. Pontellini, P. Rossi, *Dalton Trans.* **2004**, 0, 3468.
- [28] K. Dhara, S. Karan, J. Ratha, P. Roy, G. Chandra, M. Manassero, B. Mallik, P. Banerjee, *Chem. Asian J.* **2007**, 2, 1091.
- [29] D. Y. Wu, W. Huang, W. J. Hua, Y. Song, C. Y. Duan, S. H. Li, Q. J. Meng, *Dalton Trans.* **2007**, 0, 1838.
- [30] S. Mitra, D. L. Hughes, G. Rosair, C. Desplanches, *Polyhedron* **2007**, 26, 1740.
- [31] W. Cao, Y. Liu, T. Zhang, J. Jia, *Polyhedron* **2018**, 147, 62.
- [32] R.-Ş. Mezey, I. Máthé, S. Shova, M.-N. Grecu, T. Roşu, *Polyhedron* **2015**, 102, 684.
- [33] S. Rollas, Ş. G. Küçükgül, *Molecules* **2007**, 12, 1910.
- [34] B. J. Walfrido, S. A. Magna, A. A. Marina, P. R. Anayive, L. P. Gabrieli, E. C. Eduardo, E. P. Oscar, J. B. Eliezer, M. L. Lídia, B. Heloisa, *Molecules* **2011**, 16, 6902.
- [35] R. Eswaran, G. Valentina, B. Roberta, S. Paolo, N. Karuppanan, S. P. B. Nattamai, V. Alfonso, Z. Alfonso, G. Antonella, D. Alessandro, A. Alberto, M. Cristina Marzano, *J. Inorg. Biochem.* **2018**, 182, 18.
- [36] R. K. Singh, A. K. Singh, S. Siddiqui, M. Arshad, A. Jafri, *J. Mol. Struct.* **2017**, 1135, 82.
- [37] M. Sutradhar, Rajeshwari, T. R. Barman, A. R. Fernandes, F. Paradinha, C. Roma Rodrigues, M. F. C. Guedes da Silva, J. L. P. Armando, *J. Inorg. Biochem.* **2017**, 175, 267.
- [38] A. Gerpe, G. Alvarez, D. Benítez, L. Boiani, M. Quiroga, P.

- Hernández, *Bioorg. Med. Chem.* **2009**, *17*, 7500.
- [39] N. S. Cutshall, R. Onrust, A. Rohde, S. Gragerov, L. Hamilton, K. Harbol, *Bioorg. Med. Chem. Lett.* **2012**, *22*, 5595.
- [40] S. A. Carvalho, L. O. Feitosa, M. Soares, T. E. Costa, M. G. Henriques, K. Salomão, *Eur J. Med. Chem.* **2012**, *54*, 512.
- [41] S. A. Carvalho, M. Kaiser, R. Brun, E. F. Silva, C. A. M. Fraga, *Molecules* **2014**, *19*, 20374.
- [42] C. M. Leal, S. L. Pereira, A. E. Kümmerle, D. M. Leal, R. Tesch, C. M. Sant'Anna, *Eur J. Med. Chem.* **2012**, *55*, 49.
- [43] K. M. E. Tehrani, M. E. Zadeh, V. Mashayekhi, M. Hashemi, K. F. Kobarfard, F. Gharebaghi, S. Mohebbi, *Iran. J. Pharm. Res.* **2015**, *14*, 1077.
- [44] L. M. Lima, F. S. Frattani, S. J. L. Dos, H. C. Castro, C. A. Fraga, R. B. Zingali, *Eur. J. Med. Chem.* **2008**, *43*, 348.
- [45] L. Yueqin, Y. Zhiwei, Z. Minya, L. Yun, H. Jing, W. Xuehong, L. Zhengfeng, *RSC Adv.*, **2017**, *7*, 41527.
- [46] G. Ramadoss, R. Andy, M. Athiappan, *Bioinorg. Chem. Appl.* **2014**, *21539*, 1.
- [47] G. Cansu G. Ramazan, *Main Group Chemistry* **2013**, *12*, 25.
- [48] M. E. S. Mohamad, H. S. Majed, M. Nagy, M. A. A. Tayseer, *Main Group Chem.* **2014**, *13*, 187.
- [49] M. S. Niasari, A. Amiri, *Appl. Catal., A* **2005**, *290*, 46.
- [50] A. El-Motaleb, M. Ramadan, R. M. Issa, *Transition Met. Chem.* **2005**, *30*, 471.
- [51] A. Sanam, N. Nader, S. S. Mirabdullah, M. Kheirollah, F. Nazanin, *Polyhedron* **2019**, *160*, 115.

- [52] R. B Singh, T. Odashima, H. Ishii, *Analyst* **1983**, *108*, 1120.
- [53] T. Nakanishi, M. Otomo, *Anal. Sci.* **1985**, *1*, 161.
- [54] T. Nakanishi, M. Otomo, *Microchem. J.* **1986**, *33*, 172.
- [55] L. H. S. Avila, M. C. Cunha, I. Gaubeur, M. Encarnacion, V. Suarezih, *Spectrosc. Lett.* **1999**, *32*, 257.
- [56] N. A. Zatar, A. Z. Abu-zuhri, A. Al-nuri, F. M. Mahmoud, A. A. Abu-obaid, *Spectrosc. Lett.* **1989**, *22*, 1203.
- [57] M. V. Rossi, M. E. V. Suarez-Iha, M. R. Hoffman, *Spectrosc. Lett.* **1995**, *28*, 1153.
- [58] M. Salgado, C. B. Ojeda, A. G. D. Torres, J. M. C. Pavon, *Analyst* **1988**, *113*, 1283.
- [59] B. Tang, L. Zhang, J. Zhang, Z. Z. Chen, Y. Wang, *Spectrochim. Acta A* **2004**, *60*, 2425.
- [60] B. Tang, H. Zhang, Y. Wang, *Spectrochim. Acta A* **2005**, *61*, 2239.
- [61] A. Jana, S. Konar, K. Das, S. Ray, J. A. Golen, A. L. Rheingold, L. M. Carrella, E. Rentschler, T. K. Mondal, S. K. Kar, *Polyhedron* **2012**, *38*, 258.
- [62] J. A. Weil, J. R. Bolton, *Electron Paramagnetic Resonance*, Second Edition, John Wiley & Sons, Inc., **2007**.
- [63] N. M. Athorton, *Electron Spin Resonance: Theory and Applications*, Ellis Horwood Ltd. New York, **1973**.
- [64] W. Gordy, *Theory and Applications of Electron Spin Resonance. Techniques of Chemistry*. Vol. XV, John Wiley and Sons, **1979**.
- [65] A. Abragam and B. Blcancy; *Electron Paramagnetic Resonance of Transition ions*, Clarendon Pres., Oxford, **1970**.
- [66] Stoll, S. *Spectral Simulations in Solid-State Electron Paramagnetic*

- Resonance Ph. D. thesis*, ETH, Zurich, **2003**.
- [67] I.M. Procter, B.J. Hathaway, P. Nicholis, *J. Chem. Soc.* **1968**, 1678.
- [68] B.N. Figgis, *Introduction to Ligand fields*, Interscience, New York, **1996**, 295.
- [69] B.J. Hathaway, G. Wilkinson, R. D. Gillard, J. A. McCleverty, *Comprehensive Coordination Chemistry*, vol. 5, Pergamon, Oxford, **1987**, 533.
- [70] N. Aiswarya, C. Ajina, L. Tom, M. R. P. Kurup, *Chem. Select* **2018**, 3, 7031.
- [71] M. Jayendran, M. Sithambaresan, P. M. Sabura Begum, M.R. P. Kurup, *Polyhedron* **2019**, 158, 386.
- [72] D. Majumdar, J. K. Biswas, M. Mondal, M. S. S. Babu, R. K. Metre, S. Das, K. Bankura, D. Mishra, *J. Mol. Struct.* **2018**, 1155, 745.
- [73] M. A. Spackman, D. Jayatilaka, *Cryst. Eng. Comm.* **2009**, 11, 19.
- [74] B. H. Gayathri, J. P. Dasappa, N. R. Bhavya, Chandra, M. Mahendra, *J. Mol. Struct.* **2017**, 1146, 490.
- [75] SMART and SAINT, Area Detector Software Package and SAX Area Detector Integration Program, Bruker Analytical X-ray, Madison, WI, USA, **1997**.
- [76] SADABS, Area Detector Absorption Correction Program, Bruker Analytical X-ray, Madison, WI, **1997**.
- [77] G.M. Sheldrick, *Acta Crystallogr., Sect. C* **2015**, C71, 3.
- [78] L.J. Farrugia, *J. Appl. Crystallogr.* **2012**, 45, 849.
- [79] K. Brandenburg, Diamond Version 3.2g, Crystal Impact GbR, Bonn, Germany, **2010**.

- [80] A. A. R. Despaigne, L. F. Vieira, I. C. Mendes, F. B. D. Costa, N. L. Speziali, H. Beraldo, *J. Braz. Chem. Soc.* **2010**, *21*, 1247.
- [81] D. Kuriakose, A. A. Aravindakshan, M. R. P. Kurup, *Polyhedron* **2017**, *127*, 84.
- [82] N. A. Mangalam, S. R. Sheeja, M. R. P. Kurup, *Polyhedron* **2010**, *29*, 3318.
- [83] J. E. Philip, A. A. Shanty, E. S. Jose, M. R. P. Kurup, P. V. Mohanan, *Inorg. Chim. Acta* **2018**, *469*, 87.
- [84] A. A. Aravindakshan, B. Joseph, U. L. Kala, M. R. P. Kurup, *Polyhedron* **2017**, *123*, 206.
- [85] T. M. Asha · M. R. P. Kurup, *J. Chem. Crystallogr.* <https://doi.org/10.1007/s10870-018-0756-9>.
- [86] M. Kuriakose, M. R. P. Kurup, E. Suresh, *Spectrochim. Acta A* **2007**, *66A*, 353.
- [87] N. A. Mathews, A. Jose, M. R. P. Kurup, *J. Mol. Struct.* **2019**, *1178*, 544.
- [88] N. A. Mangalam, *Chelating behavior of acylhydrazones towards transition metals: Spectral and structural aspects Ph. D. thesis, CUSAT*, **2010**, 26.
- [89] M. J. Turner, J. J. McKinnon, S. K. Wolff, D. J. Grimwood, P. R. Spackman, D. Jayatilaka, M. A. Spackman, *CrystalExplorer17*, University of Western Australia, 2017.
- [90] A. Shaik, S. Kirubakaran, V. Thiruvenkatam, *Acta Crystallogr., Sect. E* **2017**, *E73*, 531.
- [91] I. Khan, P. Panini, S. Khan, U. A. Rana, H. Andleeb, D. Chopra, S. Hameed, J. Simpson, *Cryst. Growth Des.* **2016**, *16*, 1371.

- [92] S. Balachandar, M. Sethuram, P. Muthuraja, T. Shanmugavadivu, M. Dhandapani, *J. Photochem. Photobiol. B* **2016**, *163*, 352.
- [93] Yang-Hui Luo, Guo-Gan Wu, Shu-Lin Mao, Bai-Wang Sun, *Inorg. Chim. Acta* **2013**, *397*, 1.
- [94] Z. Bouhidel, A. Cherouana, P. Durand, A. Doudouh, F. Morinib, B. Guillot, S. Dahaoui, *Inorg. Chim. Acta* **2018**, *482*, 34,
- [95] W. Nbill, K. Kaabi, F. Lefebvre, W. Fujita, C. Jelsch, C. ben Nasr, *J. Coord. Chem.* **2018**, *71*, 2526.
- [96] A. A. R. Despaigne, J. G. D. Silva, A. C. M. Do Carmo, O. E. Piro, E. E. Castellano, H. Beraldo, *J. Mol. Struct.* **2009**, *920*, 97.
- [97] B. Moksharagni, K. D. Kumar, S. Chandrasekhar, K. H. Reddy, *Int. J. Pharm. Bio. Sci.* **2015**, *6(3)*, 11.
- [98] S. Pal, *Proc. Indian Acad. Sci.* **2002**, *114*, 417.
- [99] B. Joseph, M. Sithambaresan, M. R. P. Kurup, S. W. Ng, *Acta Crystallogr., Sect. E* **2014**, *E70*, 211.
- [100] P. K. Singh, K. Banerjee, S. Singla, *Int. J. Sci. Res.* **2017**, *6*, 1911.
- [101] F. A. Mautner, M. Traber, R. C. Fischer, K. Reichmann, R. Vicente, *Polyhedron* **2018**, *144*, 30.
- [102] S. Stoll, A. Schweiger, *J. Magn. Reson.* **2006**, *178*, 42.
- [103] M. Joseph, M. Kuriakose, M. R. P. Kurup, E. Suresh, A. Kishore, S. G. Bhat, *Polyhedron* **2006**, *25*, 61.
- [104] R. J. Kunnath, M. Sithambaresan, A. A. Aravindakshan, A. Natarajan, M. R. P. Kurup, *Polyhedron* **2016**, *113*, 73.
- [105] A. Sreekanth, M. R. P. Kurup, *Polyhedron* **2003**, *22*, 3321.
- [106] E. S. Jose, J. E. Philip, A. A. Shanty, M. R. P. Kurup, P. V. Mohanan, *Inorg. Chim. Acta* **2018**, *478*, 155.

- [107] L. V. Tamayo, J. G. D. Silva, M. C. Quintão, H. A. Duarte, S. R. W. Louro, H. Beraldo, *Polyhedron* **2017**, *134*, 199.
- [108] B. Bag, N. Mondal, S. Mitra, V. Gramlich, J. Ribas, M. S. E. Fallah, *Polyhedron* **2001**, *20*, 2113.
- [109] P. B. Sreeja, M. R. P. Kurup, A. Kishore, C. Jasmin, *Polyhedron* **2004**, *23*, 575.
- [110] P.F. Rapheal, E. Manoj, M. R. P. Kurup, *Polyhedron* **2007**, *26*, 818.
- [111] Y. P. Singh, R. N. Patel, Y. Singh, R. J. Butcher, P. K. Vishakarma, R. K. B. Singh, *Polyhedron* **2017**, *122*, 1.
- [112] M. A. Spackman, J. J. McKinnon, D. Jayatilaka, *Cryst. Eng. Comm.* **2008**, *10*, 377.
- [113] M. Abedi, O. Z. Yes_ilel, G. Mahmoudi, A. Bauzá, S. E. Lofland, Y. Yerli, W. Kaminsky, P. Garczarek, J. K. Zareba, A. Ienco, A. Frontera, M. S. Gargari, *Inorg. Chim. Acta* **2016**, *443*, 101.
- [114] A. D. Martin, K. J. Hartlieb, A. N. Sobolev, C. L. Raston, *Cryst. Growth Des.* **2010**, *10*, 5302.
- [115] A. W. Addison, T. N. Rao, J. Reedijk, J. Van Rijn, G. C. Verschoor, *Dalton Trans.* **1984**, 1349.
- [116] S. J. Grabowski, *Crystals* **2016**, *6*, 59.
- [117] M. C. Etter, J. C. Macdonald, *Acta Crystallogr., Sect. B.* **1990**, *B46*, 256.
- [118] M. S. Ray, A. Ghosh, R. Bhattacharya, G. Mukhopadhyay, M. G. B. Drew, J. Ribas, *Dalton Trans.* **2004**, 252.
- [119] J. Bernstein, M. C. Etter, J. C. Macdonald, *J. Chem. Soc. Perkin Trans. 2* **1990**, 695.
- [120] N. C. Jana, K. Pramanik, A. Bauzá, P. Brandão, M. Patra, A.

- Frontera, A. Panja, *Polyhedron* **2017**, *124*, 262.
- [121] S. Ferlay, T. Mallah, R. Ouahes, P. Veillet, and M. Verdaguer, *Nature* **1995**, *378*, 701.
- [122] B. Shaabani, A.A. Khandar, H. Mobaiyen, N. Ramazani, S.S. Balula, L. Cunha-Silva, *Polyhedron* **2014**, *80*, 166.
- [123] F. A. Mautner, M. Traber, R. C. Fischer, K. Reichmann, R. Vicente, *Polyhedron* **2018**, *144*, 30.
- [124] C. Adhikary, S. Koner, *Coord. Chem. Rev.* **2010**, *254*, 2933.
- [125] M. Nandy, S. Shit, E. Garribba, C. J. Gomez-Garcia, S. Mitra, *Polyhedron* **2015**, *102*, 137.
- [126] A. Jana, S. Konar, K. Das, S. Ray, J. A. Golen, A. L. Rheingold, L. M. Carrella, E. Rentschler, T. K. Mondal, S. K. Kar, *Polyhedron* **2012**, *38*, 258.
- [127] S. Banerjee, M. G. B. Drew, C.-Z. Lu, J. Tercero, C. Diaz, A. Ghosh, *Eur. J. Inorg. Chem.* **2005**, 2376.
- [128] S. S. Massoud, A. E. Guilbeau, H. T. Luong, R. Vicente, J. H. Albering, R. C. Fischer, F. A. Mautner, *Polyhedron* **2013**, *54*, 26.
- [129] C. Adhikary, D. Mal, K.-I. Okamoto, S. Chaudhuri, S. Koner, *Polyhedron* **2006**, *25*, 2191.
- [130] I. Banerjee, J. Marek, R. Herchel, M. Ali, *Polyhedron* **2010**, *29*, 1201.
- [131] W. W. Sun, X. B. Qian, C. Y. Tian, E. Q. Gao, *Inorg. Chim. Acta* **2009**, *362*, 2744.
- [132] M. A. S. Goher, T. C. W. Mak, *Inorg. Chim. Acta* **1985**, *99*, 223.
- [133] Y. Agnus, R. Louis, J. P. Gisselbrecht, R. Weiss, *J. Am. Chem. Soc.* **1984**, *106*, 93.

- [134] P. Chaudhuri, K. Oder, K. Wieghart, B. Nuber, J. Weiss, *Inorg. Chem.* **1986**, 25, 2818
- [135] S. Shit, P. Talukder, J. Chakraborty, G. M. S. Pilet, E. I. Fallah, J. Ribas, S. Mitra, *Polyhedron* **2007**, 26, 1357.
- [136] G. Chastanet, B. L. Guennic, C. Aronica, G. Pilet, D. Luneau, M. L. Bonnet, V. Robert, *Inorg. Chim. Acta* **2008**, 361, 3847.
- [137] S. Saha, S. Koner, J.-P. Tuchagues, A. K. Boudalis, K. -I. Okamoto, S. Banerjee, D. Mal, *Inorg. Chem.* **2005**, 44, 6379.
- [138] Y. Song, C. Massera, M. Quesada, A. M. M. Lanfredi, I. Mutikainen, U. Turpeinen, J. Reedijk, *Inorg. Chim. Acta* **2005**, 358, 1171.
- [139] T. C. Stamatatos, G. S. Papaefstathiou, L. R. MacGillivray, A. Escuer, R. Vicente, E. Ruiz, S. P. Perlepes, *Inorg. Chem.* **2007**, 46, 8843.
- [140] Z. L. You, H. L. Zhu, *Z. Anorg. Allg. Chem.* **2006**, 632, 140.
- [141] R. Kurtaran, K. C. Emregul, C. Arici, F. Ercan, V. J. Catalano, O. Atakol, *Synth. React. Inorg. Met. Org. Chem.* **2003**, 33, 281.
- [142] S. Koner, S. Saha, K. -I. Okamoto, J. P. Tuchagues, *Inorg. Chem.* **2003**, 42, 4668.
- [143] A. Escuer, G. Aromí, *Eur. J. Inorg. Chem.* **2006**, 4721.
- [144] S. S. Tandon, L. K. Thompson, J. N. Bridson, *J. Chem. Soc.* **1993**, 804.
- [145] Z. Hong, *Transition Met. Chem.* **2008**, 33, 797.
- [146] N. A. Bailey, S. L. Kozak, T. W. Michelsen, W. N. Mills, *Coord. Chem. Rev.* **1971**, 6, 407.
- [147] E. Diana, K. Gatterer, S. F. A. Kettle, *Phys. Chem. Chem. Phys.*

- 2016**, *18*, 414.
- [148] S. Koner, S. Saha, K.-I. Okamoto, J.-P. Tuchagues, *Inorg. Chem.* **2004**, *43*, 840.
- [149] M. Kabešova, J. Gažo, *Chem. zvesti* **1980**, *34*, 800.
- [150] R. H. Toeniskotter, S. Solomon, *Inorg. Chem.* **1968**, *7*, 617.
- [151] M. N. Uddin, T. S. Rupa, *Mod. Chem.* **2015**, *3*, 1.
- [152] A. Tomkiewicz, J. Klak, J. Mrozinski, *Mater. Sci.-Poland*, **2004**, *22*, 253.
- [153] L. Dobrzanska, G. Wrzeszcz, A. Grodzicki, F. Rozploch, *Polish J. Chem.* **2000**, *74*, 1017.
- [154] W. A. Alves, A. C. Sant'Ana, M. P. Abbott, P. Homem-de-Mello, H. Martinho, R. H. A. Santos, J. G. Ferreira, M. L. A. Temperini, A. Paduan-Filho, A. M. D. C. Ferreira, *Sci. Adv. Mater.* **2010**, *2*, 1.
- [155] W. A. Alves, R. H. A. Santos, A. Paduan-Filho, C. C. Becerra, A. C. Borin, A. M. D. C. Ferreira, *Inorg. Chim. Acta* **2004**, *357*, 2269.
- [156] W. A. Alves, S. A. de Almeida-Filho, R. H. A. Santos, A. M. D. C. Ferreira, *Inorg. Chem. Commu.* **2003**, *6*, 294.
- [157] W. A. Alves, S. A. de Almeida-Filho, R. H. A. Santos, A. Paduan-Filho, A. M. D. C. Ferreira, *J. Braz. Chem. Soc.* **2004**, *15*, 872.
- [158] W. A. Alves, I. O. Matos, P. M. Takahashi, E. L. Bastos, H. Martinho, J. G. Ferreira, C. C. Silva, R. H. A. Santos, A. M. D. C. Ferreira, *Eur. J. Inorg. Chem.* **2009**, 2219.
- [159] L. Seiroli, M. Bukowska-Strzyzewska, *Acta Crystallogr., Sect. C* **1997**, *C53*, 296.
- [160] T. Hokelek, V. Yavuz, H. Dal, H. Necefoglu, *Acta Crystallogr., Sect. E*, **2018**, *74*, 45.

- [161] C. V. Perez, I. C. Ortega, A. V. Macias, A. M. Payan, G.A. Echeverria, D. B. Soria, G. C. V. Uribe, *New J. Chem.* **2018**, *42*, 7166.
- [162] S. Mondal, P. Chakraborty, N. Aliaga-alcalde, S. Mohanta, *Polyhedron* **2013**, *63*, 96.
- [163] M. S. Ray, A. Ghosh, R. Bhattacharya, G. Mukhoppadhyay, M. G. B. Drew, J. Ribas, *Dalton Trans.* **2004**, 252.
- [164] D. Cremer, J. A. Pople, *J. Am. Chem. Soc.* **1975**, *97*, 1354.
- [165] G. G. Evans, J. A. Boeyens, *Acta Crystallogr., Sect. B* **1989**, *45*, 581.
- [166] S. T. Rao, E. Westhof, M. Sundaralingam, *Acta Crystallogr. Sect. A* **1981**, *37*, 421.
- [167] B. Machura, A. Switlicka, I. Nawrot, J. Mrozinski, R. Kruszynski, *Polyhedron* **2011**, *30*, 832.
- [168] Z. L. You, *Acta Crystallogr. Sect. C* **2005**, *61*, 466.
- [169] M. Jiang, Y. T. Li, Z. Y. Wu, Z. Q. Liu, X. Wu, *J. Inorg. Organomet. Polym. Mater.* **2008**, *18*, 448.
- [170] B. N. B. Raj, M. R. P. Kurup, E. Suresh, *Spectrochim. Acta A* **2008**, *71*, 1253.
- [171] B. N. B. Raj, M. R. P. Kurup, E. Suresh, *Struct. Chem.* **2006**, *17*, 201.
- [172] N. M. H. Salem, A. R. Rashad, L. E. Sayed, W. Haase, M. F. Iskander, *Polyhedron* **2014**, *68*, 164.
- [173] A. A. Aravindakshan, *An exploration of the coordination aspects of aroylhydrazones Ph. D. Thesis* **2017**, 306.
- [174] L. Tom, N. Aiswarya, S. S. Sreejith, M. R. P. Kurup, *Inorg. Chim.*

- Acta* **2018**, 473, 223.
- [175] A. Sreekanth, S. Sivakumar, M.R.P. Kurup, *J. Mol. Struct.* **2003**, 47, 655.
- [176] . S. Garg, D. N. Kumar, *Spectrochim. Acta A* **2003**, 59, 229.
- [177] E. D. L. Piló, A. A. R. Despaigne, J. G. D. Silva, I. P. Ferreira, J. A. Takahashi, H. Beraldo, *Polyhedron* **2015**, 97, 30.
- [178] N. Aiswarya, M. Sithambaresan, S. S. Sreejith, S. W. Ng, M. R. P. Kurup, *Inorg. Chim. Acta* **2016**, 443, 251.
- [179] L. Latheef, M. R. P. Kurup, *Spectrochim. Acta A* **2008**, 70, 86.
- [180] R. P. John, A. Sreekanth, V. Rajakannan, T. A. Ajith, M. R. P. Kurup, *Polyhedron* **2004**, 23, 2549.
- [181] J. J. McKinnon, M. A. Spackman, A. S. Mitchell, *Acta Crystallogr., Sect. B* **2004**, 60, 627.
- [182] M. A. Spackman, P. G. Byrom, *Chem. Phys. Lett.* **1997**, 267, 215.
- [183] S. K. Seth, D. Sarkar, A. Roy, T. Kar, *Cryst. Eng. Comm.* **2011**, 13, 6728.
- [184] E. Manoj, M. R. P. Kurup, *Polyhedron* **2008**, 27, 275.
- [185] V. Suni, M. R. P. Kurup, M. Nethaji, *Polyhedron* **2007**, 26, 3097.
- [186] S. Shit, J. Chakraborty, B. Samanta, A. M. Z. Slawin, V. G. S. Mitra, *Struct. Chem.* **2009**, 20, 633.
- [187] B. Samanta, J. Chakraborty, S. Shit, S. R. Batten, P. Jensen, J. D. Masuda, S. Mitra, *Inorg. Chim. Acta* **2007**, 360, 2471.
- [188] Z. Q. Hu, Y. Wu, B. Jia, S. M. Shi, X. D. Zhu, F. H. Song, *Inorg. Chem.* **2005**, 21, 1710.
- [189] K. A. Gerling, N. M. Rezayee, A. L. Rheingold, D. B. Green, J. M. Fritsch, *Dalton Trans.* **2014**, 43, 16498.

- [190] E. J. Corey, N. F. Feiner, *J. Org. Chem.* **1980**, *45*, 765.
- [191] M. Balouiri, M. Sadiki, S. K. Ibsouda, *J. Pharm. Anal.* **2016**, *6*, 71.
- [192] S. Magaldi, S. Mata-Essayag, C. Hartung de Capriles, *Int. J. Infect. Dis.* **2004**, *8*, 39.
- [193] C. Valgas, S. M. D. Souza, E. F. A. Smânia, *Braz. J. Microbiol.* **2007**, *38*, 369.
- [194] R. Jeevana *Metal Complexes of Thiosemicarbozons*, *Ph.D. Thesis*. University of Calicut **2012**.
- [195] B. Shrishailappa, H. Santhoshkumar, N. Senthilkumar; C. H. Raghu. *J. Pharmacol.* **2007**, *103*, 354.
- [196] P. J. Moldeus, Sorrhierius, L. Parker. *Methods Enzymol.* **1978**, *2*, 60.
- [197] N. P. Priya, A. P. Firdous, R. Jeevana, K. K. Aravindakshan *Indian J. Pharm. Sci.* **2015**, *77*, 655.
- [198] E. Lolis, R. Bucala, *Nat. Rev. Drug Disc*, **2003**, *2*, 635.
- [199] M. R. J. Salton, K. S Kim. Structure. In: Baron S, editor. *Medical Microbiology*. 4th edition. Galveston (TX): University of Texas Medical Branch at Galveston; 1996. Chapter 2.
- [200] A. K. Deisingh, M. Thompson, *Analyst*, **2002**, *127*, 567.
- [201] L. G. Harris, S. J. Foster, R. G. Richards, *Eur. Cells Mater.* **2002**, *4*, 39.
- [202] E. M. Cooke, *J. Hyg., Camb.* **1985**, *95*, 523.
- [203] N. G. Heatley, *Biochem. J.* **1944**, *38*, 71.
- [204] M. Balouiri, *J. Pharm. Anal.* **2016**, *6*, 61.
- [205] J. H. Jorgensen, M. J. Ferraro, *Clin. Infect. Dis.* **2009**, *49*, 1749.
- [206] F. Caron, *Anti-Infect.* **2012**, *14*, 186.

- [207] A. Marston, *J. Chromatogr., A* **2011**, 1218, 2676.
- [208] H. Liang, Y. Xing, J. Chen, *Altern. Med.* **2012**, 12, 238.
- [209] A. Imhof, S. A. Balajee, K. A. Mar, *J. Clin. Microbiol.* **2003**, 41, 5683.
- [210] S. Finger, C. Wiegand, H. J. Buschmann, *Int. J. Pharm.* **2013**, 452, 188.
- [211] A. Paparella, L. Taccogna, I. Aguzzi, *Food Control* **2008**, 19, 1174.
- [212] H. C. Neu, T. D. Gootz, *Antimicrobial Chemotherapy. Medical Microbiology*. 4th edition. Galveston (TX): University of Texas Medical Branch at Galveston; 1996. Chapter 11.
- [213] K. M. O'Connell, J. T. Hodgkinson, H. F. Sore, M. Welch, G. P. Salmond, D. R. Spring *Angew. Chem. Int. Edition* **2013**, 52, 10706.
- [214] A. S Said, A. E. Amar, H. A. El-Sayed, M. A. Al-Omae, M. M. Abdalla, *Int. J. Pharm.* **2015**, 11, 502.
- [215] N. Dharmaraj, P. Viswanathamurthi, K. Natarajan, *Transition Met. Chem.* **2001**, 26, 1.
- [216] W. Shinoda, *Biochim. Biophys. Acta*, **2016**, 1858, 2254.
- [217] J. F. Nagle, J. C. Mathai, M. L. Zeidel, S. Tristram-Nagle, *J. Gen. Physiol.* **2008**, 131, 77.
- [218] M. Patil, R. Hunoor, K. Gudasi, *Eur. J. Med. Chem.* **2010**, 45, 2981.
- [219] B. G. Tweedy, *Phytopatholo.* **1964**, 55, 910.
- [220] K. S. Kumar, C. P. Varma, V. N. Reena, K. K. Aravindakshan, *J. Pharm. Sci. Res.* **2017**, 9, 1317.
- [221] L. Mitu, N. Raman, A. Kriza, N. Stanica, M. Dianu, *J. Serb. Chem. Soc.* **2009**, 74, 1075.
- [222] M. Imran, J. Iqbal, S. Iqbal, N. Ijaz, *Turk. J. Biol.* **2007**, 31, 67.

- [223] R. Fekri, M. Salehi, A. Asadi, M. Kubicki *Polyhedron* **2017**, *128*, 175.
- [224] L. D. Popov, Y. P. Tuppolova, S. I. Lechenkova, V. V. Lukov, V.A. Kogan, *Russ. J. Coord. Chem.* **2007**, *33*, 208.
- [225] Y. L. Z. Yang, M. Zhou, Y. Li, J. He, X. Wang, Z. Lin, *RSC Adv.* **2017**, *7*, 41527.
- [226] P. S. Sathyadevi, P. Krishnamoorthi, M. Alagesan, K. Thanigaimani, P. T. Muthiath, N. Dharmaraj, *Polyhedron* **2012**, *31*, 294.
- [227] M. Alagesan, N. S. P. Bhuvanesh, N Dharmaraj, *Dalton Trans.* **2013**.
- [228] J. Xu, T. Zhou, Z.-Q. Xu, X.-N. Gu, W.-N. Wu, H. Chen, Y. Wang, L. Jia, T.-F. Zhu, R.-H. Chen *J. Mol. Struct.* **2017**, *1128*, 448.
- [229] R. K. Singh, A. K. Singh, S. Siddiqui, M. Arshad, A. Jafri *J. Mol. Struct.* **2017**, *1135*, 82.
- [230] M. Cindrić, A. Bjelopetrović, G. Pavlović, Vr Damjanović, J. Lovrić, D. Matković-C'alogović, V. Vrdoljak, *New J. Chem.* **2017**, *41*, 2425.
- [231] R. C. Borra, M. A. Lotufo, S. M. Gaglioti, F. M. Barros, P. M. Andrade, *Braz. Oral Res.* **2009**, *23*, 255.
- [232] M. Shokrzadeh, M. Modanloo, *J. Res. Med. Dent. Sci.* **2017**, *5*, 33.

List of Publications

Papers Published

- [1] Halogen/azide bridged box dimer copper(II) complexes of 2-benzoylpyridine-3-methoxybenzhydrazone: Structural and spectral studies, **M.M. Fousiamol**, M. Sithambaresan, Victoria A. Smolenski, Jerry P. Jasinski, M. R. P. Kurup, Polyhedron 141 (2018) 60–68.
- [2] Crystal structure of aqua [(E)-N'-(4-(diethylamino)-2-hydroxybenzylidene)-3-methoxybenzohydrazidato] dioxidomolybdenum(VI) dimethylformamide Monosolvate, **M. M. Fousiamol**, M. Sithambaresan, M. R. P. Kurup (Communicated).

Papers Presented in Symposia

- [1] Syntheses, spectral aspects and biological studies of bromide and azide bridged box dimer copper(II) complexes of *NNO* donor aroylhydrazone, **M. M. Fousiamol**, M. R. P. Kurup, 31st Kerala Science Congress, Fatima Mata National College Kollam (2nd and 3rd February 2019).
- [2] Syntheses, spectral studies and hirshfeld surface analysis of bromide and azide bridged box dimer copper(II) complexes of di-2-pyridylketone-3-methoxybenzhydrazone, **M. M. Fousiamol**, M. R. P. Kurup, International Conference on Advances in Materials Science - ICAMS-2018, Sree Sankara College Kalady (24th and 25th October 2018) (Best paper award).
- [3] Structural and spectral studies of chloride, bromide and azide bridged box dimer copper(II) complexes of 2-benzoylpyridine-3-methoxybenzhydrazone, **M. M. Fousiamol**, M. R. P. Kurup, Recent Advances in Chemical Sciences – RACS-2017, Sree Sankara College Kalady (13th and 14th December 2017).
- [4] Crystal structure of (2Z)-N-phenyl(pyridine-2-yl)methylidene]hydrazine carboxamide, **M. M. Fousiamol**, M. R. P. Kurup, International Conference on ‘‘Materials for the Millenium’’- MatCon-2016, CUSAT (14th – 16th January 2016).

